DIRAC METAMATERIALS: ELECTROMAGNETIC EPSILON-NEAR-ZERO METAMATERIALS THAT MIMIC RELATIVISTIC QUANTUM PARTICLES

by

ANDREW K. COOK

A DISSERTATION

Presented to the Department of Physics
and the Graduate School of the University of Oregon
in partial fulfillment of the requirements
for the degree of
Doctor of Philosophy

March 2012

DISSERTATION APPROVAL PAGE

Student: Andrew K. Cook

Title: Dirac Metamaterials: Electromagnetic Epsilon-Near-Zero Metamaterials that Mimic Relativistic Quantum Particles

This dissertation has been accepted and approved in partial fulfillment of the requirements for the Doctor of Philosophy degree in the Department of Physics by:

Dr. Mike Raymer	Chair
Dr. Jens Nöckel	Advisor
Dr. Paul Csonka	Member
Dr. Steven Van Enk	Member
Dr. Jeff Cina	Outside Member

and

Kimberly Andrews Espy	Vice President for Research and Innovation/ Dean of the Graduate School

Original approval signatures are on file with the University of Oregon Graduate School.

Degree awarded March 2012

DISSERTATION ABSTRACT

Andrew K. Cook

Doctor of Philosophy

Department of Physics

March 2012

Title: Dirac Metamaterials: Electromagnetic Epsilon-Near-Zero Metamaterials that Mimic Relativistic Quantum Particles

The central topic of this dissertation is how to make classical light, comprised of many photons, behave in a manner similar to massive quantum particles in potentials. This document describes how one can relate classical wave variables, such as ray paths, frequency scales, and group velocities, to variables associated with classical point particles. A novel Dirac-equation formulation of Maxwell's equations will be presented. We will explain the connection between classical optical and quantum mechanical spin-orbit coupling. We describe a variety of different optical phenomena, including spin-orbit coupling in epsilon-near-zero [ENZ] metamaterials and other optical systems, Darwin terms, and other pseudo-relativistic effects. Resulting mathematical techniques can be used to describe generic optical systems with spatially varying values of μ and ϵ. Further discussed is the importance of

mode-mixing in the control of polarization states of cavity fields. Also discussed is how tensor, ENZ, optical metamaterials can be constructed that give an analog of magnetic fields for light. Finally, we will discuss challenges with solving problems with a Kerr nonlinearity in ENZ materials. Additionally described are problems involved in quantizing nonintegrable optical cavities. This study is undertaken with the goal of suggesting future research directions regarding metamaterials. This dissertation includes both previously published/unpublished and co-authored material.

CURRICULUM VITAE

NAME OF AUTHOR: Andrew K. Cook

GRADUATE AND UNDERGRADUATE SCHOOLS ATTENDED:

University of Oregon, Eugene, Oregon
University of Washington, Seattle, Washington

DEGREES:

Doctor of Philosophy in Physics, 2012, University of Oregon
Bachelor of Science in Physics, 2001, University of Washington with College Honors and Degree with Distinction
Bachelor of Science in Applied Computational and Mathematical Sciences, 2001, University of Washington with Honors

AREAS OF SPECIAL INTEREST:

Electromagnetic Metamaterials, Semiclassical Electromagnetism and Mechanics, Quantum Mechanics, Photonics, Quantum Optics/Cavity Quantum Electrodynamics, Semiclassical Chemistry, Entrepreneurship, Intellectual Property and Patents

PROFESSIONAL EXPERIENCE:

Graduate Research Assistant Research Experience,
My theory research involves analytic and computational techniques to describe electromagnetic fields in 3D cavities. Additional research areas include perturbative descriptions of optical spin-orbit coupling, polarization-induced mode mixing, transfer operators, and mathematical methods for dealing with the Kerr nonlinearity. My early years as an experimental RA involved obtaining the cavity QED strong coupling limit between diamond nitrogen-vacancy

centers and high-Q microspheres.

University of Oregon, 2004 – 2008

Graduate Teaching Fellow Teaching Experience,

I have been a TA in numerous beginning to advanced undergraduate and graduate physics classes and labs. I have a great deal of experience interacting with students. I have an interest in modern physics education techniques and have attended northwest physics teaching conferences.

University of Oregon, 2008 – 2012

Lundquist Technology and Entrepreneurship Fellow Business Experience,

I was awarded a technology and entrepreneurship program fellowship from the UO business school, and enrolled in business entrepreneurship classes for the 2010-2011 school year. I incorporated VisiRay Inc., with three MBAs and a JD to commercialize millimeter wave imaging patents for building inspection and pest detection. We applied for, and received, a $50,000 Dept. of Energy technology assistance grant, and carried out millimeter wave experiments at Pacific Northwest National Laboratory.

University of Oregon/VisiRay Inc., June 2010–present

Computer Programmer,

As a college intern, and post-graduation, I worked on programs to determine the sea floor composition from multiple sonar pings using Gaussian beam models and nonlinear optimization algorithms. I performed wavelet-based singal analysis, profiled code, and found ways to significantly improve the speed of legacy algorithms. I have experience programming in C/C++, PVM/MPI, Java, Matlab, FORTRAN, TCL/Expect, Mathematica, Pyton, and Labview.

University of Washington Applied Physics Lab, 1999–2003

Sonochemistry Research,

I was a member of a NASA-sponsored undergraduate sonochemistry experiment at the UW APL. I helped design, and build, a fully automated chemistry experiment using Labview, and flew with it aboard NASA's 0-g simulating "Vomit Comet" plane.

University of Washington Applied Physics Lab, 1999–2003

Physics Technical Assistant,

I helped build shockwave physics experiments, and conducted my own shots to research the folding behavior of shocked myoglobin proteins, when hit with a projectile from a 40-foot long gun.
Washington Statue University Institute for Shock Physics, 1998

Software Testing/Design,

I worked as a software tester and survey designer for Raosoft Inc., a Seattle company specializing in network/web data collection and statistical analysis software. Raosoft Inc., 1998–1999

Survey Telephone Interviewer,

I learned the value of phone skills and persistence while working as a telephone interviewer in high school. Washington State University Social and Economic Science Research Center, 1994–1997

PUBLICATIONS:

Cook, Andrew K. and Nöckel Jens, "Spin-Orbit Coupling and Relativistic Corrections in Optical Epsilon-Near-Zero Metamaterials" Submitted to PRL

Foster, David and Cook, Andrew K. and Nöckel, Jens, "Degenerate Perturbation Theory Describing the Mixing of Orbital Angular Momentum Modes in Fabry-Perot Cavity Resonators" Phys. Rev. A, **79**, 011803(R), (2009).

Foster, David and Cook, Andrew K. and Nöckel, Jens, "Goos-Hänchen induced Vector Eigenmodes in a Dome Cavity", Optics Letters **32**, 1764, (2007).

Park, Young-Shin and Cook, Andrew K. and Wang, Hailin, "Cavity QED with Diamond Nanocrystals and Silica Microspheres", Nano Letters **6**, 2075, (2006).

Reed, Justin and Cook, Andrew K., and Matula, Tom *et. al*, "The Effects of Microgravity on Nanoparticle Size Distributions Generated by Ultrasonic Reduction of an Aqueous Gold-Chloride Solution", Ultrasonics Sonochemistry **10**, 285, (2003).

TABLE OF CONTENTS

Chapter Page

LIST OF FIGURES

Figure Page

Figure Page

Figure Page

Figure Page

CHAPTER I

INTRODUCTION

Defining a Classical System Similar to a Quantum One

This dissertation covers several topics. The foremost topic concerns the question of how one can we make electromagnetic waves in a metamaterial behave in a manner similar to quantized, relativistic charged particles. A metamaterial is a system in which subwavelength manipulation of a material's structure is used to tailor bulk material properties, such as the permittivity, ϵ and permeability, μ. Describing optical analogues of electrons is useful, because the bulk of modern electronics, including computers, ultimately exploit the behavior of quantum mechanical electrons. Unfortunately, increases in the clock speed of modern computers has stagnated due to the signicant heat generated when electrons scatter in small gates. If we could coax electron-like behavior out of photons, we could conceivably develop more energy-efficient methods of computation. Then, all-optical methods would avoid problems associated with moving massive, charged particles through wavelength-scale circuits that are prone to overheat. Supercomputers already use optical, rather than electronic, signals for energy-efficient transmission of information between nodes. Soon, similar methods may

be used to shuttle light between cores in a CPU. Additionally, there are no fast, robust, all-optical methods of processing telecommunications signals. Optical telecommunications signals are changed to electronic signals, processed and amplified, and then converted back again to optical signals. All-optical processing of telecommunications signals may one day help to replace the electronic routers that set a threshold on the speed of data transfer on the Internet. Because the aforementioned problems are important ones, we will ask how closely the energy levels of an optical system can mimic the energy levels of an quantum system. With metamaterials, we can make solutions to optical systems strikingly similar to those of quantum systems, but we will also find a number of important, and fundamental, differences.

The second major topic of this dissertation concerns generalized treatments of polarization in optical cavities and devices. As cavities and waveguides become smaller, polarization effects become more important, and advanced mathematical methods are needed to deal with effects like optical spin-orbit coupling and mode mixing. While polarization-effects are often avoided in telecommunications devices, this dissertation will describe how one can tailor cavity geometry to take advantage of the polarization of light. Chapter VII will also describe 3D matrix spin-orbit operators that can be used to handle polarization pertubatively in arbitrary opitcal cavities.

In chapter IX, we will discuss the Bogomolny transfer operator, and ongoing

work to extend its use to polarization-dependent problems. The Bogomolny transfer operator is a useful tool for quantizing the energy levels of optical cavities that can be approximated by the scalar wave equation. We will use examples of the Bogomolny operator in electron-billiard systems[4], and map them onto optical systems. Doing so, we have found this operator can robustly track modes when we move across the chaotic sea, from one integrable cavity to another. In some systems, like the dome cavity with a Bragg stack, we have discovered modes that only exist and are only stable due to the polarization of the optical field[6]. For these modes, we can't start with scalar solutions and perturb our way to vector solutions. While we have described the existence of these modes in the paraxial regime using perturbation theory[1], these techniques have not yet been extended to non-paraxial cavities. As optical cavities shrink in size, if new techniques are not developed to handle polarization, devices may have unexpected behavior. All of the mathematical techniques govered in this document can be implemented to describe generalized optical systems. However, in chapters VII through IX, we won't specifically reference epsilon-near-zero materials to make this point clear. Furthermore, in chapters X and XI, we'll furthermore describe easy-to-implement classical systems that can be made similar to quantum potentials. In other chapters, we'll discuss mathematical analogies that can't be directly implemented in metamaterials, while discussing closely related practical systems. We will note that this dissertation includes co-authored material in chapters VII, VIII, and in

appendix C. Results in chapter XIII have been published, co-authored material in chapter VII has been submitted for publication.

A Classical, Vector, Analog to a Quantum System

To describe light that behaves in a manner similar to electrons, we have devised a new matrix representation of Maxwell's curl equations. This matrix representation of Maxwell's equations takes the form of the Dirac equation of if the divergence of **E** and **H**, are zero or small:

$$\begin{pmatrix} \hbar\omega\epsilon(\mathbf{x}) & -c(\vec{\sigma}\cdot\mathbf{p}) \\ -c(\vec{\sigma}\cdot\mathbf{p}) & \hbar\omega\mu(\mathbf{x}) \end{pmatrix} \begin{pmatrix} (\vec{\sigma}\cdot\mathbf{E}) \\ i(\vec{\sigma}\cdot\mathbf{H}) \end{pmatrix} = 0 \tag{I.1}$$

The above equation, we find a 4 by 4 matrix, operating on a 4 by 2 matrix, where $\mathbf{p} = -i\hbar\nabla$. The above is Maxwell's curl equations exactly for an isotropic medium with no charges or currents. This equation very closely approximates Maxwell's equations in the limit that the divergence of **E** and **H** are small. This formulation of Maxwell's equations is significant, because with the right epsilon and mu, we can make it look like the Dirac equation:

$$\begin{pmatrix} E - mc^2 - V(\mathbf{x}) & -c(\vec{\sigma}\cdot\mathbf{\Pi}) \\ -c(\vec{\sigma}\cdot\mathbf{\Pi}) & E + mc^2 - V(\mathbf{x}) \end{pmatrix} \begin{pmatrix} \mathbf{\Psi}_{+/-} \\ \chi_{+/-} \end{pmatrix} = 0 \tag{I.2}$$

Above, $\Pi = \mathbf{p} - \dfrac{e\mathbf{A}(\mathbf{x})}{c}$ and $V(\mathbf{x}) = e\phi(\mathbf{x})$, where $\phi(\mathbf{x})$ and $\mathbf{A}(\mathbf{x})$, are the scalar and vector components of the electromagnetic field. The Dirac equation, (IV.19)

is the minimum of the action of the QED [Quantum Electrodynamics] Lagrangian which describes spinor leptons interacting with the electromagnetic field. It is possible to cast Maxwell's equations in Dirac equation form, if either epsilon, $\epsilon(r)$, is near zero [ENZ], or $\mu(r)$ is near zero MNZ, while the other is not. "Dirac Metamaterials" are metamaterials in which solutions to (I.1) satisfy Maxwell's equations, and very closely approximate solutions to the Dirac equation(IV.19). We only find such solutions in isotropic materials, or in ENZ/MNZ materials. ENZ and MNZ materials are a new and active area of research, and hold unique promise for coaxing electron-like behavior out of light. The comparison of (I.1) and (IV.19) was initially inspired by a protracted debate between my advisor, Jens Nöckel, his previous graduate student David Foster, and myself about optical spin-orbit coupling. Specifically, we observed and successfully described polarization-induced mode mixing in a three dimensional cavity using perturbation theory[1], but we debated whether it was fair to call it optical spin-orbit coupling. Though the word is frequently used in the optics community, it was unclear to us whether optical spin-orbit coupling in cavities was directly related to electron spin-orbit coupling, or if the common parlance points to a weak analogy. To this end, it helps to define a system where optical spin-orbit coupling has the same form and magnitude as quantum mechanical spin-orbit coupling. First, we studied systems in which only ϵ varied, but these systems didn't have all of the relativistic corrections found in the quantum system. Comparing (I.1), to the quantum Dirac equation will show

that simultaneous spatial variation of ϵ and μ can bring electromagnetic systems much closer to relativistic quantum systems. We will show that, by using simple techniques, a *very* close analogy can be drawn between classical optical spin-orbit coupling and quantum mechanical spin-orbit coupling. However, we also found that optical spin-orbit coupling has a different angular momentum dependence than electron spin-orbit coupling. This is unsurprising since photons are spin 1 particles, and electrons are spin 1/2 particles. We also found an optical analog to the quantum mechanical Darwin term, a small correction to energy levels that arises from a perturbative treatment of solutions to the Dirac equation. However, we found the electromagnetic analog of the Darwin term had a different sign than the quantum mechanical Darwin term, though the prefactors in the Darwin term, and in the optical spin-orbit coupling term, remained the same as in the quantum case.

We find additional differences between solutions to the Dirac equation and Maxwell's equations if we insist that fields like $\mathbf{D}$ and $\mathbf{E}$ are fundamentally real. While Maxwell's equations are mute on this point, we assume the reality of electromagnetic fields. Kramer's-Kronig relationships impose small, but unavoidable corrections to solutions to Maxwell's equations that take us very slightly further away from exact solutions to the Dirac equation. However, we also find that if we construct a classical system with quantum-mechanical spin-orbit coupling, a host of other optical analogs to quantum/relativistic effects arise, with

no additional assumptions. For instance, we find optical analogs to Bohr-like atoms de Broglie-like quantization conditions and electron-like group velocities. We will suggest that, in general, we can make light behave in a manner similar to that of electrons. We will show these analogs while taking care to characterize the limit of this analogy.

This dissertation will show how to create a classical vector field-analog of a great many phenomena involving single quantum spinor particles in potentials. It is often stated that "spin is purely quantum, something for which there is no classical analogue." This statement is untrue, in the respect that vector wave equations can be made strikingly similar to quantum counterparts. Solutions to Maxwell's equations can have spin-orbit terms strikingly similar to quantum spin-orbit terms, though with different angular momentum dependence. In spherical coordinates, we can even find solutions to the full vector Helmholtz equation (in which $\nabla(\nabla \cdot \mathbf{E}) \neq 0$)that have the same angular-momentum dependent shifts as electrons. However, we will also find that the divergence conditions of Maxwell's equations forbid these solutions for electromagnetic waves, and force light to have different angular momentum dependence in the energy shifts. We will find, thankfully, that classical descriptions of photon spin only confirm quantum predictions for the spin-1 particle.

The Importance of Defining Quantum-Like Classical Systems

Why does it matter if we can make a classical optical system behave according

to the Dirac equation? It matters because electrons are ultimately described by this equation, and the current applications of electronics were undreamt of sixty years ago. Quantum electrodynamics describes all known physics not involving cosmological, or sub-nuclear length scales. If you can imagine any interesting atomic or condensed matter physics phenomena, ultimately you can derive it from the Dirac equation. In this dissertation, we'll argue that it's *useful* to know the closest possible photonic analogy to a well understood electronic device. This document will present a number of electromagnetic analogs to different textbook quantum mechanical systems. While this doesn't amount to building an optical analog of a classical optical device that works on quantum mechanical principles, it is a necessary first step. Only by knowing the optical analog of a quantum principle, can we hope to build an optical device that functions using the same principle.

For example, there are many different optical structures that can guide light in a tight loop. Chapter XIII describes the electromagnetic metamaterial necessary to make light behave like an electrons in a magnetic field. This system can be found by constructing a vector-field analog to the quantum mechanical interaction Hamiltonian. The following modus operandi will be used: first, find a classical vector model that closely approximates a quantum system. Subsequently, one can examine whether real metamaterials can approach an idealized quantum-like classical system. We will stress that the classical model is only a effective model, but

one which we strive to make internally consistent, and one that will give accurate answers.

Classical electromagnetism is still an active area of physics research because it is a very useful way to solve problems, even while ignoring the quantum nature of single photons. For example, one can quantize the electromagnetic field and express it in terms of raising and lowering operators. However, if one wishes to quantize the energies of a 3D optical cavity, it is easier to use classical electromagnetism, rather than raising and lowering operators, to solve for the frequencies of optical modes. Subsequently we can assign $N\hbar\omega$ in energy to a mode. This gives the correct quantum answer for the amount of energy in the system.

Since the energy levels of quantum and photonic systems are so important, this dissertation will be concerned with making classical systems isospectral in frequency to quantum systems. When using the word isospectral, we will typically mean that our systems will have real energies that are proportional to energies of quantum mechanical systems comprised of massive particles. For example, a classical cavity has a set of frequencies ω_n, corresponding to photons with a quantum mechanical energy of $\hbar\omega_n$. A fermionic quantum system, say electrons in a potential, has energies $E_n^{quantum}$. A classical system is isopectral to a quantum one if $\kappa\hbar\omega_n = E_n^{quantum}$, where κ is a positive constant, usually much less than 1. In other words, we consider two systems to be isospectral if when a single energy level in a quantum

system is rescaled to match a corresponding energy level in a classical system, all other energy levels are scaled by the same constant of proportionality.

Using methods employed in this text, one can systematically think of useful physical phenomena possible with electrons, and describe exactly how close we can get with photons. We will demonstrate this by finding classical optical systems with frequencies that match real quantum systems. Classical systems with spectra close to quantum systems will be built using very simple rules. Chapter X will describe how a layered ENZ system can approach the quantum mechancial finite square well. The role of absorption in limiting the lifetime of electromagnetic bound-states will also be addressed. In chapter XII, we will argue that metamaterials in which both ϵ and μ obey the Drude model, most commonly used to construct negative refractive index materials, give us a very close electromagnetic analog to relativistic quantum systems.

Advances in Metamaterials

Optical and microwave metamaterials are devices that use periodic, subwavelength-scale structures, usually ring resonators, to engineer a material's macroscopic permeability, μ, and permittivity, ϵ. Perhaps the most famous metamaterials are negative refractive index materials, predicted by Victor Veselago [7] in which both μ and ϵ are negative, which allows for propagating wave solutions because the square of the refractive index is still positive. The first experimental demonstration

of this effect by using an optical metamaterial was by Shelby, Smith, Nemat-Nasser and Schultz in 2001 at the University of Southern California, San Diego[8]. Their experiment will be discussed later in the text. It is of particular interest, because both epsilon and mu have a dispersive Drude-like frequency, and both have ENZ/MNZ regimes. Because of this, we can relate their structures to Dirac metamaterials by using a few approximations. As a side-note, negative refractive index materials are most interesting because incoming rays will bend away from the surface normal. Also, wave packet group and phase velocities are in opposite directions, which can lead to wave packets that seem to propagate negative momentum. Later, cloaking became a new hot topic in optical metamaterials[9], and has since been an active area of research.

This dissertation postulates that a future hot-topic in metamaterials is using electromagnetic waves by reproducing some of the structure of quantum mechanics, albeit through the use of continuous vector fields. This is a contrast to simply asking that a photonic device has the same output given an input signal as a quantum device. In the not too distant future, we will be able to mimic electronic devices by using metamaterials that mimic aspects of their quantum mechanical behavior. By asking what metamaterials reproduce aspects of quantum behavior of electronics, when searching for useful new metamaterial devices, we need look no further than useful existing electronic devices.

As hinted earlier, ENZ and MNZ materials are necessary to get electron-

like behavior. Recently, ENZ metamaterials have been used for many different applications. Among these are cloaking [10], transmitting and bending light through narrow kinks that wouldn't otherwise permit it, producing optical fields with high local intensity [11], and a number of other applications from superior antennae to new types of photonic band gaps [12][13][14][15][16][17]. Additionally, ENZ materials have already been used to create some classical circuit elements [18]. One goal of this chapter will be to suggest the most basic features needed for an optical system to mimic the quantum behavior that underlies electronic circuit elements. We should also note that in the microwave regime of the electromagnetic spectrum, superconductors are ENZ materials [19][20]. The nearly-real refractive index of microwaves in superconductors has recently allowed for photons to be trapped for up to a second[21].

There are a few ENZ materials that are especially interesting. Most negative refractive index materials have an epsilon-near-zero or a mu-near-zero regime. Metals, like silver, are ENZ materials above the plasma frequency. And perhaps the most important 2D ENZ material is graphene, a likely heir to silicon in next-generation computers.

Nonlinearity in ENZ Systems

Finally, this dissertation will describe ongoing work to address the issue of Kerr nonlinearities ENZ materials. Since the linear part of the refractive index becomes

vanishingly small in our ENZ waveguides and resonators, the Kerr nonlinearity becomes much more important. Typically, $\chi^{(3)}$ Kerr nonlinearities require large intensities in order for the refractive index to deviate much from it's linear limit, usually a refractive index in the range of 1-3. In our systems, the refractive index will be much less 1, especially at the boundaries of spatially varying cavities. Because of this, the Kerr nonlinearity becomes much more important at relatively small field densities. For devices, it is fortunate to have a relatively large nonlinear component, because we seek to control optical signals with other optical signals, and this is impossible in the linear limit. In ENZ materials, however, any nonlinearity is so important that its characterization is necessary before conducting experiments.

Finally, if we wish to engineer an optical system that is isopectral to a quantum device, we must not ignore the fact that real quantum systems are nonlinear because of the Coulomb interaction, and this interaction is central to the functioning of devices. Since photons have no charge, and optical nonlinearities have long-range, $\frac{1}{r}$, behavior, approximating the nonlinear behavior of a multiple electron system presents challenges. For a single-electron quantum system, we can nearly exactly reproduce the energy level spectrum. We can only "nearly" do so because certain relativistic shifts will have altered values, spin-orbit shifts have a different angular momentum dependence, and modes with zero angular momentum violate the divergence conditions of Maxwell's equations. We will find that we *cannot* exactly optically reproduce the spectrum of every excited energy level in a multi-

electron system. We cannot do so, because the the charge distribution changes when particles are excited, and the Coulomb force is not a natural part of our optical system. However, we can engineer particular ground-state modes to have the structure of electron orbitals in screened Coulomb potentials.

We can approximate certain modes of multi-electron systems because charge density can give us a classical handle on the problem. If we use quantum mechanics to obtain probability densities from a system of many electrons, we can then ask what potential will be seen by a single point-particle electron in a particular wave packet. We will argue that given any potential, we can move it into a refractive index found either in the wave equations that emerge from the Dirac equation. We can fortunately construct a similar refractive index for solutions to Maxwell's equations. We must then tailor the linear, spatially varying part of the refractive index to be less attractive, to mimic the nonlinear contribution that arises naturally from the Dirac equation for point particles. Approximating nonlinear Coulomb force in this manner is useful if we want a mode in an electromagnetic cavity to have similar frequency dependence, and spatial variation, as an atomic mode. Lattices of semiconductor atoms, with p-orbitals electrons, are used in many electronic devices, and it may prove fruitful to make electromagnetic metamaterial analogs of such quantum systems. We can construct an optical p-orbital analog for a single electron in hydrogen. It is useful to know how we can change the refractive index to approximate a p-orbital in a multi-electron atom.

Optical cavities do not have a nonlinearity with the form of the Coulomb force. The Coulomb force is a long range nonlinearity that can be attractive or repulsive for charged particles. In optical systems, we have only the Kerr nonlinearity which is intensity dependent, and short range. We will show that the Kerr nonlinearity acts as an attractive potential in chapter XIV. We will discuss how we could use the intensity-dependent Kerr nonlinearity to shift the frequency and energy of optical modes, and thus alter trapping and tunneling behavior of photons. Furthermore, we can shift the energy levels of certain ENZ materials, like graphene, by applying a voltage, and changing the carrier density and plasma frequency. While this technique is not all-optical, it nonetheless holds a great deal of promise for the manipulation of optical signals. It is assumed that graphene will replace silicon in CPUs in coming decades. So studying the behavior of waves in such systems may some day lead to new ways in which optical signals can be used to carry information between graphene transistors, in a manner analogous to the way modern supercomputing clusters increasingly use fiber optics, rather than electrons, to transmit information between cluster elements.

Before we launch into this discussion, it is important to remind the reader that *all* of classical physics is merely a model of a more exact underlying quantum process, but it's often a very useful model. So, I urge the reader to be unconcerned when slightly different classical models are covered than those expounded upon in Jackson[22]. All of the classical models we describe will give the right quantum

answer. Whenever we describe a system that can't exactly be reproduced with Maxwell's equations, we'll aim to describe a system very close to that system which can be constructed. In this later case, we will emphasize similarities in the spectra, while insisting that Maxwell's equations are satisfied for known materials and metamaterials. The step of relating physical applications to exact and inexact models relates to the ultimate goal of this dissertation: to suggest mathematical techniques that can aid in the development of new photonic devices.

CHAPTER II

CLASSICAL SOLUTIONS TO KLEIN-GORDON AND SCHRÖDINGER EQUATIONS

Slowly Varying to EM Wave Equations above the Plasma Frequency

This chapter will describe very simple optical systems that have a connection to the radial Schrödinger equation. This chapter and the next will serve as a motivation for describing similarities between the Klein-Gordon [KG] equation and ENZ metamaterials. Classical analogues to quantum systems will be pursued futher throughout the dissertation. The connection between the KG equation and the Schrödinger equation will allow us to closely approximate ENZ materials with the nonlinear Schrödinger equation in chapter XIV.

We will first describe how vector wave solutions are obtained from scalar wave equations. Then, we will describe how a radially varying Klein-Gordon equation can be reduced the Schrödinger equations by using slowly varying envelope solutions. We will finally describe how ray tracing gives more accurate solutions than the solutions to the Schrödinger equation. Later, we will show how to obtain the underlying KG equation from the Dirac formulation of Maxwell's equations, and from the Dirac equation itself. The purpose of this exercise is to find a

fundamental classical system that is isospectral to the principle quantum energy levels of spherical potentials, like the Coulomb potential. We will use this starting system in our quest to better approximate a quantum system governed by the Dirac equation. The results here do not include optical spin-orbit coupling effects. However, the results here can be applied above the plasma frequency in any ENZ plasma medium. If we limit the discussion to 2 dimensions, we can even apply these techniques to graphene.

The Scalar Wave Equation

Given a system with the right symmetry, scalar wave equations provide a remarkably robust way to exactly solve Maxwell's equations. If a cavity is deformed from the symmetric system, frequency shifts can be obtained by using the scalar wave equation and perturbative methods[23][24]. Mode mixing, changes in vector fields, and frequency splitting due to the addition of birefringence to a symmetric cavity can also be treated by perturbative methods after using scalar solutions as a starting point[25]. For a dispersive medium with spherical symmetry, the following scalar wave equation can be used, where $n(r,\omega)^2 = \mu\epsilon$ is a purely radially varying refractive index:

$$\nabla^2\Phi + \frac{\omega^2}{c^2}n(r,\omega)^2\Phi = 0 \tag{II.1}$$

Each modal solution of the above scalar wave equation yields both a transverse

electric (TE) and transverse magnetic (TM) vector mode. Each of these modes has an $\mathbf{H}$ field related to its curl. $\mathbf{H}_{TE}$ therefore has a vector field that's similar to $\mathbf{E}_{TM}$.

$$\mathbf{E}_{TE} = \mathbf{r} \times \nabla\Phi \tag{II.2}$$

$$\mathbf{E}_{TM} = \frac{1}{k}\nabla \times \mathbf{E}_{TE} \tag{II.3}$$

In order to obtain the full vector solutions to Maxwell's equations from a scalar wave equation, we'll presume that the electric field is free of divergence, and the above solutions clearly satisfy this condition.

One radially varying scalar wave equation that has a refractive index with interesting properties is the spatially inhomogeneous KG equation:

$$\nabla^2\Phi - \frac{1}{c^2}{\partial_t}^2\Phi = \frac{{\omega_p}^2}{c^2}\Phi + \frac{2\omega_p}{\hbar c^2}V(r)\Phi \tag{II.4}$$

We'll assume that ω_p is constant, real, and large. In the next chapter, we'll show how ω_p plays a role analogous to the plasma frequency for metals. In a plasma medium, freely propagating waves are allowed only if their frequencies are above the local plasma frequency. The quantity $\frac{2\omega_p}{\hbar c^2}V(r)$ can be positive or negative at any point in space, but must be radially varying only. Optical scalar wave equations are often solved by assuming slowly varying envelope solutions. Here, we'll postulate solutions of the form $\Phi(\mathbf{x}, t) = \psi(\mathbf{x}, t)e^{(-i\omega_p t)}$. We assume that the wave envelope

changes very slowly in time compared to timescales associated with ω_p. This allows us to make the approximation:

$$\partial_t^2 \psi(x,t) e^{-i\omega_p t} \tilde{=} -\omega_p^2 \psi(x,t) e^{-i\omega_p t} - 2i\omega_p e^{-i\omega_p t} \partial_t \psi(x,t) \tag{II.5}$$

Plugging the above into the KG equation yields a Schrödinger-like equation for the wave envelope that's first order in time:

$$-\nabla^2 \psi(\mathbf{x},t) + \frac{2\omega_p}{\hbar c^2} V(r) \psi(\mathbf{x},t) = i \frac{2\omega_p}{c^2} \frac{\partial}{\partial t} \psi(\mathbf{x},t) \tag{II.6}$$

We can multiply the above by $\frac{\hbar^2}{2m}$ to obtain a more familiar formulation of Schrödinger's equation. If we treat equation (II.6) classically, $\psi(\mathbf{x},t)$ isn't a wave function, but an envelope that ultimately acts to modulate a vector field. The envelope slowly oscillates in space and carries a very high frequency wave. An optical KG medium with a plasma frequency, ω_p, corresponding to a 1.5 micron wave, could allow for the propagation and manipulation of electromagnetic waves of telecom wavelengths. Microwave plasma frequencies of superconductors make these transparent to microwave electromagnetic waves. By visual inspection, we can see that $\frac{2\omega_p}{\hbar c^2} V(r)$ plays a role similar to that of a quantum mechanical potential for charged particles. In the next section, we'll describe how rays of different frequencies bend in response to the gradient of $\frac{2\omega_p}{\hbar c^2} V(r)$. To explicitly show how classical light in a KG medium behaves in a manner similar to massive quantized particles,

we'll choose a medium with $\omega_p = \frac{mc^2}{\hbar}$, yielding the original driving term in the relativistic KG equation, also giving the Schrödigner equation:

$$-\frac{\hbar^2}{2m}\nabla^2\psi(\mathbf{x},t) + V(r)\psi(\mathbf{x},t) = i\hbar\frac{\partial}{\partial t}\psi(\mathbf{x},t) \tag{II.7}$$

If we pick m to be the mass of the electron, then optical solutions to the KG equation would have a prohibitively large frequency. In fact, light at this large frequency would be gamma radiation with a free-space wavelength equal to the Compton wavelength of the electron, $\frac{\lambda_{Compton}}{2\pi} = \frac{\hbar}{mc}$. The Compton wavelength is useful in relativistic scattering problems, and the electron can't be localized to a position less than half of the Compton wavelength, due to Heisenberg's position momentum uncertainty relationship, $\Delta x \Delta p_{rel} > \frac{\hbar}{2}$. We should note that this wavelength is less than a 40th of an Angstrom. Later, we will note that the same scalar wave equation that we are using here, falls out of solutions to the Dirac equation for spinors, so there's no particular mystery in the appearance of the Compton wavelength. However, this is the first of many steps we must take to make photons behave like massive relativistic particles.

While we may wish to choose Gaussian solutions for the envelope $\psi(\mathbf{x},t)$ for a propagating wave, for cavity solutions, it is more useful to pick: $\psi(\mathbf{x},t) = \Psi(\mathbf{x})e^{-i\omega_s t}$:

$$-\frac{\hbar^2}{2m}\nabla^2\Psi(\mathbf{x}) + V(r)\Psi(\mathbf{x}) = \hbar\omega_s\Psi(\mathbf{x}) \tag{II.8}$$

We will briefly note that the energy of a plasmon above the plasma frequency in a Drude metal is $\hbar\omega$, as a result of electrons in the material having energy proportional to frequency. Even though we have solved a spectral problem with classical assumptions, if we apply this solution to a real plasma material, we have a rough correspondence between relativistic energy and plasmon energies. However, if we treat this as a linear classical problem, we could assume no relationship between the frequency of a wave and its energy. However, an explicit relationship between frequency and energy is a general property of classical nonlinear systems[26].

The Optical Radially Varying System Lacks l=0 Modes

Since V(r) is spherically symmetric, we can also separate radial and angular parts of Schrödinger's equation with the usual ansatz of a radial function multiplied by spherical harmonics: $\Psi(\mathbf{x}) = R_{nl}(r)Y_{lm}(\theta,\phi)$. Even before we pick the form of $V(r)$, can see from equations (II.2), and (II.3), that the slowly varying approximation predicts that $\mathbf{E}_{TE}$ and $\mathbf{E}_{TM}$ optical modes **don't exist** for $l = 0$ solutions to Schrödinger's equation. If a mode of the scalar wave equation is spherically symmetric, only the radial part of its gradient survives, and the cross product of its gradient with the radial vector is zero. The conditions under which we can't have l=0 modes are as follows: The system's refractive index is scalar, radially varying and, divergence free. We can permit the electric field to have a divergence if we note that if $\nabla \cdot \mathbf{D} = 0$, then $\nabla \cdot \mathbf{E} = \frac{1}{\epsilon}(\nabla\epsilon) \cdot \mathbf{E}$, if we choose

solutions where $(\nabla\epsilon)\cdot\mathbf{E}$ is not equal to zero. Furthermore the divergence of the electric field can be non-zero if we dope the material with charge carriers to locally change the frequency. These exceptions will be discussed in chapter IV, dealing with Dirac-like formulations of Maxwell's equations.

With the Coulomb potential, approximate solutions to the scalar wave equation can be found via a wave envelope described by the textbook Laguerre polynomial and spherical harmonic solutions to the hydrogen atom. Figure 2.1. displays the electric fields corresponding to a scalar p-orbital, the fundamental modes for the hydrogen-like optical system. The vectors given by $\mathbf{E}_{TE}$ and $\mathbf{E}_{TM}$ are field amplitudes and not intensities or probability distributions. Just as each solution to Schrödinger's equation supports spin up and spin down electrons, each solution to the scalar wave equation supports two modes with different polarizations. The vector fields of these modes don't look like p-orbitals, but they occur at the same frequencies and inhabit similar regions of space.

We should briefly note that our solutions are of the form $\phi = \Psi(\mathbf{x})exp(-i(\omega_p + \omega_s)t)$. Since $\hbar\omega_s < 0$, the magnitude of the total frequency, ω of the wave will be less than ω_p. This means that traveling wave solutions only exist within the Coulombic potential of the spatially varying refractive index. The ray dynamics for a Coulombic driving term in a scalar KG medium provide an interesting connection to the Bohr atom. For this reason, we'll briefly look at ray tracing solutions to Coulombic refractive index potential in the following chapter.

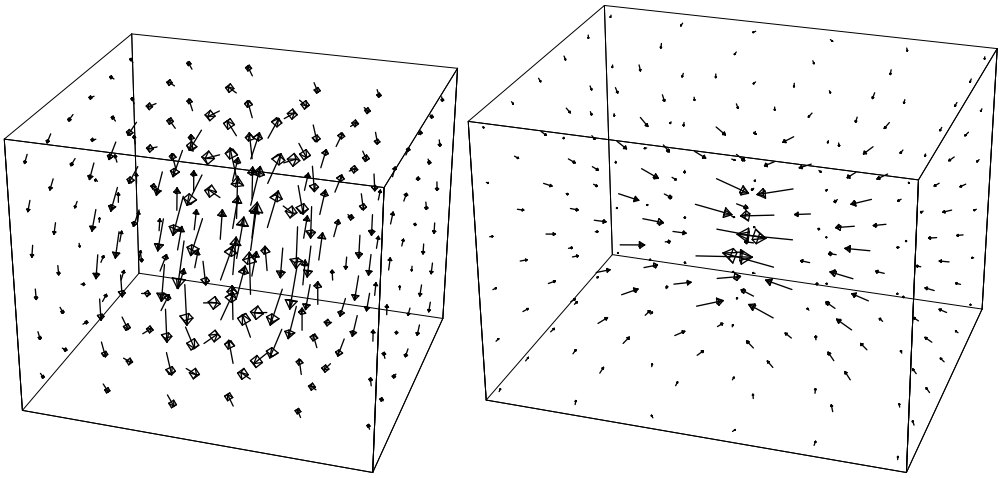

Figure 2.1. The $\mathbf{E}_{TE}$ and $\mathbf{E}_{TM}$ fields for "p-modes" of light in a KG medium with a Coulombic driving term. The two different modes are obtained from the scalar solution proportional to $\frac{-Zr}{a_o}\exp[\frac{-Zr}{2a_o}]\exp[i\phi]sin(\theta)$

CHAPTER III

RAY TRACING IN A SMOOTHLY-VARYING ENZ/KG MEDIUM

Ray Dynamics in a KG Medium

In this chapter, we will treat the KG equation as a scalar, spatially varying refractive index, and solve for its energy levels using ray-tracing methods. This approach quantizes the KG equation not by using arguments about the nonrelativistic angular momentum of of the wave, but by quantizing the phase of rays that make circular trips around the cavity. This approach is analogous to de Broglie's hypothesis that standing waves are responsible for Bohr atom quantization conditions. There are a great number of papers that quantize the KG equation using valid semiclassical arguments, and thus far we haven't found an approach identical to the one we put forth in this chapter. Some of the KG semiclassical quantization methods involve expansion of the the ground state wave function as a starting point[27]. Other approaches rely on minimizing a semiclassical energy[28]. Alexandru Popa has recently presented an approach to Bohr-like quantization of electron energy in potentials[29], and he correctly concludes that the KG equation implies that a very high phase velocity can be associated with the electron in potentials. While the starting points of reference

[29], and this chapter are similar, we use a new and different methodology. Popa still uses the classical kinetic energy of the point-particle electron, $\frac{1}{2}mv^2$, and the energy given to the electron by the Schrödigner equation, to obtain Bohr-like quantization conditions. Neither of these steps is needed in our approach. In contrast, we do not make references to quantum mechanical postulates of electron behavior in order to obtain an optical analog of the Bohr atom. Since electrons are massive particles, it would be unjustified to start by assuming electron-like kinetic energy for light in ENZ materials. We do however, obtain equations that look like quantum mechanical energy and momentum postulates along the way. And we do find a group velocity for light that mimics electron group velocity, but we find this only after quantizing the cavity. Also, our approach does not consider integrable solutions to Hamilton-Jacobi equations, as in [29]. We only need to know two things to solve this problem: the refractive index, and a rule for the radius of curvature of a ray in a spatially varying refractive index. We can take any spatially varying refractive index, quickly calculate a radius of curvature for a ray, trace the ray, and quantize closed orbits if we find $2\pi n$ phase shifts. In chapter XIV, we find arguments as to why photon energies in ENZ cavities are similar to electron energies, which will be helpful in further relating semiclassical optical problems to semiclassical chemistry problems. In chapter XIV we additionally explore methods to quantize energies if ray orbits do not close in a single trip.

Ray Models

In either optics or acoustics, a ray is a vector that describes a direction perpendicular to a level curve or wavefront at a point. Families of rays can be used to describe a wavefront that's curved due to variations in the refractive index. A ray path defines the minimum of the action for a propagating wave and is a useful starting point for understanding the behavior of waves in a system. Ray paths can be obtained through a wave equation's refractive index, $n(r, \omega)$. The KG equation's refractive index can be obtained from :

$$n(r,\omega) = \sqrt{1 - \frac{\omega_p^2 + c^2 \breve{V}(r)}{\omega^2}} = \sqrt{\epsilon\mu} \tag{III.1}$$

Later, we will the following substitution: $\breve{V}(r) = -\frac{2m}{\hbar^2} Ze^2/r$, and this will give our classical scalar wave equation the same energy levels as the Bohr atom with relativistic corrections. For now, however, we do not wish to cloud the discussion of classical ray dynamics by introducing parameters like charge, mass and Plank's constant. Here, we will assumes our material obeys the right-hand rule for energy transmission, and solves the wave equation by taking only the positive square root of the refractive index. We'll assume $\mu > 0$, since this is true of metals that can be approximated by the KG equation. In an ideal Drude metal, for example, electrons are essentially free at high frequencies. If ω is slightly larger than ω_p, where ω_p is the plasma frequency, then $\mu = 1$ and $\epsilon(\omega) \cong 1 - \frac{\omega_p^2}{\omega^2} \cong n(r,\omega)^2$ [30]. The frequencies

just above a plasma frequency are known as the ultraviolet transparency window for metals. This is the one region in which the optical scalar wave equation reduces exactly to Schrödinger's equation. We will show that many useful properties could be exploited if we add nonlinear terms to Maxwell's equations in the ultraviolet transparency regime. Waves decay exponentially in time when the total frequency is less than the local plasma frequency, these two cases will be discussed in more detail in chapter X, in which we describe how to reproduce the quantum finite square well, using microwaves in superconducting cavities.

Additionally, propagating rays are strongly reflected off of regions where the permittivity is negative, and this plays an important role in the light-trapping properties of a spatially varying KG medium. In the equation for the refractive index, we can see that $\omega_p^2 + c^2\breve{V}(r) = \Omega_{eff}(r)$ acts like a spatially varying effective plasma frequency. In materials, such an effect could be approximated by using metals with two different plasma frequencies, or by varying the surface plasma frequency by varying the refractive index of a dielectric next to a plasma material.

The refractive index gives us the phase velocity of a wavefront, v_p:

$$v_p(\omega, r) = \frac{c}{n(r,\omega)} = \frac{c}{\sqrt{1 - \frac{\omega_p^2}{\omega^2} - \frac{c^2\breve{V}(r)}{\omega^2}}} \tag{III.2}$$

Rays and waves in a medium curve towards regions of lower phase velocity with a higher refractive index and are reflected away from regions of high phase velocity. If we pick a region where $\breve{V}(r)$ trends towards zero, the phase velocity is extremely high if ω is slightly greater than ω_p. Rays will be strongly reflected from

$n(r,\omega) = 0$ boundaries. One trick for finding ray paths through a material involves the approximation that the phase velocity varies linearly over a very small region. If the phase velocity varies linearly, then rays will trace a circular arc around the point where the phase velocity is zero [31]. We derive the result from 2D ray equations in Appendix D. If we trace rays only a short distance, we can approximate any spatially varying phase velocity as linar at a given frequency. When we make such an approximation, we can choose a hypothetical point at which the phase velocity is zero, and trace rays about that particular point. The gradient of the phase velocity for a spherically symmetric medium, only has one component, that we'll call $\frac{dv_p}{dr}$. For the KG equation:

$$\frac{dv_p}{dr} = \frac{c^3 \frac{d\check{V}(r)}{dr}}{2\omega^2 n(r,\omega)^3} = \frac{\frac{d\check{V}(r)}{dr}}{2\omega^2} v_p^3 \tag{III.3}$$

Using the gradient at a certain radius, we can find what r_c would be if the medium varied linearly. Thus at any point in the cavity, there is an effective instantaneous circular orbit associated with the ray, r_c, that must obey the following equation:

$$\frac{dv_p}{dr} = \frac{v_p(\omega, r)}{r_c} \tag{III.4}$$

If we pick a ray at any non-absorbing frequency heading in any direction, if we take a small enough step, the medium will have effectively linear variation in phase

velocity. The ray will follow a circular trajectory about a radius, r_c determined by the equation:

$$r_c = \frac{2\omega^2 n^2}{c^2 \frac{d\breve{V}(r)}{dr}} \tag{III.5}$$

One way of finding frequencies of normal modes in an optical cavity is to employ the wave analogue of EBK quantization. We can look for a ray that traverses the cavity, and returns to the same wavefront with the same phase. With the spherically symmetric spatially-varying KG equation, we can ask if any trajectories trace perfectly circular arcs around the origin where $r_c = r$, where r is the current distance from the center of the cavity, and the ray's motion has no components in the radial direction. If a ray of a given frequency traces a circular arc, then $\frac{dv_p}{dr}$ doesn't change as the ray orbits, allowing for an easy determination of the frequency that allows for circular ray orbits. If we choose a Coulomb potential for $\breve{V}(r)$, we can find circular orbits for rays of any non-absorbing frequency. Here, we'll choose $\breve{V}(r) = -\frac{2m}{\hbar^2} Ze^2/r$ this is the same substitution used to obtain Schrödinger's equation through the slowly varying approximation in chapter II. The following equation describes the instantaneous radius of a circular arc that a ray will follow in a Coulombic medium:

$$r_c = \frac{r^2}{Ze^2}\frac{\hbar^2}{mc^2}(\omega^2 - ({\omega_p}^2 - \frac{2mc^2}{\hbar^2}\frac{Ze^2}{r})) \tag{III.6}$$

The above equation is valid for tracing the ray no matter what its bearing or

location in the refractive index potential. However, we could look for Bohr-like orbits, where the ray starts at a circular orbit, and stays on the same orbit. This occurs when $r_c = r$, and for this case, the equation above simplifies substantially:

$$\omega^2 - \omega_p^2 = -\frac{mc^2}{\hbar^2}\frac{Ze^2}{r} \tag{III.7}$$

Using the relationship $\omega = \omega_p + \omega_s$, we can express the condition for circular orbits in terms of the $\hbar\omega_s$ eigenvalue quantity in Schrödinger's equation for the envelope. We find:

$$\hbar\omega_s + \frac{1}{2}\frac{(\hbar\omega_s)^2}{mc^2} = -\frac{1}{2}\frac{Ze^2}{r} \tag{III.8}$$

This reduces to an equation that mirrors the virial theorem, since $mc^2 \gg \hbar\omega_s$:

$$\hbar\omega_s \cong -\frac{1}{2}\frac{Ze^2}{r} \tag{III.9}$$

In the above equation, ω_s is a vanishingly small component of the total frequency associated with the electromagnetic modes. $\hbar\omega_s$ takes the form of a quantum mechanical energy term, and the equation looks like the Bohr atom. In the Bohr atom, the total energy is half the potential energy, because the kinetic energy of the electron is half potential energy and opposite in sign. In our approach, made no assumptions about angular momentum and simply insisted that the radius of curvature of a ray is tailored not to change during its orbit. Additionally, we have made no assumptions about energy conservation. Essentially, we haven't invoked the starting assumptions for quantizing energy in the Bohr atom. Rather, we have

derived one of the starting assumptions simply by looking for self-consistent ray orbits. This is important, because we have found that there is more than one way to obtain quantum relationships. We will continue to find more quantum relationships when we add de Broglie-like quantization of phase.

Bounded Transparency Regime for Ray Orbits

We know that the kinetic and potential energy of a nonrelativistic particle is a small part of its mass-energy. We can draw a rough analogy for light in a KG medium and state that the frequency difference from the cutoff frequency is a small part of a wave's total frequency. However, we find that the ray dynamics of a wave in a KG medium are easily expressed in terms of this frequency difference, and not the total frequency, of the mode. At a given frequency, equation (III.6) tells us that any frequency less than ω_p has a ray that can trace a perfect circle around the $\breve{V}(r)$ at the radius r_c, However, as $\breve{V}(r)$ trends towards zero, we know that all frequencies less than ω_p will enter an absorptive regime because the refractive index will be imaginary. Using equation (III.6), we can express a ray's refractive index in terms of the radius at which it makes a circular orbit:

$$n(r,\omega) = \sqrt{\frac{\omega^2 - \omega_p^2 + \frac{2mc^2}{\hbar^2}\frac{Ze^2}{r}}{\omega^2}} = \sqrt{\frac{\frac{\omega_p Ze^2}{\hbar}(-\frac{1}{r_c} + \frac{2}{r})}{\omega^2}} \qquad \text{(III.10)}$$

From the above equation, we can see that a ray of a given frequency would enter an absorbing region at radii greater than $r > 2r_c$. If we find a radius at which

a ray can trace a perfect circle around a Coulombic driving potential, at exactly twice that radius, the ray of that frequency would be absorbed as it propagates, regardless of its direction of travel. In order for a ray to freely propagate at a radius outside of this sphere, its frequency would need to be increased to a frequency closer to ω_p. If the ray's frequency were increased above ω_p, the ray could propagate completely freely, of course. However, these rays would no longer be trapped, and would not correspond to a frequency with bound states. The phenomena of rays being absorbed at twice the "virial" radius is interesting because it isn't explicitly a part of its one-electron quantum mechanical analogue. Using numerical methods, we will find that any classical ray launched at a non-absorptive frequency within the refractive index potential, would very rapidly bend away from the spherical boundary determined defined by $r = 2r_c$. In order to understand why rays are reflected form this boundary, we only need look at equation (III.2), which states that the gradient of the phase velocity is proportional to the phase velocity cubed. The greater the gradient of the phase velocity, the more quickly rays bend about a smaller radius of curvature. A plot of the phase velocity for a ray with $\omega < \omega_p$ is depicted in figure 3.1..

Rays will always bend away from regions of higher phase velocity. For the KG equation with a Coulombic driving term, the phase velocity approaches infinity for $r = 2r_c$, and thus the Coulomb potential forms an infinite potential for any ray with $\omega < \omega_p$. Rays can follow rolling trajectories within the bowl-shaped

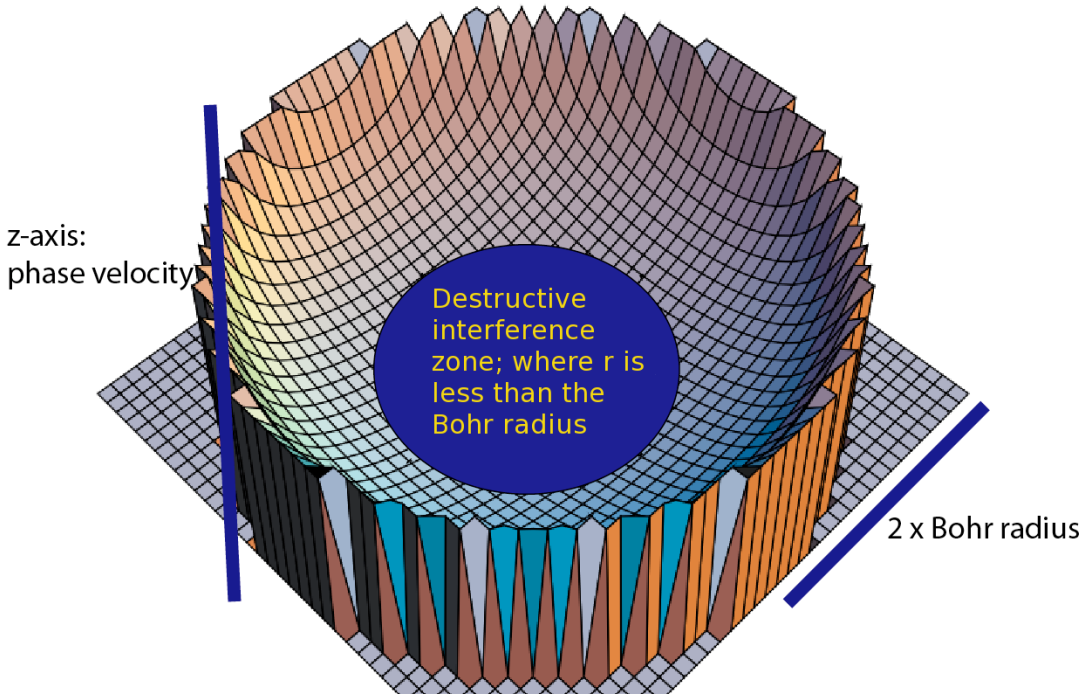

Figure 3.1. A plot of the phase velocity that a ray of a given frequency sees with a Coulombic driving term added to the KG equation. This is like a potential for waves of a given frequency. Rays will curve away from regions of higher phase velocity. Areas outside of the bowl are areas where rays are absorbed as they propagate ($r > 2r_c$). Since the rim of the bowl actually diverges to an infinite phase velocity, no classical ray path with a frequency less than the plasma frequency of the bulk material, ω_p, can escape. The rim is, of course, truncated in this plot.

potential, but can never leave. However, even in scalar wave equations, a ray path is just a step on the way to a complete description of the differential equation. A complete description of a wave equation must not only describe the minimum of the action, but also paths that surround the minimum of the action. When dealing with semiclassical wave equations, phenomena such as diffraction and tunneling are evidence of the importance of paths that don't lie on the minimum of the action. If we stick completely in the ray picture, no energy will be lost due to the absorption

of trapped rays, because these rays can't escape the $r = 2r_c$ boundary. However, with foreknowledge of tunneling, we can't discount the possibility of energy loss in this semiclassical system due to rays tunneling into an absorptive region. For now, we'll simply note that that a ray would have to deviate a great distance from the Bohr-like radius in order to tunnel into the strongly refractive index. Later, we will use a more rigorous formulation of the refractive index inspired by the Dirac equation. When we do, we will require that the refractive index have a small imaginary component even within the potential to insure that the medium can't instantaneously respond the electromagnetic field.

Adding Phase to Ray Orbits

A classical particle, like a ray, will follow a line through space defined by the minimum of the action. However, even if we ignore variations about the minimum of a ray's action, we still need to associate a phase with ray path, since it describes a wavefront. If we know a wave's phase velocity for at a given frequency, we can quickly determine its wavelength. If a ray isn't traveling on a "virial" circular orbit, its wavelength will change as it curves through regions of different phase velocity. However, the phase velocity is constant for rays on a circular orbit around the central potential. From equation (III.2) and (III.6)

$$v_p(r_c, \omega) = \frac{c\omega}{\sqrt{\frac{mc^2}{\hbar^2}\frac{Ze^2}{r_c}}} \tag{III.11}$$

From the phase velocity, we can easily determine the wavelength of a ray on a circular orbit:

$$\lambda = \frac{2\pi}{\omega} v_p = \frac{2\pi}{\sqrt{\frac{m}{\hbar^2}\frac{Ze^2}{r_c}}} \tag{III.12}$$

However, even classical, continuous waves propagating in a circular ring will destructively interfere if the wavelength isn't such that an integer number of wavelengths exist in the resonator. In other words, if n is a positive integer:

$$2\pi r_c = n\lambda = n\frac{2\pi\hbar\sqrt{r_c}}{\sqrt{mZe^2}} \tag{III.13}$$

We can see from the above equation, that if a ray follows a circular orbit, its wavelength can be expressed solely in terms of its distance from the origin. We can also see that the wavelength of a ray on a circular orbit grows proportional to the square root of the radius, while the circumference of the orbit grows linearly with the radius. Since the minimum value for $n = 1$, the minimum radius that allows constructive interference in III.13, will be equal to $\frac{\lambda}{2\pi}$. The radial dependence of the right and left hand sides of III.13 is displayed in figure 3.2..

When we solve for circular orbits that have constructive interference, we find that these orbits occur at radii proportional to n^2, or:

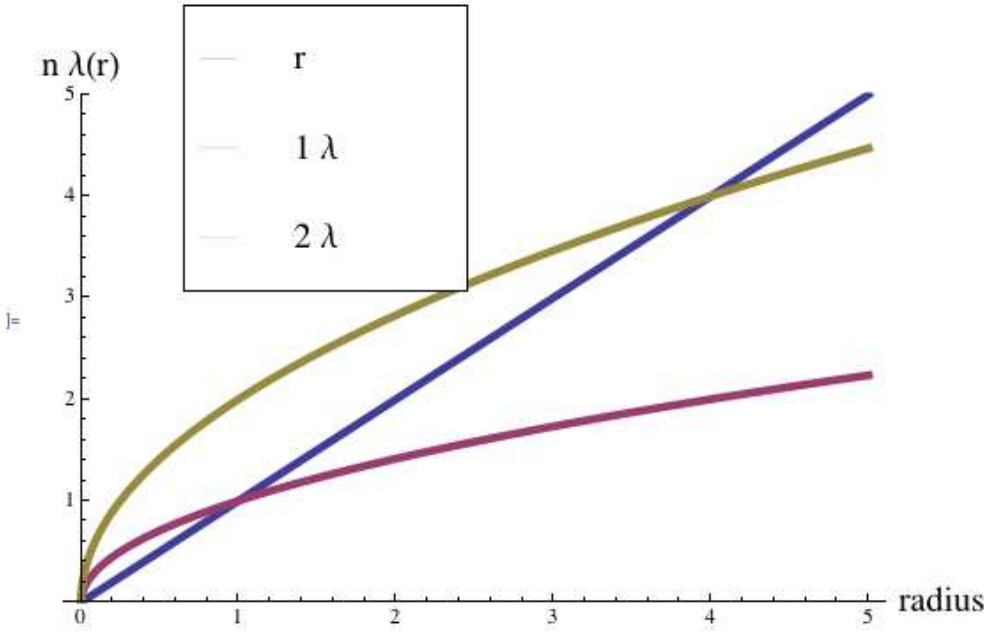

Figure 3.2. A plot of wavelength vs. raidus for circular ray orbits in a KG medium with a Coulombic driving term. The plot is the left hand side vs. the right hand side for equation, III.13, which gives ray quantization conditions based on phase velocity. Each side is divided by 2π. The straight line is the radius, and the curves are the n times the wavelength of circular orbits for $n = 1, 2$. Normal modes occur at line crossings, where constructive interference is allowed and the LHS of III.13 equals the RHS.

$$r_c = \frac{\hbar^2}{mZe^2} n^2 = a_o n^2 \tag{III.14}$$

The minimum possible radius that permits one standing wave for a circular orbit is the Bohr radius: $a_o = \dfrac{\hbar^2}{mZe^2}$. Every other circular radius will experience destructive interference. Here we can see that the scalar wave equation permits $n = 1$ and $l = 0$ solutions that we previously mentioned were absent in Chapter II. These solutions could only correspond to electromagnetic waves with a divergence. This situation can't be ignored completely, since we will later suggest that an

efficient way to produce an epsilon-near-zero potential is to locally dope a plasma medium, or metamaterial plasma medium, with charge carriers. Additionally, the scalar l=0 solutions apply if we pick solutions where $\nabla(\epsilon(r)) \cdot \mathbf{E}$ is not zero.

Return to the Classical Picture

In the preceding section we inserted quantities like $\hbar$ and m into a classical field equation simply to show the analogy between classical ray paths and the Bohr atom. However, the inclusion of these constants obscures the basic physics at work in semiclassical solutions to Maxwell's equations. If we use $\breve{V}(r) = -k_c/r$ and start with the equation:

$$\nabla^2\Phi - \frac{1}{c^2}{\partial_t}^2\Phi = \frac{{\omega_p}^2}{c^2}\Phi - \frac{k_c}{r}\Phi \tag{III.15}$$

We find more concise condition for circular orbits:

$$\omega^2 - \omega_p^2 = -\frac{k_c c^2}{2r_c} \tag{III.16}$$

Also, we find that the wavelength of circular orbits is independent of the cutoff frequency ω_p:

$$\lambda = \frac{2\pi}{\sqrt{\frac{k_c}{2r}}} \tag{III.17}$$

And finally we find a more concise and elegant condition for Bohr-like orbits,

with $a_o = \frac{2}{k_c}$:

$$r(n) = \frac{2n^2}{k_c} \tag{III.18}$$

In a KG medium with a Coulombic driving term, Bohr-like orbits occur at radii determined only by the constant that governs the magnitude of the driving Coulomb potential.

Ray Tracing Gives Leading-Order Relativistic Corrections

While the radii of circular Bohr-like orbits don't depend on the cutoff frequency ω_p, materials with different ω_p will have different total frequencies for a given n. However, if we rewrite equation III.16, and III.18, we can see that the total frequencies at which Bohr-like orbits occur is related to ω_p in a simple way:

$$\omega = \sqrt{\omega_p^2 - \frac{k_c^2 c^2}{4n^2}} \tag{III.19}$$

If we go back to equation (18), we can find the frequency quantization condition for Bohr-like circular orbits using $r = n^2 a_o$. remembering that $\omega = \omega_p + \omega_s$, we can express the above formula in terms of the $\hbar\omega_s$ quantity found in Schrödinger's equation, and the fine structure constant $\alpha = \frac{e^2}{\hbar c}$. We find:

$$\hbar\omega_s = -mc^2 \pm mc^2\sqrt{1 - \frac{\alpha^2 Z^2}{n^2}} \tag{III.20}$$

Since α is a small quantity, we can simplify this expression by Taylor expanding the square root. The negative sign corresponds to choosing a negative quantity

for the total frequency, yielding an ω with slightly smaller magnitude than $-\omega_p$. Picking the positive case where the classical Schrödinger frequency is a small negative number, we find:

$$\hbar\omega_s = -\frac{mc^2\alpha^2Z^2}{2n^2}(1 + \frac{\alpha^2Z^2}{n^2}\frac{1}{4} + ...) \tag{III.21}$$

Since $\omega = \omega_p + \omega_s = \dfrac{mc^2}{\hbar} + \omega_s$, The total frequency is less than the plasma frequency outside of the refractive index potential. We can compare the answers that ray tracing gives us, and compare it to the Dirac equation solution for electrons in a hydrogen atom, which include spin-orbit coupling and Darwin term effects:

$$E_{hyd} = -\frac{mc^2\alpha^2Z^2}{2n^2}(1 + \frac{\alpha^2Z^2}{n^2}(\frac{n}{(l \pm \frac{1}{2}) + \frac{1}{2}} - \frac{3}{4})) \tag{III.22}$$

The first term in the $\hbar\omega_s$ expression gives us the energy levels of hydrogen without fine structure. We can obtain this term directly if we drop the $\dfrac{(\hbar\omega_s)^2}{2mc^2}$ term in formula (18). All of the steps we used to get this answer are those used to solve continuous wave equations and no postulates of QM were employed that aren't a part of classical electromagnetism. Furthermore, we only used the dynamics along the minimum of the action to get good agreement with quantum results. The α^2 term matches the energy of hydrogen for some of the hydrogenic solutions, like $n = 2$, $l = 1$, (the fundamental mode for divergence free electromagnetic solutions), and $n = 3$, $l = 2$, but diverges for other values. In chapters IV-VII, we will go

beyond the scalar wave equation by taking polarization into account. This will allow us to make a connection between quantum and optical spin-orbit coupling.

Nonetheless, it is surprising to obtain the leading constants for hydrogen's fine structure when our only initial goal was to force the wave equation to yield wave envelopes that mimic wave functions. It must be emphasized that for a given frequency, many different constructively interfering ray orbits are possible that don't lie on a circle. In fact, we will show that a ray launched at any angle between $r = 0$ and $r = 2r_c$ will follow an elliptical path! Inclusion of the $\frac{(\hbar\omega_s)^2}{2mc^2}$ term in the phase velocity causes these ellipses to precess very slightly (and gives the fine structure-like correction). If we were to include constructively interfering elliptical paths in this analysis, we would need to include Maslov indices to track the phase shifts of waves at ray turning points. A valid, but absurdly general, way to solve way to solve wave equations is to employ path integrals. If we want to improve the accuracy of ray-based solutions to the scalar wave equation, we could use Huygen's principle to approximate path integrals. If we can define wave fronts and instantaneous directions of propagation, we can pick points in space and propagate them in all forward directions. For this reason, summing over all elliptical paths should give us a more accurate estimate for $\hbar\omega_s$ eigenvalues in the scalar wave equation.

It should be again emphasized that we can relate the total frequency of the electromagnetic wave $\omega_p + \omega_s$ with the total mass-energy of a relativistic particle

mc^2+E_s. We can now recognize the importance of the cutoff frequency in producing classically bound states: waves are strongly reflected from regions in which the permittivity goes from an entirely positive value to a negative value. In a scalar yet spatially inhomogeneous medium, waves of a discrete frequency are strongly confined to a region in which their permittivity has a positive value. A wave traveling into a region with a divergent phase velocity is also a hallmark of this trapping behavior in the wave equation. The quantity ω_s becomes important because the wave equation reduces to Schrödinger's equation for frequencies near the ω_p cutoff frequency. We can see that the slowly varying approximation in chapter II correctly predicted that bound states would have frequencies less than ω_p. Classically, these $\omega < \omega_p$ states are bound because they are reflected from areas with larger effective plasma frequencies. In this classical hydrogen-esque system, frequency differences between Bohr-like energy levels still agree with the quantum-mechanical frequencies of photons.

It should be noted that the $\breve{V}(r)$ potential we chose need not be Coulombic to follow the same quantization via ray-tracing approach, however, for the methods employed in this chapter, the refractive index should approach zero near the boundary of the refractive index potential. One particularly interesting system is the spherical finite well. This system is an integrable system in which we can look for splitting due to shape perturbations. We can then employ vector spherical harmonics vector basis functions to look for shape perturbations using

the methods used to perturbatively solve spin-orbit coupling problems in the Dome cavity[6]. These perturbative methods will be outlined in chapter VII. Using verified perturbation methods, we can then check extensions to techniques using the Bogomolny transfer operator described in chapter IX. We will describe the best electromagnetic analog to the 1-D finite square well, microwaves in a superconducting cavity, in chapter IX.

Non-Circular Ray Orbits in a KG Medium

Another interesting feature of an optical KG medium is that the ray dynamics of waves in such a medium approximates the trajectories that particles would follow in attractive or repulsive potentials. That the trajectories are equivalent has only been demonstrated analytically for circular orbits. Numerical models show elliptical ray paths follow the path a charged point particle in free space would follow in an attractive Coulomb potential, as show in figure 3.3.. Since the phase velocity is slower close to the origin, the rate at which the phase advances does not obey Kepler's equal area/equal time relationship. It is known that an ensemble of electron Kepler orbits can describe the time evolution of Rydberg atoms [32]. However, much of the work done in this area starts by using the quantum propagator as a starting point, or by postulating Schrödinger's equation as a starting point rather than the wave equation.

The procedure for solving for the orbits or wave mechanics problems differs from

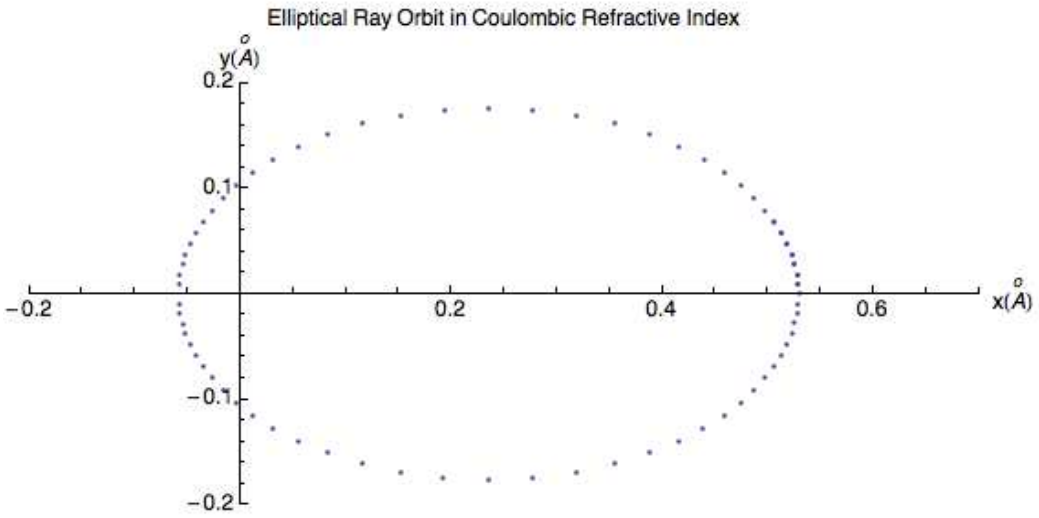

Figure 3.3. A typical elliptical orbit. In this image, the ray is launched tangentially. 100 steps separate colored pixels, and units are in Angstroms. The frequency of the ray is $\omega = \omega_p - |1.8E_{hyd}/\hbar|$. The ray is strongly confined because its energy is further below the plasma frequency than a ray with the frequency associated with quantized, circular, Bohr-like orbits.

that of finding classical orbits of point particles. Variations in phase velocity give the minimum of the action and path of the orbit, but these variations only provide indirect commentary about energy transport. To find the rate of energy transport, we must first calculate the group velocity. The group velocity of wave packets in a KG medium provides a nice connection to both the classical mechanics of point particles.

Group Velocity of KG Wave Packets

The group velocity is $v_g = \dfrac{\partial\omega}{\partial k}$. In a plasma medium, this takes the form of $v_g = n(r,\omega)c$, [30], this is discussed in more detail in chapter XIV. We will

use this to show the connection between group velocity of wave packets in a Klein-Gordon medium, and the momentum of massive particles traveling at nonrelativistic velocities. We can use the KG equation to calculate the group velocity of wave packets in a KG medium to look for a connection to classical mechanics. If k is a wave vector along a ray path, we find:

$$\omega = \sqrt{c^2k^2 + \omega_p^2 + \frac{2m}{\hbar^2}V(r)} \tag{III.23}$$

We can now find the group velocity of a wave, v_g, for some radial value:

$$v_g = \frac{d\omega}{dk} = \frac{\frac{\hbar k}{m}}{\sqrt{1 + \frac{(\frac{\hbar k}{m})^2}{c^2} + \frac{2V(r)}{mc^2}}} \tag{III.24}$$

Or, alternatively, we can express the group velocity as:

$$v_g = \frac{kc^2}{\omega} \tag{III.25}$$

If we make the approximation that $\omega = \omega_p$, we find:

$$v_g = \frac{\hbar k}{m} \tag{III.26}$$

This is the expression used in quantum mechanics to find the nonrelativistic velocity of the electron if $p = \hbar k$. It is important to note that here, we derived the nonrelativistic group velocity of the electron as a final step. In Bohr's approach, $mv_g r = h\hbar$ is the starting step, and we never used this relationship. In this chapter,

we solved the Bohr atom only by considering phase velocity, and by quantizing wavelengths. We never employed quantization of angular momentum to derive the results of this chapter. These results show a different way to derive the Bohr atom using only classical assumptions. However, we have shown that the picture of a wave packet slowly traveling in an epsilon-near-zero cavity is still consistent with the Bohr atom.

This largely closes our discussion of the scalar Klein-Gordon equation. In the last two chapters we have described how the KG equation has Schrödinger-like envelope solutions in the slowly varying limit. If we keep the KG equation in wave equation form, and pay attention to frequencies noticeably above the plasma frequency, we begin to see relativistic analogs to wave packet behavior. However, before concluding it should briefly be noted that the KG equation does have static solutions. We note this only for completeness. These static solutions would only matter in Maxwell's equations if a charge density is present in a medium, because they require an additional localized source term. In this limit, In the limit that the time derivative of the KG equation is close to zero, the field becomes localized about the charge density, and the scalar solution of the KG equation becomes: $\phi(r) = \frac{q}{r}\exp[-\frac{\omega_p^2}{c^2}r]$. For relativistic-like plasma frequencies, the static field would fall off at the compton wavelength, a factor of (1/137) smaller than the Bohr radius.

CHAPTER IV

DERIVATION OF THE QUATERNION FORM OF MAXWELL'S EQUATIONS

The Importance of the Dirac Equation

In previous sections we have argued that when the refractive index is near-zero, we can obtain the Schrödinger equation. Furthermore, if the wave equation is similar to the Klein-Gordon equation, as it is in a plasma medium, we can use ray tracing to quantize orbitals, and recover some features of classical massive particle motion. The Dirac-like formulation of Maxwell's equations will also be used to obtain the classical analogue to relatvistic corrections to hydrogenic energy levels. However, this quest was initially motivated by the question of whether optical spin-orbit coupling is truly an analog of its quantum cousin. The next dominant energy level splittings in spherical quantum systems are related to higher order relativistic effects, electron spin-orbit coupling, and the Darwin term that arises from the Dirac equation. To search for a more-complete electromagnetic analog of a quantum system with massive particles, it is therefore useful to ask what kind of correspondence we can derive between Maxwell's equations and the Dirac equation.

The Dirac equation is one of the most important equations in all of physics, and the first to convincingly merge quantum mechanics and special relativity. In

principle, almost all practical physics problems can be solved by consistently solving the Dirac equation in tandem with Maxwell's equations. Physics problems that go beyond the Dirac equation involve the behavior of quarks, gluons, gauge bosons, gravitational problems, and problems involving the Lamb shift. In fact, it was tiny Lamb-shift deviations from exact solutions to the Dirac equation that led to the development of quantum electrodynamics and quantum field theory. For now, we'll simply note that the Lamb shift defines the limit of validity of the Dirac equation. Without such a shift, for example, excited spinors would never decay to the ground state. Instead, they interact with the vacuum, and their own electromagnetic field to allow such transitions. Even today, there are still puzzles regarding quantum electrodynamics, QED, related to the Dirac equation. For example, while the Lamb shift is fleetingly small in hydrogen, the Lamb shift gives a 2 percent difference between $2S_{\frac{1}{2}}$ energy levels and $2P_{\frac{1}{2}}$ levels in muonic hydrogen. In exact spinor solutions to the Dirac equation there is no splitting between these two energy levels. The shift in muonic hydrogen is very large because the Bohr radius is inversely proportional to the muon's mass, which is hundreds of times larger than the electron's. To calculate the Lamb shift, one either needs to use QED, typically solved with Feynman diagrams, or approximate the electron as a hopping particle confined to an area the size of the Compton wavelength, a length scale an order alpha smaller than the Bohr radius, and adjust the Coulomb force accordingly. A team at the Max Plank institute was the first to measure the

rather large Lamb shift in muonic hydrogen in June of 2010. This experiment found that the Lamb shift deviated by many standard deviations from the expected value [33]. The authors concluded that either previous measurements for the Rydberg constant, $R = \frac{\alpha^2 mc}{4\pi\hbar}$, or the radius of the proton, differed from measured values by five standard deviations, or that there were problems with QED calculations of the Lamb shift. Methods in this text concern the problem of making optical systems more like the Dirac equation, and shed no light on Lamb shift discrepancies. However, we wish to stress that QED is still an active area of research with unsolved problems.

As a preview, we will discover a few important things 1) There is an optical regime in which we can make a clear argument that an optical spin-orbit shift is an analog of quantum mechanical spin-orbit coupling. 2) The spin orbit shift experienced by transverse electromagnetic fields has a different angular momentum dependence than that experienced by photons 3) Not all cases attributed to optical spin-orbit coupling are true analogs of the quantum case. Often times, angular-momentum-dependent mode splitting is an example of mode-mixing, rather than what we will come to call spin-orbit coupling. For example, we found angular momentum selection rules governing Bragg-stack induced mode-splitting in the Fabry-Perot cavities [1]. However, in retrospect, this effect was angular dependent mode-mixing and not the kind of angular momentum dependent shift that we will call optical spin-orbit coupling here. The term optical-spin-orbit coupling is one

that is overused. We will present a definition of optical spin-orbit shifts, and argue that a particular case mirrors the quantum case. When the dust clears, we will identify classical optical perturbation terms that are vector analogs of the quantum spin-orbit operator. In doing so, we will identify a host of other relativistic corrections.

In this chapter, we will show that through the use of quaternions, Maxwell's equations can be represented as the 4 by 4 matrix equation that is the Dirac equation in the absence of the electromagnetic field. When we cast Maxwell's equations in the form of the Dirac equation, we find spinor-like vectors that we'll call spatial spinors. We will show that these entities do have light-like angular momentum towards the end of this chapter. One spatial spinor is associated with the electric field, and another is associated with the magnetic field. The components of the spatial spinor that represents the electric field contains information regarding all three components of the electric field vector. The up and down components of these complex spatial spinors contain polarization information about the three dimensional electric and magnetic fields. For a plane wave, we find that spin up and spin down spatial spinors correspond to right and left circularly polarized light. We also find that Maxwell's equations in free space, and most materials, are not exactly symmetric with the Dirac equation. Only the high-energy limit of Dirac's equation looks like Maxwell's equations in free space. However, in a metamaterial with properly tuned dispersion relationships for both the electric permittivity and

magnetic permeability, Maxwell's equations could be put in a form identical to Dirac's equation. This procedure can aid us in finding vector solutions to classical electromagnetism problems that are isospectral (in shifted frequency) to particle and anti-particle spinor solutions of the Dirac equation.

Dirac-like Formulations of Maxwell's Equations

It has long been known that Maxwell's equations bear many similarities to the Dirac equation. Iwo Bialynicki-Birula commented on this similarity by putting Maxwell's equations in the following form[34][35]:

$$s^{\pm}\hbar c\nabla \times \boldsymbol{\psi} = i\hbar\frac{\partial}{\partial t}\boldsymbol{\psi} \tag{IV.1}$$

Where, $\boldsymbol{\psi} = \mathbf{E} + i\mathbf{B}$, and $s^{\pm} = \pm 1$.

Above, if the scalar $s^{\pm}$ is positive, the field is right circularly polarized, and if it is negative, the field is left circularly polarized. Ultimately, 6 equations come from (IV.1). However, a more direct analogy could be useful. When describing perturbations of cavity modes produced by polarization states of electromagnetic fields, it is often useful to use Jones vectors and classical formulations of a mode's "spin" and angular momentum[6][1]. Furthermore, Mike Raymer, David Reeb, Steven Van Enk, and Cody Leary have drawn analogies between solutions of Maxwell's equation in a fiber and the Dirac equation in cylindrical coordinates[36][37]. Here, we will endeavor to find a classical, rather

than quantum, spin-orbit operator that acts on a vector field, and we want to find a formulation that works in arbitrary 3D cavities. We will however, concentrate on cavities that vary over the radial coordinate to simplify examples. The Riemann Silberstein Dirac equation-like formulation is somewhat unsatisfying in making optical problems formally analogous to quantum ones, because it is not the form of a 4×4 matrix acting on a 4-spinor.

It could potentially be useful if we could associate classical vector field configurations with the Pauli sigma matrices and spin up and spin down spinors. Through the use of quaternions, we can draw a more explicit similarity between Maxwell's equations and the Dirac equation. To do this, we can express any vector field in Maxwell's equations as a complex, 2 by 2 matrix by dotting it with the Pauli vector, a vector of Pauli sigma matrices, usually shown in the following basis:

$$\vec{\sigma} = (\sigma_{\mathbf{x}}, \sigma_{\mathbf{y}}, \sigma_{\mathbf{z}}) \tag{IV.2}$$

$$= \left(\begin{pmatrix} 0 & 1 \\ 1 & 0 \end{pmatrix}, \begin{pmatrix} 0 & -i \\ i & 0 \end{pmatrix}, \begin{pmatrix} 1 & 0 \\ 0 & -1 \end{pmatrix} \right) \tag{IV.3}$$

For example, we can represent the electric field as:

$$\vec{\sigma} \cdot \mathbf{E} = \begin{pmatrix} E_z & E_x - iE_y \\ E_x + iE_y & -E_z \end{pmatrix} \tag{IV.4}$$

The above 2×2 formulation of the a vector is called a quaternion. From the

quaternion elements we can find the original vector, and if one vector equals another, the equality still holds if each is dotted with the Pauli vector. We can start with the curl equations to trivially recast Maxwell's equations in quaternion form. In the absence of charge, the vector fields E and H are given by the following:

$$\nabla \times \mathbf{H} = \frac{1}{c}\frac{d}{dt}\epsilon\mathbf{E} \tag{IV.5}$$

$$\nabla \times \mathbf{E} = -\frac{1}{c}\frac{d}{dt}\mu\mathbf{H} \tag{IV.6}$$

Since the above coupled equations are linear, we'll simplify them slightly by assuming $\mathbf{E}$ and $\mathbf{H}$ have the same time dependence of $\exp[-i\omega t]$.

We can choose to dot each term of Maxwell's equations with the vector of Pauli matrices, giving:

$$\vec{\sigma} \cdot (\vec{\nabla} \times \mathbf{H}) = \frac{-i\omega\epsilon}{c}\vec{\sigma} \cdot \mathbf{E} \tag{IV.7}$$

$$\vec{\sigma} \cdot (\vec{\nabla} \times \mathbf{E}) = \frac{i\omega\mu}{c}\vec{\sigma} \cdot \mathbf{H} \tag{IV.8}$$

Since $\vec{\nabla}$ is a quantity that we can treat as a vector, we change the above equation by using the identity[38]:

$$\vec{\sigma} \cdot (\mathbf{A} \times \boldsymbol{B}) = -i(\vec{\sigma} \cdot \boldsymbol{A})(\vec{\sigma} \cdot \boldsymbol{B}) + i(\boldsymbol{A} \cdot \boldsymbol{B})\mathbf{I} \tag{IV.9}$$

Rewriting the above equations to eliminate explicit reference to the curl operator, we find:

$$-i(\vec{\sigma}\cdot\vec{\nabla})(\vec{\sigma}\cdot\boldsymbol{H})+i\mathbf{I}(\vec{\nabla}\cdot\boldsymbol{H})=\frac{-i\omega\epsilon}{c}\vec{\sigma}\cdot\mathbf{E} \tag{IV.10}$$

$$-i(\vec{\sigma}\cdot\vec{\nabla})(\vec{\sigma}\cdot\boldsymbol{E})+i\mathbf{I}(\vec{\nabla}\cdot\boldsymbol{E})=\frac{i\omega\mu}{c}\vec{\sigma}\cdot\mathbf{H} \tag{IV.11}$$

The above equations are still Maxwell's equations exactly, expressed in a set of 2 by 2 matrices. Above, there are often non-vanishing divergence conditions for $\mathbf{E}$ and $\mathbf{H}$, present in terms with the identity in (IV.10), and (IV.11). Nonetheless, (IV.10), and (IV.11) may still be useful for treating spin-orbit coupling problems with large divergences. The divergence terms currently prevent us from putting a quaternion formulation of Maxwell's equations exactly in the form of the Dirac equation. However, the above equations are very similar to the Dirac equation, if both $\nabla\cdot\mathbf{E}$ and $\nabla\cdot\mathbf{H}$ are zero or small. The condition $\nabla\cdot\mathbf{E}=\nabla\cdot\mathbf{H}=0$ is strictly true if both μ and ϵ are spatially uniform. In spatially varying resonators $\nabla\cdot\mathbf{E}=-\frac{(\nabla\epsilon)\cdot\mathbf{E}}{\epsilon}=4\pi\rho$ and $\nabla\cdot\mathbf{H}=-\frac{(\nabla\mu)\cdot\mathbf{H}}{\mu}$. We have already assumed no net enclosed charge in our spatially varying potentials. To keep the divergence of the electric field close to zero, we will pick divergence free solutions to the electric field. To keep the divergence of $\mathbf{H}$ close to zero, we will explore situations in which $\mu\cong 1$ and, $\nabla(\epsilon)=(\nabla\mu)<<1$ to make the approximation that $-\frac{(\nabla\mu)\cdot\mathbf{H}}{\mu}\cong 0$. If we explore materials and solutions in which both divergence terms are very small

then Maxwell's curl equations resemble the Dirac equation. We will then compare the reformulated version of Maxwell's equations to the Dirac equation to to obtain the μ and ϵ parameters that best match the Dirac equation. Finally, we will plug these values of μ and ϵ into Maxwell's vector curl equations and look for a similarity to the solutions of the Dirac equation. Assuming $\nabla \cdot \mathbf{E}$ and $\nabla \cdot \mathbf{H}$ are both near zero, we will remove them from (IV.10) and (IV.11) and multiply each curl equation by $\hbar$.

$$c(\vec{\sigma} \cdot -i\hbar\vec{\nabla})(\vec{\sigma} \cdot \boldsymbol{H}) = -i\hbar\omega\epsilon(\vec{\sigma} \cdot \mathbf{E}) \tag{IV.12}$$

$$c(\vec{\sigma} \cdot -i\hbar\vec{\nabla})(\vec{\sigma} \cdot \boldsymbol{E}) = i\hbar\omega\mu(\vec{\sigma} \cdot \mathbf{H}) \tag{IV.13}$$

$$c(\vec{\sigma} \cdot -i\hbar\vec{\nabla})(\vec{\sigma} \cdot \boldsymbol{H}) = -i\hbar\omega\epsilon(\vec{\sigma} \cdot \mathbf{E}) \tag{IV.14}$$

$$c(\vec{\sigma} \cdot -i\hbar\vec{\nabla})(\vec{\sigma} \cdot \boldsymbol{E}) = i\hbar\omega\mu(\vec{\sigma} \cdot \mathbf{H}) \tag{IV.15}$$

We can rearrange the above equations as follows:

$$\hbar\omega\epsilon\ (\vec{\sigma} \cdot \mathbf{E}) - c(\vec{\sigma} \cdot \boldsymbol{p})i(\vec{\sigma} \cdot \boldsymbol{H}) = 0 \tag{IV.16}$$

$$\hbar\omega\mu i(\vec{\sigma} \cdot \mathbf{H}) - c(\vec{\sigma} \cdot \mathbf{p})(\vec{\sigma} \cdot \mathbf{E}) = 0 \tag{IV.17}$$

or:

$$\begin{pmatrix} \hbar\omega\epsilon & -c(\vec{\sigma}\cdot\mathbf{p}) \\ -c(\vec{\sigma}\cdot\mathbf{p}) & \hbar\omega\mu \end{pmatrix} \begin{pmatrix} (\vec{\sigma}\cdot\mathbf{E}) \\ i(\vec{\sigma}\cdot\mathbf{H}) \end{pmatrix} = 0 \tag{IV.18}$$

To obtain the above from Maxwell's curl equations, we have the additional contraint that $\nabla\cdot\mathbf{E} = -\dfrac{(\nabla\epsilon)\cdot\mathbf{E}}{\epsilon} = 0$ and $\nabla\cdot\mathbf{H} = -\dfrac{(\nabla\mu)\cdot\mathbf{H}}{\mu} \cong 0$. If these conditions aren't met we won't obtain solutions similar to Dirac equation solutions. In the above matrix equation, (IV.18), we have a matrix similar to the Dirac equation acting on a vector with 4 rows and 2 columns. There is more than one formulation that still gives us the Dirac equation. Here, we choose to group i with $\mathbf{H}$ to maintain rough symmetry with the Riemann-Silberstein vector. It is also possible to leave i out of the above equations, but when we compare this to the Dirac equation, we end up obtaining plasmon-like solutions that decay with time, but these won't be discussed here.

We're accustomed to the Dirac equation acting on a 4-component spinor. However, each column in the 4 by 2 matrix operated on by the Dirac-like matrix can be thought of as an independent spinor. In some mathematics books on Clifford algebras, spinor and quaternion formulations of the Dirac equation are used interchangeably[39]. This will be covered in chapter IX, where we also describe the relationships between quaternions and polarization states of Jones vectors. We postpone this long, but significant, discussion to maintain the reader's interest. Whenever possible, we will present simple arguments with significant results first, and then move on to more complex examples.

Now it is useful to recall the form of the Dirac equation describing the electron. We'll let ψ and χ represent the two component spinors of the Dirac equation. Below, $\mathbf{\Pi}$ is kinetic momentum operator for the Dirac equation with a value of: $\mathbf{\Pi} = \mathbf{p} - \frac{q\mathbf{A}}{c}$

$$\begin{pmatrix} (E-V) - mc^2 & -c(\vec{\sigma} \cdot \mathbf{\Pi}) \\ -c(\vec{\sigma} \cdot \mathbf{\Pi}) & (E-V) + mc^2 \end{pmatrix} \begin{pmatrix} \psi \\ \chi \end{pmatrix} = 0 \tag{IV.19}$$

Above the vector that the 4×4 matrix acts on is a 4-spinor:

$$\begin{pmatrix} \psi \\ \chi \end{pmatrix} = \begin{pmatrix} \psi_1 \\ \psi_2 \\ \chi_1 \\ \chi_2 \end{pmatrix} \tag{IV.20}$$

We can compare this to our expression for curl components of Maxwell's equations formulated using quaternions projected onto vectors. In chapter X, we will show that Maxwell's equations can also be formulated in terms of 4-spinors, and that the Dirac equation can be formulated similarly to the quaternion form of Maxwell's equations displayed in (IV.18). For now, we'll content ourselves to set the diagonal elements of the equations equal. In the Dirac equation we can make the substitution $E = \hbar\omega$, which is the total mass energy of the massive particle, including rest mass. More specifically, E is $-i\hbar\frac{d}{dt}$, provided the spinor has a time dependence of $Exp[-i\omega t]$, this matters when we address causality issues in chapter

XIII. Setting diagonal elements equal in equation (IV.19) and equation (IV.18) yields:

$$\hbar\omega\epsilon = \hbar\omega - mc^2 - V(\mathbf{x}) \tag{IV.21}$$

$$\hbar\omega\mu = \hbar\omega + mc^2 - V(\mathbf{x}) \tag{IV.22}$$

Giving:

$$\epsilon(\mathbf{x},\omega) = 1 - \frac{\omega_p}{\omega} - \frac{V(\mathbf{x})}{\hbar\omega} \tag{IV.23}$$

$$\mu(\mathbf{x},\omega) = 1 + \frac{\omega_p}{\omega} - \frac{V(\mathbf{x})}{\hbar\omega} \tag{IV.24}$$

Where $\omega_p = mc^2/\hbar$, as in chapters II and III. These are unusual material parameters for ϵ and μ. In chapter XI, we will describe how they should be given a small complex component to maintain causality spanning all frequencies. In chapter XI, we will also show that the system most-similar to the above is an ultra high-purity material in which excited electrons have extremely long lifetimes. Drude models for ϵ and μ that approximate (IV.24) will be covered in chapter XII. At this point, we will use the Dirac equation to obtain a parameterization of ϵ and μ, that is valid only over a small frequency range, for a real refractive index. We should note that the potential term in the Dirac equation can have absolutely any spatial dependence. Solving the Dirac equation for non-symmetric potentials would be

more difficult, but the solutions would still be accurate. Likewise, our solutions to Maxwell's equations could have any geometry, cylindrical, spherical or otherwise.

At this point, one could choose to solve the Maxwell formulation of the Dirac equation, (IV.18), in the same manner as one solves the Dirac equation. Doing so, one obtains similar wave equations and perturbation terms. However, in chapter V, we'll take a step back, and solve Maxwell's equations using the Dirac-like ϵ and μ, (IV.24), and see how the solutions compare to relativistic quantum mechanics. In chapter V, we'll pick the Coulomb potential, and solve much of it with classical variables, and begin to make an argument as to why certain terms can be thought of as analogues to quantum mechanical processes. However, chapter V will show a simple, easy-to-derive way to solve the cavity problem. This method is only valid in a spherical coordinate system. Furthermore, in chapter V, we won't formally cast the problem as a vector Hamiltonian that is similar to a quantum Hamiltonian. Chapter VI will begin to discuss angular momentum conservation in cylindrical and spherical coordinates.

In chapter VII, we will back away from a discussion of a vector analog to the Dirac equation, and introduce the mathematical methods that give spin-orbit and Darwin interactions.

CHAPTER V

POLARIZATION STATES OF QUATERNIONS COMPARED TO JONES VECTORS

How to Transform Quaternion Columns into 4-spinor Equations

In this chapter, we aim to make a few different points. One is that the columns of the 4×2 matrix that we obtained from Curl equations are related to left and right circular polarization states of Jones vectors, if we assume the field is propagating along a particular direction. The second point is that we can reformulate the Dirac formulation of Maxwell's equations to a form in which the Dirac matrix acts on a 4-spinor. A startling implication of this is that we can take solutions to the Dirac equation acting on a 4-spinor, and express it as a vector field equation. However, the Dirac equation itself specifies no divergence conditions if we translate it to vector fields, so Divergence terms that arise must be independently satisfied.

We'll start this chapter with the same equation we began with in the last chapter. These are Maxwell's Curl equations in quaternion form when ϵ and μ can be anything at all, provided the independent divergence equations are satisfied:

$$\begin{pmatrix} \hbar\omega\epsilon & -c(\vec{\sigma}\cdot\boldsymbol{p}) \\ -c(\vec{\sigma}\cdot\boldsymbol{p}) & \hbar\omega\mu \end{pmatrix} \begin{pmatrix} (\vec{\sigma}\cdot\mathbf{E}) \\ i(\vec{\sigma}\cdot\mathbf{H}) \end{pmatrix} = 0 \tag{V.1}$$

In the above form, we find a matrix similar to the Dirac equation acting on

a vector with 4 rows and 2 columns. There is more than one formulation that still gives us the Dirac equation. Here, we choose to group i with $\mathbf{H}$ to maintain rough symmetry with the Riemann-Silberstein vector. We're accustomed to the Dirac equation acting on a 4-component spinor. However, each column in the 4 by 2 matrix operated on by the Dirac-like matrix can be thought of as an independent spinor. In some papers relating to the Dirac equation, this is accepted as mathematically valid [39]. To make this relationship obvious, we'll split the 4 by 2 matrix representing the electric and magnetic fields into 1 column, 2 row blocks as follows:

$$\begin{pmatrix} \psi_- & -\psi_+ \\ \\ \Phi_- & -\Phi_+ \end{pmatrix} = \begin{pmatrix} (\vec{\sigma}\cdot\mathbf{E}) \\ \\ i(\vec{\sigma}\cdot\mathbf{H}) \end{pmatrix} \tag{V.2}$$

$$\begin{pmatrix} \hbar\omega\epsilon & -c(\vec{\sigma}\cdot\boldsymbol{p}) \\ \\ -c(\vec{\sigma}\cdot\boldsymbol{p}) & \hbar\omega\mu \end{pmatrix} \begin{pmatrix} \psi_- & -\psi_+ \\ \\ \Phi_- & -\Phi_+ \end{pmatrix} = 0 \tag{V.3}$$

$$\begin{pmatrix} \hbar\omega\epsilon\psi_- - c(\vec{\sigma}\cdot\boldsymbol{p})\Phi_- & -\hbar\omega\epsilon\psi_+ + c(\vec{\sigma}\cdot\boldsymbol{p})\Phi_+ \\ \\ -c(\vec{\sigma}\cdot\boldsymbol{p})\psi_- + \hbar\omega\mu\Phi_- & c(\vec{\sigma}\cdot\boldsymbol{p})\psi_+ - \hbar\omega\mu\Phi_+ \end{pmatrix} = 0 \tag{V.4}$$

Since each block matrix element above equals zero, we can relate them:

$$\hbar\omega\epsilon\psi_- - c(\vec{\sigma}\cdot\boldsymbol{p})\Phi_- + \hbar\omega\epsilon\psi_+ - c(\vec{\sigma}\cdot\boldsymbol{p})\Phi_+ = 0 \tag{V.5}$$

$$-c(\vec{\sigma}\cdot\boldsymbol{p})\psi_- + \hbar\omega\mu\Phi_- - c(\vec{\sigma}\cdot\boldsymbol{p})\psi_+ + \hbar\omega\mu\Phi_+ = 0 \tag{V.6}$$

Or, with a more suggestive grouping:

$$\hbar\omega\epsilon(\psi_- + \psi_+) - c(\vec{\sigma}\cdot\boldsymbol{p})(\Phi_- + \Phi_+) = 0 \tag{V.7}$$

$$-c(\vec{\sigma}\cdot\boldsymbol{p})(\psi_- + \psi_+) + \hbar\omega\mu(\Phi_- + \Phi_+) = 0 \tag{V.8}$$

Each of the quantities in parentheses is a two-component vector! Now we can express Maxwell's equations in the form of the Dirac-like matrix, acting on a 4-spinor-like vector with 4 components:

$$\begin{pmatrix} \hbar\omega\epsilon & -c(\vec{\sigma}\cdot\boldsymbol{p}) \\ -c(\vec{\sigma}\cdot\boldsymbol{p}) & \hbar\omega\mu \end{pmatrix} \begin{pmatrix} \psi_+ + \psi_- \\ \Phi_+ + \Phi_- \end{pmatrix} = 0 \tag{V.9}$$

Where our spinor-like "spatial spinors" compents are the following:

$$\psi_+ = \begin{pmatrix} -E_x + iE_y \\ E_z \end{pmatrix} = -(\vec{\sigma}\cdot\mathbf{E}) \begin{pmatrix} 0 \\ 1 \end{pmatrix} \qquad \psi_- = \begin{pmatrix} E_z \\ E_x + iE_y \end{pmatrix} (\vec{\sigma}\cdot\mathbf{E}) \begin{pmatrix} 1 \\ 0 \end{pmatrix} \tag{V.10}$$

$$\Phi_+ = i \begin{pmatrix} -H_x + iH_y \\ H_z \end{pmatrix} = -i(\vec{\sigma}\cdot\mathbf{H}) \begin{pmatrix} 0 \\ 1 \end{pmatrix} \quad \Phi_- = i \begin{pmatrix} H_z \\ H_x + iH_y \end{pmatrix} = i(\vec{\sigma}\cdot\mathbf{H}) \begin{pmatrix} 1 \\ 0 \end{pmatrix} \tag{V.11}$$

Our total spinor can be thought of as a superposition of the two spatial spinors components.

$$(\psi_+ + \psi_-) = \begin{pmatrix} -E_x + iE_y + E_z \\ \\ E_z + E_x + iE_y \end{pmatrix} \tag{V.12}$$

$$(\Phi_+ + \Phi_-) = i \begin{pmatrix} -H_x + iH_y + H_z \\ \\ H_z + H_x + iH_y \end{pmatrix} \tag{V.13}$$

If we know the vector components, of the electric field, we can simply insert them into ψ_+ to find a non-normalized spin-up spinor. If we add both the ψ_+ and ψ_- vectors, we have the overall spin state of the electromagnetic field. In a subsequent section, we'll show how to relate the spatial spinors to Jones vectors. For now, we'll note that we can add different weightings of the spatial spinor components, in a manner similar to what we do if we want to superimpose quantum mechanical spin states.

$$\psi_e = \frac{1}{\sqrt{2}} (\alpha_+ \psi_+ - \alpha_- \psi_-) \tag{V.14}$$

$$\psi_e = \begin{pmatrix} \psi_u \\ \\ \psi_d \end{pmatrix} = \frac{1}{\sqrt{2}} \begin{pmatrix} \alpha_+(-E_x + iE_y) - \alpha_- E_z \\ \\ \alpha_+ Ez - \alpha_-(E_x + iE_y) \end{pmatrix} \tag{V.15}$$

We think of ψ_+ and ψ_- as orthogonal vectors that correspond to polarization states of the electromagnetic field. If we have unique values for E_x, E_y and E_z, and we perform a spin measurement on our total spatial spinor, we know exactly what value we'll obtain for the spin measurement. However, if we perform a spin

measurement on a spatial spinor, this doesn't correspond to a unique state of the vector field. Instead, an ensemble of distinct field states could have produced this measurement. Therefore, spin measurement on a spatial spinor gives an incomplete characterization of the vector field. All possible normalized field configurations are possible if we independently vary α_+ and α_- from -1 to 1 respectively.

In this sense, a quantum measurement doesn't specify a distinct electromagnetic field configuration. Rather, it eliminates the possibility of some configurations, and allows for others with varying probability. A $(S_x+S_y)/\sqrt{2}$ measurement that would collapse a quantum mechanical wave function, only partially determines the state of a higher dimensional electromagnetic field.

We have previously described optical spin-orbit interaction using semiclassical Jones vectors, σ^+, σ^-[1][6]. If a paraxial cavity is aligned with the z-axis, or if a mode is propagating in the z direction, the electric field can be represented as a sum of Laguerre-Gauss Polynomials $LG^l_P(\rho,\phi)$ multiplied by Jones vectors. Explicitly:

$$\begin{pmatrix} E_x \\ \\ E_y \end{pmatrix} = \sum_{p,l} \frac{1}{\sqrt{2}} \left(A^l_p \begin{pmatrix} 1 \\ \\ i \end{pmatrix} + B^l_p \begin{pmatrix} 1 \\ \\ -i \end{pmatrix} \right) LG^l_p(\rho,\phi) \tag{V.16}$$

Where:

$$\sigma^+ = \frac{1}{\sqrt{2}} \begin{pmatrix} 1 \\ i \\ 0 \end{pmatrix} = e^{i\phi} \tag{V.17}$$

$$\sigma^+ = \frac{1}{\sqrt{2}} \begin{pmatrix} 1 \\ -i \\ 0 \end{pmatrix} = e^{-i\phi} \tag{V.18}$$

For a Laguerre-Gauss Polynomial with given p (radial node number) and l (angular momentum), we know its total angular momentum, j, around the z-axis will be $j = l + s$. Where $s = \pm 1$ corresponding to $\sigma^{\pm}$. We can now compare states of our spatial spinor to the Jones vectors. A spin up spatial spinor is:

$$\psi_+ = \begin{pmatrix} E_x - iE_y \\ 0 \end{pmatrix} \qquad if \qquad E_y = iE_x \qquad (\sigma^+, \qquad s = 1) \tag{V.19}$$

$$\psi_- = \begin{pmatrix} 0 \\ E_x + iE_y \end{pmatrix} \qquad if \qquad E_y = -iE_x \qquad (\sigma^-, \qquad s = -1) \tag{V.20}$$

We have found a natural analogy between quaternions reformulated as 4-vectors, and traditional 3D descriptions of the polarization of vector fields. We have a spin up solution, if we set $E_y = iE_x$. We can quickly see that this field configuration is a σ^+ Jones vector with $s = +1$. Likewise, the spin down component of ψ_e is

possible only if $E_y = -iE_x$. This corresponds to the Jones vector with a negative spin quantum number.

It should be noted, that if we have solved the Dirac equation, in 4-spinor form, to find ψ_e, we can easily find E_x and E_y:

$$E_x = \frac{\psi_+ + \psi_-}{2} \tag{V.21}$$

$$E_y = \frac{\psi_- - \psi_+}{2i} \tag{V.22}$$

We can do the same for B_x and B_y by using Φ_h. To find the spin of a particle about an axis, we can take the expectation of its spin. We can do the same for, spatial-spinors, for example, to measure the spin expectation for a spin down spatial-spinor:

$$S_z = \frac{\langle \hbar\sigma_z \rangle}{\langle \psi_-^* \psi_- \rangle} = \frac{(0, E_x^* - iE_y^*) \cdot (0, -(E_x + iE_y))}{(0, E_x^* - iE_y^*) \cdot (0, (E_x + iE_y))} = -\hbar \tag{V.23}$$

Expectation values for S_x and S_y are, of course, exactly what we would expect them to be in using quantum mechanics for spin 1 particles. In other words, a spin up spatial-spinor won't have an expectation of spin along the x and y axis. From a semiclassical perspective, we know that the electric and magnetic field vectors aren't rotating around those axes, or have no net rotation along those axes.

CHAPTER VI

PERTURBATIVE TREATMENT OF SPIN-ORBIT COUPLING FOR THE OPTICAL HYDROGEN ATOM

The Vector Wave Equation with Spin-Orbit Coupling

Below is the most general vector wave equation that solves Maxwell's equations. A complementary equation exists for the magnetic quadrature if we make the substitutions $\mathbf{E} \rightarrow \mathbf{H}$ and $\epsilon \rightarrow \mu$.

$$\left(-\nabla^2 - \frac{\omega^2}{c^2}\epsilon\mu\right)\mathbf{E} - \frac{\frac{\partial \mu}{\partial r}}{\mu}\hat{\mathbf{r}} \times (\nabla \times \mathbf{E}) = 0 \tag{VI.1}$$

As written, we use the vector Laplacian, rather than the double curl for two reasons. First, we will later show that the most convenient way to produce quantum-like, spatially-varying optical potentials is ENZ materials is to change the number density in a plasma medium that obeys the Drude model. If we do so, we will have a local charge density that accompanies the electromagnetic potential, and a component of the electric field will have a divergence. Furthermore, as written, we can explore non-zero divergence conditions in Dirac-like equations. Some of these solutions will be interesting, because they have spectra closer to electrons than divergence-free fields.

If ϵ and μ vary according to a spherical coordinate system, vector spherical harmonics are used to construct solutions, and we can look at the behavior of the LS/Darwin term acting on these spherical harmonics and determine whether an effective photon g is better expressed with $g \cong 1$ or $g \cong 2$. Here, we'll pick the susceptibility and permittivity potentials that give us the spectrum of the hydrogen atom, we do this using the parameters that give us the Dirac equation, derived in chapter IV. Here, however, we'll pick a strictly radially varying potential:

$$\epsilon(r,\omega) = 1 - \frac{\omega_p}{\omega} - \frac{V(r)}{\hbar\omega} \tag{VI.2}$$

$$\mu(r,\omega) = 1 + \frac{\omega_p}{\omega} - \frac{V(r)}{\hbar\omega} \tag{VI.3}$$

With the same $V(r)$ appearing in ϵ and μ, the vector wave equation (VI.1) for both $\mathbf{E}$ and $\mathbf{H}$ is invariant under the transformation $\epsilon \rightarrow \kappa\epsilon$ if $\mu \rightarrow \frac{1}{\kappa}\mu$. Where κ is a dimensionless constant. For every solution to (VI.1), there exist a wide range of choices for ϵ and μ that also have the same solutions. Chapter XII discusses using Drude models for ϵ and μ to closely approximate (VI.3). If we pick a Coulomb potential, $V(r) = -\frac{e^2}{r}$, our material parameters look odd because they are expressed in terms of quantum rather than classical parameters. This is no problem, because whenever we see charge squared, we can remember that it's proportional to a Bohr-like length scale. And, whenever we see a mass, we can remember that the classical analog is frequency. As such, we can express a Bohr

radius as $a = \frac{\hbar^2}{me^2} = \frac{\hbar c^2}{\omega_p e^2}$, or $e^2 = \frac{\hbar c^2}{\omega_p a}$. We can now substitute our paramteters into VI.3, and solve a now classical wave equation. We have: $\epsilon = 1 - \frac{\omega_p}{\omega} + \frac{c^2}{\omega_p \omega}\frac{1}{ar}$ and $\mu = 1 + \frac{\omega_p}{\omega} + \frac{c^2}{\omega_p \omega}\frac{1}{ar}$.

We can next multiply VI.1 through by $\frac{\hbar^2}{2m}$, and assume $\omega = \omega_p + \omega_s$ where $\frac{\omega_s}{\omega_p} << 1$. Generally, we will find the refractive index term in the wave equation is written, as the following, if expanded in powers of $\frac{\omega_s}{\omega_p}$:

$$\frac{\hbar^2}{2m}\frac{\omega^2}{c^2}n^2(r,\omega) \;=\; \hbar\omega_s - V(r) + \frac{1}{2mc^2}\left[\hbar\omega_s - V(r)\right]^2 \qquad \text{(VI.4)}$$

Since we are dealing with a spherically symmetric system, we will use vector spherical harmonics to express our vector fields. There are three vector spherical harmonics, and we express them as $\mathbf{Y}^j_{lm}$. Our vector fields can be expressed as $\mathbf{E}(r,\theta,\phi) = R_{nl}(r)\mathbf{Y}^j_{lm}$. After truncating the expansion of $\frac{\omega^2}{c^2}\epsilon\mu$, we can express our wave equation in the form of a vector Hamiltonian, in which the vector fields independently satisfy the vector wave equation, and conserve J^2 and J_z. With the truncation of the refractive index expansion as the only approximation, the wave equation becomes:

$$\mathbf{H_0}R_{nl}(r)\mathbf{Y}^j_{l,m} + (\mathbf{H_1} + \mathbf{H_2})R_{nl}(r)\mathbf{Y}^j_{l,m} = \hbar\omega_s R_{nl}(r)\mathbf{Y}^j_{l,m} \qquad \text{(VI.5)}$$

Where the primary and perturbative Hamiltonian elements are:

$$\mathbf{H_0} = \frac{\hbar^2}{2m}\left(\nabla^2 + \frac{2}{ar}\right) \tag{VI.6}$$

$$\mathbf{H_1} = \frac{-1}{2mc^2}\left((\hbar\omega_s)^2 + \frac{2(\hbar\omega_s)e^2}{r} + \frac{e^4}{r^2}\right) R_{nl}(r)\mathbf{Y}^j_{l,m} \tag{VI.7}$$

$$\mathbf{H_2} = -\frac{\hbar^2}{2m}\frac{\frac{\partial\mu(r,\omega)}{\partial r}}{\mu(r,\omega)}\hat{\mathbf{r}} \times (\nabla \times R_{nl}(r)\mathbf{Y}^j_{l,m}) \tag{VI.8}$$

Above, $\mathbf{H}_2$ isn't truly in a Hamiltonian from, in which a matrix acts on a vector, yielding an eigenvalue. However, we can take the curl of a radial function multiplied by a vector spherical harmonic, and then take the cross product of the result with the radial unit vector to simplify $\mathbf{H}_2$. When we do so, we find:

$$\mathbf{H_2} = -\frac{\hbar^2}{2m}\frac{\frac{\partial\mu(r,\omega)}{\partial r}}{\mu(r,\omega)}\left(\frac{\mathbf{L}\cdot\mathbf{S}}{r} - \frac{\partial}{\partial r}\right)R_{nl}(r)\mathbf{Y}^j_{l,m} \tag{VI.9}$$

The quantity $\mathbf{L}\cdot\mathbf{S}$ will be defined in the following chapter. For now, we'll simply note that it depends only on the angular momentum index of the vector spherical harmonic. Taking this approach, still isn't a true Hamiltonian formalism, but it's a fast way to get the right answer. Perturbation terms can be handled by acting on the field with $\mathbf{H}_i$, multiplying the result by the complex conjugate of the field, and integrating over all space.

Where

$$\nabla^2 R_{nl}(r)\mathbf{Y}^j_{l,m} = R_{nl}(r)\begin{cases} L_{l+1}(r), & \text{if } l = j+1 \\ L_1(r), & \text{if } l = j \\ L_{l-1}(r), & \text{if } l = j-1 \end{cases} \tag{VI.10}$$

Or $\nabla^2 R(r) = L_j(R(r))\mathbf{Y}^j_{l,m}$ where the radial operator is the same operator found in the radial Schrödinger equation: $L_l = \frac{\partial^2}{\partial r^2} + \frac{2}{r}\frac{\partial}{\partial r} - \frac{l(l+1)}{r^2}$

We can show:

$$\frac{\frac{\partial \mu}{\partial r}}{\mu} = \frac{-c^2}{\omega_p a r^2} \frac{1}{(\omega + \omega_p + \frac{c^2}{w_p a r})} \tag{VI.11}$$

$$= \frac{-c^2}{2\omega_p^2 a r^2 (1 + \frac{\omega_s}{2\omega_p} + \frac{c^2}{2w_p^2 a r})} \tag{VI.12}$$

$$\cong \frac{-c^2}{2\omega_p^2 a r^2}(1 - \frac{\omega_s}{2\omega_p} - \frac{c^2}{2w_p^2 a r}) \tag{VI.13}$$

$$\cong \frac{-c^2\hbar^2 m e^2}{2m^2 c^4 \hbar^2 a r^2}(1 - \frac{\omega_s}{2\omega_p} - \frac{c^2}{2w_p^2 a r}) \tag{VI.14}$$

$$\tag{VI.15}$$

Substituting $\hbar\omega_p = mc^2$ and $a = \hbar^2/(me^2)$, we find:

$$\frac{-\hbar^2}{2m}\frac{\frac{\partial \mu}{\partial r}}{\mu} \cong \frac{\hbar^2}{2m}\frac{c^2\hbar^2 m e^2}{2m^2 c^4 \hbar^2 r^2}\left(1 - \frac{\hbar\omega_s}{2mc^2} - \frac{me^2}{2m^2c^2 r})\right) \tag{VI.16}$$

$$= \frac{\hbar^2 e^2}{4m^2 c^2 r^2}\left(1 - \frac{1}{2mc^2}\left(\hbar\omega_s - \frac{e^2}{r}\right)\right) \tag{VI.17}$$

$$\tag{VI.18}$$

So our perturbative term is:

$$H_{\mathbf{LS}} \cong \frac{\hbar^2 e^2}{4m^2 c^2 r^3}(\mathbf{L}\cdot\mathbf{S}) \tag{VI.19}$$

In the nonrelativistic hydrogen atom, the electron sees an effective magnetic field from the proton, orbiting in its frame of reference:

$$\mathbf{B} = \frac{-\mathbf{v} \times \mathbf{E}}{c} = \frac{1}{mc}\frac{1}{r}\frac{\partial V}{\partial r}\mathbf{L} \tag{VI.20}$$

The electron magnetic moment is:

$$\mu = \frac{-g_s \mu_B \mathbf{S}}{\hbar} = \frac{-g_s e}{2mc}\mathbf{S} \tag{VI.21}$$

Furthermore, we have to tack on a value of 1/2 to account for Thomas precession. Using parentheses to group factors of common origin, and denoting the quantum perturbation term $H^Q_{\mathbf{LS}}$, we find:

$$H^Q_{\mathbf{LS}} = (\frac{1}{2})\left(\frac{-ge}{2mc}\right)\left(\frac{1}{mc}\frac{1}{r}\frac{\partial V}{\partial r}\right)(\mathbf{L}\cdot\mathbf{S}^Q) \tag{VI.22}$$

If we compare the above and below equations, it appears that the photon g should be proportional to 1, unless we include a 1/2 in the spin part of the spin-orbit operator. It should be noted that expanding μ to higher orders in the Schrödinger frequency over the plasma frequency produces similar corrections to g as those found when one starts from the Dirac equation for the electron, and expands to higher orders in the Schrödinger energy over the electron rest mass.

$$H^C_{\mathbf{LS}} \cong -\frac{1}{2}\frac{e}{2mc}\left(\frac{e}{mc}\frac{1}{r}\frac{\partial V_{class}}{\partial r}\right)(\hbar^2\mathbf{L}\cdot\mathbf{S}) \tag{VI.23}$$

Review of Quantum Spin-Orbit Coupling Wavefunctions

In QM, the spin-orbit term acts on a sum of two scalar functions, one multiplied

by spin up spinor, and the other by a spin down spinor, each with different m. These two functions are : $\psi_{l+1/2,m+1/2} = R_{nl}(r)(C1(l,m)Y_{lm}\chi_+ + C2(l,m)Y_{l,m+1}\chi_-)$ and $\psi_{l-1/2,m+1/2} = R_{nl}(r)(C2(l,m)Y_{lm}\chi_+ - C1(l,m)Y_{l,m+1}\chi_-)$, where C1, and C2 normalize the wave functions. We'll find that each of these composite wave functions act like two single non-transverse vector spherical harmonics that independently satisfy the unperturbed radially varying vector wave equation. The quantum $\mathbf{L}\cdot\mathbf{S}$ acts on these as follows:

$$\mathbf{L}\cdot\mathbf{S}(\psi_{l+1/2,m+1/2},\psi_{l-1/2,m+1/2}) = \frac{\hbar^2}{2}(l\psi_{l+1/2,m+1/2},-(l+1)\psi_{l-1/2,m+1/2}) \quad \text{(VI.24)}$$

$$\langle\psi_{l\pm1/2,m+1/2}|H^Q_{\mathbf{L}\cdot\mathbf{S}}|\psi_{l\pm1/2,m+1/2}\rangle \quad \text{(VI.25)}$$

$$= \frac{g_s\hbar^2e^2}{8m^2c^2}\int_0^\infty \frac{R_{nl}(r)}{r^3}r^2dr \begin{cases} l, & \text{if } j = l+1/2 \\ -(l+1), & \text{if } j = l-1/2 \end{cases} \quad \text{(VI.26)}$$

Below is the classical result, we make use of orthogonality of vector spherical harmonics when integrated over all space:

$$\langle R_{nl}(r)\mathbf{Y}^j_{lm}|H_{\mathbf{LS}}|R_{nl}(r)\mathbf{Y}^j_{lm}\rangle \tag{VI.27}$$

$$\cong \frac{\hbar^2 e^2}{4m^2c^2}\int_0^\infty \frac{R_{nl}(r)}{r^3}r^2dr \begin{cases} l, & \text{if } j = l+1 \\ -1, & \text{if } j = l \\ -(l+1), & \text{if } j = l-1 \end{cases} \tag{VI.28}$$

We will justify the angular momentum eigenvalues produced by the vector spherical harmonics in the next chapter, which is intended to be medium-independent discussion of spin-orbit coupling. The angular momentum eigenvalues So, we find that the two vector spherical harmonics that aren't divergence free act like the quantum wave functions that diagonalize the spin-orbit wave function in a radial potential. These two vector wave solutions also satisfy the vector wave equation, in which the double curl is replaced by the vector Laplacian with a nonvanishing $\nabla(\nabla\cdot)\mathbf{E}$). So, in principle, vector fields can give similar spectra to quantum systems, at least in spherical coordinates. However, not all of those vector solutions are permitted with divergence-free solutions to Maxwell's equations. If however, we vary the number density in order to create quantum-like potentials for electromagnetic waves, solutions with non-zero divergence must be considered.

At this point, it is important to remember that there are only two free constants in our classical analog to the Coulomb potential: the Bohr-like length scale, and the plasma frequency. In order to make our classical system isospectral to the quantum system, we needed to define particular values for those two constants.

Any quantum potential will have a factor charge squared, e^2. The factor of e^2 will always be divided by $\hbar$ in the equations for ϵ and μ (VI.3). We must therefore replace $e^2/\hbar$ with classical variables to obtain a classical version of any quantum potential:

$$\frac{e^2}{\hbar} = \frac{1}{\hbar}\frac{\hbar c^2}{\omega_p a_0} = \frac{c^2}{\omega_p a_0} \tag{VI.29}$$

Above, a_0 can be any Bohr-like radius, and ω_p can be any metamaterial plasma frequency. This relationship, combined with $\omega_p = \frac{mc^2}{\hbar}$ alows us to translate from quantum energies and frequencies to classical frequencies. In figure 6.1., optical wave equation shifts are evaluated and compared to quantum shifts. Based on the energy of plasmons in a plasma medium, and by Liouville Hamiltonian arguments in chapter XIV, we expect the total photon energy per photon to be $\hbar\omega = \hbar\omega_p + \hbar\omega_s$. In a real material, a the length scale associated with the Bohr radius will be much less than the real Bohr radius. And the plasma frequency of the metamaterial will be much less than $\omega_p = mc^2/\hbar$. Formally, the classical energies are obtained by expressing the fundamental and perturbative optical Hamiltonians, (VI.6)(VI.7)(VI.8), in terms of $\alpha = \frac{e^2}{\hbar c} \cong \frac{1}{137}$, and $\hbar\omega_p = mc^2$.

Perturbative Hamiltonians are evaluated with the integral:

$$\int_0^\infty R_{nl}(r)(\mathbf{Y}^j_{l,m})^*\mathbf{H}_i R_{nl}(r)(\mathbf{Y}^j_{l,m})r^2 sin(\theta)drd\Omega \tag{VI.30}$$

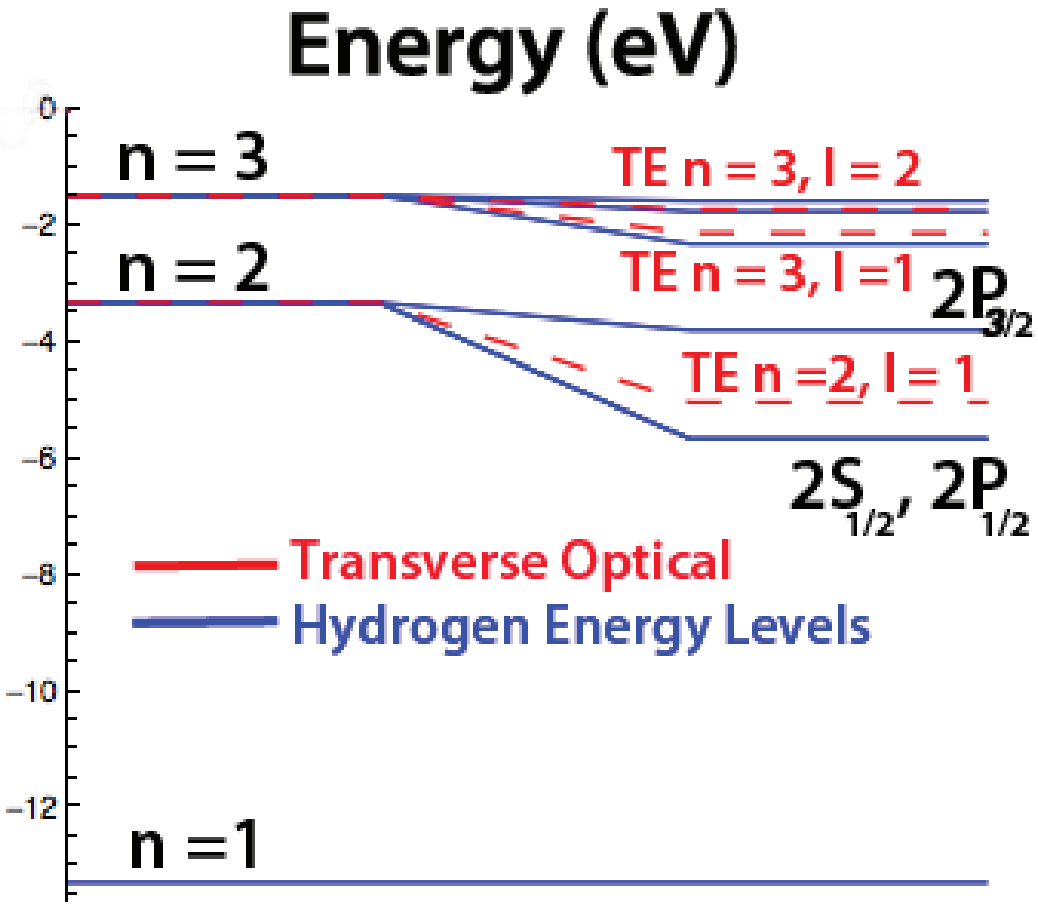

Figure 6.1. Optical perturbations (red and dashed) are evaluated and compared to quantum mechanical energy levels of hydrogen (blue and solid). The quantum energy splittings include relativistic shifts, SO coupling, and the QM Darwin term, discussed in chapter VII. The QED lamb shift is not evaluated in this diagram. Optical shifts include relativistic-like shifts, and optical SO shifts for transverse modes, the optical Darwin shift is zero for transverse modes in a hydrogen-like cavity. All optical and quantum fine structure shifts are scaled by the same large constant for visibility. Optical energies are made isospectral to quantum energies with two substitutions, $\omega_p = \dfrac{mc^2}{\hbar}$ and $\dfrac{e^2}{\hbar} = \dfrac{c^2}{\omega_p a_0}$. The scale for optical energy levels is $\hbar\omega_s$, where ω_s is the frequency difference from ω_p. Only TE modes are pictured, since only TE modes have exact solutions. Differences between the diagrams arises because only non-transverse vector spherical harmonics have the same $\mathbf{L}\cdot\mathbf{S}$ shifts as the electron. And because transverse vector spherical harmonics do not allow for s-orbital solutions. The fundamental modes for quantum and classical cases are the same: $E_{hyd} = -\dfrac{1}{2}\dfrac{mc^2\alpha^2}{n^2}$ for the quantum case, and $\hbar\omega_s = -\dfrac{1}{2}\dfrac{\hbar\omega_p\alpha^2}{n^2}$ for the classical case.

Above $d\Omega$ is the solid angle element. Fundamental energies are $\hbar\omega_s = -\frac{1}{2}\frac{\hbar\omega_p\alpha^2}{n^2}$, for $n > 1$, or to find frequency, divide each side by $\hbar$. We can make use of expectations of hydrogenic radial wave functions, and the orthogonality of vector spherical Harmonics to evaluate the above integral. Relativistic optical frequency shifts of $\mathbf{H}_1$ (VI.7) are:

$$\Delta_{rel}\omega_s = -\frac{1}{2}\omega_p\alpha^4\left(\frac{1}{n^3 l(l+1/2)} - \frac{3}{4n^4}\right) \tag{VI.31}$$

Optical SO coupling shifts are:

$$\Delta_{SO}\omega_s = \frac{1}{4}\omega_p\alpha^4\left(\frac{-1}{n^3 l(l+1/2)(l+1)}\right) \tag{VI.32}$$

Later we will find that optical Darwin shifts are near zero for this charge-free system, since there is negligible envelope overlab with the origin. The perturbed optical energy levels of 6.1. are obtained with the sum $\hbar\omega_s + \hbar\Delta_{rel}\omega_s + \Delta_{SO}\omega_s$, and then substituting mc^2 in place of $\hbar\omega_p$. Also, since $\alpha = \frac{e^2}{\hbar c}$, we can parameterize α in terms of classical variables using (VI.29), or $\alpha = \frac{c}{\omega_p a_0}$. In chapter XIII, we will further find that one of the terms in the relativistic perturbation is modified slightly if we insist that both ϵ and μ follow the Drude model. However, the example in chapter XIII is one possible Drude model parameterization of ϵ and μ, out of many, that still give the Schrödinger equation. The Drude model is necessary for vector fields that have loss, and are fundamentally real, discussed in chapter XI. As a curiosity, we note that vector fields satisfying a vector wave equation, with a the

vector Laplacian given by (VI.10), and ϵ and μ given by (VI.3) can be made nearly isopectral to the quantum energy levels displayed in figure 6.1.. These modes have hydrogen-like energy levels, allow for s-orbitals and Darwin shifts. However, these vector fields do not obey the divergence conditions of Maxwell's equations.

Currently, there is no known analytic TM solution in this system. A possible problem with pursing TM modes in the vector wave equation (VI.1), where $\mathbf{E} \to \mathbf{H}$ and $\epsilon \to \mu$, is that $\frac{1}{\epsilon}\partial_r \epsilon$ is *not* small, since we chose ϵ to be the parameter near zero. One possible solution is to construct a second TE mode using the two remaining vector spherical harmonics with non-zero divergence. If further numerical work indicates this is a good solution, then the second mode would also have a SO shift approximately equal to 1. However, this approach also yields no analytic solutions. To find numerical solutions, one would expand the vector using vector spherical Harmonics and radial functions and find coefficients such that (VI.1) is satisfied. Until an optimum numerical solution is found, the SO shift of the orthogonal mode remains unknown.

One final possible concern for real materials is that ϵ and μ are singular at the origin for the Coulomb potential. However, this system can still be made isospectral to the quantum case, with finite ϵ and μ, by adding a Yukawa potential correction to the Coulomb potential. The profile of a Yukawa-corrected refractive index (VI.33) is displayed in figure 6.2.. If the fundamental $R_{21}(r)\mathbf{Y}^j_{l,m}$ mode has little overlap with the Yukawa correction, hydrogenic energy levels are changed minimally. Spatially

dependent terms in ϵ and μ are smaller than those in (VI.33) by a factor of 2. The square of refractive index, also displayed in figure 6.2., has a slightly modified $V(r)$:

$$n^2(r, omega) \cong 1 - \left(\frac{\omega_p}{\omega}\right)^2 + 2\frac{c^2}{\omega_p \omega a_0 r} - \frac{2c^2 \exp(-\frac{r}{d})}{\omega_p \omega a_0}\left(\frac{1}{r} + \frac{1}{d}\right) \qquad \text{(VI.33)}$$

To summarize the results of this chapter, after translating between quantum and classical variables, we found that three leading-order relativistic terms had the same pre-factors as the leading-order quantum mechanics terms. In addition, we found that both the spin-orbit coupling term, and the non-Hermitian term, which

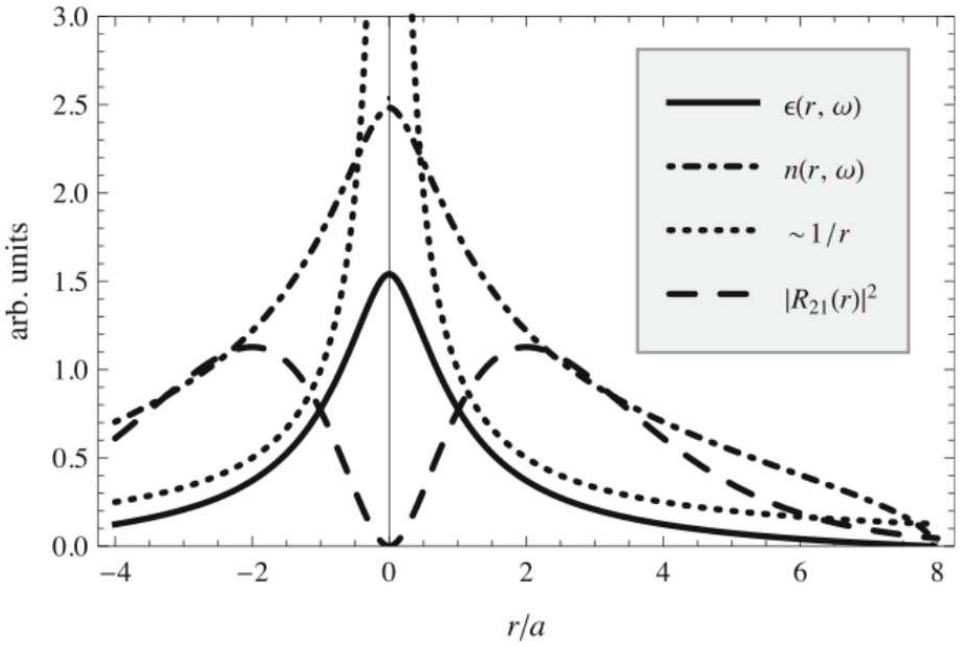

Figure 6.2. This figure displays the Coulombic ϵ and Coulombic refractive index modified by a Yukawa correction to avoid divergence at the origin (VI.33). Modes are confined because the refractive index goes to zero outside of the confining refractive index potential. Also displayed is the radial intensity profile of the fundamental mode.

we will show takes the form as the Darwin term had the same constants as the quantum mechanical case. In the previous chapter, we argued that we could use quaternions to define classical vector analogs of spinor systems. This chapter is one example that such a transformation indeed transfers dominant relativistic fine structure shifts from the spinor picture to the vector picture. This is not to say that we can do everything with light that we can with electrons, and we already have seen that transversality prohibits some quantum solutions. Additionally, transversality changes angular momentum values in the spin-orbit coupling term. However, this result can lend some confidence to the idea that we can begin to construct optical devices with behavior highly similar to quantum counterparts.

CHAPTER VII

DERIVATION OF THE ELECTROMAGNETIC VECTOR INTERACTION HAMILTONIAN

In this chapter, we will use the angular momentum operator, the spin angular momentum operator, and the total angular momentum operator to begin to define spin orbit operator in spherical coordinates. This chapter contains material co-authored by my advisor Jens Nöckel and myself, and has been submitted for publication. As an example, we will briefly note the role of these operators for a wave propagating along the z-axis. In the previous chapter, we found that gradients of μ and ϵ gave us a perturbation term that, using the Dirac-like ϵ and μ, gave us the same prefactors as a spin-orbit coupling term. In this section, we will argue that certain terms have the form of Spin-Orbit and Darwin terms by invoking angular momentum arguments, and Hermiticity arguments. All of the results of the previous chapter can be extended by the work in this chapter, but the results in this chapter can stand on their own. To refresh one's memory, the term that concerns us has appears in the vector wave equation (VI.1) and has the following generalized form:

$$(\nabla V(\mathbf{x})) \times (\nabla \times \mathbf{E}) \tag{VII.1}$$

We will call the above, the spin-orbit/Darwin term. This term perturbs the vector wave equation(VI.1). We assume that $V(\mathbf{x})$ describes the spatial variation of the permittivity and permeability, and make no additional assumptions. We can pick a given basis, pick any spatially varying permeability, find solutions to the vector wave equation, and evaluate the expectation of the above after operating on the field $\mathbf{E}$. However, this won't show us how the above term relates to spin orbit coupling in 3 dimensions. We would prefer to have a matrix operator that acts on a vector, and gives an eigenvalue. To this end, we will discuss 3D spin and angular momentum operators, and discuss the features necessary for a polarized vector field to be a well-behaved solution to a 3D problem. To begin to simplify the above, we first make note of the angular momentum operator used to derive vector spherical harmonics:

$$\mathbf{L} = -i\hbar(\mathbf{r} \times \nabla) \tag{VII.2}$$

The above is the angular part of our classical spin-orbit operator, and the $\mathbf{L}$, in $\mathbf{L} \cdot \mathbf{S}$. We add $\hbar$ to $\mathbf{L}$ only to draw a connection to the quantum operator, for the same reason, we will add it to the spin operator. The closest classical analog that we have to spin is the polarization state of the electromagnetic wave, most often described by Jones vectors. We want a set of 3×3 matrices for which the Jones vectors as eigenvectors. For this, we use the Levi-Civita tensor:

$$(S_n)_{j,k} = -i\hbar\epsilon_{n,j,k} \tag{VII.3}$$

Explicitly:

$$\hat{S}_x = -i\hbar \begin{pmatrix} 0 & 0 & 0 \\ 0 & 0 & -1 \\ 0 & 1 & 0 \end{pmatrix} \tag{VII.4}$$

$$\hat{S}_y = -i\hbar \begin{pmatrix} 0 & 0 & 1 \\ 0 & 0 & 0 \\ -1 & 0 & 0 \end{pmatrix} \tag{VII.5}$$

$$\hat{S}_z = -i\hbar \begin{pmatrix} 0 & -1 & 0 \\ 1 & 0 & 0 \\ 0 & 0 & 0 \end{pmatrix} \tag{VII.6}$$

Each of the above matrices defines the optical spin angular momentum along the axis corresponding to its subscript. They obey the commutation relationships $[S_i, S_j] = -iS_k$. The quantities $\hat{S}_z$ and $\hat{L}_z$ are most famous to those in the optics community, who are familiar with attacking problems with cylindrical symmetry. For example, we can consider the angular momentum around the z-axis:

$$\hat{L}_z = -i\frac{\partial}{\partial\phi} \tag{VII.7}$$

If a function in cylindrical coordinates has a ϕ coordinate dependence of $e^{il\phi}$, then it is an eigenfunction fo the $\hat{L}_z$ operator with eigenvalue l. A vector field can be represented by a Jones vector multiplied by a scalar function. We need our vector fields to be eigenfunctions of the total angular momentum operator, $\hat{J}_z$, where $\hat{J}_z = \hat{L}_z + \hat{S}_z$. As formulated, the S_z rotates a vector field around the z-axis, and $\hat{L}_z$ advances the phase of the polar coordinate, as we can see by casting it as a generator: $Exp(-i\hat{L}_z\alpha)\vec{E}(\rho,\phi) = \vec{E}(\rho,\phi+\alpha)$. The Jones vectors that are eigenvectors of $\hat{S}_z$ are the following:

$$\vec{\sigma}_{\pm} = \begin{pmatrix} 1 \\ \pm i \\ 0 \end{pmatrix} \tag{VII.8}$$

The above Jones vectors have eigenvalues of $s = \pm 1$. If the following is true:

$$\vec{E}(\rho,\phi) = \vec{\sigma}_{\pm} f(\rho) e^{il\phi} \tag{VII.9}$$

Then

$$J_z\vec{E}(\rho,\phi) = (l+s)\vec{E}(\rho,\phi) = (l\pm 1)\vec{E}(\rho,\phi) \tag{VII.10}$$

Polarization complicates quantization of modes when ray-tracing, because a ray must not only return to a wavefront with the same phase, but it must return to a wavefront with both the same phase and polarization. Polarization of a vector field

also changes what fields are good eigenfunctions. If we operate on our vector field with only the angular momentum operator, we will change its polarization as well. Likewise, if we operate on our vector field with only the spin rotation generator, this effects the angular momentum. We want solutions that are eigenfunctions of the total angular momentum operator along the z-axis. The complete rotation operation requires the application of both spin, and angular momentum generators: $Exp(-i\hat{S}_z\alpha)Exp(-i\hat{L}_z\alpha)$. If we find such solutions that are eigenfunctions of the total angular momentum operator, as in the above example, we can guarantee that our solutions are invariant under a complete rotation operation.

As we'll discuss in chapter VIII, degenerate modes are likely to mix if they have the same total angular momentum, while they can have completely different orbital angular momentum structure. Though the mixing problem invokes angular momentum-dependent rules for splitting, the mixing of modes itself is not an example of optical spin-orbit coupling, which we will argue is a spectral shift experienced by a single polarized mode interacting with a gradient.

The 3D Vector Spin-Orbit/Darwin Vector Hamiltonian

The goal in this next section is to parameterize the RHS of the wave equation, (VI.1), in the form of a spin-orbit operator, using classical assumptions. Furthermore, we want to show that if we set a frequency scale and length scale in (IV.24) that gives us Schrödinger's equation, we also spin-orbit and Darwin

terms with the correct prefactors. Spin-Orbit coupling described by Rytov rotation, [40][41] starts by fomulating the problem through the divergence of the electric field. Here we will assume divergence-free solutions, and show that even for divergenceless modes, the RHS of (IV.24) is nonzero. Furthermore, this technique generalizes approaches used to calculate spin-orbit shifts in spherical optical resonators[42]. The Spin-Orbit/Darwin term, (VII.1), can be expressed in component form:

$$[(\nabla V)\times(\nabla\times E)]_\alpha = \sum_{\beta\gamma}\varepsilon_{\alpha\beta\lambda}V_\beta\sum_{\mu\nu}\varepsilon_{\lambda\mu\nu}\partial_{mu}E_\nu \tag{VII.11}$$

Here, we use the following conventions:

$$V_\beta = \partial_\beta V \tag{VII.12}$$

$$V_{\alpha\beta} = \partial_\alpha V_\beta \tag{VII.13}$$

Contraction and anti-cyclic properties of the Levi-Civita tensor are employed to obtain:

$$[(\nabla V)\times(\nabla\times E)]_\alpha = [-i\mathbf{S}\cdot((\nabla V)\times\nabla)]_\alpha - ((\nabla V)\cdot\nabla)\mathbf{E} + (\nabla V)(\vec{\nabla}\cdot\mathbf{E}) \tag{VII.14}$$

This result can be checked in spherical coordinates using vector spherical harmonics. Additionally, this result is broadly true in any coordinate system using Mathematica's vector analysis package in Appendix C. At this point, it is helpful to have a more detailed discussion about vector spherical harmonics. We can

decompose our vector Laplacian into a part that acts on the radial part of the solution, and a part that acts on the angular coordinates:

$$\nabla^2 R(r)\mathbf{Y}^j_{l,m} = \mathbf{Y}^j_{l,m}\frac{1}{r^2}\frac{\partial R(r)}{\partial r} - R(r)\frac{1}{r^2}\hat{\mathbf{L}}^2\mathbf{Y}^j_{l,m} \tag{VII.15}$$

The square of the angular momentum operator acts as follows, where $Y_{lm}(\theta,\phi)$ is a spherical harmonic:

$$\hat{\mathbf{L}}^2 Y_{lm}(\theta,\phi) = l(l+1)Y_{l,m}(\theta,\phi) \tag{VII.16}$$

The vector spherical harmonics attractive properties with regard to both the angular operator, the 3D spin angular momenutm vector, and the $\hat{J}_s$ operator:

$$\mathbf{S}^2\mathbf{Y}^j_{l,m} = 2\mathbf{Y}^j_{l,m} \tag{VII.17}$$

$$\hat{\mathbf{L}}^2\mathbf{Y}^j_{l,m} = l(l+1)\mathbf{Y}^j_{l,m} \tag{VII.18}$$

$$\hat{J}_z\mathbf{Y}^j_{l,m} = m\mathbf{Y}^j_{l,m} \tag{VII.19}$$

$$\hat{\mathbf{J}}^2\mathbf{Y}^j_{l,m} = j(j+1)\mathbf{Y}^j_{l,m} \tag{VII.20}$$

$$\tag{VII.21}$$

All of the above relationships act on the angular part of the solution, and not on scalar radial part of the solution. Here, we can find a similar relationship to deriving the spin-orbit operator in quantum mechanics:

$$(\mathbf{S}\cdot\mathbf{L})\mathbf{Y}^j_{l,m} = \frac{1}{2}\left(\hat{\mathbf{J}}^2 - \hat{\mathbf{L}}^2 - \mathbf{S}^2\right)\mathbf{Y}^j_{l,m} \tag{VII.22}$$

$$= \frac{1}{2}\left(\hat{\mathbf{J}}^2 - \hat{\mathbf{L}}^2 - \mathbf{S}^2\right)\mathbf{Y}^j_{l,m} \tag{VII.23}$$

For the 3 vector spherical harmonics we can have 3 cases: $j = l+1, 1, l-1$. The spin-orbit term, as metioned earlier, gives us the following eigenvalues for those three cases:

$$\mathbf{L}\cdot\mathbf{S}\mathbf{Y}^j_{lm} = \mathbf{Y}^j_{lm}\begin{cases} l, & \text{if } j = l+1 \\ -1, & \text{if } j = l \\ -(l+1), & \text{if } j = l-1 \end{cases} \tag{VII.24}$$

For completeness, we'll define the 3 vector spherical harmonics, in terms of the scalar spherical harmonics, $Y_{lm}(\theta,\phi)$. For the transverse optical case, we have:

$$\mathbf{Y}^{j=l}_{lm} = \frac{1}{\sqrt{l(l+1)}}\mathbf{L}Y_{lm}(\theta,\phi) \tag{VII.25}$$

We can also construct transverse solutions by the appropriate superposition of the two vector spherical harmonics with non-zero divergence:

$$\mathbf{Y}^{j=l-1}_{lm} = \frac{1}{\sqrt{j(2j+1)}}\left(-j\hat{\mathbf{r}} + i\hat{\mathbf{r}}\times\mathbf{L}\right)Y_{lm}(\theta,\phi) \tag{VII.26}$$

$$\mathbf{Y}^{j=l+1}_{lm} = \frac{1}{\sqrt{(j+1)(2j+1)}}\left((j+1)\hat{\mathbf{r}} + i\hat{\mathbf{r}}\times\mathbf{L}\right)Y_{lm}(\theta,\phi) \tag{VII.27}$$

Hamiltonian Formulation for Vector Fields

We can now return to the perturbative spin-orbit coupling/Darwin term in Maxwell's equations:

$$\begin{aligned} \mathbf{A} \times \left(\vec{\nabla} \times \mathbf{E} \right) &= \left[\frac{\mathbf{S}}{i\hbar} \cdot \left(\mathbf{A} \times \vec{\nabla} \right) \right] \mathbf{E} + \mathbf{A} \left(\vec{\nabla} \cdot \mathbf{E} \right) \\ &\quad - \left(\mathbf{A} \cdot \vec{\nabla} \right) \mathbf{E} \end{aligned} \tag{VII.28}$$

Using the above, Mawell's wave equation takes the form:

$$\begin{aligned} &\nabla^2 \mathbf{E} + \left(\frac{\omega}{c} \right)^2 \epsilon \, \mu \, \mathbf{E} \\ &= -\frac{1}{\mu} \left\{ \left[\frac{1}{i\hbar} \mathbf{S} \cdot \left(\left(\vec{\nabla} \mu \right) \times \vec{\nabla} \right) \right] - \left(\left(\vec{\nabla} \mu \right) \cdot \vec{\nabla} \right) \right\} \mathbf{E}. \end{aligned} \tag{VII.29}$$

The first term on the right can now be compared to the SO interaction as it appears in the quantum-mechanical Pauli Hamiltonian with an external electric field $\mathbf{F}$: $\frac{e}{2m^2c^2} \hat{\mathbf{s}} \cdot (\mathbf{F} \times \mathbf{p})$ where $\mathbf{p} = -i\hbar\vec{\nabla}$ is the momentum operator and $\hat{\mathbf{s}} = \hbar\vec{\sigma}/2$ the spin. For spin-one-half particles, $\vec{\sigma}$ is the vector of 2×2 Pauli matrices. The formal analogy to Eq. (VII.30) becomes clear if we interpret $\vec{\nabla} \ln \mu \equiv \mathbf{F}$ as a fictitious external electric field. The last term in Eq. (VII.30) will be shown below Eq. (VII.36) to correspond to the relativistic Darwin term.

Assuming $\mu = \mu(r)$, the SO term takes the familiar $\mathbf{S} \cdot \mathbf{L}$ form which explicitly

contains the interaction of the intrinsic and orbital angular momenta:

$$\mathbf{S}\cdot\left(\left(\vec{\nabla}\ln\mu\right)\times\mathbf{p}\right)=\frac{1}{r}\frac{d\ln\mu}{dr}\mathbf{S}\cdot\mathbf{L}, \tag{VII.30}$$

where $\mathbf{L}=\mathbf{r}\times\mathbf{p}$. The SO term in Schrödinger's equation for a radial potential has the same form, with $\mathbf{S}$ replaced by $\hat{\mathbf{s}}$. The Pauli matrices in $\hat{\mathbf{s}}$ are generators of SU(2), whereas the S_n generate three-dimensional rotations, thus forming a spin-1 irreducible representation of SO(3) with $\mathbf{S}^2=2\hbar^2\mathbf{1}$. The eigenvectors of S_z with eigenvalue $\pm\hbar$ are the *Jones vectors* $(1,\pm i,0)/\sqrt{2}$, and the eigenvalue 0 of S_z corresponds to $\hat{z}$.

In quantum mechanics, Eq. (VII.30) appears as a perturbation term, and the perturbed eigenstates are also eigenfunctions of $\hat{\mathbf{s}}\cdot\hat{\mathbf{L}}$ with eigenvalue $\hbar^2\left(j\left(j+1\right)-\ell\left(\ell+1\right)-s\left(s+1\right)\right)/2$, where $\hbar^2\ell\left(\ell+1\right)$ is the eigenvalue of L^2, and $\hbar^2 j\left(j+1\right)$ is the eigenvalue of the squared total angular momentum. The quantities that are actually coupled by SO "coupling" are the components S_z and L_z which in the unperturbed problem are conserved. The same happens in our optical system, except that $j=\ell$ is required if we focus on the TE solutions of Eq. (VII.30). These solutions are proportional to the vector spherical harmonics, denoted by $\mathbf{Y}^{\ell}_{\ell,m}(\theta,\phi)$. We obtain optical solutions from the one independently transverse vector spherical harmonic:

$$\mathbf{Y}^{\ell}_{\ell,m}(\theta,\phi)\equiv\frac{1}{\hbar\sqrt{\ell\left(\ell+1\right)}}\mathbf{L}\,Y_{\ell,m}(\theta,\phi), \tag{VII.31}$$

obtained by applying the orbital angular momentum operator, $-i\hbar(\mathbf{r}\times\nabla)$, to the

spherical harmonic $Y_{\ell,m}(\theta,\phi)$. Here, $m=-\ell,\ldots\ell$, and $\hat{\mathbf{r}}\cdot\mathbf{Y}^{\ell}_{\ell,m}=0$ by construction. Because $\mathbf{L}\,Y_{0,0}(\theta,\phi)=0$, there are no $\ell=0$ states (corresponding to s orbitals) in the vector wave equation. The vector spherical harmonics are eigenstates of the squared orbital and spin angular momenta, but not of S_z or L_z (the "magnetic number" m is the z-component of the total angular momentum S_z+L_z of $\mathbf{Y}^{\ell}_{\ell,m}$). The TE fields given by Eq. (VII.31) always yield $\frac{1}{\hbar^2}(\mathbf{S}\cdot\mathbf{L})\,\mathbf{E}(\mathbf{r})=-\mathbf{E}(\mathbf{r})$, but we shall keep $\mathbf{S}\cdot\mathbf{L}$ in the following to emphasize the correspondence to quantum mechanics.

It should be stressed that the results presented so far are independent of any particular model of ϵ and μ, however, to illustrate the connection of the spin-orbit and Darwin terms to quantum mechanics we can employ the previously derived models of ϵ and μ obtained from the Dirac equation:

$$\left\{\begin{array}{c}\epsilon(r,\omega)\\ \\ \mu(r,\omega)\end{array}\right\}=1\mp\frac{\omega_p}{\omega}-\frac{V(r)}{\hbar\omega} \tag{VII.32}$$

And further use a definition of the Schrödinger energy.

$$\varepsilon_{\mathrm{S}}\equiv\hbar\omega_s\equiv\varepsilon-\hbar\omega_p. \tag{VII.33}$$

The approximations used here are also valid for Drude models of ϵ and μ, described in chapter XII. Next, by multiplying Eq. (VII.30) by $\hbar^2/(2m)$ and inserting Eqs. (VII.32), (VII.33) allows us to recover the optical version of the spin-orbit interaction term:

$$\frac{1}{\mu}\frac{\hbar^2}{2mr}\frac{d\mu}{dr}(\mathbf{S}\cdot\mathbf{L})\mathbf{E}\;\approx\;\frac{1}{4m^2c^2r}\frac{dV}{dr}(\mathbf{S}\cdot\mathbf{L})\,\mathbf{E} \tag{VII.34}$$

Here, we have used the non-relativistic limit in which $\hbar\omega_p = mc^2 \gg \varepsilon_{\rm S} - V(r)$ to expand the denominator. The above allows us to compare directly to the quantum-mechanical SO interaction, $\mathcal{H}_{\rm SO}$, for a charged particle of gyromagnetic ratio g,

$$\mathcal{H}_{\rm SO} = \frac{g}{4m^2c^2r}\,\frac{dV}{dr}\,\hat{\mathbf{s}}\cdot\mathbf{L} \tag{VII.35}$$

Equations (VII.34) and (VII.35) are identical with the replacement $g\hat{\mathbf{s}} \leftrightarrow \mathbf{S}$. We also insert Eq. (VI.4) into Eq. (VII.30), so that Maxwell's wave equation takes the form of an eigenvalue problem $\hbar\omega_s\mathbf{E} = \mathcal{H}_{\rm opt}\mathbf{E}$ with an optical Hamiltonian

$$\begin{aligned}\mathcal{H}_{\rm opt} \;&=\; \frac{p^2}{2m} + V - \frac{p^4}{8m^3c^2} + \\ &\quad + \frac{1}{4m^2c^2}\left(\frac{1}{r}\frac{dV}{dr}\,(\mathbf{S}\cdot\mathbf{L}) + (\mathbf{p}V)\cdot\mathbf{p}\right).\end{aligned} \tag{VII.36}$$

We use the same expansion as in Eq. (VII.34) to approximate the last term: $\frac{1}{\mu(\mathbf{r})}\left(\left(\vec{\nabla}\mu\right)\cdot\vec{\nabla}\right)\mathbf{E} \;\approx\; -\frac{1}{2\hbar\omega_p}\left(\frac{dV}{dr}\right)\frac{\partial\mathbf{E}}{\partial r}$. This is non-selfadjoint, so that the optical Hamiltonian $\mathcal{H}_{\rm opt}$ is not directly amenable to perturbation theory. The physical reason for the non-Hermiticity of $\mathcal{H}_{\rm opt}$ is the coupling between $\mathbf{E}$ and $\mathbf{H}$ in our spatially varying medium, which leads to an interchange of energy between the electric and magnetic fields. To make $\mathcal{H}_{\rm opt}$ self-adjoint, we rescale the electric field by introducing

$$\mathbf{E}_{\rm S} \;=\; \left(1 + \frac{1}{8m^2c^2}\mathbf{p}^2\right)\mathbf{E}, \tag{VII.37}$$

where the smallness of $1/\left(m^2c^2\right)$ can be exploited to write an approximate inverse relation, $\mathbf{E} = (1 - \frac{1}{8m^2c^2}\mathbf{p}^2)\mathbf{E}_{\rm S}$. If $\mathbf{E} \propto \mathbf{Y}^{\ell}_{\ell,m}$ then the same holds for $\mathbf{E}_{\rm S}$. Using

the substitution (VII.37) in the eigenvalue equation $\hbar\omega_s \mathbf{E} = \mathcal{H}_{\rm opt}\mathbf{E}$, the last term in Eq. (VII.36) becomes a "contact term" proportional to $\left(\nabla^2 V\right)$. To show this, note that switching to $\mathbf{E}_{\rm S}$ adds a commutator to $\mathcal{H}_{\rm opt}$,

$$\hbar\omega_s \mathbf{E}_{\rm S} \approx \left\{ \mathcal{H}_{\rm opt} - \frac{1}{8m^2c^2}\left[\mathbf{p}^2, \mathcal{H}_{\rm opt}\right] \right\} \mathbf{E}_{\rm S}. \tag{VII.38}$$

where $\left[\mathbf{p}^2, \mathcal{H}_{\rm opt}\right] \approx \left[p^2, V\right]$ if only terms up to linear order in $1/(m^2c^2)$ are kept in Eq. (VII.38). Inserting Eq. (VII.36),

$$\left[\hbar\omega_s \mathbf{E}_{\rm S} = \left\{ \frac{\mathbf{p}^2}{2m} + V(r) - \frac{\mathbf{p}^4}{8m^3c^2} + \frac{1}{4m^2c^2r}\frac{dV}{dr}\left(\mathbf{S}\cdot\mathbf{L}\right) + \frac{1}{4m^2c^2}\left((\mathbf{p}V)\cdot\mathbf{p} - \frac{1}{2}\left[\mathbf{p}^2, V\right] \right) \right\} \mathbf{E}_{\rm S}. \right] \tag{VII.39}$$

The last two terms can now be combined using $(\mathbf{p}V)\cdot\mathbf{p} - \frac{1}{2}\left[p^2,\, V\right] = -\frac{1}{2}\left(p^2 V\right)$, to get for the rescaled optical Hamiltonian that mirrors its quantum counterpart:

$$\begin{aligned} \mathcal{H}_{\rm S} \;=\; & \frac{\mathbf{p}^2}{2m} + V(r) - \frac{\mathbf{p}^4}{8m^3c^2} + \frac{1}{4m^2c^2r}\frac{dV}{dr}\left(\mathbf{S}\cdot\mathbf{L}\right) \\ & - \frac{1}{8m^2c^2}\left(\mathbf{p}^2 V\right). \end{aligned}$$

With this Hamiltonian, the optical modes of the metamaterial system can now be treated in complete formal analogy to standard quantum mechanics textbook calculations of the spin-orbit shift [38], except that the transversality condition requires $j = \ell$.

CHAPTER VIII

OPTICAL MODE-MIXING, OPTICAL SPIN-ORBIT COUPLING, AND TAILORING THE RADIATION PATTERN

Perturbative Approaches to Analyze Polarization Dependent Mode Mixing

Any lengthy discussion about polarization effects in cavities would be incomplete without a description of polarization-induced mode-mixing. The purpose of this chapter is to suggest a generalized approach towards characterizing polarization-induced optical mode mixing, using perturbative approaches and the Poincaré Surface of Section (SOS). This chapter contains previously published material co-authored by myself, David Foster, and Jens Nöckel. Optical mode mixing is a very important polarization-dependent phenomenon that isn't directly related to optical spin-orbit coupling. On the basis of previous chapters, spin-orbit coupling is a predictable spectral shift caused by the polarization of light rays interacting with the geometry of a cavity. Generally speaking, polarization-dependent mode mixing will be a part of any 3D optical cavity that doesn't exactly adhere to one of a handful of geometries, given in Morse and Feshbach [43] in which the vector Helmholtz equations can be solved. The drawback to mode mixing is that if one applies textbook solutions to real-world cavities, solutions will deviate slightly

from textbook conditions, the polarization structure of modes sharing the same total angular momentum quantum number can deviate dramatically from textbook conditions, but in a way that can be tuned by turning geometrical knobs. For example, if you think textbook Laguerre Gauss modes of a Vertical Cavity Surface Emitting Laser (VCSEL) will describe the polarization structure of the laser, this is unlikely to be the case for TE and TM modes that share the same total angular momentum quantum number. However, one can intelligently design geometrical properties of the cavity, such as length and radius of curvature of mirrors, to produce robust circularly polarized modes, with foreknowledge of the mixing behavior.

A second drawback to polarization induced mixing is that it can confuse attempts to confirm a strong coupling regime between qubits and cavities, necessary for quantum computing. One hallmark of strong coupling is an avoidant crossing that produces a strong peak if the cavity is tuned on resonance with the quantum bit. However, if one changes the geometry of the cavity to tune such a resonance, polarization-induced mixing can create the same effects. I worked with Hailin Wang at the University of Oregon to couple diamond NV center qubits to deformed microsphere whispering gallery modes. We observed what looked like strong coupling[44], however we didn't have sufficient collection efficiency to observe photon anti-bunching. Reviewers and a visiting researcher protested that perhaps it was some classical effect. Without a rigorous framework to say why this wasn't a cavity effect, we weren't able to publish the results in the first journal

to which we submitted. Additionally, the dome cavity described in this chapter was designed to interact with qubits, but upon a detailed study, we found that some modes would split due to optical mixing, risking confusion with coupling to a quantum dot.

In the paper "Degenerate perturbation theory describing the mixing of orbital angular momentum modes in Fabry-Perot cavity resonators" [1], my group was able to describe polarization dependent mode mixing by using a perturbative approach, which will be briefly described here. Specifically, we found that polarization effects had a very large effect on the splitting of some modes as the length of the cavity was varied, even if the cavity was nearly paraxial, with an almost flat curved mirror.

If we have a close-to flat Fabry-Perot dome cavity, we can expand the vector in terms of Laguerre-Gauss Polynomials multiplied by Jones vectors defined by the 3×3 spin matrix for the z-axis, $\hat{S}_z$. Studying numerical model of this cavity, mode splittings will appear when a perfectly reflecting metal mirror is replaced by a Bragg Stack. To first order, a resonance condition is met if, where L is the length of the cavity:

$$2kL = 2\pi n \tag{VIII.1}$$

However, the TE and TM cavity modes are only split a small amount in a metal cavity. This splitting is due to the fact that the TE and TM modes are affected by

the slight curvature of the mirror[45]. However, we noticed the splitting generally did not obey this formula. The textbook mode splitting is[24]:

$$\delta k = \pm \frac{m}{4kLR} \tag{VIII.2}$$

Where m is the total angular momentum of the modes, and R is the radius of curvature of the mirror. We can make an electric field plot at the surface of the Bragg stack, and compare TE and TM modes. The vector field on the Bragg stack changes character as the geometry of the cavity is modified. The TE mode will start to look like the TM mode, and vice versa, until they are indistinguishable. For these reasons, we want to look for a mixing matrix that has off-diagonal elements, that takes one mode, mixes it with another mode, to produce the resulting vector field. Since we know that mixed modes with have an avoidant crossing, we can guess that this is responsible for the effect.

To account for observed deviations, we can add a reflection phase acquired by each mode, $\langle\phi\rangle_{TE}$. The modified Fabry-Perot quantization conditions become:

$$2k_{TE}L + \langle\phi\rangle_{TE} = 2\pi n \tag{VIII.3}$$

$$2k_{TM}L + \langle\phi\rangle_{TM} = 2\pi n \tag{VIII.4}$$

The observed effect can be described by a mixing matrix, which only has diagonal elements of $\pm\frac{m}{8kLR}$, and zero for off-diagonal elements if there is no

mixing or differential phase shifts. For the off-diagonal elements, we wish the absolute value to be proportional to the phase shift differences, which are zero for metal cavities, in which no mixing was observed. So, we wish the magnitude of off-diagonal elements to be:

$$\frac{|\langle\phi\rangle_{TM} - \langle\phi\rangle_{TE}|}{4L} \tag{VIII.5}$$

Our mixed modes can now be described as follows:

$$\begin{pmatrix} \Psi_{N,m,1} \\ \Psi_{N,m,2} \end{pmatrix} = \begin{pmatrix} \cos\alpha & -\sin\alpha \\ \sin\alpha & \cos\alpha \end{pmatrix} \begin{pmatrix} \mathrm{LG}^{m-1}_{(N-m+1)/2}\hat{\boldsymbol{\sigma}}_1 \\ \mathrm{LG}^{m+1}_{(N-m-1)/2}\hat{\boldsymbol{\sigma}}_{-1} \end{pmatrix}. \tag{VIII.6}$$

Since our geometry is nearly paraxial, and our TE and TM modes are nearly textbook, we can expand their different reflection phase shifts over a small polar angle, θ:

The reflectivity of the Bragg mirror for TE (s-polarized) plane waves, r_{s}, and the corresponding TM (p-polarized) reflectivity, r_{p}, can be approximated as $r_{\mathrm{s/p}} \approx \exp(i\phi_{\mathrm{s/p}})$ where the phase is expanded in the plane wave angle of incidence, θ_{k}.

$$\phi_{\mathrm{s/p}}(k, \theta_{\mathrm{k}}) \approx \phi_0(k) + \epsilon_{\mathrm{s/p}}(k)\theta_{\mathrm{k}}^2. \tag{VIII.7}$$

We expect our mixing angle to be:

$$\alpha = \frac{1}{2}\arctan\left(\frac{\epsilon_{\mathrm{p}}(k) - \epsilon_{\mathrm{s}}(k)}{\Delta\epsilon}\right), \tag{VIII.8}$$

The denominator in the arctangent can be described by the divergence angle of the modes, when one takes into account the extremes of the mixing matrix, and is only dependent on geometrical parameters and mode numbers, as described in [1].

$$\Delta\epsilon(L/R, N, m) = \frac{1}{2}\sqrt{\frac{(L/R)(1 - L/R)}{(N + 1 + m)(N + 1 - m)}}. \tag{VIII.9}$$

The above result means that using only cavity length and radius, one can tune the mixing angle, and polarization output of the cavity. If one has an FDTD model for a 3D cavity, then given a particular geometry, one could indeed predict a given output. Pertubation theory shows explicity how splitting depend on mode parameters. Vector-based pertubation techniques allow an engineer to readily predict what cavities will have the most advantageous properties.

To test our predictions, we can break our TE and TM modes into s and p polarizations, and numerically calculate the angular dependent expectation of the phase shift for a given Bragg stack. Integrating over small angles, we can then obtain the expectation of the phase shifts and test the theoretical wavenumber splitting and mixing angle verses the numerical results. The sound agreement between analytical and numerical results is shown in figure 8.1., which displays agreement with both wavenumber splitting and with the mixing angle.

The approach used in this paper can be generalized to various geometries. If there exist two near-degenerate modes, sharing total angular momentum quantum numbers, we can expect these modes to have different phase shifts at boundaries

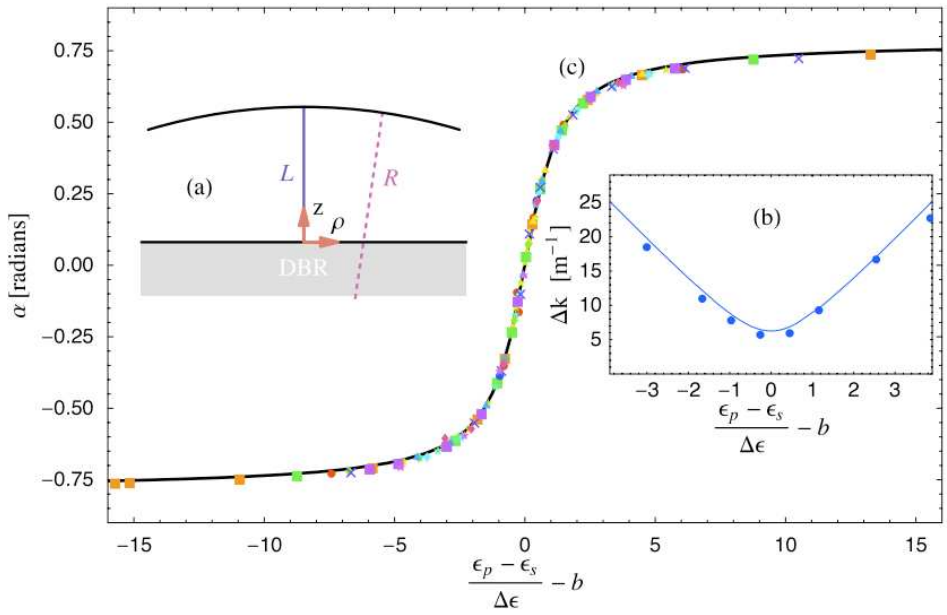

Figure 8.1. The dots are numerical measurements of mixing angle and wavenumber splitting for cavities of different length and radius. The lines are the theoretical result of a largely analytical mixing-matrix approach to describing the splitting and mixing angle. The only numerical modeling that went into the curve was a measurement of the reflection phase shift for s and p polarized rays when incident on the Bragg stack at different small angles. From reference [1].

unless silver mirrors are used for the boundary. Where the phase shift is most pronounced, the greater the effects of mode mixing. If one can define a normal to a boundary, then modes of the cavity can be decomposed into s and p polarized components on a reflecting boundary that introduces different phase shifts for each polarization. The most promising systems in which to next test this approach are on deformed spheres or on a deformed torus.

CHAPTER IX

PROPAGATORS AND THE BOGOMOLNY SEMICLASSICAL TRANSFER OPERATOR

Handling Polarization in Nonintegrable Cavities

In the previous chapters, we described two methods for handling polarization-dependent phenomena in three-dimensional cavities. One method is to develop a vector Hamiltonian with spin-orbit and Darwin terms. The second method was to look at the polarization of s and p components of vector fields at a surface of section in order to generate a polarization-dependent mixing matrix that coupled TE and TM modes. Both of these approaches assumed that we already knew the form of the vector field that we wished to perturb. In this chapter, we ask how we could find the full vector field if we start with an optical cavity that is non-integrable. We will present the Bogomolny Transfer Operator method, that does a great job at finding the modes of non-integrable cavities that obey the scalar wave equation. We will show that we can continuously deform fields from one integrable cavity (in the scalar limit) to another, keeping track of modes as the cavity crosses a chaotic regime. However, dealing with scalar fields is unsatisfying for a number of reasons. One is that modes are often degenerate in the scalar limit. And these

modes are no longer degenerate for vector solutions of the cavity. This is a problem because degenerate modes can have different spatial mode structure. If a mode is not degenerate, we can use Green's functions to reproduce the amplitude of the scalar field at any point in the cavity. But if a mode is degenerate, and a cavity is non-integrable, it is unclear how we can find the amplitude of the field within the cavity. For this reason, we would like to extend methods of the Bogomolny transfer operator to characterize and quantize vector fields.

Bogomolny's semiclassical transfer operator is a useful tool for solving many problems in electromagnetism and quantum mechanics. Bogomolny's operator is powerful because it gives the frequencies and energies of semiclassical and quantum systems that are highly accurate approximations to path integral methods. In contrast to earlier approaches Bogomolny's method does not require closed paths to obtain quantization. Additionally, once the frequency is obtained that corresponds to an optical mode in a cavity, information about the electromagnetic field on the boundary and within the cavity can be obtained with relatively little extra computational overhead. To our knowledge, this operator has only been used to solve scalar problems in optics. It is our hope that a higher dimensional generalization of Bogomolny's quantization technique will give us accurate answers to problems involving birefringent phenomena and optical spin-orbit coupling. We also believe that Bogomolny's technique can be extended to optical problems with continuously varying permittivity. Also, Bogomolny's technique has yet to

be extended to solving scalar problems in lossy cavities. This document describes some problem solving techniques using Bogomolny's operator and suggests ways in which the operator can be used to solve more complex problems.

In 1991, E. B. Bogomolny proposed a new semiclassical transfer operator that provides a powerful tool for solving problems in quantum mechanics and classical electromagnetism. Initially, this operator was used to solve quantum mechanics problems, but the method was quickly adapted for solving scalar optical problems. The primary initial motivation for the development of the Bogomolny transfer operator was to take a step beyond the Gutzwiller trace formula that determines the density of states of a quantum mechanical system. The Gutzwiller trace formula has been widely used in quantum chaos, but its achilles' heel is the necessity for defining closed orbits[3]. Bogomolny's technique gives us the energy and frequency spectrum of non-integrable closed systems without recourse to semiclassical orbits. Furthermore, the matrices produced to solve for the spectrum also give us valuable information about the wave function of quantum mechanical problems, and the three dimensional field of modes in optical problems. Extensions to Bogomolny's technique will allow us to describe three-dimensional vector electric and magnetic fields in Maxwell's equations. We have previously used perturbative techniques to study optical spin-orbit coupling and mode mixing in a 3D paraxial cavity geometry. If extended to vector space, Bogomolny's operator can be used to study optical spin-orbit coupling problems even in non-integrable cavities with non-trivial phase

shifts at boundaries. Such a study would enhance our ability to design microcavities with customized polarization properties. Additionally, this approach may allow us to better characterize optical spin-orbit coupling in cavities. The first section of this paper will introduce the operator. Sections 2. and 3. will give semiclassical background behind the operator. Section 4. describes the implementation of the operator for the dome cavity.

The Bogomolny Transfer Operator

When solving electromagnetic problems with the Bogomolny semiclassical transfer operator, one must first define a Poincaré surface of section (SOS). If there are k dimensions, the surface of section represents a k-1 dimensional phase space. Phase space is a volume of variables that represent all possible states of a classical system. The axes of phase space are typically positions and momenta of classical particles or rays. The Poincaré SOS is a map that intersects all orbits and trajectories. In other words, there are no closed ray orbits that fail to periodically intersect the SOS. We can therefore represent continuous motion in the larger phase space as discretized into points on the map [46]. Figure 9.1. displays a surface of section, Σ, within a bounded region that allows wave or wave packet propagation. Bogomolny's technique for solving quantum problems is to reduce a solution for the wavefunction ψ in real space to a solution to ψ on a k-1 dimensional map [2].

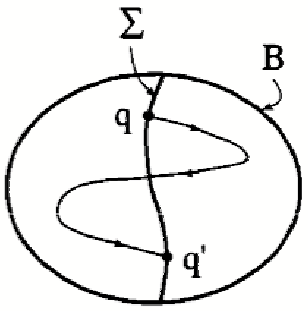

Figure 9.1. Surface of Section, Σ, of a two dimensional cavity with boundary B. A new point is added to the SOS when a trajectory enters the SOS from a single side only[2].

The integral equation on the surface, Σ, defines the Bogomolny transfer operator.

$$\psi(\mathbf{q}'', \omega) = \int_{\Sigma} T(\mathbf{q}'', \mathbf{q}', \omega)\psi(\mathbf{q}', \omega)\, \mathbf{dq}' \tag{IX.1}$$

$$T(\mathbf{q}'', \mathbf{q}', \omega) = \sum_{class.traj.} \frac{1}{(2\pi i\hbar)^{(k_\Sigma/2)}} \sqrt{det \left| \frac{\partial^2 S(\mathbf{q}'', \mathbf{q}', \omega)}{\partial \mathbf{q}'' \partial \mathbf{q}'} \right|} exp(-i\hbar S(\mathbf{q}'', \mathbf{q}', \omega) - i\frac{\pi}{2}\nu) \tag{IX.2}$$

In the above equation, $S(\mathbf{q}, \mathbf{q}', \omega)$ is the classical action, parameterized by frequency.

$$S(\mathbf{q}, \mathbf{q}', \omega) = \int_{\mathbf{q}}^{\mathbf{q}'} \mathbf{p}\, d\mathbf{q} \tag{IX.3}$$

Bogomolny's transfer operator is like a propagator, but it relates the value of the wave function on one part of the surface of section to its value on another part of the surface of section. If the left hand side of IX.1 equals the right hand side everywhere

on the surface of section, at that frequency, there is a resonance or energy level. At other frequencies, destructive interference prevents the formation of normal modes. The wavefunction $\psi(\mathbf{q}, \omega)$ can represent either a quantum mechanical wave function, or a scalar field proportional to the magnitude of the electromagnetic field. Blümel, Ott, and Prange were among the first to adopt Bogomolny's operator for use in optical problems, and they made the simple argument that Helmholtz equation has the same form as the quantum mechanical Hamiltonian.

$$\mathbf{H_{QM}}\psi = E_n\psi \tag{IX.4}$$

$$\updownarrow \tag{IX.5}$$

$$\left(\nabla^2 - u(x)V_0\right)\Psi = k^2\Psi \tag{IX.6}$$

In semiclassical optics, we substitute the square of the wavenumber in place of the quantum mechanical energy eigenvalue. We can find complete equivalence between the two equations if we subsequently take the limit that $\frac{\hbar^2}{2m} - > 1$, or $\hbar = 1$, $m = \frac{1}{2}$. Look at the the equation IX.2, we can use the Bogomolny transfer operator to hop between semiclassical electromagnetism and quantum mechanics by taking limit of $\hbar$ going to 1. In contrast, to derive the classical mechanics of Newtonian point particles, which have no phase-dependent behavior, we must take the limit of $\hbar$ going to zero.

The physical significance of different parts of the $T(\mathbf{q}'', \mathbf{q}', \omega)$ operator will be explained in the next few sections.

The Jacobian Determinant

In this section, we'll let $S_t(\mathbf{q}'', t'', \mathbf{q}', t')$ represent the action, parameterized in time.

$$S_t(\mathbf{q}'', t'', \mathbf{q}', t') = \int_{t'}^{t''} L(\dot{\mathbf{q}}_\mathbf{0}, \mathbf{q}_\mathbf{0}, \tau)\, d\tau \tag{IX.7}$$

If a path $\mathbf{q}(\mathbf{t})$ minimizes the action between points $\mathbf{q}'$ and $\mathbf{q}''$, the behavior of adjacent trajectories/ray paths still effect the frequencies of resonances in phase-dependent semiclassical problems (those involving quantum wavefunctions, or classical, continuous fields). The density of adjacent ray paths appears as a prefactor in the Bogomolny transfer operator, and is also related to the quantum mechanical amplitude. Let's assume that $\mathbf{p}'$ is a starting momentum at point $\mathbf{q}'$, and $\mathbf{p}'_\mathbf{0}$ is the momentum along the minimized trajectory. The spreading of rays about a minimum of the action, with perturbed starting momenta, is depicted in Figure 9.2.. To find the density of rays around the endpoint, $\mathbf{q}''$, we can use the Jacobi matrix to expand the ending position as a function of the vector perturbation of the starting momentum. Assuming linearity about the starting point:

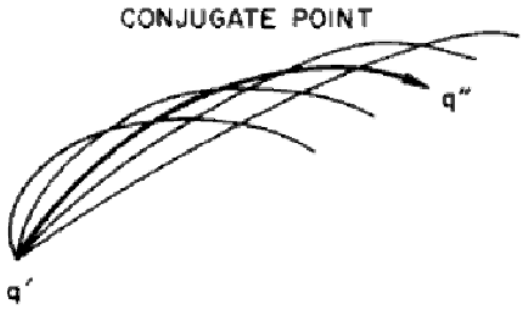

Figure 9.2. A depiction of the density of rays about the minimum of the action connecting points $\mathbf{q}'$ and $\mathbf{q}''$. This figure is from "Chaos in Classical and Quantum Mechanics"[3].

$$\mathbf{q}''(\mathbf{p}') \cong \mathbf{q}''(\mathbf{p}'_\mathbf{0}) + \begin{pmatrix} \nabla_{\mathbf{p}'} q''_1(\mathbf{p_0}) \\ \vdots \\ \nabla_{\mathbf{p}'} q''_n(\mathbf{p_0}) \end{pmatrix} (\mathbf{p}' - \mathbf{p}'_\mathbf{0}) \tag{IX.8}$$

We can differentiate and invert the above expression if the Jacobi matrix is invertible. This yields:

$$\delta\mathbf{q}'' = \begin{pmatrix} \delta q''_1 \\ \vdots \\ \delta q''_n \end{pmatrix} = \left(\frac{\partial p'}{\partial q''}\right) \delta\mathbf{p}' \tag{IX.9}$$

Since $\mathbf{p}' = -\nabla_{\mathbf{q}'} S_t$ we can rewrite the matrix in terms of derivatives of the action at the endpoints.

$$\delta\mathbf{q}'' = \mathbf{N}\delta\mathbf{p}' \tag{IX.10}$$

Where $\mathbf{N}$ is defined by:

$$\mathbf{N^{-1}} = \left(-\frac{\partial^2 S_t}{\partial \mathbf{q_i''} \partial \mathbf{q_j'}} \right) \tag{IX.11}$$

If the matrix N isn't invertible, then the ray passes through an unstable fixed point at point $\mathbf{q}''$. Likewise, if the matrix is singular, the assumption of linearity is invalid. Additionally, if rays converge at caustic or focus, this would imply an infinite energy density at a point unless we carefully consider the wave nature of energy ascribed to a ray. For example, if a single ray passes through a focus, half of its energy will pass to the left of the focus, and half to the right. But any tiny deviation of the ray's momentum on the left side of a focus can launch a ray on a path radically to one direction. At unstable points, linear classical mechanics fails, but it fails for perfectly sensible reasons. If a ray enters a caustic, its energy belongs to all of its neighbors that also enter that caustic at the same point in time.

The determinant of the Jacobi matrix is the Jacobian, and is the ratio of a volume element defined by $\delta \mathbf{p}'$ elements over $\delta \mathbf{q}''$ elements. Essentially the Jacobi determinant tells us the concentration of ray paths about the endpoint as we perturb ray momenta at the starting point. The square root of the Jacobi determinant also defines the quantum mechanical amplitude for a particle to propagate between points.

$$C(\mathbf{q}'', \mathbf{q}', t) = \left| -\frac{\partial^2 S_t}{\partial \mathbf{q_i''} \partial \mathbf{q_j'}} \right| \tag{IX.12}$$

The root of $C(\mathbf{q}'', \mathbf{q}', t)$ is a prefactor in the Van Vleck propagator, (IX.25), that semiclassically solves Schrödinger's equation. However, the square root of the Jacobi determinant also appears as a prefactor of Gaussian beams propagating in several dimensions.citeJensen. The root of the Jacobi determinant has clear meaning in both quantum and semiclassical descriptions of propagation. However, it is only semiclassically defined away from caustics.

Propagators and Green's Functions

A propagator is a tool that moves a field or wave function from an initial to final spatial distribution in a given period of time. Propagators used to describe Bogomolny's operator were initially employed to solve Schrödinger's equation:

$$H\psi(q,t) = -\frac{\hbar^2}{2m}\nabla^2\psi(q,t) + V(q)\psi(q,t) = i\hbar\frac{\partial}{\partial t}\psi(q,t) = E_n\psi(q,t) \qquad \text{(IX.13)}$$

Solutions to Schrödinger's equation can be expressed as a sum of complex, orthonormal functions, $\phi_n(q)$:

$$\psi(q,t) = \sum_n c_n e^{-i\frac{E_n t}{\hbar}}\phi_n(q) \qquad \text{(IX.14)}$$

Where the coefficients are defined by and integral over d spatial dimensions:

$$c_n = \int \phi_n^*(q)\psi(q,0)\, d^d q \qquad \text{(IX.15)}$$

In this section, we'll use Gutzwiller's notation[3] where q is a generalized coordinate, q' is a starting position, and q'' is an ending position. Rewriting our expansion of the wave function we find:

$$\psi(q'', t) = \int K(q'', q', t)\psi(q', 0)\, d^d q' \tag{IX.16}$$

Where $K(q'', q', t)$ is:

$$K(q'', q', t) = \sum_n \phi_n(q'')\phi_n^*(q')e^{-i\frac{E_n t}{\hbar}} \tag{IX.17}$$

The Fourier transform of the time-dependent propagator gives the energy-dependent Green's function. Using Gutzwiller's notation

$$G(q'', q', E) = \frac{-i}{\hbar}\int_0^\infty K(q'', q', t)e^{\frac{iEt}{\hbar}}\, dt \tag{IX.18}$$

If a vanishingly small imaginary component is added to the Green's function, we can simplify the expression for the Green's function:

$$G(q'', q', E + i\epsilon) = \frac{-i}{\hbar}\sum_n \phi_n(q'')\phi_n^*(q')\int_0^\infty e^{-\frac{i(E-E_n+i\epsilon)t}{\hbar}}\, dt \tag{IX.19}$$

$$= \sum_n \frac{\phi_n(q'')\phi_n^*(q')}{E - E_n + i\epsilon} \tag{IX.20}$$

The density of states of a closed system can be found by taking the trace of the Green's function.

$$Tr\left(G(q'', q', E + i\epsilon)\right) = \int_0^\infty K(q'', q', t)\, d^q q = \sum_n \frac{1}{E - E_n + i\epsilon} \qquad \text{(IX.21)}$$

This quantity gives a Dirac delta function for the energy in the limit that epsilon trends towards zero. The density of states of a closed system can now be obtained if we know the Green's function:

$$d(E) = \sum_n \delta(E - E_n) = -\pi^{-1} \lim_{\epsilon \to 0} Im[Tr\left(G(q'', q', E + i\epsilon)\right)] \qquad \text{(IX.22)}$$

Gutzwiller's central contribution to quantum chaos entailed dividing the Green's function into two parts. One part is an oscillatory part obtained from "long" periodic orbits, $d_{osc}(E)$. The second part, labeled $d_{short}(E)$, corresponds to short trajectories. Both of these Green's functions are used in the derivation of Bogomolny's transfer operator. Both of these Green's functions relate to the Van Vleck propagator, which was discovered shortly after Schrödinger derived his famous equation. One method, not covered here, is to derive the Van Vleck propagator through the WKB ansatz and conservation arguments, $\psi(q,t) = A(q,t)Exp[i(S(q)/\hbar]$. Here, we will justify its use simply by the fact that it satisfies the Schrödinger equation. Since the wavefunction $\Psi(q'', t)$ satisfies the Schrödinger equation, so must the propagator $K(q'', q', t)$. The second condition that we impose on the propagator is that the time evolution of $\psi(q'', t)$ follows the Hamiltonian (IX.16). Together, these conditions are:

$$\lim_{t\to 0} K(q'', q', t) = \delta(q'' - q') \tag{IX.23}$$

$$H(p, q)K(q'', q', t) = i\hbar\frac{\partial}{\partial t}K(q'', q', t) \tag{IX.24}$$

The above equations are valid if the potential is not time varying. The solution to these equations is the Van Vleck Propagator:

$$K_c(q'', q', t) = \frac{1}{(2\pi\hbar)^{d/2}}\sqrt{C(q'', q', t)}Exp[(i/\hbar)R(q'', q', t) - i\nu\frac{\pi}{2}] \tag{IX.25}$$

In the above equation, $R(q'', q', t)$ is defined by the action: $S(q'', q', E) = \int_{q'}^{q''} p,\, dq = R(q'', q', E) + Et$. The phase shift of $-i\nu\frac{\pi}{2}$ was derived by Gutzwiller[3] using Feynman's path integral formulation of quantum mechanics. We will later show that the ν takes the role of a Maslov index that tracks phase shifts at turning points when we extend the quantum mechanical formulation of this problem to the optical domain. We use the notation K_c rather than K to emphasize that the Van Vleck propagator, IX.25, solves the Schrödinger equation only when we make assumptions regarding the validity of classical mechanics. For now we'll simply state that the Van Vleck propagator is a very good approximation to Feynman path integrals for static potentials, provided that paths aren't too short.

The Bogomolny Operator and the Dome Cavity

In our initial attempts to describe mode mixing in the paraxial dome cavity,

the Bogomolny transfer operator seemed a promising avenue. However, we found that Cheng-Hung Chang had already quantized the scalar dome cavity using the transfer operator in the year 2003[4]. Chang quantized the cavity as an electron billiard, using the transformation mentioned earlier in this chapterIX.6. Chang put the surface of section on the top part of the dome as labeled in figure 9.3., from his article[4].

The action can be easily expressed in terms of the lengths of the two different

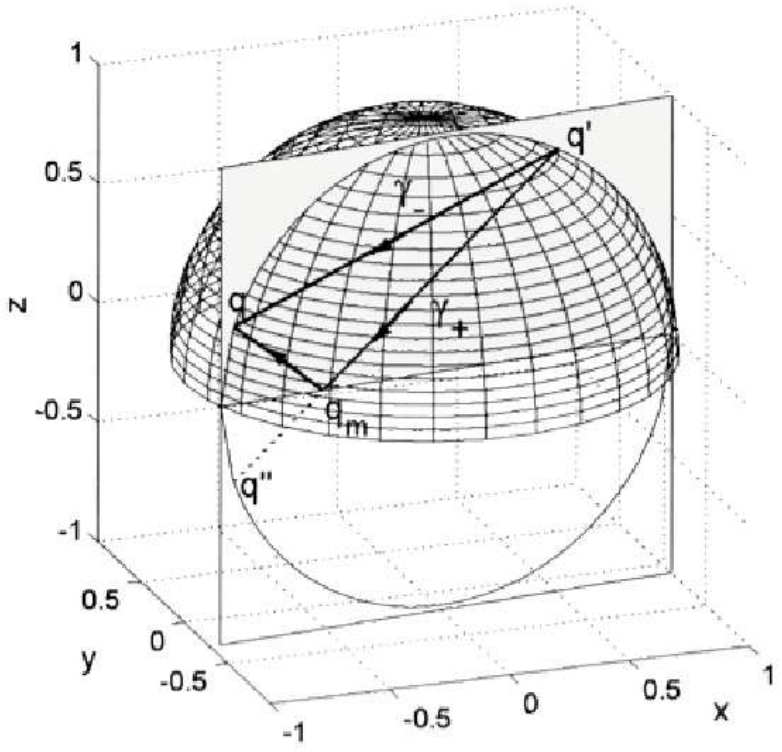

Figure 9.3. Two paths in the dome cavity, from reference [4]. There are two possible trajectories that connect initial and final points on the SOS.

ray paths that can travel from one coordinate on the SOS to another. An extra phase shift must be added to the reflecting path.

$$S_{\mp}(q'', q', E) = \sqrt{2mE} L_{\mp} \tag{IX.26}$$

The transfer operator takes the following form, where the phase shift, ν, for the reflecting path is double that of the straight path. There is a phase shift for each ray, because the rays must pass the SOS going in the same direction to count as a crossing.

$$\mathbf{T}_{\alpha\beta} = \frac{\Delta_{area}}{2\pi i\hbar} \sum_{L\pm} \sqrt{\left| det\left(\frac{\partial^2 S(q''_\alpha, q'_\beta, E)}{\partial q''_\alpha \partial q'_\beta} \right) \right|} exp(iS(q''_\alpha, q'_\beta, E)/\hbar - i\nu\frac{\pi}{2}) \tag{IX.27}$$

Once parameterized, we can grid up the dome into points, and form a matrix connecting points α and β. The resonance condition is met if the determinant of the identity minus the transfer matrix is zero.

$$det[\mathbf{I} - \mathbf{T}_{\alpha\beta}] = 0 \tag{IX.28}$$

Using Bogomolny's Operator to Continuously Deform Between Integrable Systems

We coded up Chang's results and found they agreed well with the integrable, half-sphere case. Subsequently, we decided to see how well the operator performed by continuously deforming from the half sphere, to half paraboloid, both integrable

cases. The deformed cavity between the two integrable cases, is non-integrable, and its phase space is chaotic. We wish to know the efficacy of the Bogomolny transfer operator in chaotic systems. If we can track a mode from one integrable system, to a different mode in another integrable system, then we can be confident that the operator adequately characterizes stable SOS islands in a chaotic system. The profile of the geometries we studied are depicted in figure 9.4..

The equation giving the cylindrical radius, $\rho(\theta, \phi)$ is the following:

$$\rho(\theta, \phi, d) = (\epsilon + 1)\left(-\frac{\cos(\theta)}{\sin(\theta)} + \sqrt{1 + \left(\frac{\cos(\theta)}{\sin(\theta)}\right)^2}\right) \tag{IX.29}$$

Where $0 < \theta < \frac{\pi}{2}$, and the ϵ is the deformation parameter, and $0 < \epsilon < 1$.

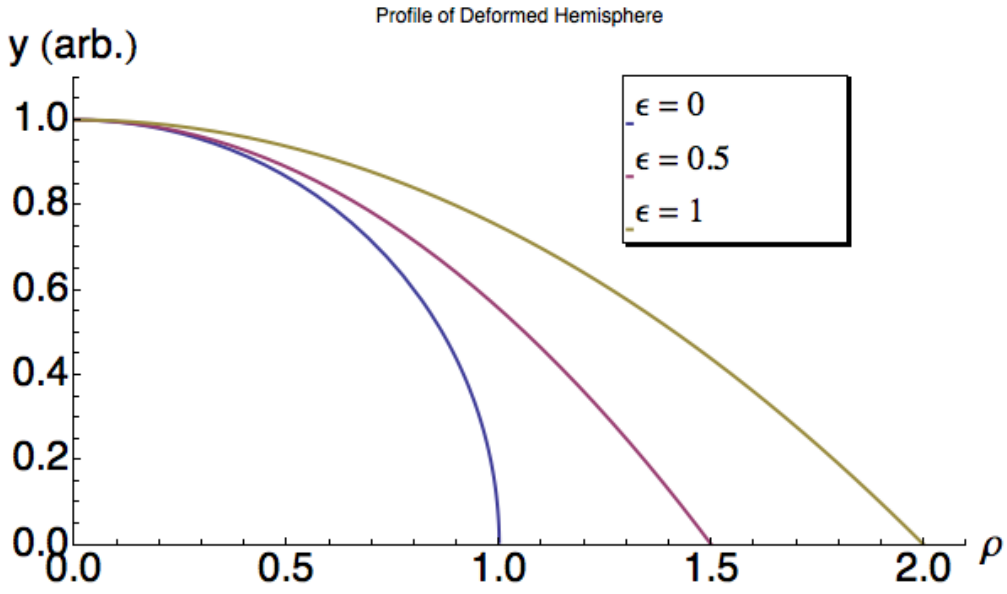

Figure 9.4. Graph depicting $y(\rho)$ vs. ρ as the cavity is deformed from one integrable geometry (spherical) to another (parabolic). The shape is defined in equation (IX.29).

$\epsilon = 0$ corresponds to the half sphere, $\epsilon = 1$ corresponds to the half parabola, and intermediate values of ϵ are nonintegrable cavities. The azimuthal angle, ϕ varies from 0 to 2π. We found that Bogomolny's transfer operator performed admirably, linking up modes from one integrable geometry to the next, shown in chosing zeroes of the transfer operator in figure 9.5..

In this approach, there was little evidence of avoidant crossings, but there seemed to be some irregularity in the zeros as we approached the half-paraboloid limit. This technique can be especially useful for quickly identifying the centers of

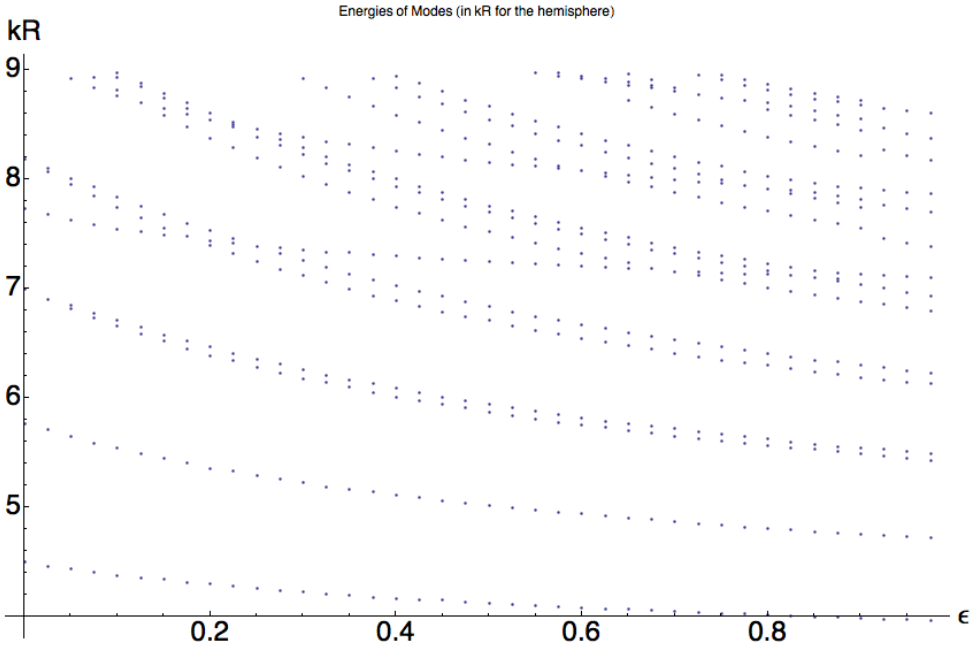

Figure 9.5. Zeroes of the transfer operator as the cavity is deformed from a spherical to parabolic geometry. The y axis is wavenumber, and the x-axis is the deformation parameter, ϵ. The hemispherical cavity corresponds to $\epsilon = 0$ and the parabolic cavity corresponds to $\epsilon = 1$, and the shape is described by (IX.29). The left axis gives correct exact energies for the hemisphere, and the right axis, $\epsilon = 1$, gives the correct exact energies for the half parabola.

stable islands in chaotic billiards, without the use of a monodromy matrix. When we discuss plotting chaotic phase space in color, in order to quickly identify related island chains, traversing an island directly from the edge to the center, and vice versa, is essential, otherwise, the neatly colored islands become a mess of static color, and one is unable to differentiate like from unlike island chains especially as the islands grow smaller and the cavity becomes more chaotic.

Bogomolny Operator in Ray Splitting Systems

One inspiration for solving the problem of extending the Bogomolny operator to vector space comes from the study of the transfer operator in ray-splitting systems, covered by several authors[47][48][5]. An example geometry of this system is shown in figure 9.6., discussed in in [5]. One feature of the ray splitting system that could be advantageous for treating polarization dependent problems is that a single ray will meet the SOS with a reduced amplitude than when it left the SOS, dependent on how much of the ray was transmitted and how much of the ray was reflected.

To add polarization to the Bogomolny operator, we can split the ray into s and p polarized components. A p polarized component of a ray will generally return to the surface of section as a ray that is both s and p polarized, with the amplitude of the p-polarized ray contained in each component. An s polarized ray will likewise be split into both s and p polarized components. The change in amplitude of an s or p polarized component can be treated in a way analogous to the change

in amplitude of the double the dimensionality of the Transfer matrix to account for both s and p polarized rays. Splitting a ray into components at the SOS is a method analogous to splitting TE and TM modes into s and p polarized components to solve the paraxial dome cavity problem. However, if such an approach works with the Bogomolny transfer operator, mode mixing can be handled in arbitrary cavity geometries.

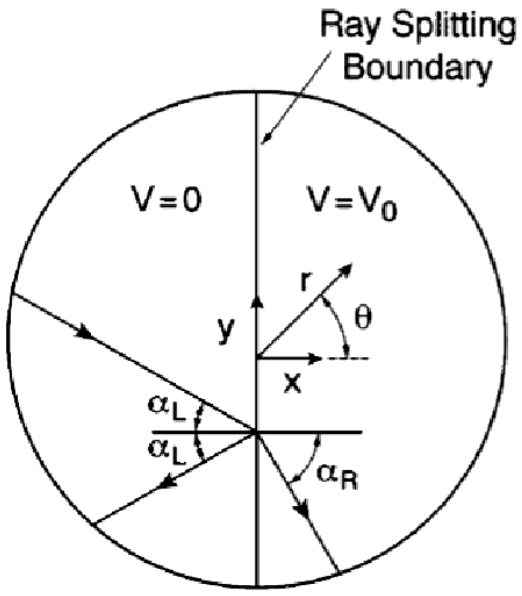

Figure 9.6. The geometry of ray-splitting in a scalar quantum system [5]. In an optical system, V is replaced by the index of the refraction, and angles $\alpha_{L/R}$ are determined via Snell's Law.

CHAPTER X

DRUDE MODEL FINITE SQUARE WELL MODES, WITH DISSIPATION

In this chapter, we wish to begin to explore practical ENZ systems in which electromagnetic waves emulate the quantum behavior of electrons in 1D systems. In this chapter, μ is taken as a constant, while ϵ follows the Drude model, and may vary spatially. This chapter will show that electromagnetic modes can only approach quantum "stationary states" if the refractive index is nearly real, or if disspation is offset by gain. This chapter will also show how the lifetime of trapped ENZ modes is limited by the imaginary part of ϵ.

The Drude Model

Materials with a permittivity described by the Drude model are extremely useful for manipulating optical signals. One frustrating feature of EM waves is that it is extremely difficult to trap photons in cavities for timescales approaching a second. This chapter suggests that optical confinement is impossible if the mirrors of a cavity have both finite real, and imaginary components of its permittivity. When imaginary components of a material's permittivity approach zero, this chapter will demonstrate that it is possible to hold wave packets for very long timescales. We will suggest that cavities can, in principle, be made isospectral with linear quantum

systems. The results we'll present are for a one-dimensional cavity. A Kramers-Kronig Drude model is considered in this chapter, where[30]:

$$\epsilon(\omega) = 1 - \frac{\omega_p^2}{\omega(\omega + i\gamma)} \tag{X.1}$$

To find modes with long lifetimes, in media where there is no gain, we want a material to have $\gamma \cong 0$. In this chapter we'll consider electromagnetic waves confined in one dimension between higher plasma frequency materials that act as mirrors. Waves propagate along the x-axis and Maxwell's equations for the transverse electromagnetic field take the following form[49][50]:

$$\frac{\partial}{\partial x} B_y = \frac{\epsilon(\omega)}{c} \frac{d}{dt} E_x \tag{X.2}$$

$$\frac{\partial}{\partial x} E_z = \frac{1}{c} \frac{d}{dt} B_y \tag{X.3}$$

This chapter will consider two different materials with a Drude permittivity (X.1). One material with $\epsilon = \epsilon_1$ has a plasma frequency ω_{p1}, and the other material has $\epsilon = \epsilon_2$ with a plasma frequency ω_{p2}. We assume $\omega_{p1} < \omega_{p2}$, allowing traveling wave solutions of frequency ω, where $\omega_{p1} < \omega < \omega_{p2}$. This sets up the finite square well geometry:

$$\epsilon(\omega) = \begin{cases} \epsilon_2(\omega) & \text{if} - a < x < a \\ \\ \epsilon_2(\omega) & \text{if} |x| > a \end{cases} \tag{X.4}$$

We can pick the following solutions for the time-varying electric field, provided that we pick a frequency that gives a positive permittivity if $|x| < a$, and a negative permittivity outside of the the central Drude material. The frequency, ω, can be complex, but k and α are positive and real.

$$E_1(x,t) = C_1 e^{kx} e^{i\omega t} \qquad x < a \tag{X.5}$$

$$E_2(x,t) = \left(A\cos(qx) + B\sin(qx)\right) e^{-\alpha x} e^{i\omega t} \qquad a < x < a \tag{X.6}$$

$$E_3(x,t) = C_2 e^{kx} e^{i\omega t} \qquad x > a \tag{X.7}$$

Since wave solutions only exist when the permittivity is real, the higher plasma frequency material acts as a mirror at $x = a$. Above the plasma frequency, these fields can still propagate. Our time-varying transverse magnetic fields are:

$$B_1(x,t) = C1\frac{ick}{\omega} e^{kx} e^{-i\omega t} \qquad x < -a \tag{X.8}$$

$$B_2(x,t) = \frac{icq}{\omega}\left(-\left(A + \frac{\alpha B}{q}\right)\sin(qx) + \left(B - \frac{\alpha A}{q}\right)\cos(qx)\right) \quad e^{-\alpha x} e^{-i\omega t} (-a < x < a) \tag{X.9}$$

$$B_3(x,t) = C2\frac{-ick}{\omega} e^{-kx} e^{-i\omega t} \qquad x > a \tag{X.10}$$

If we maintain continuity of the electric and magnetic fields at the boundaries, we find the following set of equations.

$$C_1 e^{-(k+\alpha)a} = A\cos(qa) - B\sin(qa) \tag{X.11}$$

$$C_2 e^{-(k-\alpha)a} = A\cos(qa) + B\sin(qa) \tag{X.12}$$

$$kC_1 e^{-(k+\alpha)a} = q((A + \frac{\alpha B}{q})\sin(qa) + (B - \frac{\alpha A}{q})\cos(qa)) \tag{X.13}$$

$$kC_2 e^{-(k-\alpha)a} = q((A + \frac{\alpha B}{q})\sin(qa) - (B - \frac{\alpha A}{q})\cos(qa)) \tag{X.14}$$

The $\alpha \to 0$ limit occurs if each region has a strictly real permittivity. In the $\alpha \to 0$ limit, the above equations are exactly the solutions for the finite square well that can be found in any undergraduate quantum mechanics text[51]. In Appendix B we show that slowly varying envelope solutions to Maxwell's equations provide the the same reflection and transmission coefficients as 1D quantum mechanics problems. Obtaining finite square well boundary conditions in a low loss limit of a Drude material is a stronger statement than that made in Appendix B. Here, we did not invoke the slowly varying approximation.

The surprisingly explicit symmetry between the approaches of QM and electromagnetism is broadly related to the fact that components of the magnetic field, times frequency, are partial derivatives of the electric field(X.2). In the ENZ finite square well, continuity of the electric electric field in the no-loss limit(X.11)(X.12), give us the same equations that ensure that a QM wave function is continuous in the finite square well. In quantum mechanics, ensuring flux conservation amounts to insuring that the derivative of a quantum mechanical

solution is continuous at the boundary. Because the components of the magnetic field can be expressed as derivatives of the electric field, the continuity equations for the magnetic field(X.13)(X.14) give us the same equations imposed by quantum mechanical flux conservation in the finite square well. Thus we will find both the frequency, and spatial amplitude dependence of the electromagnetic field agrees with quantum mechanics.

Drude Model Finite Square Well with Negligible Damping

The central difference that exists between real-world ENZ cavities and quantum mechanics problems is the fact that the electromagnetic permittivity for electromagnetic materials has both real and imaginary components. We will soon note the corrections to resonant wavelengths and trapping times due to a complex refractive index. First, we'll study solutions to the boundary conditions in the low loss limit. Combining the boundary conditions, we find:

$$AB + \frac{\alpha}{2q}B^2 \sin^2(qa) - \frac{\alpha}{2q}\cos^2(qa) = 0 \tag{X.15}$$

If ϵ_2 is real and $\alpha = 0$, the either the coefficient A or B must be zero. Thus, we have the same chose of even or odd solutions provided in the quantum mechanical finite square well. As in the quantum mechanical case, the even solution always exists.

$$k = \begin{cases} q \cdot \tan(qa) & \text{even} \\ -q \cdot \cot(qa) & \text{odd} \end{cases} \tag{X.16}$$

We'll concentrate on the even solution for the remainder of the paper. If α is real, but much smaller than q, the even solution has a small odd correction to the wavenumber. This occurs if there is an imaginary component to the permittivity in the cavity or in the mirrors.

$$\frac{k}{q} = \tan(qa) - \frac{1}{2}\frac{\alpha}{q}\sin(qa) + O((\frac{\alpha}{q})^2) \tag{X.17}$$

The correction to the wavenumber due to imaginary components of $\epsilon_2(\omega)$ usually insignificant, since solutions will usually occur where the tangent and cotangent curves have very large values. However, the exact correction can easily be calculated by matching intersecting curves in the same manner than we do in the case where there is no correction. In quantum mechanics, k and q are related by the depth of the potential well and the energy of the particle. In this electromagnetic problem, k and q are related by frequency. Maxwell's equations give us our permittivity-dependent dispersion relationships.

$$\omega^2 = \frac{(q^2 - \alpha^2)c^2 + 2\alpha q c^2}{\epsilon_2(\omega)} = \frac{-k^2c^2}{\epsilon_1(\omega)} \tag{X.18}$$

We will first assume that γ is negligible and demonstrate the overall form of solutions to equation X.16. In the next section, we'll show that a finite γ requires

a complex frequency and introduces decay of trapped wave packets. Taking the scattering-free limit:

$$\omega^2 = \frac{q^2c^2}{\epsilon_2(\omega)} = \frac{-k^2c^2}{\epsilon_1(\omega)} \tag{X.19}$$

As in the quantum mechanical case, intersections of the left and right hand sides of the above equation give us eigenmodes of the problem. The reason for this correspondence is outwardly simple. In the quantum mechanical case, q^2 and k^2 are both proportional to the absolute value of the bound particle's energy. Here, q^2 and k^2 are both proportional to square of the frequency of the electromagnetic wave. We will briefly note that we generally think of electromagnetic waves as having energies quadratic in frequencies and quantum systems having energies linear in frequency. However, in a plasma above the plasma frequency, we can express the total frequency as a sum of a large plasma frequency, and small Schrödinger frequency. In this case, $\omega^2\epsilon(\omega) = \omega^2 - \omega_p^2 = 2\omega_p\omega_s + \omega_s^2$. If $\omega_p >> \omega_s$, then the Schrödinger frequency varies in an approximately linear way with k^2 and q^2. Energy density in a classical plasma material will be briefly discussed in chapter XIV. For now, we will note that a quantum mechanical treatment of electromagnetic plasmons in a Drude material tells us that a plasmon's energy is proportional to $\hbar\omega$. This quantum energy of plasmons assumes the electrons in the plasma evolve according to Schrödinger's equation. We do see quadratic ω_s^2 corrections to k^2 in our ENZ plasma. However, we should also note that the energy of relativistic

quantum systems is actually quadratic in frequency, but for this to be noticeable, a particle must have a kinetic energy that compares appreciably with its rest mass. These show up as p^4 relativistic corrections in solutions to the KG equation or Dirac equation.

Going back to our solutions, the $\gamma = 0$ limit also allows us to simplify the expression for the permittivities of a plasma medium.

$$\epsilon_1(\omega) = 1 - \frac{\omega_1^2}{\omega^2} \tag{X.20}$$

Provided that we assume that $\epsilon_1(\omega)$ is a lossless plasma, and that the frequency of trapped wave is above the plasma frequency, we can rewrite equation (X.16) in a form identical to that found in the quantum mechanical square well problem:

$$\frac{\sqrt{\kappa - (qa)^2}}{qa} = \tan(qa) \tag{X.21}$$

In figure 10.1., κ is a dimensionless parameter and its value depends on the permittivity of the medium that allows for propagation.

Two forms of lambda are compared, one for free space, $\epsilon_2 = 1$ and one for the case when ϵ_2 is another plasma medium with a lower plasma frequency. If the central cavity is free space, the frequency of the mode, ω must be less than the surrounding plasma frequency, ω_1. In this case, κ is:

$$\kappa = \frac{\omega_1^2 a^2}{c^2} \tag{X.22}$$

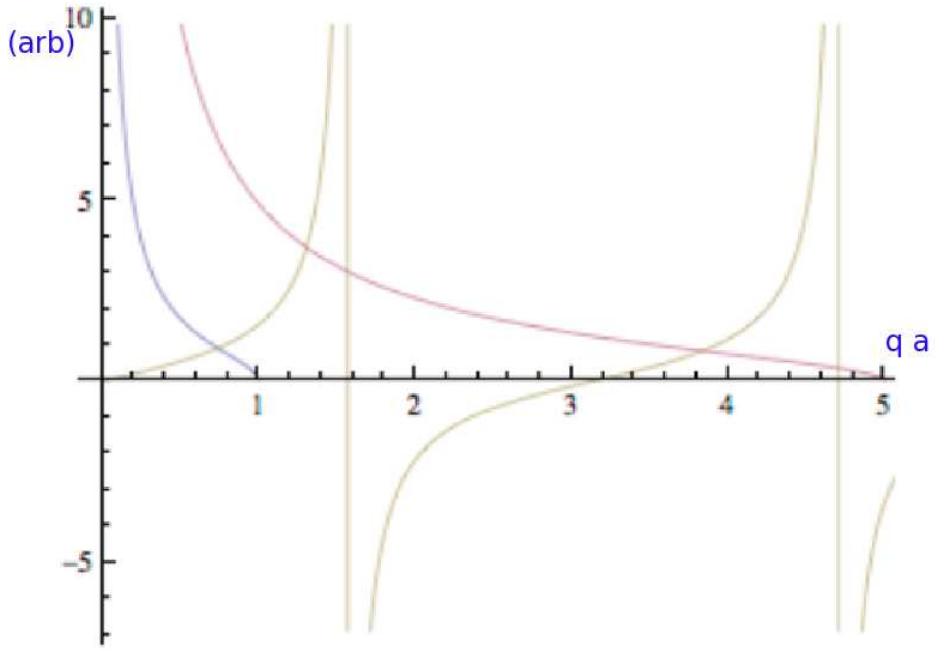

Figure 10.1. Even solutions to the electromagnetic finite square well, with negligible γ. The x-axis is (qa) And eigenmodes are at (qa) with intersecting curves. The blue curve has $\kappa = 1$ and the mauve curve has 5 times that value. The behavior of even and odd solutions are qualitatively and quantitatively similar to the quantum mechanical finite square well.

If the central cavity is composed of another scattering-free Drude material with plasma frequency ω_2, we can use the relationship $\omega^2 = q^2 + \omega_2^2$ along with a modified version of X.21, giving:

$$\frac{\sqrt{\kappa - (qa)^2}}{qa} = \tan(qa) \tag{X.23}$$

The $\alpha \to 0$ limit in which trapped ENZ boundary condidtions approach QM solutions is only reached if dissipation is offset by loss, or in the limit that the scattering rate vanishes, where $\gamma \to 0$. We will briefly note that microwaves

in superconductors obey the Drude model of ϵ and have the smallest imaginary permittivity for a system that allows electromagnetic waves. The Drude model for superconductors takes a somewhat more complicated form[49][50][52][53]:

$$\epsilon_{sc}(\omega) = \epsilon_c - \frac{\omega_{ps}^2}{\omega^2} - \frac{\omega_{pm}^2}{\omega(\omega + i\gamma)} \tag{X.24}$$

Tachiki and Bulaeveski's papers note that the scattering constant, γ, in the superconductor goes to zero as the temperature goes to zero[49][50]. The above model for ϵ is valid if the energy of photons kT is less than the energy required to break cooper pairs, and describes a lossless plasma combined with a plasma with finite damping. We can put the permittivity for superconductors in Drude form, if we exaggerate the role of damping and assume ω_p in (X.1), is given by $\omega_p^2 = \omega_{ps}^2 + \omega_{pm}^2$, and assume the low frequency permittivity constant $\epsilon_c = 1$. We note the Drude form of permittivity for mircrowaves in superconductors only to describe the material that appraoches the $\gamma \to 0$ limit.

Number of Supported Modes

As mentioned before, the trapped frequency must lie between the two plasma frequencies, above the central cavity frequency and below the frequency of the surrounding cavity.

$$\kappa = \frac{(\omega_1^2 - \omega_2^2)a^2}{c^2} \tag{X.25}$$

If the length of the cavity is constant, then a superconducting cavity medium will support a dramatically smaller number of modes than a free-space central cavity. The reason for this difference is that the phase velocity in the central plasma material will be extremely large if $\omega \cong \omega_2$. We can make the central cavity fairly thick, and still have it only support one even electromagnetic mode of a well-defined frequency. If we wish the cavity to support additional modes, we must pick a much larger cavity length, or lower plasma frequency, ω_2. Electromagnetic signals are typically very difficult to manipulate on the scale of the wavelength, since fabrication techniques will invariably produce imperfections on the scale of the free-space wavelength. An ENZ finite square well cavity can support fundamental modes when its dimension is much larger than the free space wavelength of microwaves that we seek to manipulate. Thus, ENZ plasma materials may allow us accurately filter electromagnetic signals by dramatically increasing a signal's wavelength. It is suggested that that we can use ENZ microcavities as effective nano-scale cavities. It should also be noted that such cavities may be ideal for manipulating extremely short pulses as well. The group velocity in a plasma medium close to the plasma frequency is almost zero. This is apparent in the dispersion relationship of a plasma medium [49] and has been experimentally demonstrated. The group velocity of of a plasma medium with nonlinearity will be discussed in more detail in chapter XIV.

Lifetime of a Finite Square Well Mode with Dissipation

When the scattering rate, γ, is non-zero, the Drude permittivity is complex. We'll take the same Drude model that we used before, but assume scattering is significant. Expanding the complex permittivity, we find:

$$1 - \frac{\omega_p^2}{\omega^2} + \frac{i\gamma\omega_p^2}{\omega^3} \tag{X.26}$$

In a generic, low temperature metal, γ is the inverse of the mean free collision time between electrons. The final term is a damping mechanism for the electromagnetic field, since the transverse electromagnetic field is carried by electron oscillations. If we allow the frequency, $\omega = \omega_r + i\omega_I$ to be complex, we can describe how quickly our modes decay with time. If ω_I is small, the amplitude of the field will changed negligibly with each cycle, and the earlier expressions for the even and odd form of the modes will remain the same. For now, we'll assume that there is no damping in the central cavity, but we'll still give that central field a complex wave vector so Maxwell's equations can be satisfied, For the field in the bounding Drude materials, we'll explicitly set $k = |k|$, so for $x > a$, $\mathbf{E} \propto Exp[-i(\omega_r + i\omega_I)t]$. Maxwell's equations (X.3) are still explicitly satisfied provided:

$$(\omega_r + i\omega_I)^2\epsilon(\omega) = -c^2k^2 \tag{X.27}$$

The imaginary part of the above equation yields:

$$2i\omega_r\omega_I + i\frac{\gamma\omega_1^2}{\omega_r} = 0 \tag{X.28}$$

Or:

$$\omega_I = \frac{-\gamma}{2}(\frac{\omega_1}{\omega_r})^2 \tag{X.29}$$

For the electromagnetic waves to be trapped, ω_r must be less than the plasma frequency. The lowest losses for trapped modes will occur at frequencies just below the plasma frequency. The constant γ, the scattering rate, is inversely proportional to the relaxation time $\gamma = \frac{1}{\tau_s}$. It should be noted that γ is not actually a constant in real materials, but has an additional quadratic dependence[54]. In pure, low temperature, non-superconducting metals, the relaxation time is on the order of $\tau_s = 10^{-9}$ seconds. The energy, U, of the field is proportional to its modulus squared. From this relationship we can obtain an expression for the quality factor.

$$U \propto e^{-(\omega/Q)t} \propto e^{-\gamma\frac{\omega_1^2}{\omega^2}t} \tag{X.30}$$

$$Q = \frac{\omega^3}{\gamma\omega_1^2} \tag{X.31}$$

The maximum Q occurs at in the vicinity of the plasma frequency.

$$Q_{max} = \omega_1\gamma = \omega_1\tau_s \tag{X.32}$$

For ultraviolet plasma frequencies, in pure, non-superconducting metals this gives a Q on the order of a million. However, the real promise of these cavities lies in divergence of Q in the regime where the relaxation time goes to zero. For the same reason that electrons don't scatter off of one another in a cavity, there is promise that coherent trapped modes of microwaves in superconducting cavities can persist for very long times. In the case of a superconducting medium in the central cavity, we can use the equation (X.18) to calculate the imaginary part of the frequency in the same manner as above, to obtain the same general result. However, if two Drude materials with mismatched plasma frequencies had different relaxation times of γ, the highest value would necessarily determine the lifetime of the mode. Without mapping a photon's quantum state to a particle's spin, electromagnetic waves can only be confined for a time proportional to the imaginary component of the permittivity. Explicitly, if the maximum photon confinement time allowed by Maxwell's equations is T_{max}, then:

$$T_{max}(\omega) = \frac{\omega}{2} Im[\epsilon(\omega)] \tag{X.33}$$

This sets an upper limit on the trapping a photon's quantum state in a box. Scattering off of wavelength-scale roughness could dramatically constrain the above relationship. However, in ENZ cavities, the effective wavelength is much larger than the free space wavelength. For this reason, if the interior of a cavity is a Drude material with a slightly different plasma frequency, the cavity will appear

to be optically smooth to the trapped mode. Currently, the maximum trapping time for photons between superconducting mirrors is on the order of a second[21]. This means that if one wishes to construct a a microwave analog of an electronic computer, all operations must be done in under a second, which is a relatively long timescale. Unfortunately, imaginary components of other materials are huge when compared to that of superconductors. In materials with high loss, some optical gain mechanism would need to be in place to offset loss without destroying the signal. Another application of ENZ cavities may be to act as optical buffers in quantum computers with superconducting qubits, entangled by microwaves. ENZ materials could act as buffers since the group velocity of a pulse can be slowed to zero at the plasma frequency. If the plasma frequency is lower with an intense pulse, the pulse can enter a central cavity. As intensity decays due to damping, the pulse could be trapped.

The boundary conditions used here can easily be extended to a quantum-like electromagnetic well in which two finite-width potential/frequency walls allow electromagnetic bound states to form in a central cavity. This would require the walls be thick enough to discourage escape by tunneling. However, to get the waves in the cavity in the first place may require shifting the plasma frequency of the surrounding medium slightly. One way to shift the plasma frequency in an ENZ plasma material is to dope the number of charge carriers, by applying a voltage to

the material. In chapter XIV, we will aslo explore the use of the Kerr nonlinearity to lower the effective plasma frequency.

Conclusion

Without electron-electron scattering, Maxwell's equations in an ENZ material mimic 1D solutions to quantum mechanics problems. Not only are the wave equations that govern the time evolution of the fields similar, but the boundary conditions imposed on these fields are identical, if we ignore dissipation. The presence of an electron relaxation and scattering term, however, reveals a significant difference between an electron in a potential and electromagnetic waves in cavity. Thus layered ENZ cavities described by the Drude model with small γ are ideal both for their high Q and their high phase velocity. Furthermore, we can insure that ENZ finite square well solutions support only a single, sharp, well-defined mode at a precise wavelength. The results for mode lifetimes in this section translate to cavities with geometries very different than the square well, by using the same technique of separating temporal and spatial parts of the electromagnetic wave.

CHAPTER XI

DERIVING DRUDE MODELS FOR DIRAC METAMATERIALS VIA A CONDUCTIVITY ANALOGY, WITH CAUSALITY CONSIDERATIONS

In this chapter, we will argue that employing a complex Drude model for both ϵ and μ give a very good approximation to vector analogs of the Dirac equation. This discussion is intended to give a physical motivation for using Drude models for ϵ and μ, rather than using the models obtained in chapter IV (IV.24). We will make this argument by pointing out that when we transform the Dirac equation to vector space, certain terms take the form of the conductivity term in Maxwell's equations. We will then discuss how the conductivity term in Maxwell's equations must be complex if a medium is to respond to fields in a non-instantaneous manner. We can then pick the limit in which a complex, causality-kosher term gives us the appropriate terms in the Dirac equation. We can use the non-approximated conductivity, now complex, and apply causality arguments. These semiclassical arguments assuming finite electron response times lead to the Drude formula for the wavenumber. In other words, if we transform the Dirac equation to vector space, certain terms are malformed, because they would describe a material responding instantaneously to fields. We can make these terms causal in the same way that we make Maxwell's equations obey causality for real fields. When we do so, however,

we are guided towards ϵ and μ parameters more frequently used in the metamaterial community. We undertake this approach because it is more physically motivated than simply expanding epsilon and mu about a plasma frequency and comparing one Taylor expansion to another. Also, in this treatment, we bring certain previously ignored aspects of the Dirac equation to the forefront.

In chapter IV we described how columns of the 4×2 quaternion matrix arising from Maxwell's equations could be superimposed into a 4-vector that was also a solution to the Dirac equation. We used this to suggest that solutions to the 4×4 Dirac Matrix acting on a 4 spinor could be related to solutions of the Dirac equation acting on a 4×2 quaternion Matrix that represents a vector field with electric and magnetic quadratures. In chapter IV, in which we introduced the quaternion matrix formalism, we dropped the conductivity term in Maxwell's equations. Soon, we'll suggest a reason why its inclusion may have been useful. First, recall the form of the Dirac equation acting on a 4-spinor with the 2 electron elements represented by ψ and the two positron elements represented by χ:

$$\begin{pmatrix} i\hbar\dfrac{\partial}{\partial t} - V - mc^2 & -c(\sigma \cdot \mathbf{\Pi}) \\ -c(\sigma \cdot \mathbf{\Pi}) & i\hbar\dfrac{\partial}{\partial t} - V + mc^2 \end{pmatrix} \begin{pmatrix} \begin{pmatrix} \psi_+ \\ \psi_- \end{pmatrix} \\ \begin{pmatrix} \chi_+ \\ \chi_- \end{pmatrix} \end{pmatrix} = 0 \qquad \text{(XI.1)}$$

In the above, it is important to note that the time derivative only acts on the first term in the diagonal element. The $\pm mc^2 - V$ terms contain no time derivatives.

In chapter IV, we supposed a time derivative that acted on the entire diagonal element of the Dirac matrix. If we want a vector system that is truly faithful to a vector analog of the Dirac equation, we must have terms in the diagonal elements of the Dirac matrix that aren't acted on by a time derivative. So, in this chapter, we will briefly explore a model in which vector fields better approximate the Dirac equation. However, we'll then argue that we need to invoke causality considerations, and this will make our solutions a little less like the Dirac equation, because it will give a complex element to our vector wave equation. Right now, we're going to take a mathematical step that might seem a little odd. Instead of working forward from Maxwell's equations to the Dirac equation, we're going to work backward from a quaternion formulation of the Dirac equation. At an intermediate step, it may appear that we have wound up in trouble. However, we assure the reader that we will emerge from this exercise unscathed. We will end up suggesting that a complex Drude model for both ϵ and μ is a very good way, probably the best way, to describe a Dirac metamaterial. The fact that loss and spectral shifts will be introduced to our model is of no grave concern; these features are an inescapable part of real-world electromagnetic cavities. Even more importantly, we should remind the reader that not even exact solutions to the Dirac equation exactly describe states of spinors in single-electron atoms. Quantum electrodynamics and path integrals introduce features like spectral shifts, and finite excited state lifetime. We will see qualitative analogs to these processes when we make our classical system

causal, though we can claim no quantitative correspondence. The reason we are taking this particular approach is to explicitly make a Dirac-like formulation of Maxwell's equations causal. This approach will transform an initially unfamiliar problem involving causality to a more familiar one: that of electrons responding to electromagnetic fields in a pure metal. Finding a connection to the Drude model isn't the purpose of this exercise, but a bonus.

As a starting point, let's undertake a thought experiment: let's say I present equation (XI.1), and don't tell you whether it's meant to describe actual point-particle spinor wavefunctions, or if it is meant to describe Maxwell's equations, and the 4-vector is a superposition of Jones vectors given by the columns of a quaternion matrix. One could check if (XI.1) is Maxwell's equations by replacing the 4-spinor by quaternion matrix, as follows:

$$\begin{pmatrix} i\hbar\dfrac{\partial}{\partial t} - V - mc^2 & -c(\sigma\cdot\mathbf{p}) \\ -c(\sigma\cdot\mathbf{p}) & i\hbar\dfrac{\partial}{\partial t} - V + mc^2 \end{pmatrix} \begin{pmatrix} (\vec{\sigma}\cdot\vec{\psi}) \\ (\vec{\sigma}\cdot\vec{\chi}) \end{pmatrix} = 0 \qquad \text{(XI.2)}$$

In the above formulation, we get get 2 equations that are symmetric when we block multiply the matrices, and make the substitution $\vec{\psi} \to \vec{\chi}$ except for the sign of the mc^2 term. One of the equations, for example, gives us:

$$(\vec{\sigma}\cdot\vec{\mathbf{p}})(\vec{\sigma}\cdot\vec{\chi}) = \frac{1}{c}(i\hbar\partial_t - V - mc^2)(\vec{\sigma}\cdot\vec{\psi}) \qquad \text{(XI.3)}$$

We can perform the same operation as we did going foward, $(\vec{\sigma}\cdot\vec{\mathbf{p}})(\vec{\sigma}\cdot\vec{\chi}) =$

$i\vec{\sigma} \cdot (\tilde{\mathbf{p}} \times \vec{\chi}) + \vec{\mathbf{p}} \cdot \vec{\chi}$. In this section, we will assume that $\vec{\mathbf{p}} \cdot \vec{\chi} \cong \vec{\mathbf{p}} \cdot \vec{\psi} \cong 0$. This assumption will put our vector wave equations in a form rougly similar to Maxwell's equations. In chapter XIII, we derived a vector wave equation version of the Pauli interaction Hamiltonian in order to look for a tensor refractive index that can make light bend, as if in response to a magnetic field. In chapter XIII, we assume that $\Pi \cdot \vec{\psi} = \Pi \cdot \vec{\chi} = 0$, where $\Pi = (-i\hbar\nabla - e\frac{\mathbf{A}}{c})$. This assumption results in a vector analog of the Pauli interaction Hamiltonian. Assuming that divergence is small or zero, the vector equations take the following form:

$$\nabla \times \vec{\chi} = \frac{i}{c}\frac{\partial}{\partial t}\vec{\psi} - \frac{mc^2 + V(\mathbf{x})}{\hbar c}\vec{\psi} \tag{XI.4}$$

$$\nabla \times \vec{\psi} = \frac{i}{c}\frac{\partial}{\partial t}\vec{\chi} - \frac{-mc^2 + V(\mathbf{x})}{\hbar c}\vec{\chi} \tag{XI.5}$$

We can perform one of several transformations to make the vector wave equations look more like Maxwell's equations:

$$\nabla \times (-i\vec{\chi}) = \frac{1}{c}\frac{\partial}{\partial t}\vec{\psi} + i\frac{mc^2 + V(\mathbf{x})}{\hbar c}\vec{\psi} \tag{XI.6}$$

$$\nabla \times \vec{\psi} = -\frac{1}{c}\frac{\partial}{\partial t}(i\vec{\chi}) + i\frac{mc^2 - V(\mathbf{x})}{\hbar c}(-i\vec{\chi}) \tag{XI.7}$$

The above equations are meant to loosely approximate $\mathbf{E}$ and $\mathbf{H}$ in a material. The far right terms of the above equations both look like current terms. Without magnetic monopoles, we could never hope to exactly match both of the above with Maxwell's equations. When we introduced the Dirac equation in chapter

IV, (IV.18), we used the same equations as above, but assumed that the time derivative acted on every term, giving us $\epsilon/\mu = 1 \mp \omega_p/\omega - V(r)/(\hbar\omega)$(IV.24). These parameters will still be justified in a certain limit. Also, we mentioned that a scalar term, of the form $\vec{\mathbf{p}} \cdot \vec{\chi}$, also needed to be satisfied to move from the quaternion equation to the curl equations, and this sets divergence conditions for each quadrature. The divergence condition means that the divergence of the right hand side of each of the above curl equations should be equal to zero. Let's take a moment to compare the $\nabla \times (i\vec{\chi})$ to the Curl[$\mathbf{H}$] term of Maxwell's equations:

$$\nabla \times \mathbf{H} = \frac{1}{c}\frac{\partial}{\partial t}\mathbf{E} + \frac{4\pi}{c}\sigma\mathbf{E} \tag{XI.8}$$

Here, we see a similarity between the current term in Maxwell's equations, and the $i\dfrac{mc^2 + V(\mathbf{x})}{\hbar c}\vec{\psi}$ term in the Dirac equation. We will find that if we make this analogy explicit, it only applies within a narrow frequency range. The closest analogy is an ultra-pure metal in which there are extremely long electron relaxation times. To make this analogy, we'll take a moment to review the conductivity term in Maxwell's equations.

Non-instantaneous Response of Conductivity in Pure Metals

In this section, as in the rest of the dissertation, we use cgs units, and follow the approach of Wooten[30]. We'll use a semiclassical model of the electrons. If a

field excites a given number of electrons, we assume that the number that have yet to experience a collision is given by:

$$n(t) = n(0)e^{-t/\tau} \tag{XI.9}$$

Where τ is the relaxation time. We'll assume that the electromagnetic field driving the electrons has the form of $\mathbf{E}_0 \exp[-i\omega t]$. We can find the average velocity, $\bar{v}$ of electrons by defining a response function, $G(t-t')$, that gives electrons $dv(t)$ increments of velocity in a dt' time increment:

$$G(t-t') = -\frac{e}{m}e^{-\frac{(t-t')}{\tau}} \tag{XI.10}$$

This gives an average electron velocity of:

$$\bar{\mathbf{v}} = \int_{-\infty}^{t} \mathbf{E}(t')G(t-t')dt' = -\frac{e\mathbf{E}}{m}\frac{\tau}{1-i\omega\tau} \tag{XI.11}$$

We can now relate the macroscopic conductivity to the electron velocity:

$$\sigma = \frac{-Ne^2}{m}\frac{\tau}{1-i\omega\tau} \tag{XI.12}$$

Since the plasma frequency, in terms of the number density is defined as:

$$\omega_p^2 = \frac{4\pi Ne^2}{m} \tag{XI.13}$$

We can characterize the complex conductivity of a metal as follows:

$$\sigma = \frac{\omega_p^2}{4\pi} \frac{\tau}{1 - i\omega\tau} \tag{XI.14}$$

For a moment, we'll take the limit in which the $V(\mathbf{x})$ term in the Dirac equation is small, or consider it part of a spatially varying plasma frequency. If we compare the $\frac{4\pi}{c}\sigma\mathbf{E}$ term in Maxwell's equations, to the conductivity-like term in the Dirac equation, we find:

$$i\frac{mc^2}{\hbar c} \cong \frac{1}{c}\omega_p^2 \frac{\tau}{1 - i\omega\tau} \tag{XI.15}$$

We can make this correspondence only in the limit of long relaxation times, where $\omega\tau >> 1$. And the equivalence between the two is reached only when $\omega \cong \omega_p$. What we have discovered is that if we wish to make a material analogy between the Dirac equation and Maxwell's equations, the complex conductivity term ends up being odd in omega. Giving the vector version of the Dirac equation the same kind of temporal behavior as Maxwell's equations with conductivity, means that we have to insert $(1 - i\omega t)$ in the denominator of the LHS of (XI.15). If we want $\vec{\Psi}$ and $\vec{\chi}$ to approximate real fields, with a response function given by (XI.10), then we have no choice but to use the RHS of (XI.15) in place of the LHS of (XI.15). If the response function does not decay exponentially, we would have to add gain terms to offset scattering loss. Therefore, real semiclassical field can only approximate the factor $i\frac{mc^2}{\hbar c}$ if $\omega\tau >> 1$, and $\omega \cong \omega_p$. This is not a statement about the Dirac equation,

but an assertion that causality imposes unavoidable limits the approximation of the Dirac equation with real, semiclassical vector fields.

If we want to give the curl equations (XI.7) a frequency response that agrees with a complex conductivity for metals, we necessarily deviate from exact solutions to the Dirac equation. Assuming $V(\mathbf{x}) = 0$, and $\omega_p = mc^2/\hbar$, we make the transformation:

$$i\frac{mc^2}{\hbar c} \rightarrow \frac{1}{c}\omega_p^2 \frac{\tau}{1 - i\omega\tau} \tag{XI.16}$$

Again, we'll assume the long lifetime limit, $\omega\tau >> 1$. If we want to move the modified term in (XI.7) into the time derivative, we have to divide it by $-i\omega$, since $\partial_t \vec{\psi} = -i\omega\vec{\psi}$. This is used to obtain a now-corrected refractive index for the right hand side of the $\nabla \times \vec{\chi}$ equation. We find:

$$\nabla \times \vec{\chi} = \frac{-i\omega}{c}\partial_t \epsilon \vec{\psi} \tag{XI.17}$$

This is the same semiclassical model for conductivity used to derive the Drude model for permittivity in pure metals. We find:

$$\epsilon = 1 + \frac{\omega_p^2 \tau}{-i\omega(1 - i\omega\tau)} \tag{XI.18}$$

If we divide by the relaxation time, then we can cast the above in terms of the scattering rate, $\gamma = \frac{1}{\tau}$. Doing so, we find we've arrived at the Drude model:

$$\epsilon(\omega) = 1 - \frac{\omega_p^2}{\omega^2 + i\gamma\omega} \tag{XI.19}$$

If we add considerations of causality, a Drude model is very necessary if we want to approximate the Dirac equation with Maxwell's equations. In chapter XIII, we use a Drude model for ϵ and μ, and show that it works fairly well. The above is an argument as to why it is necessary. Drude models for ϵ and μ, with loss, are used near-universally within the metamaterials community, especially for negative refractive index materials [8]. These models are used because they obey Kramers-Kronig relationships, which will be discussed in the next section.

Kramers-Kronig Relations for Real Vector Fields

In the last section, it was argued that the vector formulation of the Dirac equation needed to be modified to compare it to Maxwell's equations with a complex conductivity. This had the effect of making imaginary terms odd in powers of ω, which is a general principle for modeling permittivities and permeabilities in real materials. Also, in chapter IV, I asserted that we could represent 4-vectors obeying the Dirac equation as vector fields, and vice-versa. Do these two arguments combined mean that the Dirac equation must be fixed in the same way as Maxwell's equations to ensure causality? No; Kramers-Kronig relations don't describe spinor fields, which may spread outside of a potential, but don't decay in time. Furthermore, when the Dirac equation is transformed

to vector space, its causality constraints are not as stringent on those imposed on solutions to Maxwell's equations. One reason is that in order to force the Dirac equation into the form of Maxwell's equations, I forced the fields approximating electron and positron quadratures to be intrinsically complex. Without grouping an i with either the $\vec{\psi}$ or $\vec{\chi}$ field, curl equations can't be put in the same form as Maxwell's equations. And since either quadrature can be obtained by taking the curl of the other, they can't both be real fields. This implies that there are intrinsic extra degrees of freedom in vector formulations of the Dirac equation. Kramers-Kronig relations assume reality of of both **D**, and **E**, and likewise **B** and **H**. This assumption results in the rule that odd powers of frequency in ϵ and μ are multiplied by the imaginary number i and that even powers are real. This rule forbids real, odd in ω terms used in (IV.24). Here, we will follow the approach in Jackson[22] in deriving Kramer's-Kronig relations. If we assume that:

$$\mathbf{D}(\mathbf{x},\omega) = \epsilon(\omega)\mathbf{E}(\mathbf{x},\omega) \tag{XI.20}$$

It is not generally true that $\mathbf{D}(\mathbf{x},t) = \epsilon(\omega)\mathbf{E}(\mathbf{x},t)$. Instead, we will introduce a transfer function, $G(\tau)$, where:

$$G(\tau) = 1/(2\pi)\int_{-\infty}^{\infty}(\epsilon(\omega)-1)e^{-i\omega\tau}d\omega \tag{XI.21}$$

We'll further assume the transfer function is 0 at times less than t=0, at which point the incident field began to affect a particular part of the medium. So,

$$\epsilon(\omega) = 1 + \int_0^\infty G(\tau) e^{(-i\omega\tau)} d\tau \tag{XI.22}$$

Using the transfer function, we can find an expression for $\mathbf{D}(\mathbf{x}, t)$:

$$\mathbf{D}(\mathbf{x}, t) = \mathbf{E}(\mathbf{x}, t) + \int_0^\infty G(\tau) \mathbf{E}(\mathbf{x}, t - \tau) d\tau \tag{XI.23}$$

In order to obtain textbook Kramers-Kronig relationships for electromagnetic fields, we have to assume that $\mathbf{D}$, $\mathbf{E}$, and $G(\tau)$ are all real fields. If we do so, we arrive at the familiar relationship:

$$\epsilon(-\omega) = \epsilon^*(\omega^*) \tag{XI.24}$$

Generally, one assumes $G(\tau) \to 0$ as $\tau \to \infty$. This is not true for conductors where $G(\tau) \to \sigma$ as $\tau \to \infty$, allowing $\epsilon \to \frac{i\sigma}{\omega}$, as $\tau \to \infty$. Even if we want to crudely and semiclassically model vector fields that are isospectral to the Dirac equation, we can only do so with complex vector fields. We can see this by referring to (XI.7), and noting that $\vec{\chi}$ and $\vec{\psi}$ can't be simultaneously real. Since electromagnetic waves are constrained to be real fields, we find a number of arguments as to why we must use the Drude model to approximate (IV.24)

CHAPTER XII

IMPLEMENTING DIRAC METAMATERIALS USING DRUDE MODELS FOR EPSILON AND MU

Metamaterial Drude Models

Drude models for both epsilon and mu are most commonly used in the metamaterials community. With a Drude model for ϵ and μ, we can obtain the same leading-order behavior for the spin-orbit coupling and Darwin terms as Dirac metamaterials, but other relativistic corrections take on a slightly different form than those found in quantum systems. The most famous experiment that employed a metamaterial for simultaneously varying mu and epsilon was the first experiment to observe negative refractive index metamaterials[8]. This phenomenon was, of course, was demonstrated in a regime where both epsilon and mu were less than zero. Negative refractive index materials also have a Dirac-like regime, but this won't be discussed here. The model used in the negative refractive index experiment, commonly used in many others, is the following, its analog derived in a roundabout way in the last chapter(XI.19):

$$\epsilon(\omega, r) = \left(1 - \frac{(\omega_{ep}(r)^2 - \omega_0^2)}{(\omega^2 - \omega_0^2) + i\gamma\omega}\right) \tag{XII.1}$$

$$\mu(\omega, r) = \left(1 - \frac{(\omega_{mp}(r)^2 - \omega_0^2)}{(\omega^2 - \omega_0^2) + i\gamma\omega}\right) \tag{XII.2}$$

In the above, ω_0 is a resonance frequency, which can differ between the two parameters, but this will be unimportant for our purposes. We can pick either epsilon or mu to be near zero, and here we will chose epsilon. We should note that as long as wave solutions are permitted, and one parameter is near zero, the methods of chapter VI and VII are still perfectly valid for predicted spatial spin-orbit coupling and Darwin-term behavior. However, the constants before those terms will vary according to the size of one of the large parameter verses the other. We will be slightly more restrictive in this chapter, and make sure our perturbation terms have the same prefactors, at least to low orders in expansions.

Now, we'll make note of the following: In previous chapters, when we wanted correspondence to the Dirac equation, the large parameter μ was around 2, and varied slowly in frequency, where the small parameter was around zero. This is somewhat problematic, because most Drude models pick high frequency limiting values of μ around 1. There is one particular geometry of resonators that in which μ is near 2, and declining, where ϵ is 1, but we will stick to more generalizable examples. Earlier, we noted that most of the amplitude of the EM field was carried in the electric quadrature, and other than the refractive index, the magnitude of

the term $\frac{1}{\mu}\partial_r\mu$ affected the magnitude of spin-orbit coupling. This means that we can scale mu by any constant, and the spin orbit coupling term will be unchanged, but furthermore, we need to scale epsilon by the inverse of that constant so we don't change the magnitude of the refractive index. Explicitly we can make the transformation $\mu \rightarrow \frac{1}{\kappa}\mu$ while $\epsilon \rightarrow \kappa\epsilon$. Keeping this in mind, no matter what mu is when epsilon is zero, we can map the resulting wave equation onto the vector wave equations expressed in chapters IV through VII. Likewise, the equation for the **H** field is translated in a symmetric way because $(\epsilon)^{-1}\nabla\epsilon$ is unchanged. Here we can state a general principle: there are a huge range of materials that show Dirac-like spin-orbit coupling, and they are characterize by one parameter near zero, and similar spatial variation. In other words, mu or epsilon need not be $\pm$ 2 while the other parameter is zero in order for wave equation solutions to be formally identical, and isospectral near the plasma frequency, to wave equation solutions of the Dirac equation.

If we look our material parameters, XII.2, we see that we can either simultaneously vary the resonant frequency for each, or vary the plasma frequency for each to obtain a Dirac-like metamaterial. Most papers read by this author that derived magnetic resonant frequencies had resonant frequencies less than the magnetic plasma frequencies[55]. This affects both the choice of which parameters we should vary to produce a refractive index potential, and the degree to which the Drude models for epsilon and mu can match the refractive index that arises

from the Dirac equation. We should briefly note that the refractive index from the Dirac equation need not be a refractive index that affects a vector field, but a refractive index that affects a 2 spinor field, that arises from traditional textbook wave equation solutions to the Dirac equation[38].

To simplify the refractive index, we will assume both terms have the same resonance frequency. We can simplify the form of the refractive index to the following:

$$\epsilon\mu = \frac{(\omega^2 - \omega_{ep}^2)(\omega^2 - \omega_{mp}^2)}{(\omega^2 - \omega_0^2)^2} \tag{XII.3}$$

To simplify the above further, we'll pick non-spatially-varying magnetic plasma frequency to be about zero, while the electric plasma frequency will be large. We'll also pick a negligible resonant frequency. As mentioned earlier, this is wholly unnecessary, since we can map epsilon and mu onto the Dirac equation, but it simplifies the math. Specifically, $\omega_{mp}^2 \to 0 + f(r)$, and $\omega_{ep}^2 \to \omega_{ep}^2 + f(r)$.

$$\epsilon\mu = \frac{(\omega^2 - \omega_{ep}^2 - f(r))(\omega^2 - f(r))}{\omega^4} \tag{XII.4}$$

The Dirac equation gives the following refractive index:

$$n_{Dirac}^2(r,\omega) = 1 - \left(\frac{\omega_p}{\omega}\right)^2 - 2\frac{V(r)}{\hbar\omega} + \left(\frac{V(r)}{\hbar\omega}\right)^2 \tag{XII.5}$$

Earlier, we showed that with the above refractive index, obtained either from the Pauli equation, or by transforming the Dirac equation to vector space, we could exactly match the relativistic corrections of the hydrogen. These corrections are on the order of α^2 the Bohr energy, or to better than 1 part in 18,000 times the Bohr energy. Even with the refractive index given by the Drude models, we can match the relativistic corrections to the same order of accuracy.

If we expand (XII.4), we can begin to match leading order relativistic corrections in the refractive index obtained from a Drude equation in both mu and epsilon. To obtain the best fit, you would want to optimize f(r) by matching a Taylor expansion at a frequency of $\omega_p + \omega_s$. However, the small parameter dwarfs the large one by a ratio of $13.1/(5 * 10^5)$. Additionally, the relativistic corrections are near unmeasurable in modern metamaterial cavities. We undertake this exercise to emphasize that we're not kidding when we assert that electromagnetic systems can be tailored to behave like quantum systems, even taking into consideration the restrictions that Kramers-Kronig relationships impose on real vector fields. For these reasons, we can eyeball the equation and match the Drude refractive index to Dirac equation refractive index about the frequency $\omega = \omega_p$.

$$n_{Drude}^2 = 1 - \frac{\omega_p^2}{\omega^2} - \frac{2f(r)}{\omega^2}(1 + \frac{\omega_p^2}{\omega^2}) + \frac{f(r)^2}{\omega^4} \tag{XII.6}$$

We can now solve the following equation for f(r):

$$n^2_{Drude}(r,\omega_p) = n^2_{Dirac}(r,\omega_p) \tag{XII.7}$$

$$-2\frac{2f(r)}{\omega_p^2} + \frac{f(r)^2}{\omega_p^4} = -2\frac{V(r)}{\hbar\omega_p} + \left(\frac{V(r)}{\hbar\omega_p}\right)^2 \tag{XII.8}$$

If we choose $f(r)\dfrac{\omega_p}{2\hbar} = V(r)$, then the refractive index given by Drude models will only differ in the $V(r)^2/(mc^2)^2$ term, by a factor of 4. The other two terms in the refractive index expansion exactly match those given by the strange-looking, odd-in ω, *epsilon* and *mu* that we employed by direct analogy with the Dirac equation. Again, this difference is negligible unless the metamaterial analog of α^2 is much larger than $\dfrac{1}{137^2}$.

Here, that we have shown that simultaneous spatial variation of the electric and magnetic plasma frequency can produce Dirac-like quantum potentials. In practice, we can vary both plasma frequencies by changing the number of free conduction electrons. The square of the electric plasma frequency is directly proportional to the number density. Furthermore, the magnetic plasma frequency can be defined by the the amount of current that carried by sub-wavelength coils, which is most often changed by altering the number of coils in a sub-wavelength volume element[55][56]. However, if these coils are not connected, then we can change the amount of current carried by the coils by changing the relative number of electrons in coils in one area vs. those in another. Formally, if we want a lower plasma frequency, we apply a positive voltage to a volume or area element, and this creates an attractive potential. By applying a negative voltage, we can create a less attractive potential, or even a

repulsive barrier for light of a given frequency. This would require electrical leads going to different volume elements of the metamaterial. By applying voltage we could trap light, and subsequently release it. We should note that when we have varying charge density, there will be an extra charge density term in the divergence condition for the electric field. In spherical coordinates, this would require the use of vector spherical harmonics with non-zero divergence.

Conclusion

In this chapter, we aimed to illustrate that any ENZ system can be intelligently mapped onto wave equations given by the Dirac equation. We furthermore illustrated that replacing the Dirac version of epsilon and mu with the Drude model for each parameter results in a very small shift that can be constructed to differ only slightly from the relativistic result. The purpose of this exercise was to show that even if we change the form of epsilon and mu by altering a term proportional to an inverse power of omega, we can still accurately map a quantum system onto an optical one. In the example outlined in this chapter, we would need to apply different voltages to different metamaterial elements to make ENZ attractive potentials on the fly. In the next chapter, we will ask how can we make light, in a metamaterial curve as if under the influence of a strong magnetic field.

CHAPTER XIII

USING A TENSOR INDEX OF REFRACTION IN A METAMATERIAL TO APPROXIMATE THE EFFECT OF A UNIFORM MAGNETIC FIELD FOR LIGHT

For spinor solutions to the Dirac equation to describe electrons under the influence of magnetic fields, it is necessary to replace the momentum operator with the canonical momentum operator: $(\vec{\sigma} \cdot \mathbf{p}) \rightarrow (\vec{\sigma} \cdot \mathbf{\Pi})$. We would like to describe electromagnetic waves in a cavity bending, as if under the influence of a magnetic field. If a quantum device employs a magnetic field, we would like to know how a pseudo-magnetic metamaterial could spoof a magnetic field for charge-free electromagnetic waves.

Once again, we will use the vector formulation of the Dirac equation to construct this analogy. And once again, we will take the same approach as we did in previous chapters. We will first take liberties and attempt to model a spinor process with vector fields as accurately as possible. Having done so, we will then find the closest possible metamaterial analogy to the quantum process, one that is in strict accordance with Maxwell's equations. We take this approach because it is easier to model a process if you give yourself more freedom, rather than less freedom. In our initial unconstrained model, we will explain why certain terms correspond

to quantum terms by pointing out term-by-term which quantum perturbations are analogs to which terms in the vector wave equation. In this particular case, we will initially ignore the divergence conditions of Maxwell's equations to obtain a vector wave equation isospectral to the quantum one. Imposing a particular set of divergence conditions on our system introduces additional constraints. When we impose these constraints, solutions to Maxwell's equations will become less like solutions to the Pauli interaction Hamiltonian. But, we will argue that certain essential features and terms remain. With the approach of first describing a highly accurate model and then imposing constraints, we can show which features in an optical system are necessarily different from those in a spinor system. In essence, we will initially sidestep a problem, and later fix it having gained additional insight with a tangential approach. For example, in the last chapter we showed that we can approximate some relativistic perturbation terms very well by using the Drude model, but the optical system will then be off by a factor of 4 for terms that take the form $V(r)^2/(mc^2)^2$, that are α^2 smaller than principal quantum energy levels. Since we understand the system that has better agreement, we know why we can't do better with Drude models. In chapter V we found that the angular momentum dependence of the spin-orbit operator acting on optical modes has a different angular momentum dependence than when it acts on electrons. However, we can see which divergence conditions forbid and allow a closer correspondence.

The canonical momentum operator is $\Pi = (-i\hbar\nabla - e\frac{\mathbf{A}}{c})$, for negative charge

carriers, where e is the magnitude of a Coulomb. Using Helmholtz potentials, the vector potential $\mathbf{A}$ is part of both the electric and magnetic quadratures of our field. For example $\mathbf{E} = -\nabla V - \frac{1}{c}\frac{\partial \mathbf{A}}{\partial t}$. When all is said and done, we will assert that the curl of the vector potential, representing the magnetic field, can be spoofed by making a tensor ENZ refractive index. In practice, $\mathbf{A}$ will be related to metamaterial parameters, and will not be an independent field. We could insert $\mathbf{A}$ into the Dirac equation represented in terms of $(\vec{\sigma} \cdot \mathbf{E})$ and $i(\vec{\sigma} \cdot \mathbf{H})$, but we will not use this convention because it the reader may be confused and assume that a change in the magnitude of $\mathbf{A}$ changes the magnitude of the electric and magnetic quadratures, and this is not at all what we are suggesting. Also, to be clear, spinor fields in the Dirac equation are distinct from electromagnetic fields, though they are coupled in the QED Lagrangian.

We will begin with the approach outlined in earlier chapters to obtain vector fields isospectral to the Dirac equation. We replace scalar, 2 component spinors with with vector fields in quaternion form. If ψ is an electron spinor and χ is a positron spinor, we transform the full Dirac equation (with vector potentials) to vector initial conditions by making the substitutions: $\psi \to \vec{\sigma} \cdot \vec{\psi}$ and $\chi \to \sigma \cdot \vec{\chi}$.

$$\begin{pmatrix} \hbar\omega - V - mc^2 & -c(\sigma \cdot \mathbf{\Pi}) \\ -c(\sigma \cdot \mathbf{\Pi}) & \hbar\omega - V + mc^2 \end{pmatrix} \begin{pmatrix} (\sigma \cdot \vec{\vec{\psi}}) \\ i(\sigma \cdot \vec{\chi}) \end{pmatrix} = 0 \qquad \text{(XIII.1)}$$

Once again, the diagonal elements will correspond to effective epsilon and mu parameters, and we consider these models as only valid near the plasma frequency

for electromagnetic fields. To appropriately deal with them in metamaterials with real fields, the elements should be approximated by Drude models for epsilon and mu. This can be done with the approach outlined in the previous chapter. Once again, we will use spherically varying material parameters, but we chose spherical potentials only to simplify the example. So, here, $\epsilon_d/\mu_d = 1 \mp \frac{\omega_p}{\omega} - \frac{V(r)}{\hbar\omega}$, and where the diagonal elements in the Dirac equation above are $\hbar\omega\epsilon_d$, and $\hbar\omega\mu_d$ respectively. At the end, we will make this vector wave equation obey solutions to Maxwell's equations. After this final transformation, we will then be able to roughly associate $\vec{\sigma}\cdot\vec{\psi}$ with $\vec{\sigma}\cdot\mathbf{E}$, and $i\vec{\sigma}\cdot\vec{\chi}$ with $i\vec{\sigma}\cdot\mathbf{H}$.

As a starting point, we use the same approaches outlined in previous chapters and transform the Dirac equation to vector space. Here, we find that the following vector wave equation relationships can be obtained if $\mathbf{\Pi}\cdot\vec{\psi} = 0$ and $\mathbf{\Pi}\cdot\vec{\chi} = 0$, yielding the following curl equations:

$$\nabla\times\vec{\psi} - \frac{ie}{\hbar c}\left(\mathbf{A}\times\vec{\psi}\right) = i\frac{\omega}{c}\left(1+\frac{mc^2}{\hbar\omega}\right)\vec{\chi} - \frac{iV}{\hbar c}\vec{\chi} = \frac{i\omega}{c}\mu_d\vec{\chi} \tag{XIII.2}$$

$$\nabla\times\vec{\chi} - \frac{ie}{\hbar c}\left(\mathbf{A}\times\vec{\chi}\right) = -i\frac{\omega}{c}\left(1-\frac{mc^2}{\hbar\omega}\right)\vec{\psi} + \frac{iV}{\hbar c}\vec{\psi} = \frac{-i\omega}{c}\epsilon_d\vec{\psi} \tag{XIII.3}$$

The equations above can be recast as a very complex tensor refractive index iff we know which vector fields satisfy the wave equation without a vector potential. To do so for the first equation, $(\mathbf{A}\times\vec{\psi})$ can be moved to the right hand side, and the second equation can be used to solved to express $\vec{\psi}$ solely in terms of $\vec{\chi}$, giving

a tensor μ. The $(\mathbf{A} \times \vec{\chi})$ can also be moved to the right hand side of the second equation, and expressed in terms of $\vec{\psi}$ to give a tensor epsilon. A constant B field can give a simplified vector potential. This means we would translate $(\mathbf{A} \times \vec{\chi})$ to a particular tensor refractive index for a particular mode. However, all other modes would not be shifted in energy in the appropriate way. This is useful only if we know the mode that we wish to shift with the metamaterial addition of a fake magnetic field. If we choose a particular $\vec{\chi} = R_{nl}(r)\mathbf{Y}^{j}_{lm}$ to shift a particular $\vec{\psi}$ mode in a quantum way, all other modes will experience shifts that don't correspond to the Dirac equation. In real atoms, the vector potential is produced when spinor fields make a quantum mechanical current, so if the spinor is excited to a higher energy level, the vector potential will also change. Since our vector potential itself is related to metamaterial parameters, we have no such freedom.

However, for now we will assume, in our semiclassical vector model, that $\mathbf{A}$ and V are meant to evolve by Maxwell's equations, and we will see where the analysis takes us. The terms $1 \pm \dfrac{\omega_p}{\omega}$ acts like free space permeabilities and permittivities for massive electron/positron-like vector fields in the absence of the electromagnetic force.

Vector Analog of the Pauli Interaction Hamiltonian

Next, we look for a vector wave equation that describes these fields; we will find

that the above satisfy a vector Laplacian where the gradient of the divergence of the vector field is nonzero.

$$\nabla \times \nabla \times \vec{\psi} - \frac{ie}{\hbar c} \nabla \times \left(\mathbf{A} \times \vec{\psi} \right) = \frac{i\omega}{c} \left(\mu_d (\nabla \times \vec{\chi}) + \nabla \mu_d \times \vec{\chi} \right) \tag{XIII.4}$$

The two vector product identities expanding $\nabla \times (\mathbf{A} \times \mathbf{B})$ and $\nabla(\mathbf{A} \cdot \mathbf{B})$ can be combined to form:

$$\nabla \times (\mathbf{A} \times \mathbf{B}) = \nabla(\mathbf{A} \cdot \mathbf{B}) - \mathbf{A} \times (\nabla \times \mathbf{B}) - \mathbf{B} \times (\nabla \times \mathbf{A}) - 2(\mathbf{A} \cdot \nabla)\mathbf{B} + \mathbf{A}(\nabla \cdot \mathbf{B}) - \mathbf{B}(\nabla \cdot \mathbf{A}) \tag{XIII.5}$$

In terms of our fields, we find:

$$\nabla \times (\mathbf{A} \times \vec{\psi}) = \nabla(\mathbf{A} \cdot \vec{\psi}) - \mathbf{A} \times (\nabla \times \vec{\psi}) - \vec{\psi} \times (\nabla \times \mathbf{A}) - 2(\mathbf{A} \cdot \nabla)\vec{\psi} + \mathbf{A}(\nabla \cdot \vec{\psi}) - \vec{\psi}(\nabla \cdot \mathbf{A}) \tag{XIII.6}$$

We can substitute the above into the vector wave equation:

$$\nabla \times \nabla \times \vec{\psi} -$$
$$\frac{ie}{\hbar c} \left(\nabla(\mathbf{A} \cdot \vec{\psi}) - \mathbf{A} \times (\nabla \times \vec{\psi}) - \vec{\psi} \times (\nabla \times \mathbf{A}) - 2(\mathbf{A} \cdot \nabla)\vec{\psi} + \mathbf{A}(\nabla \cdot \vec{\psi}) - \vec{\psi}(\nabla \cdot \mathbf{A}) \right)$$
$$= \frac{i\omega}{c} \left(\mu_d (\nabla \times \vec{\chi}) + \nabla \mu_d \times \vec{\chi} \right) \tag{XIII.7}$$

After many steps with no approximations (in appendix G) we find the following:

$$
\begin{aligned}
&(-\nabla^2 - \frac{\omega^2}{c^2}\epsilon_d\mu_d)\vec{\psi} \\
&= \frac{\nabla\mu_d}{\mu_d} \times \left(\nabla \times \vec{\psi} - \frac{ie}{\hbar c}\left(\mathbf{A} \times \vec{\psi}\right)\right) \\
&+ \frac{ie}{\hbar c}\left((\nabla \times \mathbf{A}) \times \vec{\psi} - 2(\mathbf{A} \cdot \nabla)\vec{\psi}\right) - \frac{e^2A^2}{\hbar^2c^2}\vec{\psi}
\end{aligned}
\tag{XIII.8}
$$

It should be noted that we did chose the Coulomb gauge, and the vector Laplacian has a non-zero grad div term. One important feature of this new vector wave equation is that the new states are the j!=l vector spherical harmonics, which give an spin-orbit splitting like that of electrons. We can multiply through by $\hbar^2/2m$ to put the above wave equation in Schrödinger form:

$$
\begin{aligned}
&\frac{\hbar^2}{2m}(-\nabla^2 - \frac{\omega^2}{c^2}\epsilon_d\mu_d)\vec{\psi} \\
&= \frac{\hbar^2}{2m}\frac{\nabla\mu_d}{\mu_d} \times \left(\nabla \times \vec{\psi} - \frac{ie}{\hbar c}\left(\mathbf{A} \times \vec{\psi}\right)\right) \\
&+ \frac{ie\hbar}{2mc}\left((\nabla \times \mathbf{A}) \times \vec{\psi}\right) - \frac{ie\hbar}{mc}(\mathbf{A} \cdot \nabla)\vec{\psi} - \frac{e^2A^2}{2mc^2}\vec{\psi}
\end{aligned}
\tag{XIII.9}
$$

If we express the above in terms of vector spherical harmonics, we obtain a scalar wave equation that is a vector the Pauli interaction Hamiltonian for a spinor electron interacting with an electromagnetic field. The extra term that appears in the spin-orbit term also arises from the spinor Dirac equation if we don't make the approximation that the vector potential is zero. The $\nabla \times \mathbf{A}$ term is equal to the magnetic field $\mathbf{B}$, if we assume that $\mathbf{A}$ and V are the vector and scalar

components of the electromagnetic field in the Coulomb gauge. This magnetic field has the same magnitude as the quantum case. Since the magnetic field field in the hydrogen atom can be approximated by $\mathbf{B} = \nabla \times \mathbf{A} = (\mathbf{v} \times -\nabla\phi(\mathbf{r}))/c$, and $v \cong \alpha c/n$ in the hydrogen atom, we expect the magnetic field term to dominate over relativistic corrections for large magnetic fields.

Modifying the Vector Interaction Hamiltonian for a Tensor Metamaterial

Earlier, we mentioned that expressing the Dirac equation in terms of vector fields gave us terms that were not transverse. Now, we would like to take our final vector wave equation, and fix it to allow for transverse electromagnetic modes. Specifically, the equation we don't like are $\mathbf{\Pi} \cdot \vec{\psi} = 0$ and $\mathbf{\Pi} \cdot \vec{\chi} = 0$, which gives a similar divergence equation for each quadrature: $\nabla \cdot \vec{\psi} = \dfrac{-ie}{\hbar c}\mathbf{A} \cdot \vec{\psi}$. However, we used this relationship to obtain the non-divergent vector Laplacian found in our vector interaction Hamiltonian. We would like to make the transformation $\nabla^2\mathbf{E} \rightarrow \nabla \times \nabla \times \mathbf{E}$. So, we'll simply manually invoke this transformation in our vector wave equation. Also, for now, we'll assume that $\nabla \times \mathbf{A}$ is large, meaning that there is a large magnetic field, and that this term dominates the vector interaction Hamiltonian. If we make these assumptions, we can obtain a modified transverse vector interaction Hamiltonian with the following form:

$$\nabla \times \nabla \times \mathbf{E} - \frac{\omega^2}{c^2}(\epsilon\mu - \frac{c^2}{\omega^2}\frac{ie}{\hbar c}(\mathbf{B_{fake}} \times \mathbf{E})) = 0 \qquad \text{(XIII.10)}$$

We'll also make the assumption that we're near the plasma frequency to fix the magnitude of the magnetic term:

$$\nabla \times \nabla \times \mathbf{E} - \frac{\omega^2}{c^2}(\epsilon\mu - \frac{c^2}{\omega_p^2}\frac{ie}{\hbar c}(\mathbf{B_{fake}} \times \mathbf{E})) = 0 \tag{XIII.11}$$

A tensor refractive index is often used in optics if phase velocities are different along different optical axes. We'll use a tensor refractive index for a different purpose. To see that we have the form of a tensor refractive index if we express the curl operation as a matrix, and pick a fake metamaterial magnetic field in the z-direction, B_z. If our scalar refractive index is $n_0^2 = \epsilon\mu$, for any value of epsilon or mu, and $\hat{\mathbf{I}}$ is the identity matrix, then our modified tensor refractive index is the following:

$$\hat{n}^2 = n_0^2\hat{\mathbf{I}} + i\kappa B_z \begin{pmatrix} 0 & -1 & 0 \\ 1 & 0 & 0 \\ 0 & 0 & 0 \end{pmatrix} \tag{XIII.12}$$

Where κB_z defines the magnitude of the fake magnetic field. One important thing to note about the magnetic tensor, is that its components are imaginary, but have different sign. Imaginary components of different sign in a scalar refractive index correspond to gain or loss, depending on the sign. The above tensor refractive index tells us that when there is loss along the x-axis, there is an equal and opposite gain for the field along the y-axis, and vice versa. This means that if an incident

field is polarized along the x-axis, it will gradually decrease in intensity along that axis, but y-axis polarization components increase in intensity. This is the result that we were hoping to find. We wanted light traveling in one direction to bend in response to the fake magnetic field, without increasing or decreasing the magnitude of the Poynting vector.

A Metamaterial Analog for a Constant B-Field for EM Waves

How could we implement such a metamaterial system? If an antenna is parallel to the x-axis, it absorbs electromagnetic energy as a field passes over it. We want this energy to be re-radiated in an orthogonal direction. So, the x-axis antennae must cause a y-axis antenna to emit radiation. This can be accomplished by making the center of the antenna an inductor that wraps around the y-axis antenna. Current in the inductor will drive a current in the y-axis antenna. We also want the y-axis antenna to absorb radiation and emit it along the x-axis. For this reason, there must be an inductor near the center of the y-axis antenna that wraps around the x-axis antenna. If we want light to bend sharply, we would need lots of antennas with large inductive couplings. Why might such a system be useful? Let's suppose we want an electromagnetic wave to bend at right angles with minimal reflective losses, in a small photonic circuit. Here, we propose that such a scheme is realizable.

CHAPTER XIV

NONLINEAR EFFECTS IN ENZ METAMATERIALS

This chapter begins a discussion regarding the Kerr nonlinearity in ENZ metamaterials. In this section, the Kerr nonlinearity is treated approximately, and equations for group velocity are also only approximate. No exact solutions to the nonlinear wave equation are described. This chapter suggests ways that the Kerr nonlinearity can be used that are unique to ENZ materials. However, all results should be considered approximate and preliminary. This discussion focuses on using the Kerr nonlinearity to lower the effective plasma frequency for an ENZ material. In chapter XII, we described how changing the plasma frequency could be used to switch optical signals. By changing the plasma frequency of an ENZ material, we can create a cavity where none was before, or create an optical barrier where none was before. Unfortunately, this method relies on electrical signals to control light. All-optical switching of optical signals has long been a goal of physicists and engineers. Most telecommunications signals are amplified, buffered, and routed by changing the signal to an electronic signal, before changing the signal back into a pulse of light. All-optical switching would allow optical signals to be processed by other beams of light, skipping the conversion to an electronic signal. However, some kind of optical or optical-mechanical nonlinearity

is necessary to perform all optical switching, and the nonlinear part of an optical signal is usually very small compared to the linear part. In this chapter, we will discuss the Kerr effect and approaches to quantizing nonlinear effects in optical cavities. We will assert that the Kerr nonlinearity plays the role of the $2V(r)/(\hbar\omega)$ refractive index term discussed in most chapters of this book, except it is always attractive, and always a short-range potential. We will discuss attempts to extend the ray-based quantization methods in chapter III to quantize an oversimplified nonlinear system. We will also discuss how chaos makes ray-based quantization methods very difficult in non-integrable systems, and show early results. We will begin by noting that Maxwell's equations with a nonlinear Polarization response yield:

$$\nabla \times \nabla \times \mathbf{E} - \frac{\omega^2 n^2}{c^2}\mathbf{E} = \frac{4\pi\omega^2}{c^2}\mathbf{P}_{NL} \tag{XIV.1}$$

We expand the nonlinear polarization in powers of intensity. Most generally, each $\chi^{(n)}$ component is a tensor. In this chapter we'll only deal with the Kerr nonlinearity and assume it is a scalar. Furthermore, we'll assume one central frequency dominates the problem. For ϵ to be near zero, a narrow frequency range is required. Also, in ENZ materials, waves of modestly different frequency propagate with radically different group velocities and phase velocities. Expanding the nonlinearity in different powers of the electric field without consideration of dispersion is a risky endeavor. The second order nonlinearity vanishes for most

crystals, and we'll concentrate on the Kerr nonlinearity, which is always present in any electromagnetic medium. For us, $\mathbf{P}^{NL}(\omega) = \chi^{(3)}|\mathbf{E}(\omega)|^2\mathbf{E}(\omega)$. In this approximation, we assume that matching conditions are such that 3rd harmonic generation is negligible. No oscillator is completely linear, and this is true for electrons in materials when acted upon by light. The polarization response of a material can be expanded in powers of ω, but for all but non-centro-symmetric crystals, the $\chi^{(3)}$ component of the nonlinearity, proportional to the cube of the electric field, is the dominant non-vanishing component. Typically, the linear part of the refractive index of a material is on the order of one, and thus even in materials with a large $\chi^{(3)}$ nonlinearity, a very intense field is required for the nonlinear part of the refractive index. Usually, it is advantageous to increase the intensity of light to study all-optical nonlinear effects. However, more intensity requires more energy, so typical approaches to this problem involve concentrating light in small mode volumes. Photonic crystal fibers and surface plasmons are often used to create such localized and intense fields. However, photonic crystal fibers can often be expensive. High frequency surface plasmons decay rapidly in time because part of the plasmon is in a medium that doesn't independently allow propagating wave solutions. However, there are a number of reasons why ENZ materials can provide an excellent nonlinear medium, and a few technical hurdles that must be respected. We note again that solutions to (XIV.1) are very approximate in nature, and have not been tested with numerical models.

We'll begin this discussion by briefly noting the refractive index of an ENZ material with a Kerr nonlinearity. In this section, we'll assume that the permeability is 1, as in most metals, and that the refractive index is entirely determined by the permittivity. If light in the cavity is dominated by a single frequency, we can move the Kerr nonlinearity into the refractive index as follows:

$$n^2(x,\omega) = 1 - \frac{\omega_p^2 - 4\pi\chi^{(3)}\omega^2|E(x,\omega)|^2}{\omega^2 + i\gamma\omega} \tag{XIV.2}$$

Here, we will treat the damping, γ, as independent of temperature and intensity. If we do so, we should group the Kerr term in the numerator, rather than treating it as a strictly real term. Otherwise, the effect of damping will be entirely independent of the intensity of the field. This is especially important as the linear part of the refractive index approaches zero near the plasma frequency. However, keeping the intensity term strictly real will not affect any arguments that we present here. The first reason that ENZ materials are ideal nonlinear materials is simply because the linear part of the refractive index is small. Relative to the linear part, the nonlinear part of the refractive index takes on an increasing importance. As seen above, when $1 - \frac{\omega_p^2}{\omega^2}$ trends to zero, the nonlinear term and the loss term are all that remains. In an ENZ material, the nonlinear component of the refractive index is important even at a modest field intensity. Also, we can see from the above that $4\pi\chi^{(3)}\omega^2|E(x,\omega)|^2$ appears in the same place that that we reserved for an attractive potential in previous chapters. In previous chapters, we made cavities with smoothly varying refractive indexes that served the purpose of bending light

towards the center of the cavity. In the presence of the Kerr nonlinearity, light creates its own cavity, and bends rays towards regions of greater intensity.

Group Velocity and the Kerr Nonlinearity

The fastest way to calculate the group velocity in a Drude material is to invert the partial derivative of the wave vector with respect to the frequency. Ignoring polarization effects, the scalar wave equation gives us:

$$k = \frac{\omega n}{c} \tag{XIV.3}$$

We can take the Kerr type refractive index given above, (XIV.2), assume the damping compared to frequency, γ/ω, is small, and find $\left(\frac{\partial k}{\partial \omega}\right)^{-1}$, which yields:

$$\frac{\partial \omega}{\partial k} = \frac{c\sqrt{1 - \frac{\omega_p}{\omega^2} + 4\pi\chi^{(3)}\mathbf{E}^2}}{1 + 4\pi\chi^{(3)}(\mathbf{E}^2 + \omega\mathbf{E}\frac{\partial \mathbf{E}}{\partial \omega})} \tag{XIV.4}$$

The Kerr term in the denominator, $4\pi\chi^{(3)}\mathbf{E}^2$, drops out because it is small compared to 1. However, $4\pi\chi^{(3)}\omega\mathbf{E}\dfrac{\partial \mathbf{E}}{\partial \omega}$ may remain if the frequency is large enough. Dropping terms much less than 1, we find an expression for the group velocity:

$$v_g = \frac{\partial \omega}{\partial k} = \frac{c\sqrt{1 - \frac{\omega_p^2}{\omega^2} + 4\pi\chi^{(3)}\mathbf{E}^2}}{1 + 4\pi\chi^{(3)}\omega\mathbf{E}\frac{\partial \mathbf{E}}{\partial \omega}} \tag{XIV.5}$$

The quantity $1 - \dfrac{\omega_p^2}{\omega^2}$ is near zero but negative. When $4\pi\chi^{(3)}\mathbf{E}^2 = \left|1 - \dfrac{\omega_p^2}{\omega^2}\right|$, the group velocity will be equal to zero, but this can occur before the intensity of the pulse is equal to zero.

If we couple a wave from a high index material into an ENZ waveguide, the signal is compressed in the propagation direction, resulting in an additional enhancement in the energy density per unit volume. In order to couple a signal from a high refractive index material to an ENZ material, it is necessary to gradually vary the index of refraction from $n > 1$ to $n \cong 0$, or we will experience substantial reflection losses due to the near zero refractive index. If we do couple into an ENZ material adiabatically, we find a high energy density per unit volume despite the high phase velocity. If a signal starts in a medium with a group velocity on the order of the speed of light, and ends propagating with a group velocity close to zero, the tail of the signal will be closer to the lead of the signal, resulting in a net increase in $\mathbf{E}(\mathbf{x}, \omega)$. Thus, there are two features of ENZ materials that enhance nonlinear effects: an increase in energy density, and a near-removal of the linear component of the index of refraction.

We can use the enhanced nonlinear effects of ENZ materials to create a low-power all-optical switch. To test this, we could split a signal in the arms of an interferometer, in which each arm is an ENZ material. A tiny shift in the refractive index in one of the arms of any interferometer can determine whether there is constructive or destructive interference at the output port of the interferometer. Let us suppose that one arm of our interferometer is immediately adjacent to another ENZ waveguide, which will act as a switch. This waveguide must be separated only on the order of a wavelength to allow tunneling between the waveguide and

the arm. The intensity of radiation in the switch waveguide will then alter the intensity of radiation in one arm of the interferometer. Thus, the presence, or absence, of radiation in the switch waveguide can result in a signal appearing in the output port of the ENZ interferometer. This is similar to a diode, which allows for the propagation of electrical current based on a bias voltage, which acts as a switch. Our optical interferometer can also act as a switch for other ENZ interferometers, allowing for rudimentary all-optical signal processing. Using nonlinearity in interferometers as as switch is not new, but we argue here that ENZ materials are specifically well tailored to the task. Very recently, switching using ENZ gratings, with substantial nonlinear effects, was demonstrated by Nader Engheta and Andrea Alú[57].

We should briefly note that it is important to pick ENZ materials with a relatively small imaginary component of ϵ, where ϵ is zero. Some materials, like silver, have a peak in the imaginary component of the refractive index near the ENZ regime[58]. In cases, where the imaginary component is large, it would be preferable to keep the ENZ region of a waveguide short, to avoid loss. The other advantage to keeping a relatively short ENZ region is when one wants to decrease the time required to switch signals with low group velocities. Other metamaterial ENZ resonators, however, have very small imaginary components of ϵ where μ is near zero[59]. In the case of designed ENZ materials, loss can be limited by

keeping a separation between the resonant frequency and the plasma frequency of a material.

The third reason that ENZ materials are good nonlinear materials is that we can create ENZ cavities that are optically smooth. For a photon in in an $n \cong 1$ medium, a defect that is on the scale of the wavelength, will be much smaller than the wavelength in an ENZ material, thus limiting scattering losses due to surface roughness. Furthermore, in cavities, photons have more time to interact further enhancing the nonlinear effect.

Pulse Slowing in Response to Loss

In this section, we will explore the possibility that wave packets in an ENZ medium may stop completely with non-zero intensity. The arguments presented are preliminary, and more research is necessary before we can authoritatively make this claim. We can view the numerator of Kerr-type refractive index, (XIV.2) as a spatially varying plasma frequency $\omega_{p-effective} = \omega_p^2 - 4\pi\chi^{(3)}\omega^2|\mathbf{E}(\mathbf{x},\omega)|^2$. A wave packet in an ENZ medium carries with it a lower plasma frequency than the surrounding medium. Thus, an intense ENZ pulse can propagate through a medium even if its frequency is slightly below the plasma frequency. Here, we can illustrate an interesting feature related to modest loss in an ENZ material. If the frequency of a wave is less than the plasma frequency when a sufficient Kerr-nonlinearity is present, it can propagate through the medium, due to the locally lowered plasma

frequency. However, the pulse will experience loss as it travels. As the pulse loses intensity, the group velocity will decrease. This raises an important question: can a pulse stop in a medium because the Kerr nonlinearity decays to a threshold value, resulting in a refractive index of zero, even if the intensity is not yet zero? The Kerr nonlinearity can keep the refractive index positive if the intensity of the pulse is large, but the group velocity hints that the refractive index, and group velocity, could equal zero before the intensity is zero. From equation (XIV.5) we can see that the near-zero group velocity will get closer and closer to zero as the intensity decreases, and can equal zero if we chose a frequency such that $1 - \omega_p^2/\omega^2 < 0$, or $\omega_s < 0$.

In this discussion, we must take extra care to recognize that any pulse must be spectrally broad if it has a finite width. In chapter X, we described the exponential-in-time decay of a trapped wave packet due to the imaginary component of the refractive index. However, assuming a near-single frequency pulse is strictly valid only for cavities. We must check to make sure the assumption is justified in a propagating pulse. Therefore, we must consider multiple frequencies near the plasma frequency to construct our pulse. Here, we will consider a Gaussian pulse, and follow the derivation in reference [51]. Also, we will assume propagation only in the x direction, and temporarily ignore the polarized nature of the electromagnetic wave. This approach is by no means rigorous, because it involves superimposing electromagnetic waves in a nonlinear medium, so in the next section, we will

essentially treat the nonlinear part of the refractive index as if it were linear. This is arguably permissible, but only if we time evolve the pulse for time scales that see negligible change in the wave envelope, which propagates at the group velocity.

The Gaussian pulse will be altered because waves near the front edge of the pulse are slowed, and waves near the back edge of the pulse are accelerated, due to repulsion from areas of high phase velocity in areas of low intensity. With a linear superposition, we won't see this effect. While we don't expect the pulse shape to be maintained, we do expect this to give a reasonable estimate of the group velocity stopping condition, which we will compare to the stopping condition obtained from soliton solutions. Additionally, Gaussian wave packets can lead to Gaussian solitons [60], which give good agreement with exact Sech soliton solutions. For now, this approach will address the non-monochromatic nature of the pulse in a very dispersive, lossy, medium. Taking the very rough approximation that the pulse can be approximated as a superposition, we find:

$$E(x,t) = \int_{-\infty}^{\infty} g(k) \exp i(kx - i\omega(k))t dk \tag{XIV.6}$$

Here, we'll assume a Gaussian function in k space: $g(k) = \exp[-\alpha(k-k_0)^2]$. The width of the Gaussian wave packet in position space will initially be equal to $\sqrt{\alpha}$. This will result in the familiar relationship that a broad spectrum in wavenumber will produce a narrow pulse in position space and vice versa. To construct a Gaussian pulse, we will expand the frequency of a plane wave as a

function of wave number, about a central wave number, and assume the pulse is relatively localized in wave number:

$$\omega(k) \cong \omega(k_0) + (k - k_0)\left(\frac{d\omega}{dk}\right)_{k_0} + (k - k_0)^2\left(\frac{d^2\omega}{dk^2}\right)_{k_0} \tag{XIV.7}$$

Localizing the wave number in the ENZ pulse, requires that it be broad in time, since the wavevector will vary substantially at the plasma frequency. Above, we can see the group velocity $v_g = \frac{d\omega}{dk}$. The second expansion parameter will describe the expansion of the wave packet in time, and we'll label it: $\beta = \frac{d^2\omega}{dk^2}$. As in chapter X, we will allow frequency to be complex to allow the wave to decay in the presence of a complex refractive index. If $k' = k - k_0$, we can derive our Gaussian pulse as follows:

$$E(x,t) = e^{i(k_0 x - \omega(k_0)t)} \int_{-\infty}^{\infty} e^{\alpha k'^2} e^{ik'(x - v_g t)} e^{ik'^2 \beta t/2} dk' \tag{XIV.8}$$

Solving this integral gives:

$$E(x,t) = e^{i(k_0 x - \omega(k_0)t)} \left(\frac{\pi}{\alpha + i\beta t}\right)^{1/2} \exp[-(x - v_g t)^2/(4(\alpha + i\beta t))] \tag{XIV.9}$$

In an ENZ material, this describes a wave traveling with a very fast phase velocity, inside a Gaussian envelope moving at a very slow group velocity. The group velocity is given by XIV.5, and above we can see that the group velocity

goes to zero, the Gaussian envelope stops moving. We can also estimate the rate of spreading of the pulse, which again, is only valid in the linear limit:

$$\beta = \frac{dv_g}{dk} = \frac{dv_g}{d\omega}\frac{d\omega}{dk} = c^2\frac{\omega_P^2}{\omega^3} \cong \frac{c^2}{\omega_p} \tag{XIV.10}$$

We derived the imaginary component of the frequency from the complex Drude model in chapter X, X.29, and found that it is proportional to the scattering rate, $\omega_I = \frac{\gamma}{2}$. Due to damping, modulus squared of the electromagnetic field decreases in time:

$$|E(x,t)|^2 = \exp[-\gamma t]\left(\frac{\pi^2}{\alpha^2+\beta^2t^2}\right)^{1/2}\exp[-(x-v_gt)^2/(2(\alpha^2+i\beta^2t^2))] \tag{XIV.11}$$

We take care to remember that we choose a Schrödinger frequency that was negative in sign, so that the frequency of propagation in the bulk is less than the plasma frequency. Since $v_g = nc = c\sqrt{\frac{-2|\omega_s|}{\omega_p} + 4\pi\chi^{(3)}|E(x,t)|^2}$, we realize that the Gaussian wave envelope will stop moving before the field has reached zero intensity!

In 1-D isotropic nonlinear media, there are also exact soliton solutions for the envelope of the electromagnetic wave. These solutions are very accurate so long as the wave envelope slowly varies, which is true if the group velocity is much less than the phase velocity. The derivation for the nonlinear Schrödinger equation can be found in "The Principles of Nonlinear Optics" by Y.R. Shen[61], and virtually any other nonlinear optics book. We will outline the results here,

using Shen's conventions for the refractive index and soliton solutions. First, the electromagnetic field is separated into an x-dependent part and a transverse spatial profile $\mathbf{E} = \mathbf{F}(\rho)A(x,\omega)\exp(i(kx - i\omega)t)$. Next, it is assumed that the envelope, $A(x,\omega)$ varies slowly over the spatial coordinate, and second derivatives in the spatial coordinate are thrown out. This is a very similar approach to that used to derive the Schrödinger equation from the KG equation in chapter II, except we only threw out second derivatives in the envelope with respect to time. Not simplifying the spatial pulse dependence was important in chapter II, because the fundamental modes varied on the scale of the Coulombic cavity. The result of the more traditional nonlinear optics approach is the following, exactly solvable, envelope equation:

$$\left(\frac{\partial}{\partial x} + \frac{1}{v_g}\frac{\partial}{\partial t}\right) A(x,t) = -i\frac{\partial v_g^{-1}}{2\partial\omega}\frac{\partial^2}{\partial t^2}A(x,t) - i\frac{8\pi^2\omega^2}{ikc^2}\chi^{(3)}|A(x,t)|^2 A(x,t) \quad \text{(XIV.12)}$$

The fundamental, single soliton, solution for the envelope takes the form:

$$A(x,t) = \frac{1}{T}\sqrt{\frac{ikc^2}{16\pi^2\omega^2\chi^{(3)}}\frac{\partial v_g^{-1}}{\partial\omega}}sech(\frac{t - v_g x}{T}) \quad \text{(XIV.13)}$$

Above, T is the width of the hyperbolic secant pulse, which propagates unchanged, as long as there is no loss. This equation assumes no loss, and the total pulse area integrated over time is constant, given by the equation $Area = \int_{-\infty}^{\infty} A(x,t)dt$. With the Gaussian approximation, we found that the

pulse stopped moving when the refractive index and group velocity reached zero. Soliton solutions for the wave envelope also approach a group velocity of zero as the refractive index goes to zero. The unusual feature of ENZ materials is that the group velocity has such a radical dependence on the intensity of the pulse. In any other material, when the nonlinear part of the refractive index decays, the index of refraction and group velocity are still larger than zero. This analysis is preliminary, and serves to motivate further research into the possibility that intense pulses can be frozen in place in an ENZ medium with a Kerr nonlinearity.

Here, we propose an experiment, with relevant, time-dependent frequencies illustrated in figure 14.1.. One could send a pulse into a plasma medium at a frequency just below the plasma frequency. The plasma medium could be just thick enough so no signal arrives from a single pulse. However, if a second, higher intensity pulse is sent at a later time, before the first signal has decayed, both signals could arrive on the other side. If the second pulse has a known, but different pulse shape than the first, a resulting signal would not look like either of the input pulses. Of course, since the nonlinearity is significant in a Kerr medium, the resulting signal cannot possibly be a true superposition of either pulse. In the accompanying figure, we roughly expect a pulse to hit a wall when the Kerr nonlinearity is in equal magnitude to $1 - \frac{\omega_p^2}{\omega^2}$, where the pulse frequency, ω, is less than the plasma frequency.

The process we describe is somewhat analogous to stopping pulses using

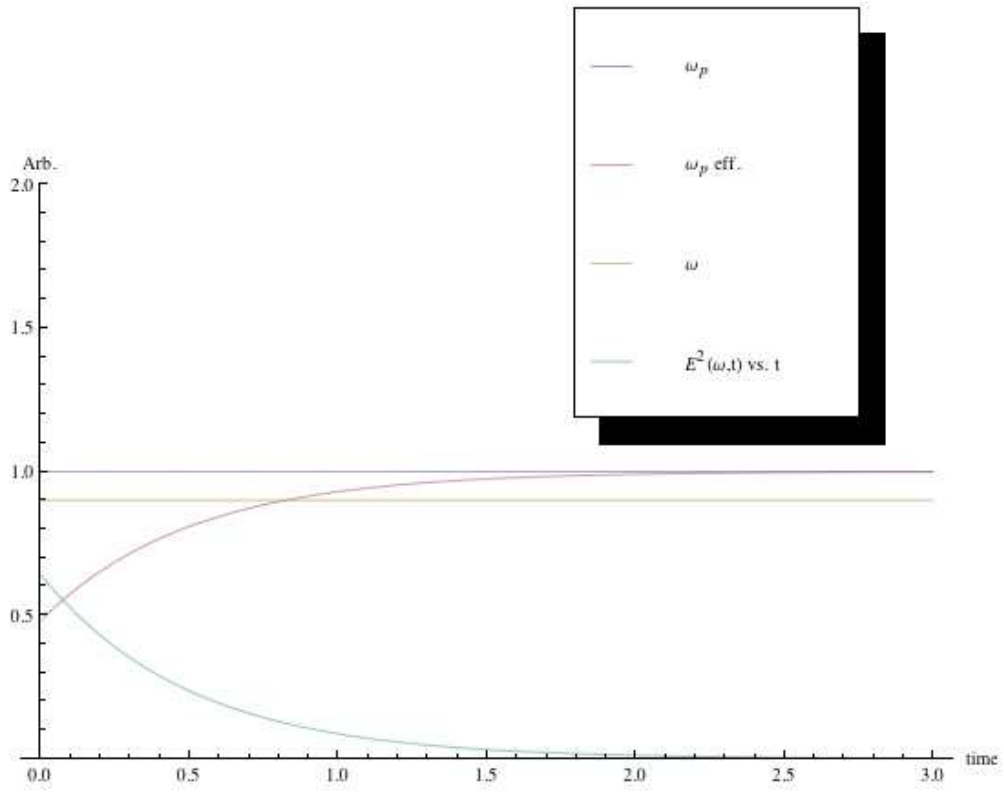

Figure 14.1. This figure displays an exaggerated change in effective refractive index as a pulse propagates through a Kerr medium, undergoing loss due to imaginary components of the refractive index. At the point in time where the effective plasma frequency exceeds the frequency of a pulse, it can no longer propagate. This crossing occurs here when time, in arbitrary units approaches 1.

electromagnetically induced transparency [EIT][62]. In this case, however, the pulse stops on its own accord, but requires another pulse to be freed. An often-touted benefit of EIT is that it may one day allow for all-optical buffering of telecommunication signals, so this experiment may be of interest to those outside the academics community with the development of telecom wavelength ENZ metamaterials.

In the above discussion, we ignored the transverse spatial profile, and we will only briefly touch on it here. As in any Kerr medium, sufficient intensity results in self-focusing is present in the transverse beam. ENZ materials represent the radical extreme of self-focusing, and this is another way in which ENZ materials are unique.

The focal length for a self-focusing Gaussian beam, when the linear component of the refractive index is small, is given by[61][63]:

$$z_f = \frac{kw^2}{\sqrt{P/P_{crit} - 1}} \tag{XIV.14}$$

In the limit of a vanishing linear refractive index, $P = cw^2|E(x,\omega)|^2$ and $P_{crit} = c/(k^2 4\pi\chi^{(3)})$, where w is the Gaussian beam width, and k is the very large wave number.

$$z_f = \frac{kw^2}{\sqrt{w^2k^2 4\pi\chi^3 - 1}} \tag{XIV.15}$$

If the beam power equals the P_{crit}, the transverse component of the Gaussian pulse is unaltered, but at modestly high intensities in ENZ materials, the beam very rapidly will collapse to a point, since the wave number and wave vector are simultaneously large due to a vanishing refractive index.

Deriving the Energy of Modes in a Kerr-type Medium

We will begin by recalling that Drude materials can be made isospectral the KG equation, if we ignore spin:

$$\nabla^2\Psi - \frac{1}{c^2}{\partial_t}^2\Psi = \frac{{\omega_p}^2}{c^2}\Psi + \frac{2\omega_p}{\hbar c^2}V(r)\Psi \tag{XIV.16}$$

In chapter II, we showed that the KG equation can give us the refractive index necessary to arrive at the Schrödinger equation. In appendix F, we will derive the result that the KG equation gives us an approximate way to solve single electron problems in the Dirac equation, if we ignore the effects of quantum mechanical spin-orbit coupling. While above Ψ is a 4-spinor, henceforth, we'll just treat it as a scalar function, knowing that we've already dropped spin-dependent terms from the Dirac equation. Furthermore, in chapter II we derived the Schrödinger equation from the KG equation. The Schrödinger equation is useful because solutions to the nonlinear Schrödinger equation, with a Kerr-type nonlinearity, have a known energy. We will show that the energy of the nonlinear Schrödinger equation in an electromagnetic Kerr-type medium can be related to the nonrelativistic energy of quantum mechanical problems. We will soon find that the energy of modes in 1D ENZ potentials has a correspondence to the quantum mechanical energy of electrons in 1D potentials. First, we'll recall that we reduced the KG equation to the Schrödinger equation in chapter II:

$$-\frac{\hbar^2}{2m}\nabla^2\psi(\mathbf{x},t)+V(r)\psi(\mathbf{x},t)=i\hbar\frac{\partial}{\partial t}\psi(\mathbf{x},t) \tag{XIV.17}$$

If we were solving a scalar quantum mechanical problem, with normalized solution $\psi_0(x,t)$ and we added a perturbation potential to $V(\mathbf{x})=V_0(\mathbf{x})+V_{pert}(\mathbf{x})$, we would simply take the overlap integral of the perturabtion potential to find the new energy:

$$\Delta E=\int \psi_0(\mathbf{x},t)^* V_{pert}(\mathbf{x})\psi_0(\mathbf{x},t)dV \tag{XIV.18}$$

This approach suggests that a perturbation theory estimate for a Kerr nonlinearity can be obtained by simply treating it as a spatially varying perturbation potential, and integrating over it. In the optical case, since the Kerr nonlinearity is proportional to the square of the electric field, the perturbative estimate for the energy shift should be proportional to the field to the square of intensity of the field. Most perturbative methods for solving Kerr nonlinearity start with soliton solutions, and perturb those solutions. Since the ENZ cavities that we have discussed are wavelength scale, we know that at low intensities, the Kerr nonlinearity will perturb the cavity field, rather than the other way around. Furthermore, we have yet to find 3D soliton solutions in the cavities discussed thus far. Fortunately, the nonlinear Schrödigner [NLS] equation gives us integrals of motion for the energy and norm. We'll start with the 1D nondimensional NLS, with a 1D potential following the conventions of Bishop[64]:

$$\psi_{xx} + \gamma|\psi|^2\psi - V(x)\psi = -i\psi_t \tag{XIV.19}$$

We have already found solutions to Schrödinger's equation without the nonlinear perturbation in ENZ cavities, one example is the ENZ finite square well analog in chapter X. For most perturbing potentials, the above equation is nonintegrable. Nonetheless it possesses 2 conserved integrals of motion, the norm, N, and the Energy[64][65]:

$$N = \int_{-\infty}^{\infty} |\psi|^2 dx \tag{XIV.20}$$

$$H = \int_{-\infty}^{\infty} |\psi_x|^2 + V(x)|\psi|^2 - \frac{\gamma}{2}|\psi|^4 dx \tag{XIV.21}$$

The NLS equation arises from the above Hamiltonian, when it is placed in Liousville equation:

$$\frac{d\psi}{dt} = \{\psi, H\} + \frac{\partial\psi}{\partial t} \tag{XIV.22}$$

In a continuum, which is true if V(x) is a perturbation, the Poisson bracket, where Π is the cannonical momentum, is:

$$\{F, H\} = \int \left(\frac{\delta F}{\delta\psi}\frac{\delta H}{\delta\Pi} - \frac{\delta F}{\delta\Pi}\frac{\delta H}{\delta\psi} \right) d^3x \tag{XIV.23}$$

For this system, the following conservation equations hold:

$$\{\psi(x,t), \psi^*(y,t)\} = -i\delta(x-y) \tag{XIV.24}$$

$$\{\psi(x,t), \psi(y,t)\} = \{\psi^*(x,t), \psi^*(y,t)\} = 0 \tag{XIV.25}$$

From looking at the energy given by the Hamiltonian, we find that we can't simply fold the Kerr nonlinearity into the potential $V(x)$ and integrate mindlessly. If we did, we would expect the energy of the Kerr term to be equal to $\int_{-\infty}^{\infty} \gamma|\psi|^4 dx$. However, we will get the right energy contribution if we decrease the Kerr term by a factor of 2, before treating it simply as a spatially varying refractive index. If the Kerr nonlinearity is large compared to the Schrödinger frequency, then a finite square well may begin to approach a parabolic potential for the lowest energy mode; this is at least one limit in which we know that we have broken perturbation theory. For the spatial variation of the potential, however, we get exactly what we would have guessed by drawing an analogy to the energy shifts of a scalar quantum system.

At this point, we ask if the energy given by the classical Hamiltonian has a correspondence to energies of quantum mechanical systems; we find this is indeed the case. Previously, we only asserted that the frequencies of ENZ cavities could be made isospectral to the frequencies of quantum systems, while noting that the energy of plasmons was equal to $\hbar\omega$. Here, we will find that the kinetic and potential terms in our NLS Hamiltonian are exactly what we would expect from solving a quantum problem. We can nondimensionalize the Schrödinger equation

by parameterizing it in terms of dimensionless variables. The one for position takes the form $\chi = x/a$, where a is a length scale, best parameterized after choosing a potential form, and $\tau = \omega_o t$. However, we can also simply rearrange Schrödinger's equation to make it into an equation for inverse length, where the still-dimensional left hand side mirrors the nondimensional NLS, and the right hand side is:

$$\Psi_{xx} + \gamma|\Psi|^2\Psi - \frac{2m}{\hbar^2}V(x)\Psi = -i\frac{2m}{\hbar}\Psi_t = \frac{E_s}{(\hbar^2/(2m))}\Psi_t \tag{XIV.26}$$

Above, $\gamma = 4\pi\chi^{(3)}$ if we use the single-frequency approximation mentioned earlier. If we put it in this form, we would have to multiply resulting energies from the Hamiltonian by $\hbar^2/(2m)$. Since the Poission brackets and partial derivatives in Liouville's equation commute with scalars, we'll start with the NLS equation with Gaussian units:

$$\frac{\hbar^2}{2m}\Psi_{xx} + \gamma|\Psi|^2\Psi - V(x)\Psi = -i\hbar\partial_t\Psi \tag{XIV.27}$$

And again, we are still treating the spatial variation as a perturbing potential [64]. The first term in the Hamiltonian looks like a kinetic energy term, the spatially varying potential looks like the contribution to potential energy.

$$E = \int_{-\infty}^{\infty}\left(\frac{\hbar^2}{2m}|\psi_x|^2 + V(x)|\psi|^2 - \frac{\gamma}{2}|\Psi|^4\right)dx \tag{XIV.28}$$

Ignoring the Kerr nonlinearity for a moment, let's ask if this interpretation is consistent with our quantum mechanical expectations for energy. We have shown

that we can make a broad class of ENZ problems isospectral to quantum problems in frequency, with the substitution $m = \hbar\omega_p/c^2$. Here we suggest that the energies of our systems are likewise analogous, even from a classical standpoint. The infinite square well is the deep-well limit of the finite square well, and we described the electromagnetic analog in chapter X. If the well starts at zero, and ends at length a, the solutions are $\Psi(x) = \sqrt{2}a\sin(\frac{n\pi x}{a})$. From XIV.30, we expect energies of:

$$E = \frac{\hbar^2 n^2}{2ma^2} - \gamma\frac{3}{2a} \tag{XIV.29}$$

The kinetic term gives us the exact quantum mechanical energies of the infinite square well. In classical variables $m = \frac{\hbar\omega_p}{c^2}$, and the energy takes the from: $E_n = \frac{\hbar c^2 n^2}{2\omega_p a}$, where ω_p in the plasma frequency of an ENZ material, and we again assume we are in the ENZ limit to make the NLS equation valid even at small field amplitudes. When the Kerr term approaches the magnitude of the linear term, we can be certain that linear solutions for the strongly confining potential are no longer valid. We again note that the Kerr term is something we don't see in quantum mechanics. This is an effect unique to electromagnetic fields. However, it is nonetheless a useful feature because it gives us the chance to manipulate light with light. And again, since this is a system where we ignore loss, we also expect $N = \int \Psi^2 dx$ to be a conserved quantity. For solutions outside of potential wells, we expect to find N solitons traveling through the medium, but we will not discuss that further here.

To better assert the kinetic-energy analog in our Hamiltonian, we can pick the quantum solutions for a nonrelativistic momentum, $\exp[ipx]$, and realize that the kinetic term in our Hamiltonian gives: $E = \frac{p^2}{2m}$, and we again find a correspondence with the quantum case from our classical Hamiltonian. The nonrelativisitc momentum can be related to classical parameters of the wave packet through the wave number. If $k = p/\hbar$, is related to the classical group velocity, $v_g = \frac{kc}{\omega_p}$, the velocity of the wave envelope. To construct the classical Hamiltonian, we assumed that the energy was proportional to $\hbar\omega_s$, and thus we should only see these energies as correction to the energy of a photon in a plasma medium, which is $E \cong \hbar\omega_p$. The appearance $p^2/2m$ hints at why the classical kinetic energy term agrees with the quantum, the ∂_x operator is best thought of as part of the radial momentum operator: $|-i\hbar\partial_x|$, and thus we should instead suggestively rearrange the term, and we will write our energy equation as follows:

$$E = \int_{-\infty}^{\infty} \left(\frac{1}{2m} |\hbar\psi_x|^2 + V(x)|\psi|^2 - \frac{\gamma}{2}|\Psi|^4 \right) dx \tag{XIV.30}$$

If we can find a good mode through perturbation theory, then we can use the above integral to look for a local minimum in the energy by perturbing mode parameters. For example, if the curvature of the mode increases, the kinetic energy term will increase, but may not have much of an effect on the Kerr term. Increasing the magnitude of the field may lead to self-focusing, which increases the magnitude

of the Kerr term. Mode parameters such as wavenumber/frequency, and amplitude are all parameters that could be modified.

We would like to extend the Liouville's equation formulation of the energy density to spherical, ENZ, NLS cavities. The power of this formulation is that we have classically conserved quantities. However, we can't simply bootstrap up from the scalar 1D case without proving its validity in 3D. A search for the extension of this approach to 3 dimensions is ongoing. Ideally, we would like one term in this Hamiltonian to be proportional to the energy of the wave, and a kerr term and potential energy term similar to the 1D case. Use of the radial Laplacian operator, (VI.10), in place of $|\psi_x|^2$ in (XIV.30) gives vector fields good empirical agreement with nonrelativistic electron energies, but we have yet to prove its validity in a 3D classical system.

If we simply want to estimate a classical electromagnetic energy density in a nonlinear medium, we would use Poynting's theorem. If fields are time averaged[66]:

$$U = \frac{1}{8\pi}\mathbf{D}\cdot\mathbf{E} \tag{XIV.31}$$

Where $\mathbf{D} \cong n^2\mathbf{E}$, where we use the nonlinear n^2 given earlier (XIV.2). This non-dispersive energy density gives an answer that doesn't agree with the Liouville Hamiltonian. The energy of the pulse is zero if epsilon is zero, and the corrections in energy disagree with experimental fact and quantum prediction that a plasmon has $\hbar\omega$ energy. For a propagating pulse in an ENZ material, dispersion in the linear

refractive index means we should use the dispersive form of energy density. If the material is still roughly linear, an approximation here, then energy density takes the form[22]:

$$\frac{1}{8\pi}\frac{d(\omega\epsilon)}{d\omega}\mathbf{E}\cdot\mathbf{E} \tag{XIV.32}$$

In the above, for example if $\epsilon = 1 - \omega_p^2/\omega^2$, then XIV.32 gives $1 + \omega_p^2/\omega \cong \frac{2}{\omega_p}(1-\omega_s-V)$. In this formulation, if the Schrödinger frequency is a larger negative value, then the state has a larger energy, which is does not agree with the Liouville Hamiltonian. However, the dispersive energy density does a better job than the linear energy density, because it doesn't predict that the energy of a pulse will go to zero if it adiabatically travels from an $n = 1$ material into an $n \cong 0$ metamaterial. In an ENZ material, the linear refractive index is small, the Kerr nonlinearity itself changes the dispersive nature of the pulse, allow for the formation of soliton wave packets. This is another reason why the 1D Liouville's equation approach should be extended to multidimensional vector fields in cavities.

Approximating a Repulsive Coulomb Potential with a Linear Refractive Index

Here, we wish to discuss how to approximate a nonlinear quantum effect on a single energy level by perturbing the linear part of the spatially varying index of refraction. These results are rough and preliminary, but illustrate how we can partially overcome real differences between charged electrons and photons.

Additionally, the results will be used in the exploration of ray-based quantization methods in Appendix F, which may one day be useful in dealing with the Kerr nonlinearity. Most electronic devices have multiple electrons, and the repulsive Coulomb interaction shifts the energy levels of electrons. Here, we begin to explore how one can shift the linear spatially varying refractive index to try to make a single mode governed by the wave equation in an ENZ material roughly isospectral to a mode in an multiple-electron atom. In this approach we want to make a linear ENZ refractive index less attractive to create optical states in which the Schrödinger frequency, ω_s, is smaller in magnitude.

Unfortunately, we need to approximate many body interactions with a single scalar potential, and only then can we have a quantity that we can insert into the refractive index. We could start adding arbitrary shape perturbations to an optical refractive index potential until we find a shape perturbation that shifts the optical refractive index by the right frequency for a given mode. However, it is preferable to add perturbations that are physically motivated. Use of Hartree Fock methods[67][68] to find an effective potential for an electron would be a better approach than the argument that we will outline here. But a decent guess at an effective potential is all that is necessary for a starting point. If we find a good answer, and perform higher order perturbation theory, we can fine-tune the magnitude of those perturbations if they initially show some agreement with the desired frequency shift.

We will consider only pairwise interaction of electrons through the long range Coulomb force. We will make a very crude attempt to approximate this interaction with an effective potential, and we will find that it gives decent agreement with experimental predictions. We have taken time to argue that we can make ENZ systems that are similar to single-particle quantum systems. We suggested that since so many useful devices are electronic, perhaps we could someday design optical metamaterial devices that worked based on similar principles. However, no useful electronic devices are single electron systems. If we can't find a way to at least approximate the effect of Coulombic repulsion via metamaterial engineering, then the range of electron-like ENZ photonic applications will be limited. In this approach we should emphasize that we refer to a static change in the refractive index. Also, we will only look at solutions corresponding to the scalar wave equation. We will describe a perturbative effect on zero angular momentum modes, and the vector spherical harmonics that solve the wave equation, and that are associated with these $l = 0$ modes have non-zero divergence. We will use the resulting perturbed potential to study numerical ray-tracing quantization methods in Appendix F.

Earlier, we asserted that given an arbitrary spatially varying potential $V(\mathbf{x})$, we could find a refractive index profile that gave the same energy spectrum, though scaled in frequency by some constant. It would be difficult to classically approximate a point particle electron jumping around in a probability

cloud. However, charge density is a parameter that we can relate both to quantum mechanics and classical electromagnetism. Let us assume, as a crude approximation, that one electron in a ground state in the helium atom doesn't budge in response to the repulsive force from the other electron. In this case, each probability density is determined by solutions to the hydrogenic atom. However since electron 2 is a point particle, it doesn't feel its own charge density, while it affected by the charge density of the other electron. We can very roughly approximate the first electron as having a never-changing charge density. We can couple this charge density to the electric field from Maxwell's equations, and estimate the radially varying potential created by the charge density. The probability density for the ground-state electron, in an ion of arbitrary charge Z, is:

$$P(x,t) = R_{10}(r)^2 = \left(2(Z/a)^{(3/2)} \exp[-Z * r/a]\right)^2 \tag{XIV.33}$$

The vector wave equation analog for probability density is energy density. The vector spherical harmonic doesn't have a radial dependence of $R_{10}(r)$ that satisfies the Schrödginer equation. But if we picked state $\mathbf{E}(\mathbf{x},t) = R_{20}(r)\mathbf{Y}^l_{lm} \exp[-i(\omega_p + \omega_s)]$, the energy density is $R_{20}(r)^2\mathbf{Y}^l_{lm}(\mathbf{Y}^l_{lm})^*$. To calculate change in the ground state electron's approximate charge density, we solve Maxwell's equations in the Coulomb gauge: $\nabla \cdot \mathbf{E} = 4\pi e \int_0^\infty R_{10}(r)^2 r^2 dr$. Since the problem is spherically symmetric, then we can use Gauss's law with a spherical surface to find $\mathbf{E}$, and use

the fact that the electric field is the gradient of the scalar potential to solve for the scalar potential. The above was an ugly mix of quantum and classical arguments, but it still yields good agreement with perturbation theory. Our repulsive scalar potential, multiplied by the charge e is:

$$V_{repulsive}(r) = e^2 \left(\frac{1}{r} - Exp[\frac{-2Zr}{a_0}] \left(\frac{1}{r} + \frac{Z}{a} \right) \right) \tag{XIV.34}$$

We need the potential to be proportional to e^2, by multiplying by $-e$, because this was necessary to obtain hydrogenic solutions in chapter VI, and $2V(r)/(\hbar\omega_p)$ must be dimensionless. Earlier, we demonstrated that we could find an optical system isospectral to a quantum system by inserting a potential into the following refractive index:

$$n^2(x,\omega) = 1 - \frac{\omega_p^2}{\omega^2} - \frac{2V(r)}{\hbar\omega_p} \tag{XIV.35}$$

This refractive index also corresponds to the KG equation, well approximated by the Schrödinger equation. Here we will assume $V(r) = -Ze^2/r + V_{repuslive}(r)$. We already solved the optical scalar wave equation for $V(r)$ in chapter VI. In chapter VI and VII we showed how we could evaluate terms like $(\frac{Ze^2}{r})^2$, which arose when we varied both ϵ and μ, as perturbations to a vector Hamiltonian, and this gave the same result we would get by taking on a perturbation for $V(r)$ into the refractive index. The same KG equation that is given if we insert the above refractive index into Maxwell's equations is given in the spin-free approximation of

the Dirac equation derived earlier in the chapter. For these reasons, we know that if we add the repulsive potential to the refractive index to solve the scalar wave equation, it will also show an energy shift that approximates the 2-electron ground state of helium. This approach will only loosely approximate helium, because we assumed that the Ground state s-orbitals in helium would keep the same Bohr radius regardless of the addition of new charged particles, which is certainly untrue. For this reason, we should check that this estimate of the perturbation to the refractive index gives a shift that agrees with the perturbation of the ground state in a 2-electron atom. Evaluating $V_{repulsive}$ as a perturbation, we find, substituting $Z = 2$ in the last steps:

$$\Delta E \cong \int_0^\infty V_{repulsive} R_{10}(r)^2 r^2 dr = \frac{Ze^2}{a} - \frac{1}{4}\frac{Ze^2}{a} - \frac{1}{8}\frac{Ze^2}{a} \tag{XIV.36}$$

$$= \frac{5}{8}\frac{Ze^2}{a} = \frac{5}{4}(\frac{1}{2}mc^2\alpha^2) = \frac{5}{4}13.3eV \tag{XIV.37}$$

This is the same expression for the repulsive energy shift in ground electrons obtained in quantum mechanics textbooks[51]. Here, we know that we will get a shift of this order if we modify the linear refractive index of a Coulombic ENZ cavity with the new potential, $V(r) = -Ze^2/r + V_{repuslive}(r)$. However, we can only shift the energy of a single mode of an electromagnetic analog with this technique. In the helium atom, if the one electron is excited ot $n = 2$, it will certainly affect the energy of the inner electron, thus modifying the Coulomb potential seen by the outer

electron. However, we crudely assumed that the wave function of neither electron changed when a second electron was added to a ground state of the helium ion. However, even this approximation does a decent job. The gound state of a single electron for the helium ion has an energy of $E = -\frac{1}{2}\frac{mc^2\alpha^2 Z^2}{n^2} = -2mc^2\alpha^2$, or -54.4 eV. If there were no electron-electron repulsion, the ground state of helium would have an energy of twice that value, or -108.8 eV. We find that our perturbation to the linear refractive index, would give a frequency shift of +16.6 eV, this energy shift would add to the ion ground energy, to produce a new ground frequency for the photon proportional to -36.4 eV. Since there are two electrons with the same ground-state energy in helium, and each would have an energy of -36.4 eV, this provides an estimate -74.8 eV for the ground state energy. The experimental ground energy of helium is -78.975 eV[51]. The perturbation theory estimate differs by a little more than 5 percent from the actual value. At least for this system, we can use crude estimates about the repulsive potential of electrons to produce spectral shifts that mimic electron repulsion, with around 5 percent accuracy. This is still a hybrid quantum/classical system.

At this point, we have a new potential to insert into our refractive index. This is a system in which we know for certain that first order perturbation theory does a good job of solving, but can't exactly solve. We can add our perturbing potential to $V(r)$, modify the refractive index, and use semiclassical methods to quantize the cavity. An exact solution to the scalar wave equation is not guaranteed to be

closer to the experimental answer for ground state in helium because the multi-electron system is fundamentally different than a linear, spatially varying, optical system. Here, we assumed that the ground state wave functions didn't change with the addition of a new electron, and that is most certainly untrue for the helium atom. However, we know that if we find a way to nearly exactly solve the linear, nonintegrable scalar wave equation, we will get a different answer than the perturbation theory estimate, and it would be interesting to know whether it is closer, or further away from from the quantum estimate. While we could add a Kerr nonlinearity to the 3D cavity, we will have no experimental answer as a reference point. So, the next step is to quantize this cavity using semiclassical methods, and this step is not easy. If we add $V_{repuslive}$ to the potential of the of the helium atom, $V_{He} = -2e^2 r$, we obtain:

$$V_{ground}(r) = e^2 \left(-\frac{1}{r} - \exp[\frac{-4r}{a_0}] \left(\frac{1}{r} + \frac{2}{a} \right) \right) \tag{XIV.38}$$

The new refractive index is:

$$n^2(x, \omega) = 1 - \frac{\omega_p^2}{\omega^2} - \frac{2V_{ground}(r)}{\hbar \omega_p} \tag{XIV.39}$$

In appendix F, we will begin tracing rays in this new refractive index, as we did in chapter III for the Coulombic refractive index. The reason why this problem was first picked is for testing numerical ray-based quantization methods is because rays in a Coulombic refractive index follow circular and elliptical trajectories, and

always return to virtually the same point in the potential. In undertaking this problem, it was hoped that ray paths would still trace almost closed ellipses. If an elliptical ray path returns to the same point, the phase quantization condition is: $-\omega t + N_{turns}\frac{\pi}{2} = 2\pi n$, where$n$ is an integer, t is a travel time, and N_{turns} is the number of turning ray turning points. Additionally, in appendix F we will postulate that we can treat the Kerr nonlinearity as an ENZ refractive index potential. On time scales associated with the phase velocity this potential is effectively static. For this reason, ray-based quantization methods that use the phase velocity and quantization conditions may help solve the nonlinear problem. The results of this chapter indicate that we can mimic the most basic aspects of quantum mechanical electron-electron Coulomb interaction for a single mode in a cavity. More broadly, inserting perturbative potentials into the spatially varying refractive index can describe what frequency shifts we would expect if an ENZ cavity is perturbed from an integrable shape. If we want to have an ENZ cavity to have a particular spectrum, perturbation theory can be used to get us closer to that spectrum. To shift the spectrum of more than one mode, we would need to introduce shape perturbations that more strongly affect selected modes.

CHAPTER XV

CONCLUSIONS

In this dissertation we have introduced and discussed a wide variety of interesting semiclassical physics problems. In chapter II, we described how the use of the Schrödinger equation can be used to describe epsilon-near-zero materials, which include Drude metals. We went on to describe how ray-tracing techniques can be used to quantize modes in cavities, and define an optical analog to the Bohr atom. We further introduced a new Dirac equation-like quaternion formulation of Maxwell's equations, which confirmed the importance of ENZ materials, and simultaneously hinted that simultaneous spatial variation of ϵ and μ could provide a close analog to the Dirac equation. We find that columns of the quaternion matrix in Dirac formulations of Maxwell's equations are related to right and left Jones vector circular polarization states of light. We also found that we could express Maxwell's equations in the form of a Dirac matrix acting on a 4-vector. We further find that using vector spherical harmonics and Dirac-like ϵ and μ values simultaneously gives us the Schrödigner equation, relativistic corrections to the Schrödinger equation, the spin orbit coupling term and a Darwin-like term, all in vector space but with appropriate leading-order constants, which are set by the Schrödinger equation alone.

In chapter VII, we described how we could put the vector wave equation, in the form of a vector interaction Hamiltonian, for generic ϵ and μ parameters. We believe this approach can aid in handling polarization-sensitive 3D problems in any cavity. We further found that in 3D space we could derive a matrix spin orbit operator, and account for energy lost to the magnetic quadrature with a Darwin-term that acts on vectors. This approach can be extended to describe optical spin-orbit energy shifts in arbitrary optical cavities. Using spatially varying ϵ and μ obtained through an analogy with the Dirac equation, we showed that spin-orbit and relativistic shifts had the same magnitude as we would expect from relativistic solutions to the Dirac equation. However, vector spherical harmonics with the same angular momentum dependence as electron spin-orbit shifts are not transverse. In chapter VIII, we described how optical mode-mixing could also create split modes, but that this was a distinct phenomenon then the near-literal analogy to quantum mechanical spin-orbit coupling that we found in previous chapters. We found that perturbation theory could accurately describe cavity mode-mixing, and that intelligent manipulation of mode-mixing could aide in the development of micro-lasers with well-defined polarization states. We also discussed quantization of optical cavities using the Bogomolny transfer operator, and showed how we could watch modes in an integral cavity traverse chaotic phase space, and often merge, to form modes in a different, integrable, cavity geometry. We described ongoing attempts to apply this operator to polarization-sensitive problems.

Next, we began to describe real epsilon-near-zero materials that yield the Schrödinger equation and Klein-Gordon equation. In chapter X, we noted that microwaves in superconducting cavities, or low-loss Drude materials, could be made isospectral to the quantum mechanical finite square well problem. We also discussed how loss could limit the lifetime of quantum-like "stationary" states, but noted that superconductors had the lowest losses for low-frequency electromagnetic waves. Next, we took a closer look at the Dirac equation, and concluded that some terms had the form of a conductivity. We noted that if we took these conductivity-like terms and adjusted them so materials don't respond instantaneously to a field, we found that they took the form of a conductivity, in the limit of long lifetimes for electron-relaxation times. However, we also found that the now-complex conductivity had a direct correspondence to the Drude equation. We suggested that Drude equations for both ϵ and μ were the best way to obtain a causality-sensitive result. However, we also noted that even-odd relationships in Kramer's-Kronig relationships are valid only if $\mathbf{D}$ and $\mathbf{E}$ are real fields. The method we used to transform the quantum Dirac equation into Maxwell's equations is to multiply one of the Dirac equation terms by i. Furthermore, a quantum mechanical spinor is inherently complex. Thus, we concluded that only complex fields could exactly reproduce the spectra of the Dirac equation. In chapter XII, we implemented the Drude model for both ϵ and μ, and we found it gave exceedingly good agreement with non-Drude models of ϵ

and μ, differing only in a particular term of order α^4. We also found that a certain transformation of ϵ and μ meant that a very large class of ENZ, and MNZ materials gave wave equations and spin-orbit coupling terms that were nearly isospectral to the Dirac equation. The only requirement is that the refractive index match ϵ and μ, and that one parameter be small. We are exploring the situation in which $\frac{1}{\mu}\frac{\partial \mu}{\partial r} \cong \frac{1}{\epsilon}\frac{\partial \epsilon}{\partial r}$, while $\mu >> \epsilon$. This situation allows transverse magnetic and electric modes to have the same spin-orbit shift.

Next, we asked if metamaterials could affect the dynamics of a light wave in a the same way that a magnetic field affects the dynamics of electrons. By using the Dirac equation, we were able to show that we could make a vector system that had the same form of the Pauli interaction Hamiltonian, but we found this vector system didn't obey favorable divergence conditions. But we did suggest how a tensor refractive index could give terms that produced the same vector-potential-dependent shifts. Looking at the tensor refractive index, we concluded that a metamaterial with orthogonal antennae, coupled through inductance, could serve as a magnetic analog for light, and make electromagnetic fields bend around tight corners in a waveguide. We finally described why the Kerr nonlinearity was especially important and favorable in ENZ materials, and suggested ways that one pulse of light could control another using this nonlinearity. We also described how one could make a refractive index less attractive to very roughly approximate energy level shifts for electrons. Current areas of study involve whether transfer operators

or numerical ray tracing techniques can be employed to solve for perturbations of refractive index potentials due to a Kerr nonlinearity.

The most pressing problem related to this thesis is to find better ways to characterize nonlinear ENZ cavities in more than one dimension. Without a good understanding of the pronounced nonlinear effects, ENZ devices will be difficult to build. Perturbation theory, transfer methods, and even ray tracing may help in estimating nonlinear effects in ENZ materials. Despite uncertainties related to three-dimensional nonlinear effects, ENZ metamaterials present promising avenues for future research. ENZ metamaterials provide an ideal system for the demonstration that light can behave in a manner similar to the electron.

APPENDIX A

VECTOR HEMHOLTZ EQUATIONS AND THE GENERAL FORM OF VECTOR WAVE EQUATIONS

Another way to attack the problem of three-dimensional modes in nonspherical cavities is to use the Vector Helmholtz equations, also called Hertz vectors. This approach will be briefly outlined, as it will be useful in several different non-spherical coordinate systems in which the full vector wave equation can be derived in spherical coordinates. Consult Morse and Feshbach [43] for the 5 different coordinate systems in which vector Helmholtz equations can be employed directly. Understanding this approach for spherical coordinates guides the wave for using vector Helmholtz equations in other coordinate systems. The mathematics behind this approach doesn't give more information than solving the problems using vector spherical harmonics (emphasized in the text), but this is included for completeness.

To start, we'll assume a dispersive medium with spherical symmetry, the following scalar wave equation can be used, where $n(r,\omega)^2 = \mu\epsilon$ is a purely radially varying refractive index. The Vector Helmholtz equations are used to solve the following vector wave equation in a system with spherical symmetry.

$$\nabla \times \nabla \times \mathbf{C} - \nabla\nabla \cdot \mathbf{C} + \mu\epsilon \frac{\partial^2}{\partial t^2}\mathbf{C} = 0 \tag{A.1}$$

Where:

$$\mathbf{C} = c_1 \nabla \Phi + c_2 \nabla \times \mathbf{r}\Phi + c_3 \frac{1}{k} \nabla \times \nabla \times \mathbf{r}\Phi \tag{A.2}$$

Above, c_i are arbitrary amplitude coefficients and the transverse terms can be chosen to represent either the **E** or **H** vector fields. The above equation is exactly satisfied by solving the following scalar wave equation:

$$\nabla^2 \Phi + \frac{\omega^2}{c^2} n(r,\omega)^2 \Phi = 0 \tag{A.3}$$

Each optical solution of the above scalar wave equation yields both a transverse electric (TE) and quasi-transverse magnetic (TM) vector mode. Each of these modes has an **H** field related to its curl. $\mathbf{H}_{TE}$ therefore has a vector field that's similar to $\mathbf{E}_{TM}$.

$$\mathbf{E}_{TE} = -\mathbf{r} \times \nabla \Phi \tag{A.4}$$

$$\mathbf{E}_{TM} = \frac{1}{k} \nabla \times \mathbf{E}_{TE} \tag{A.5}$$

In order to obtain the full vector solutions to Maxwell's equations from a scalar wave equation, the electric field must be divergence-free, and the above solutions clearly satisfy this condition. One radially varying scalar wave equation that has a refractive index with interesting properties is the spatially inhomogeneous KG equation:

$$\nabla^2 \Phi - \frac{1}{c^2} {\partial_t}^2 \Phi = \frac{{\omega_p}^2}{c^2} \Phi + \frac{2\omega}{\hbar c^2} V(r) \Phi \tag{A.6}$$

We'll assume that ω_p is constant and real. ω_p plays a role analogous to the plasma frequency for metals, and we'll show this equation gives the permittivity of a plasma medium. However, a very large value of ω_p will give us Schrödinger's equation identically. $\frac{2\omega}{\hbar c^2}V(r)$ can be positive or negative at any point in space, but must be radially varying only. We can assume the following solution for the above linear wave equation: $\Phi(r,t) = R(r)Y_l^m(\theta,\phi)Exp[-i\omega t]$. If we plug in this solution, use the Laplacian in spherical coordinates, and multiply though by $r^2\hbar^2$ We find:

$$\frac{1}{R(r)}\frac{\partial}{\partial r}(r^2\frac{\partial}{\partial r}R(r)) + r^2\hbar^2\frac{(\omega^2-\omega_p^2)}{c^2} - r^2\hbar^2\frac{2\omega}{\hbar c^2}V(r) \tag{A.7}$$

$$= -\frac{1}{Y_l^m(\theta,\phi)}(\frac{1}{\sin^2(\theta)}\frac{\partial}{\partial\theta}(\sin(\theta)\frac{\partial}{\partial\theta} - \frac{1}{\sin^2(\theta)}\frac{\partial^2}{\partial\phi^2})Y_l^m(\theta,\phi) \tag{A.8}$$

$$= \frac{\mathbf{L}^2Y_l^m(\theta,\phi)}{Y_l^m(\theta,\phi)} = l(l+1)\hbar^2 \tag{A.9}$$

If we make the substitution $\frac{2\omega}{\hbar c^2}V(r) = \frac{2m}{\hbar^2}V(r)$, we can put the optical scalar wave equation in a form analogous to a quantum mechanical potential. After making this substitution and multiplying through by $2m$, we can put the radial wave equation form of Schrödinger's equation and use those well-known solutions.

$$\frac{\hbar^2}{2m}\frac{1}{r^2}\frac{d}{dr}(r^2\frac{d}{dr}R(r)) - \frac{l(l+1)}{r^2}R(r) - V(r)R(r) = -\frac{\hbar^2}{2m}\frac{(\omega^2-\omega_p^2)}{c^2}R(r) \tag{A.10}$$

or:

$$-\frac{\hbar^2}{2m}(\frac{1}{r}\frac{d}{dr}(r\frac{d}{dr})+\frac{1}{r}\frac{d}{dr}-\frac{l(l+1)}{r^2})R(r)+V(r)R(r)=\frac{\hbar^2}{2m}\frac{(\omega^2-\omega_p^2)}{c^2}R(r)=E_{nlm}R(r) \tag{A.11}$$

Where E usually appears in Schrödinger's equation, we have: $E_{nlm} = \frac{\hbar^2}{2m}\frac{(\omega^2-\omega_p^2)}{c^2}$. Thus energy eigenvalues for solutions to Schrödinger's equation are related to the square of frequencies of solutions to the scalar wave equation. Solving for frequency, we find:

$$\omega^2=\frac{2mc^2}{\hbar^2}E_{nlm}+\omega_p^2 \tag{A.12}$$

Where, upon reduction to the quantum problem:

$$E_{nlm}=-\frac{\hbar^2}{2m}\frac{Z^2}{a_o^2n^2} \tag{A.13}$$

However, these solutions do not completely satisfy Maxwell's wave equation for a spatially varying permittivity:

$$\nabla\times\nabla\times\mathbf{E}=\epsilon\mu\frac{\omega^2}{c^2}\mathbf{E}-\frac{i\omega}{c}(\mathbf{H}\times\nabla\mu(r)) \tag{A.14}$$

$$\nabla\times\nabla\times\mathbf{H}=\epsilon\mu\frac{\omega^2}{c^2}\mathbf{H}+\frac{i\omega}{c}(\mathbf{E}\times\nabla\epsilon(r)) \tag{A.15}$$

Going through steps similar to those in Chapter IV, we find, if $\omega=\omega_p+\omega_s$, and $E_s=E_{nlm}=\hbar\omega_s$:

$$\frac{\hbar^2}{2m}\nabla \times \nabla \times \mathbf{E} = (E_s - V)\mathbf{E} + \frac{p^4}{8m^3c^3}\mathbf{E} + \frac{\hbar^2 Zq^2}{4m^2c^2r^3}(-\mathbf{r} \times \nabla \times \mathbf{E}) \qquad \text{(A.16)}$$

APPENDIX B

HOW TO RELATE ONE-DIMENSIONAL QUANTUM SCATTERING TO MAXWELL'S EQUATIONS

On the surface, it may seem that a 1D scattering problem has different mathematics than a 1D optical problem with boundary conditions. If ENZ materials are used, this is not the case. In this appendix, we aim to show why the math behind the two approaches is the same. We first approach this problem by assuming the frequency of a wave in an ENX material is close to the plasma frequency, and invoke the slowly varying approximation.

The eigenvalue problem for the Schrödinger-like equation for dielectrics explicitly contains a frequency. While frequency is a distinction between the Schrödinger-like equation for dielectrics from its quantum counterpart, it is not the most important distinguishing feature between the systems. The requirement to obtain a bound optical state is simple: For a given frequency, there must be a region in which that frequency can freely propagate, surrounded by a region in which that frequency cannot propagate at all. That is, the wave vector must be purely real and be surrounded by regions in which wave vectors for that frequency are purely imaginary. In order to make optical wave packets time evolve in a

similar way to electron wave functions, there furthermore must be a frequency at which the permittivity approaches zero.

To illustrate slowly varying bound solutions in 1-D, we'll assume cartesian coordinates we will rewrite equation (1), assuming $\mu = 1$.

$$\frac{\partial^2}{\partial x^2}E + \frac{\omega^2}{c^2}(\epsilon(x,\omega) - 1) - \frac{1}{c^2}\frac{\partial^2}{\partial t^2}E = 0 \tag{B.1}$$

Above, we assume that ω is the total frequency of oscillation of the electric field. It is useful to separate the contribution of $\epsilon(x,\omega)$ that doesn't explicitly depend on $\partial_t^2 E$, so we can employ the slowly varying approximation. Additionally, the inclusion of $\epsilon(x,\omega)$ in the expression allows us to compare slowly varying solutions to those yielded by classical electromagnetism. Above, the wave travels in the x direction, E is the magnitude of the electric field, and the electric and magnetic fields are perpendicular to the direction of travel. We can assume solutions of the form: $E = \xi(x,t)e^{-i\Omega t}$. Schödinger's equation describes the evolution of the envelope:

$$-\frac{\partial^2}{\partial x^2}\xi + \frac{\omega^2}{c^2}(1 - \frac{\Omega^2}{\omega^2} - \epsilon(x,\omega))\xi = \frac{2i\Omega}{c^2}\frac{\partial}{\partial t}\xi \tag{B.2}$$

The quantity $\frac{\omega^2}{c^2}(1 - \frac{\Omega^2}{\omega^2} - \epsilon(x,\omega))$ plays the role of a potential in 1-D quantum mechanics problems. In optical problems, this potential-like term is always dependent on ω^2 unless the permittivity is that of a Drude metal: $\epsilon = 1 - \frac{\omega_p^2}{\omega^2}$. In a Drude material, $\omega_p = \frac{4\pi N 2^2}{m}$, where N is the number of conduction electrons

and m is their effective mass. We can employ separation of variables by assuming solutions of the form: $\xi(x,t) = u(x)T(t)$. This yields:

$$\frac{1}{u(x)}(-\frac{d^2}{dx^2}u(x) + \frac{\omega^2}{c^2}(1 - \frac{\Omega^2}{\omega^2} - \epsilon(x,\omega))u(x)) = \frac{2i\Omega}{c^2}\frac{\dot{T(t)}}{T(t)} = \breve{E} \tag{B.3}$$

Above, $\breve{E}$ is simply a constant and we can't assume it is related to energy in this linear model. $T(t)$ has solutions of the form:

$$T(t) = exp(-i\frac{\breve{E}c^2}{2\Omega}t) \tag{B.4}$$

In order for the slowly varying approximation to be valid, the envelope must oscillate much more slowly than Ω:

$$\breve{E} \ll \frac{2\Omega^2}{c^2} \tag{B.5}$$

The spatial part of the envelope obeys the equation:

$$\frac{d^2}{dx^2}u(x) + \kappa u(x) = 0 \tag{B.6}$$

Where:

$$\kappa = \breve{E} - \frac{\omega^2}{c^2}(1 - \frac{\Omega^2}{\omega^2} - \epsilon(x,\omega)) \tag{B.7}$$

If κ is positive, free wave propagation is allowed. If κ is negative, only decaying exponential solutions are allowed. Bound solutions to Schrödinger's equation are those that have wave-like solutions surrounded by a region where only decaying exponential solutions are allowed. We will thus define "bound" wave envelope solutions to Maxwell's equations in the same way. If the wave envelope has a

solution that would be a bound state in quantum mechanics, we'll classify it as a bound state of Maxwell's equations. In order for a region to exclude propagation of electromagnetic waves, the constant κ must be negative. Since we've solved the temporal part of the envelope equation, we can now express the total frequency frequency in terms of $\breve{E}$. If we employ the condition for a slowly varying envelope, we can express ω^2 as:

$$\omega^2 \cong \Omega^2 + \breve{E}c^2 \tag{B.8}$$

This yields:

$$\kappa = \epsilon(x,\omega)(\frac{\Omega^2}{c^2} + \breve{E}) \tag{B.9}$$

If we insist that the envelope propagate in the same direction as the the high frequency wave that it modulates, the permittivity must be negative to allow bound solutions. Even if we relax this restriction, the permittivity must be very close to zero to allow bound solutions for negative $\breve{E}$ values. We can also express the condition for decaying exponentials in terms of the frequency of oscillation of the envelope, $\Delta\omega$.

$$\epsilon(x,\omega)(\Omega + 2\Delta\omega) < 0 \tag{B.10}$$

Since the permittivity for free space is one, and dielectrics have a positive permittivity greater than 1, we typically don't observe confinement of optical wave packets. However, for an ideal Drude material near the plasma frequency, the slowly

varying envelope equation reduces to Schrödinger's equation and we should expect optical wave packets to behave more like particle wave functions.

Though we have shown that solutions to 1D optical problems can be cast reduced to identical separable differential equations as the 1D Schrödinger equation, we still must show that the boundry conditions used in QM are consistent with those used in optics. In quantum mechanics, boundary conditions are handled by ensuring the continuity of probability current. In optics, we assume that reflected and transmitted intensities conserve energy, while imposing continuity of electric and magnetic field components. We can easily check to see whether associating a quantum mechanical flux of the wave envelope agrees with BC's applied to fields in Maxwell's equations. To do so, we'll treat the spatial scalar wave equation as quantum mechanical potential step problem. First, we'll postulate intensity of the wave packet as the classical analogue of the quantum probability density:

$$I(x,t,\omega) = \xi^*\xi \cong P(x,t) \tag{B.11}$$

The intensity for our electromagnetic wave packet is similar to an unnormalized, non-quantized, frequency-dependent probability distribution. Using equation (34) and its complex conjugate gives us a flux for our classical envelope.

$$\frac{\partial}{\partial t}\xi^*\xi = \frac{\partial}{\partial t}\xi^*\xi + \xi^*\frac{\partial}{\partial t}\xi \tag{B.12}$$

We'll assume that $\epsilon(x,\omega)$ is real, and this yields the same result as a real electric

potential in a quantum problem. The potential-like terms cancel and we're left with the relationship:

$$\frac{\partial}{\partial t}(\xi^*\xi) = \frac{\partial}{\partial x}\frac{-ic^2}{2\Omega}(\xi^*\frac{\partial}{\partial x}\xi - \frac{\partial}{\partial x}\xi^*\xi) \tag{B.13}$$

Using the conservation relationship:

$$\frac{\partial}{\partial t}I(x,t) + \nabla \cdot \mathbf{j}(\mathbf{r},t) = 0 \tag{B.14}$$

We define a wave envelope flux similar to the QM probability current:

$$j(x,t,\Omega) = \frac{-ic^2}{2\Omega}(\xi^*\frac{\partial}{\partial x}\xi - \frac{\partial}{\partial x}\xi^*\xi) \tag{B.15}$$

We can now solve our electromagnetic reflection/transmission problem as a generalized quantum potential step problem, that should work for any Ω and any permittivity provided that the slowly varying approximation is accurate. The quantum problem is a special case, where $\Omega = \omega_p = \frac{mc^2}{\hbar}$, and the permittivity is that of a Drude metal with a plasma frequency $\omega_p = \omega_p$. When we solve the potential step problem, $\breve{E}$ plays a role related to Energy in the quantum problem. $\breve{E}$ is related only to the frequency of modulation of the wave envelope in the classical problem. We can assume that the permittivity changes at $x = 0$ from ϵ_1 on the left, to ϵ_2 on the right. For convenience:

$$\kappa(\epsilon_1) = k^2 \tag{B.16}$$

$$\kappa(\epsilon_2) = q^2 \tag{B.17}$$

For $x < 0$

$$u(x) = e^{ikx} + Re^{-ikx} \tag{B.18}$$

For $x > 0$

$$u(x) = Te^{iqx} \tag{B.19}$$

For $x < 0$, the total flux is:

$$j_- = \frac{c^2}{\Omega} k(1 - R^* R) \tag{B.20}$$

For $x > 0$, the total flux is:

$$j_+ = \frac{c^2}{\Omega} q(T^* T) \tag{B.21}$$

Applying flux conservation gives us:

$$\frac{c^2 k}{\Omega}(1 - R^* R) = \frac{c^2 q}{\Omega} T^* T \tag{B.22}$$

If we insure continuity of the wave envelope, we find:

$$ik(1 - R) = iqT \tag{B.23}$$

We can now solve for reflection and transmission coefficients of the scalar wave equation:

$$R = \frac{k-q}{k+q} \tag{B.24}$$

$$T = \frac{2k}{k+q} \tag{B.25}$$

If the slowly varying limit is valid, the equations for the two fluxes are as follows:

$$j_- = \frac{c^2 k}{\Omega}(1 - R^* R) = c\sqrt{\epsilon_1}(1 - (\frac{\sqrt{\epsilon_1} - \sqrt{\epsilon_2}}{\sqrt{\epsilon_1} + \sqrt{\epsilon_2}})^2) \tag{B.26}$$

$$j_+ = \frac{c^2 q}{\Omega} T^* T = c\sqrt{\epsilon_2}(\frac{2\sqrt{\epsilon_1}}{\sqrt{\epsilon_1} + \sqrt{\epsilon_2}})^2 \tag{B.27}$$

Fluxes are proportional to intensities, and in classical electromagnetism, intensities are broken down into reflected and transmitted parts. The $x < 0$ flux has two different intensities, reflected in the two different terms in the flux equation. We'll define incident flux as:

$$j_I = c\sqrt{\epsilon_1} \tag{B.28}$$

The ratio of the reflected flux to the incident flux is:

$$(\frac{\sqrt{\epsilon_1} - \sqrt{\epsilon_2}}{\sqrt{\epsilon_1} + \sqrt{\epsilon_2}})^2 \tag{B.29}$$

The ratio of transmitted flux to incident flux is:

$$\frac{\sqrt{\epsilon_2}}{\sqrt{\epsilon_1}}(\frac{2\sqrt{\epsilon_1}}{\sqrt{\epsilon_1}+\sqrt{\epsilon_2}})^2 \tag{B.30}$$

The above equations are the ratios of reflected and transmitted intensities to the incident intensity that we would find if we solved Maxwell's equations without the use of the slowly varying approximation. Applying "quantum" rules to classical envelope equations provides the correct boundary conditions to solve problems in classical electromagnetism. Knowing the connection between the 1-D Maxwell's equation version of Schrödinger's equation is useful since so many optics problems have been exhaustively solved for one dimensional systems. Future work involves adding a Kerr nonlinearity to the 1D equation and studying the properties of Gaussian pulses in spatially varying KG/Drude material.

Showing Equivalence without Invoking the Slowly Varying Approximation

One last note is we can also perform separation of variables on our original wave equation without making use of the slowly varying approximation to obtain a more exact temporal equation.

$$\Psi(\mathbf{x})^{-1}(-\frac{\hbar^2}{2m}\nabla^2\Psi(\mathbf{x})+V(r)\Psi(\mathbf{x}))=\breve{E}=\frac{-\hbar^2}{2mc^2}(\frac{\ddot{T}(t)}{T(t)}+1) \tag{B.31}$$

For a Coulomb potential, we already know the solutions to $\breve{E}$. We can use the spatial eigenvalues to solve for the frequencies at which the temporal component oscillates:

$$\omega = \frac{mc^2}{\hbar}\sqrt{1 - \frac{(Z\alpha)^2}{n^2}} \tag{B.32}$$

These are the same frequencies that we find from the Bohr-like ray orbits. The frequency difference from the plasma frequency is given by in chapter III, which we previously derived from ray equations without separation of variables. We take this result as a confirmation of the validity of the frequencies obtained from the ray model.

APPENDIX C

VERIFYING THE MATRIX SPIN-ORBIT OPERATOR

This chapter contains co-authored material that supplements the co-authored material in chapter VII. We can use Mathematica to verify the identity:

$$[(\nabla V)\times(\nabla\times E)]_\alpha = [-i\mathbf{S}\cdot((\nabla V)\times\nabla)]_\alpha - ((\nabla V)\cdot\nabla)\mathbf{E} + (\nabla V)(\vec{\nabla}\cdot\mathbf{E}) \quad \text{(C.1)}$$

First, the vector analysis package must be loaded with: Needs[“VectorAnalysis‘”];, and coordinates should be set to Cartesian. We can define a vector with an x, y, and z dependence with:

$$\mathbf{A} = Through[Array[a_{\#}\&, 3][x, y, z]]; \quad \text{(C.2)}$$

The same command is used for vector **B**. We define:

$$s = Table[Normal[LeviCivitaTensor[3][[i]], i, 3]]; \quad \text{(C.3)}$$

$$s1 = -Sum[s[[i]]Cross[\mathbf{A}, dx, dy, dz][[i]], i, 3]; \quad \text{(C.4)}$$

We now define the spin orbit operator:

$$LSOp[e\_] := Table[Sum[sl[[n, i]]/.dx \to D[e[[i]], x], dy \to D[e[[i]], y], dz \to D[e[[i]], z], i, 3], n, 3]; \quad \text{(C.5)}$$

We can check that the identity holds by verifiying that this equality is true:

$$Simplify[Cross[\mathbf{A}, Curl[\mathbf{B}] == LSOp[\mathbf{B}] + \mathbf{A}Div[\mathbf{B}] - Map[\mathbf{A}.Grad[\#]\&, \mathbf{B}]] \tag{C.6}$$

APPENDIX D

DERIVATION OF CIRCULAR RAY TRAJECTORIES WITH A LOCALLY LINEARLY VARYING PHASE VELOCITY

In chapter III, we argued that ray paths follow circular trajectories in a medium with a linearly varying phase velocity. Here, we assume a 2D system in which phase velocity, $v_p(z)$, that varies linearly in the z direction. This approach is based on "Computational Ocean Acoustics", by Jensen[31].

We start with the wave equation with a delta function source, where $v_p((x)) = \frac{c}{n(\mathbf{x})}$:

$$\nabla^2\psi + \frac{\omega^2}{v_p^2(\mathbf{x})}\psi = -\delta(\mathbf{x} - \mathbf{x_0}) \tag{D.1}$$

We can now expand the wave, and look for solutions:

$$\psi(\mathbf{x}) = \exp\left(i\omega\tau(x)\right)\sum_{j=0}^{\infty}\frac{A_j(\mathbf{x})}{(i\omega)^j} \tag{D.2}$$

When we insert the expansion into the wave equation, we search for, and group, the terms with the largest powers of frequency. The terms that have an order of ω^2 form the eikonal equation for a ray:

$$|\nabla\tau|^2 = \frac{1}{v_p^2(\mathbf{x})} \tag{D.3}$$

The quantity $\nabla\tau$ is perpindicular to the wavefront. We can define a ray trajectory vector with unit length in the direction of the wavefront:

$$\frac{d\mathbf{x}}{ds} = v_p \nabla\tau \tag{D.4}$$

We can differentiate the above with respect to s, a length along the ray, combine it with the eikonal equation, to obtain:

$$\frac{d}{ds}\left(\frac{1}{v_p}\frac{d\mathbf{x}}{ds}\right) = -\frac{1}{v_p^2}\nabla v_p \tag{D.5}$$

This can be transformed to first order form with the following variable substitutions:

$$\frac{dr}{dz} = \frac{\xi}{\zeta} \tag{D.6}$$

$$\frac{d\zeta}{dr} = -\frac{\frac{dv_p}{dz}}{\xi v_p^3} \tag{D.7}$$

$$\frac{d\xi}{dr} = -\frac{\frac{dv_p}{dr}}{\xi v_p^3} \tag{D.8}$$

The above equations can be used to derive the 2D wave equation for the ray:

$$\frac{d^2y}{dz^2} = \frac{1}{v_p}\frac{dy}{dz}\frac{v_p(z)}{dz}\left(1 + \left(\frac{dy}{dz}\right)^2\right) \tag{D.9}$$

The following equation for the slope $\dfrac{dy}{dz}$ satisfies the above differential equation:

$$\frac{dy}{dz} = \frac{av_p(z)}{\sqrt{1 - a^2 v_p(z)^2}} \tag{D.10}$$

We can also solve this equation for the integration parameter a, which will determine the radius of curvature of a ray based on its depth and angle with respect to the phase velocity gradient:

$$a = \frac{1}{v_p(z)} \frac{\left(\frac{dy}{dz}\right)}{1 + \left(\frac{dy}{dz}\right)^2} \tag{D.11}$$

For now, we will integrate $D.10$ to obtain the range vs. depth ray trajectory.

$$y(z) = y(z_0) + \int_{z_0}^{z} \frac{av_p(z')}{\sqrt{1 - a^2 v_p(z')^2}} dz' \tag{D.12}$$

If

$$\frac{dv_p(z)}{dz} = g \tag{D.13}$$

Then we can integrate over the phase velocity instead:

$$y(z) = y(z_0) + \int_{v_p(z_0)}^{v_p(z)} \frac{av_p}{g\sqrt{1 - a^2 v_p^2}} dv_p \tag{D.14}$$

The resulting equation, in which everything is constant except for z and y is:

$$\left(\frac{c_0 + gz}{g}\right)^2 = r_c^2 - (y - (y(z_0) - b))^2 \tag{D.15}$$

Here, $r_c = \dfrac{1}{ag}$, and $b = r_c\sqrt{1 - a^2(c_0 + gz_0)^2}$. The above tells us that as the ray depth will follow a circular arc as a function of range, y. We illustrate the circular

ray orbits associated with this coordinate system in figure D.1.. In chapter III, we traced ray orbits in which the rays were to the gradient of the phase velocity, and picked tangential ray orbits in which the radius of the curvature of the ray was equal to the radius in the cavity. In this case, the rays would trace circular orbits. Usually, we want to make sure that over the short element traced by the ray, that the phase velocity varied approximately linearly. For tangential ray orbits, we can find orbits in which the phase velocity never varies, so this assumption is automatically satisified.

In this strictly linear example parameteriezed in y and z varibles, we know that the ray is perpendicular to the gradient of phase velocity when z is at an extereme.

Figure D.1. The following figure, from Computational Ocean Acoustics, by Jensen, describes ray curvature in a medium where phase velocity increases linearly in the depth, or z direction. The parameter a will depend on the initial starting depth, and the ray angle. Rays trace circular orbits in a medium of linearly varying phase velocity, and approximating a medium as linearly varying was used to trace rays.

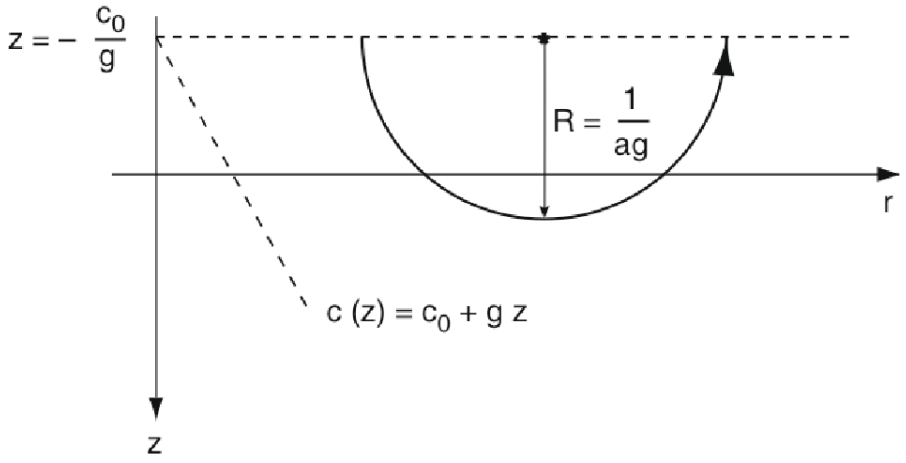

This occurs where:

$$(y - (y(z_0) - b))^2 = 0 \tag{D.16}$$

When the ray is tangential, we can know the radius of curvature of the ray without evaulating $(\frac{dz}{dy})^{-1}$, and we find:

$$r_c = \frac{c_0 + gz}{g} = \frac{v_p(z)}{\left(\frac{dv_p(z)}{dz}\right)} \tag{D.17}$$

Two methods were used to trace rays, one was to project the phase velocity gradient onto an a hypotentical plane, and then draw a turning arm at right angles until it meets point on on the plance of zero phase velocity that the ray curves around. This method worked better than associating an angle of curvature of the ray based on the radius of curvature of the ray and the ray phase velocity.

APPENDIX E

ORDER IN THE CHAOTIC SEA: RIGHT AND WRONG WAYS TO COLOR-CODE A CHAOTIC SOS

The Chaotic SOS

This chapter discusses the advantages to plotting chaotic phase space by using multiple colors, and describes right and wrong ways to do this. The initial motivation for color plots of chaotic phase space was to quickly visually identify which stable orbits are related to others. In chapter XIII, we described how to construct a perturbation Hamiltonian that can describe mode-mixing in the dome cavity. Our initial attempt to solve the mode-mixing problem was to identify stable orbits in the non-integrable limit of the dome cavity, associate s and p polarized rays with these orbits, and then quantize these polarization-dependent orbits. Generally, a stable orbit is at the center of an island in phase space. However, as we move a cavity from a half dome configuration to a non-integrable half-dome configuration, stable islands rapidly fragment into smaller stable islands. In the chaotic regime, it is difficult to even visually identify which stable orbits are related, since many small island chains are the same size. However, we found that if we plotted the phase space in color, different stable islands would have a unique set of

colors. Thus, even adjacent stable islands of the same size can be readily identified as belonging to different ray trajectories.

We found that in order to preserve the unique color-coding of stable islands, one cannot traverse phase space haphazardly. The rules for color-coding islands are as follows. First, while traversing phase space, the edge of a stable island can be identified if a ray repeatedly returns to the same area of phase space, and these repeated returns trace out an ellipse in phase space. All of these ray bounces should share the same color in the plot. The center of this ellipse can be associated with a quantized orbit. However, having identified a stable island, one must next take a step perpendicular to the edge of the edge of the ellipse, towards its center. Then, one can pick a new color, and trace a smaller ellipse inside the first ellipse. This process is repeated until one reaches the center of the ellipse. Next, it is just as easy to maintain the same perpendicular trajectory back through to the edge of the ellipse, thus color it twice, as it is to jump to the edge and resume traversing phase space.

When we follow this procedure, we find brilliant color is added to the fractal patterns that define the minimum of the action on the SOS. We first illustrate this in figure E.1..

Figure E.1. illustrates the theta phase space action-angle variables of ray position and momentum. The y-axis of the figure is the theta coordinate, and the x-axis describes the momentum. This is simply a cross section of a higher

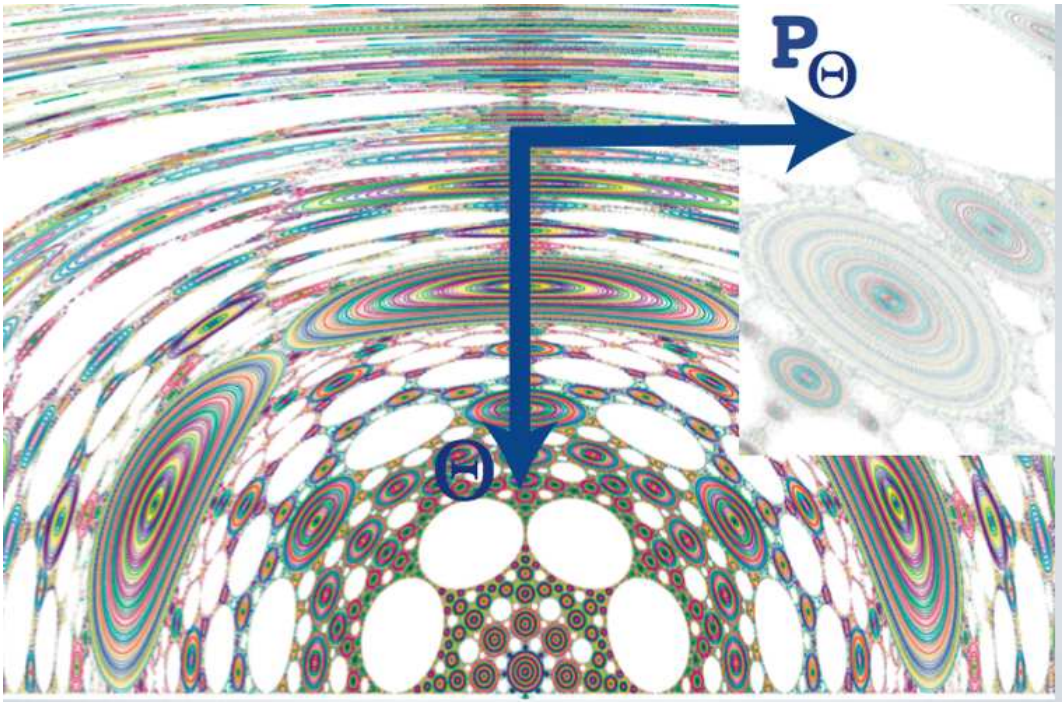

Figure E.1. This phase space plot depicts a 2 dimensional cross section of the higher dimensional phase space, for a non-integrable dome cavity. In this instance, we fix the the value of the phi component of angular momentum, p_ϕ. The top of the z-axis in this picture is the top of the rounded dome cavity, where $\theta = 0$. The bottom of the z-axis is $\theta = \frac{\pi}{2}$. The y-axis is the theta component of ray momentum, and the inset depicts the kinds of patterns we see if we zoom in and map a particular rectangle of phase space.

dimensional phase space, because if we change the phi component of angular momentum, we will a different configuration of ellipses in the phase space plot. More angular momentum about the z-axis results in increasing break-up of large stable islands, and less angular momentum pushes the cavity slightly towards the linear regime.

The use of color plots of phase space also hints that there is a great degree of order in the chaotic sea that can't be seen in a similar black and white plot. Figure

E.2. displays a traditional black-and-white phase space plot of the dome cavity, this time deformed more than in the last figure E.1., to the point that elliptical stable islands become triangular shaped, this cavity was deformed 7 percent away from the integrable half dome. If one looks at regions not directly adjacent stable islands, there appears to be no rhyme or reason to the speckle. This is the kind of plot one invariably sees in articles discussing quantum chaos. However, this type of plot is insufficient for both identifying which similar-similar sized islands are connected, and for identifying which areas of phase space in the speckle-laden chaotic sea are related. If we plot the same figure in color, E.3., new patterns are apparent.

In the color plot, it is much easier to pick out stable island chains, and similar

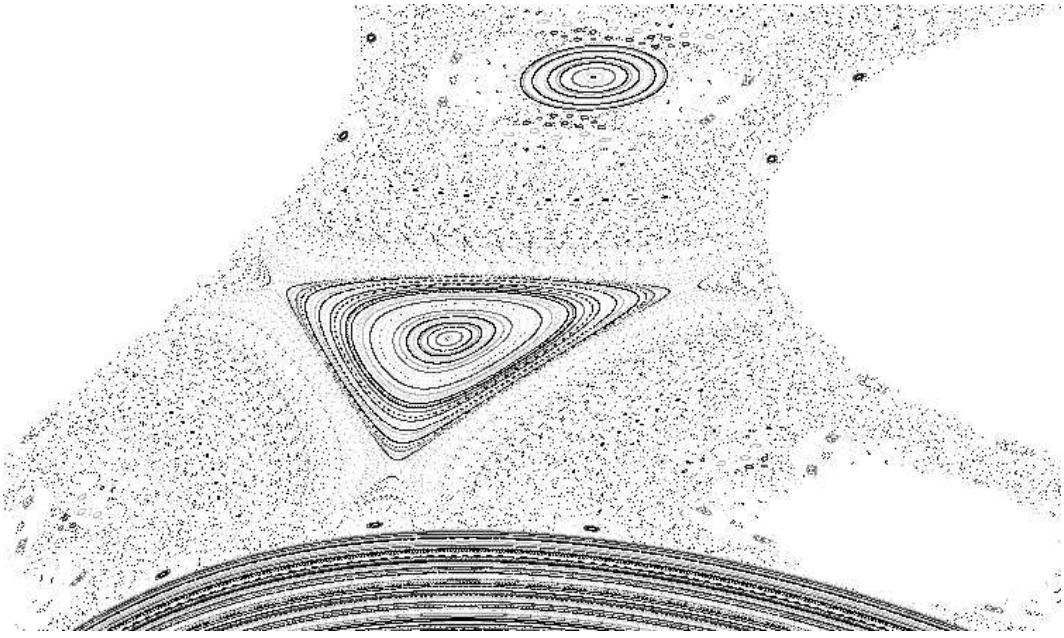

Figure E.2. This is a black and white SOS plot of a fairly chaotic region of phase space in the truncated dome cavity. In this figure, the onset of the chaotic sea is "clearly" identifiable. We see a few tiny related islands in a mess of supposedly unrelated speckle.

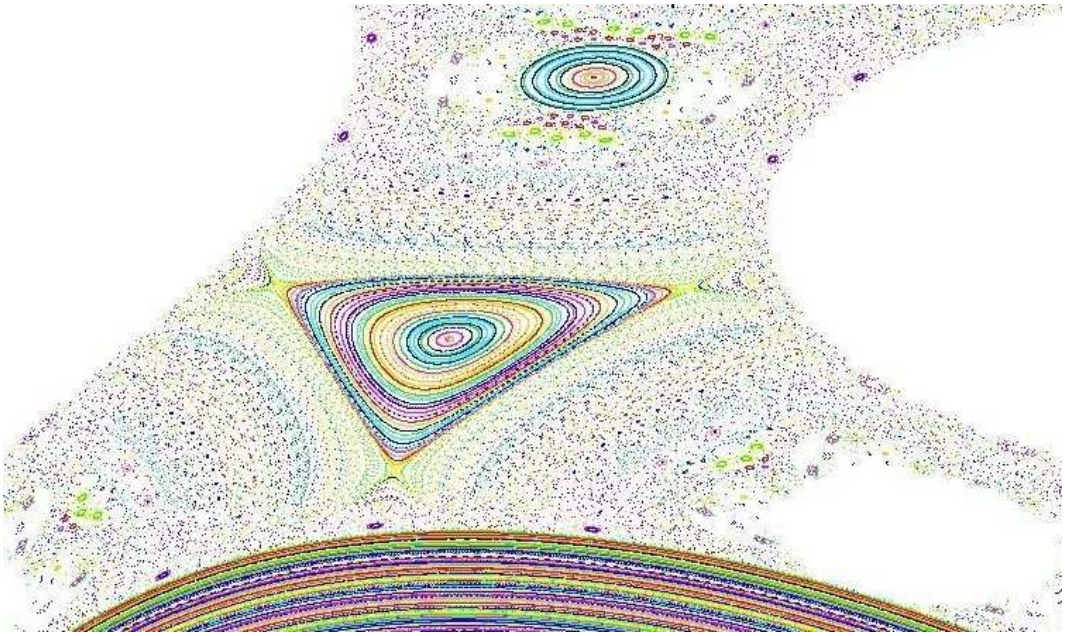

Figure E.3. This is the same SOS plot as on the previous page, but this time each stable island chain has a unique set of This is a black and white SOS plot of a fairly chaotic region of phase space in the truncated dome cavity. In this figure, the onset of the chaotic sea is "clearly" identifiable. We see a few tiny related islands in a mess of supposedly unrelated speckle.

patterns of coloration even exist on all three sides of the central stable island. patterns of coloration even exist on all 3 sides of the central triangular island. We can zoom in even further to attempt to better resolve features seen in figure E.4..

We expect some of the points to truly be aperiodic points due to the KAM theorem, which won't be discussed in detail here. However, it should briefly be noted the KAM theorem has not been proven for higher dimensional systems, described by the SOS plots.

The entire phase space of this cavity is included in figure E.5., for reference. We picked one of the most chaotic areas of the cavity to zoom in on.

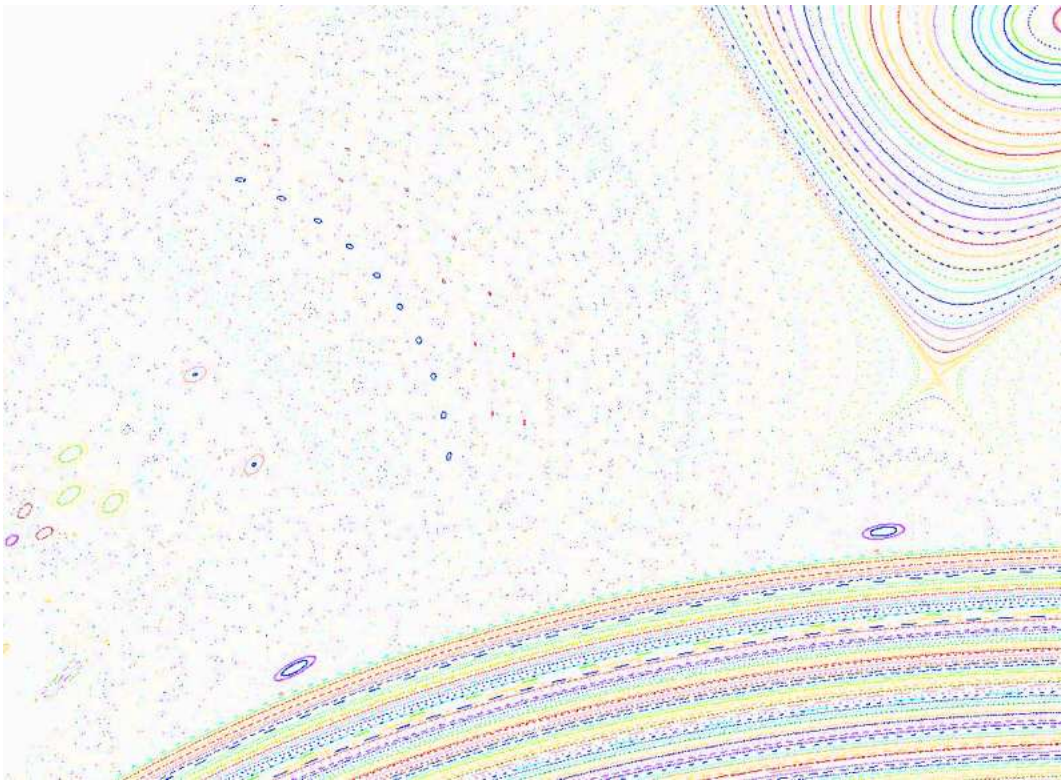

Figure E.4. An additional level of zoom on the chaotic sea. To obtain this figure, and to begin to fill out island chains, the ray tracing program was run overnight. The artifact in the lower right corner is due to the inclusion of the flat bottom of the cavity in the SOS. Ray orbits are not present near the dome of the cavity, because we insisted the cavity have a substantial angular momentum in about he z-axis for this particular SOS slice.

The Wrong Way to Color Phase Space

Finally, we mentioned that there's a wrong way to color phase space. If you don't traverse directly towards the center of stable islands, then each point in an island is colored an inordinate number of times. In this case, the colorful patterns unique to each stable island are washed out, and tiny island chains in the chaotic

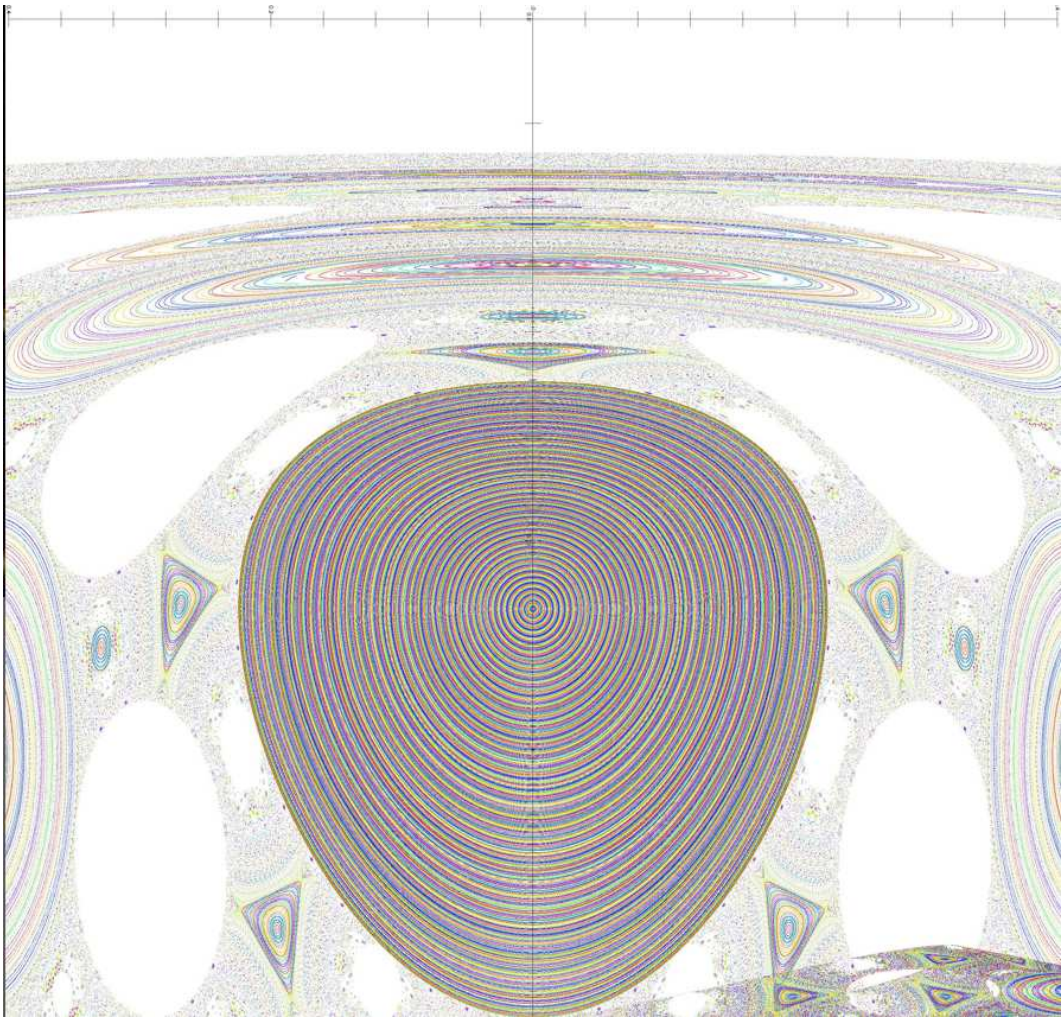

Figure E.5. The entire phase space of the deformed dome cavity, with a height 7 percent less than the radius is displayed.

sea are more likely to be uniformly colored, and the chaotic sea looks much more like an uninformative black-and-white chaotic sea.

In figure E.6. we traversed a straight line through phase space that didn't go through the centers of island chains, in violation of the rules mentioned in the previous section. The result is a cavity that looks much more chaotic than the

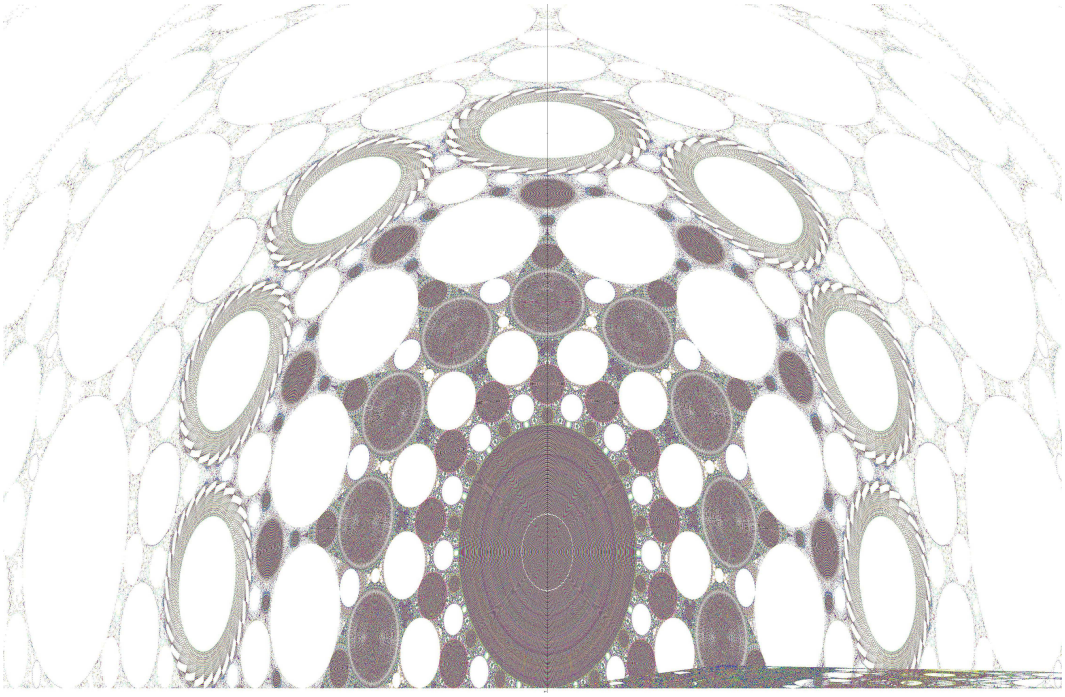

Figure E.6. When care isn't taken to traverse phase space by traveling through the center of an island, the resulting phase space plot is a mess. The cavity looks more chaotic because each island is a random mix of colors.

others, but in this case, is a more integrable case than most of the examples listed before.

Conclusion

Patterns emerge in previously unpatterned areas of the chaotic sea if the phase space is plotted in color. More care must be taken with regard to how one traverses the phase space in order to bring it into colorful relief. However, this author feels the extra care is worth the effort. When plotted in color, the fractal nature of the SOS becomes obvious. Additionally, it's fascinating to note that the minimum

of the action for any non-integrable ray cavity has such patterns on the SOS. The minimum of the action for most real-world optical and electronic systems is literally a fractal. Of course, the path-integral nature of quantum mechanics can rapidly disguise these fractals. As the wavelength of particles or light approaches the scale of the stable islands, these patterns are disguised, since nothing is truly a ray.

At some future time, it would be interesting to run these ray-tracing simulations on a cluster to grant the ability to fill in the hidden details in close-zooms of the chaotic sea. Additionally, future ray tracing implementations of these cavities will use a larger color palette. These color plots were simply constructed by using the standard pre-defined colors in Java, without specifying unique RGB values. Whether or not this exercise will teach us anything new about chaos theory, or help to solve the frustrations that accompanying lower dimensional theorems to high dimensional systems, exploring these techniques have their own aesthetic rewards.

APPENDIX F

EXTENDING RAY THEORY TO QUANTIZE NONLINEAR, NONINTEGRABLE SYSTEMS

The work here is preliminary, so is left as an appendix. In order to test semiclassical quantization methods, one would like an exact soliton, or integrable solution to an inhomogenous 3D radial cavity; we have no such luxury. Yet unobtained experimental results giving the spectrum of a nonlinear ENZ resonator at different frequencies and intensities would also be a sanity check for testing ray-based quantization methods. Without knowing an exact solution, there is no hope showing that a semiclassical quantization method, whether based on ray quantization, or transfer operator methods, outperforms perturbation theory. Here is one way to attack the problem:

1) We first can approximate a Kerr nonlinearity as a scalar perturbation potential. We gave a motivation for the effectiveness of this approach in the previous section. If the nonlinearity is a Kerr nonlinearity, we must half the magnitude of the nonlinear coefficient, before treating it as a linearly varying spatial refractive index, in order to give agreement NLS conservation equations.

2) Using perturbed solutions, modify the refractive index, and treat it as a spatially varying cavity.

3) Quantize the cavity, which we will now treat as a linear, but spatially varying refractive index. Since wave packets time evolve so slowly in ENZ systems, we know that rays can traverse the cavity on a timescale much smaller than the time it takes the envelope to change. However quantizing even a very, very simple cavity is difficult, as we will demonstrate.

4) After finding energy minima, perturb length, amplitude, a frequency parameters in the wave envelope used to estimate the refractive index.

5) Quantize the cavity again, seeking to minimize energies of modes.

Currently, even quantizing the cavity is a stumbling block because nonintegrable cavities are chaotic. Another problem is finding a nonlinear problem in 3D space, with known solutions, that is ammenable to ray methods. Since the proposed approach is to treat a nonlinear cavity as a linear one on time scales much slower than the group velocity, the nature of the nonlinearity is not of crucial importance for solving the sub-problem finding solutions for the nonintegrable cavity. Furthermore, since we know that a Coulombic refractive index gives closed orbits, a perturbation to such a system would be an ideal testing ground. We can add a Kerr nonlinearity to the ray-based quantization methods outlined in chapter III, but if we find a solution, we can't know if it outperforms perturbation theory.

However, we know one important, somewhat-Coulombic nonlinear system in which quantum mechanical perturbation theory gives a decent answer, and for which the exact solution is known, and this is the ground state of the helium

atom. For this particular case, there is no optical solution because there are no zero angular momentum modes. However, it is still a solution to the scalar wave equation, and as we showed in chapter III, we can find $l = 0$ modes in the scalar wave equation that have no transverse solutions in the vector wave equation. We choose helium because the electrons in helium have a spherically symmetric charge density, which gives a relatively easy scalar wave equation to solve by perturbative methods. Even for this oversimplified system, we will find that the nonintegrable and chaotic nature of the wave equation makes ray-oriented quantization methods difficult. We will show that applying perturbation theory to the scalar wave equation agrees with first-order quantum mechanical perturbation theory, but we can't assume to match rigorous quantum mechanical solutions. One reason this problem was chosen is because it approximates a nonlinear problem and scalar wave equation gives the right answer. First, we will show why we can very roughly approximate an two particle Schrödinger equation by a scalar wave equation, with a mixture of quantum arguments and semiclassical approximations. The reason that ray tracing gave relativistic hydrogen atom in chapter III, is because the single-electron Dirac equation can be cast in the form of the Klein Gordon wave equation, which in turn, resembles the refractive index of Drude material, as illustrated in previous sections. The goal of this approach is to transform a hard problem, with no known theoretical or experimental answer, to a distinct, but related problem. If the exact energies of a ray-friendly system with a Kerr nonlinearity were known, that problem would be

a better place to start. Since we are dealing with a roughly Coulombic potential, if ray tracing methods don't work, then it's best to try a different approach.

Perturbative Treatment of Nonlinearity, and Attempts at Ray-Based Solutions

In this section, we wish to discuss difficulties involved with solving the nonlinear wave equation in a 3D, inhomogeneous, ENZ cavity. Since we are dealing with three dimensional cavities that have phase velocities vastly different from group velocities, many FDTD results would be extremely computationally intensive, as is the case even in a single dimension. FDTD methods are even slow when the refractive index is larger than unity. Thus, it is interesting from both a practical and a mathematical standpoint to calculate the effect of the Kerr nonlinearity on a wave packet in an ENZ cavity. Finite difference time domain methods are attractive because we can temporally evolve a pulse interacting with a cavity in a nonlinear medium. However, the phase advances at the a rate of c/n, when the refractive index is near zero, while the group velocity, and the envelope of the pulse evolve at a rate of $v_g = cn$. If we time evolve the phase, we will wait forever for the refractive index to appreciably change. Here, we propose one approach to solving this problem. First, we can calculate the nonlinear refractive index based on on the input wave packet. Next, we use semiclassical methods to quantize the cavity, temporarily treating the Kerr term as a linear, but inhomogeneous, contribution to the refractive index. Finally, we could perturb the input wave packet, again

treat it as a spatial variation to the linear component of the refractive index, and search for a lower energy state. We will soon discuss a particular example related to the perturbation of cavity solutions. The first problem with testing this approach is quantizing a 3D, nonintegrable, spatially varying cavity. This is a difficult and interesting problem in and of itself.

In chapter III, we found that tracing rays gave Bohr-like quantization conditions in the optical analogue of the hydrogen atom, where the spatial part of the square of the refractive index varied proportional to the Coulomb potential: $n^2 = 1 - \omega_p^2/\omega^2 - \frac{2V_{Coulomb}(r)}{\hbar\omega_p}$. In this case, ray quantization did a better job than solving the Schrödinger equation, giving leading higher-order relativistic corrections. However, one feature of this system made it ideal for numerical ray tracing: the rays traveled in circular or elliptical closed orbits. In general, if a ray makes a single trip around a cavity, it will return to the same wavefront, but not the same point on that wavefront. Therefore, this is happens to be an optimal system for trying out new approaches to quantizing a highly nonlinear electromagnetic cavity.

The goal is to develop a quantization model that beats perturbation theory, and ray-based quantization methods showed some promise in that regard in chapter III, which performed significantly better than approximate, wave-envelope approaches. The most reliable approach to quantize a cavity is to treat the nonlinear part of the refractive index as a perturbative term, pick a known solution to the linear wave equation, and calculate the overlap integral. For spatially varying ENZ

cavity, we could use the same Hamiltonian approach outlined in chapter VII, making the replacement $V(r)/(\hbar\omega_p) \rightarrow 4\pi\chi^3|\mathbf{E}|^2$. In chapter VII, however, we assumed spherical symmetry in $V(\mathbf{x})$, which simplified the spin-orbit/Darwin term, $\nabla V(\mathbf{x}) \times \nabla \times \mathbf{E}$ to obtain the final result. This term can be evaluated directly for an arbitrary spatial variation, with a frequency-shift proportional to the follwing overlap integral:

$$\int \left((\nabla V(\mathbf{x})) \times (\nabla \times \mathbf{E})\right) \mathbf{E}^* dV \tag{F.1}$$

In this chapter, we will ignore polarization entirely, since the problem is already difficult, and resort to looking for ray-based quantization solutions to to scalar KG wave equation, which is equivalent to a Drude model refractive index. Numerical ray tracing is time-dependent, and computationally cheap. As described in chapter III, and also in Appendix 4, to lowest order with a scalar wave equation we need only know the gradient of the refractive index to know the curvature of the ray, and the location of the ray tells us the phase velocity with which it propagates. The group velocity of the wavefront arises because waves of a slightly different frequency propagate at a different speed. Interference between these rays results in a slower group velocity, arrived at in the Gaussian approximation described in the previous section. Most importantly, in chapter III, we used the phase velocity to quantize the cavity. If part of the cavity is a nonlinear refractive index, phase velocity quantization methods could still be robust, because the refractive index

won't change in the time that it takes a launched ray to return to its wavefront. Additionally, we would like to describe a time-dependent signal entering, and leaving the cavity. While perturbation theory can estimate the frequency of a mode within the cavity, this does not tell us the dynamics of a time-dependent signal interacting with cavity modes. First however, we will discuss perturbative approaches to finding the energy of a mode in a nonlinear ENZ cavity. We will begin comparing the energy levels of scalar quantum problems and optical problems. Now we will make an argument as to why we shouldn't be surprised if a rough correspondence can be drawn. The wave equation given by ENZ materials can be related to the KG equation, and the KG equation can accurately approximate the Dirac equation if we ignore polarization effects.

Here, we propose an analogy between an effective potential and a Kerr potential. If the coefficient in the Kerr nonlinearity is γ, we would have to divide by 2 to obtain a perturbation that has the properties of an effective potential:$V_{effKerr} = \frac{\gamma}{2} R_{10}(r)^2$. We could insert $V_{effKerr}$ into the refractive index, and pretend that it is a purely spatial shift. The factor of 2 is there because it appears in the Liouville Hamiltonian with a Kerr nonlinearity. Again, we don't yet know exact solutions to a mode in a 3D cavity with a large Kerr nonlinearity, so we'll first try quantizing rays in a different nonintegrable system with known solutions.

Numerical Ray Tracing and Phase Quantization

It was hoped that rays traced in the refractive index given in chapter XIV, XIV.39, would still have elliptical orbits that returned to roughly the same point in phase space after a single orbit. This is not the case. There is still hope of quantizing the ray orbits without formally defining the wavefronts. The ENZ refractive index can be approximated as:

$$n = \sqrt{\frac{2}{\omega_p}\left(-|\hbar\omega_s| + |V(r)|\right)} \tag{F.2}$$

If $\hbar\omega_s > 0$, then rays are free to propagate into the surrounding plasma medium, and won't be bound. If the potential term isn't correspondingly positive, the refractive index is no longer real. When the refractive index is decreased, to mimic a electron-electron repulsion, the wavelength becomes larger. The total ray frequency is $\omega_p + \omega_s$, and $\omega_s = \frac{1}{\hbar}E_q$, where E_q is a quantum energy. With the addition of the repulsive potential, rays with a frequency corresponding to the ground state of helium make the refractive index negative, and can't propagate. If we use a frequency corresponding to -36.4 eV, the perturbation theory estimate, we find an ellipse that precesses substantially.

Since the ray doesn't come back to the starting point, it's very difficult to determine what constitutes an orbit. If we knew the wavefront of this system at this frequency, we would simply wait until the wave returns to its wavefront, and

then check if there is constructive interference. However, at this point, it's hard to figure out how to define the wavefront. On the bright side, tangentially launched rays form the outer extreme of the ray orbit. This means if we pick different radial ray launch locations, we will cover the phase space of possible ray orbits. We can see another pattern emerging if we vary the frequency: Orbits with a frequency closer to the plasma frequency bend less strongly and their ellipses precess less radically. Rays with a Schrödinger frequency of greater magnitude precess more rapidly and bend more strongly because they experience a refractive index that's closer to zero. Precessing ray orbits are illustrated in figure F.1..

One way to estimate how many obits a ray will experience is to measure the precession angle of rays at the maxima. However, this angle is large. If we watch a ray progress for multiple orbits, we see another pattern emerge, seen in figure F.2..

We find the ray launched with the perturbation theory estimate precesses one fifth of the way around the central potential with every orbit. Furthermore, this ray happens to satisfy the relationship: $\frac{2\pi 5}{t} - \omega \cong 0$, where t is travel time to return to the same point in phase space, and 5 is the number total number of orbits experienced before returning to phase space. In general, we don't know the point in the rays trajectory when it returned to its wavefront. However, if a ray orbits 3 times, and returns to the same point, and the time of the trip equals $t = 3*2*\pi/\omega = t$, then arguably that ray passed its wavefront 3 times somewhere in the journey, and will pass the wave front 3 times again before it returns to the same

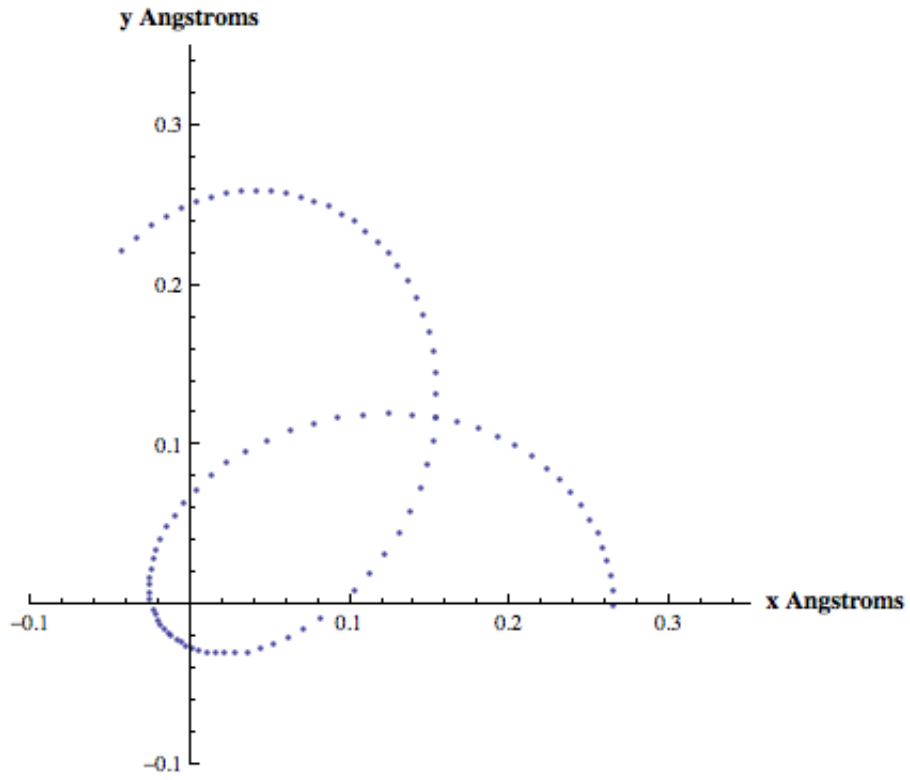

Figure F.1. Rather than ellitical orbits, we find ray orbits with high precession, making quantization difficult. This ray was launched at the Helium ion Bohr radius with an energy of -36.4 eV, which corresponds to a pertubation theory estimate of the energy.

point in phase space. We can vary the frequency to find the ray that closes after 3 orbits, and we find that this ray, like most, does a poor job at phase quantization conditions.

One point that we must be wary of is whether we should advance the phase of the ray by $\pi/2$ at each turning point[31][69]. This changes the phase condition to $2\pi n - \omega t + \pi/2 N_{turns}$. We have tested adding these phase shifts to the system, and it certainly changes the location of matching, quasi-periodic orbits. One argument against adding this phase shift is to consider a constructively interfering circular

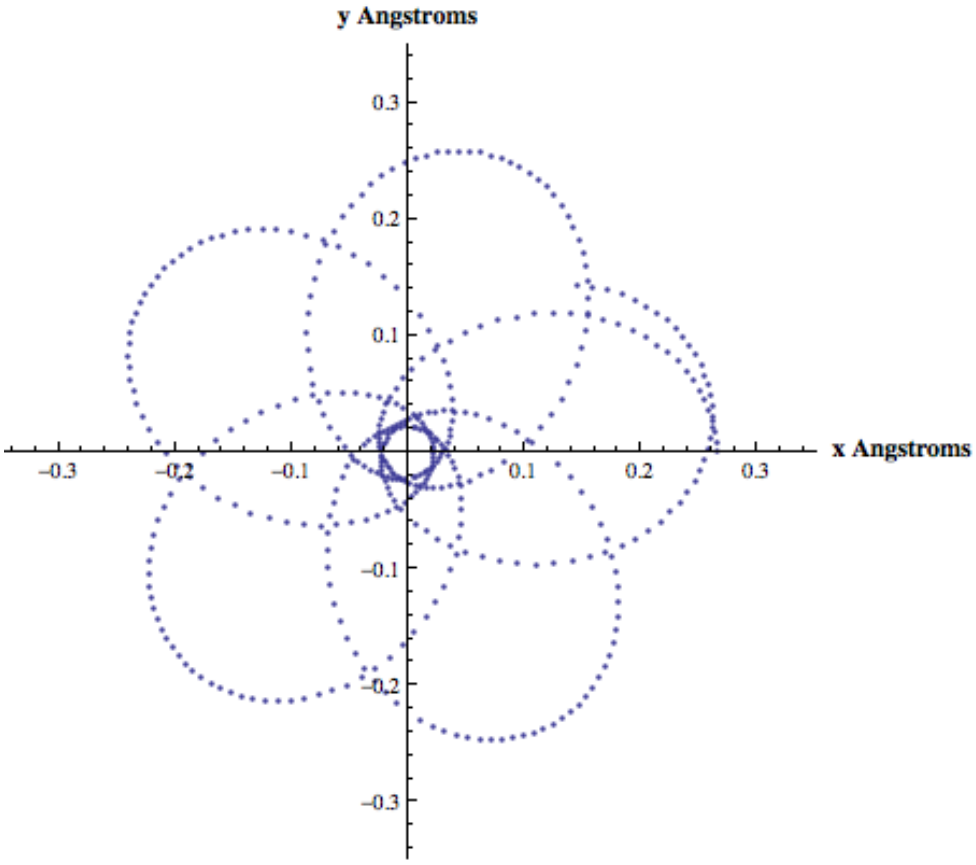

Figure F.2. This ray corresponds to the perturbation theory estimate for the energy of the cavity, -36.4 eV. In 5 orbits, this ray returns to its starting point. Also, $\frac{2\pi n}{t} - \omega \cong 0$, where n is the orbit number and $\omega = (mc^2 + Energy)/\hbar$. This means that this ray will continue to almost constructively interfere every 5 orbits. Adjacent ray paths require many more orbits before returning to the same point in phase space, parameterized in launch angle and radius.

orbit, and and perturb it slightly to form an ellipse. In a Coulombic refractive index, the ray will still return to the same point, in very roughly the same time if the perturbation is small. However, by perturbing the ellipse we have added one maximum and one minimum. Instead of experiencing a 2π phase shift, it will experience a 3π phase shift, and would have to orbit an extra time before the

interference condition is met. Using the Bogomolny operator to quantize this cavity should help to resolve this issue. Leaving the turning point phase shift out seemed to give better interference conditions for more orbits. The figure F.3. displays the phase match results without turning point phase shifts in blue, and with turning point shifts in red. This run seemed to give somewhat encouraging quantization conditions.

However, if we relax restrictions on what counts as close enough to returning

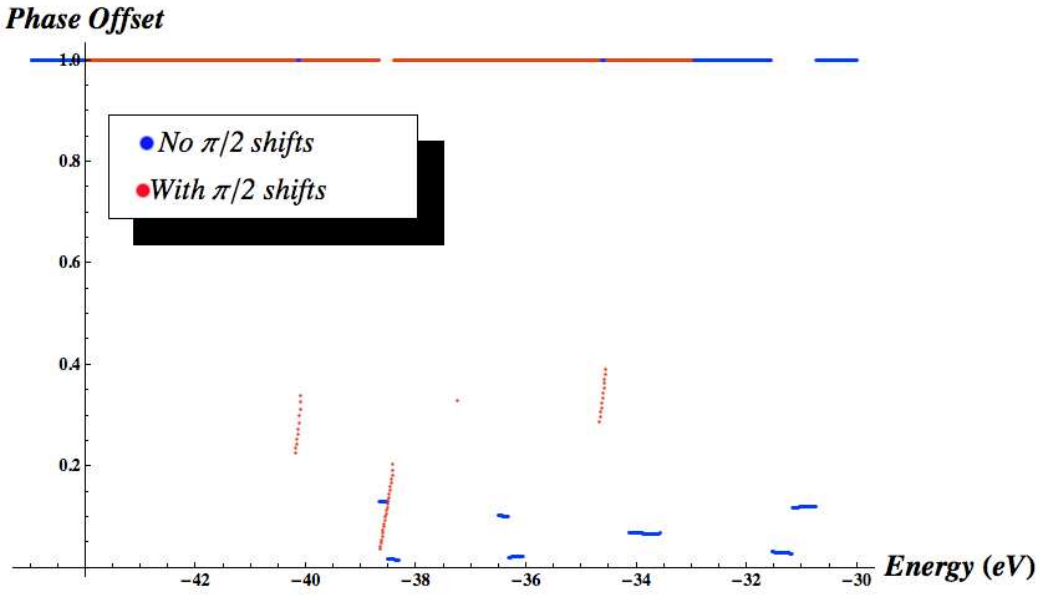

Figure F.3. This figure displays phase matching effectiveness for rays of varying frequency in a perturbed Coulombic refractive index. If a ray returned to the same point in phase space after n, integer orbits, the phase match condition was: $2\pi n - \omega t + \pi/2 = 0$, where t is the ray travel time, and $\hbar\omega = mc^2 + Energy$ gives the ray frequency. This refractive index is meant to mimic the 2 electron helium atom. 36.4 eV is the pertubation theory prediction, and 39.5 eV corresponds to the ground state of helium. Rays were launched tangential to the cavity at the Bohr radius of helium. A phase shift was added at turning points for the red data, and was not present for the blue data.

to the same radius and angle, we find many, many more constructively interfering orbits. Also, if we substantially increase the number of trips allowed around the cavity we find a huge number of constructive orbits as we sweep through frequency. The goal in this exercise was to find a good minimum close to the perturbation theory frequency. In the displayed run, we find one matching orbit with five lobes at around -36 eV the perturbation theory, and another constructive orbit with 11 lobes at around -38.5 eV, displayed in figure F.4.. At -40 eV we find a 6 lobe orbit with destructive interference conditions.

We chose to start at the Bohr radius of helium because that is the peak of the radial probability distribution for the wave function that we used to construct the perturbation potential. If we change the starting radius by five percent, closed quasiperiodic orbits no longer close and don't change dramatically. Our quasiperiodic frequency quantizaiton doesn't give robust agreement with somewhat quantized frequencies at smaller frequencies. This again hints at the presence of chaotic phase space. Plotting this phase space on an SOS is another important next step. It doesn't seem necessary to change ray starting launch angles, because these orbits will correspond to a different maximum frequency.

The explosion of orbits that eventually return to the spame point in phase space is of concern. This also hints we are treading into the chaotic regime of this nonintegrable cavity. Also, this is not a paraxial system, modes bend on the order of the wavefront, so it may be that we should count rays as returned to the same

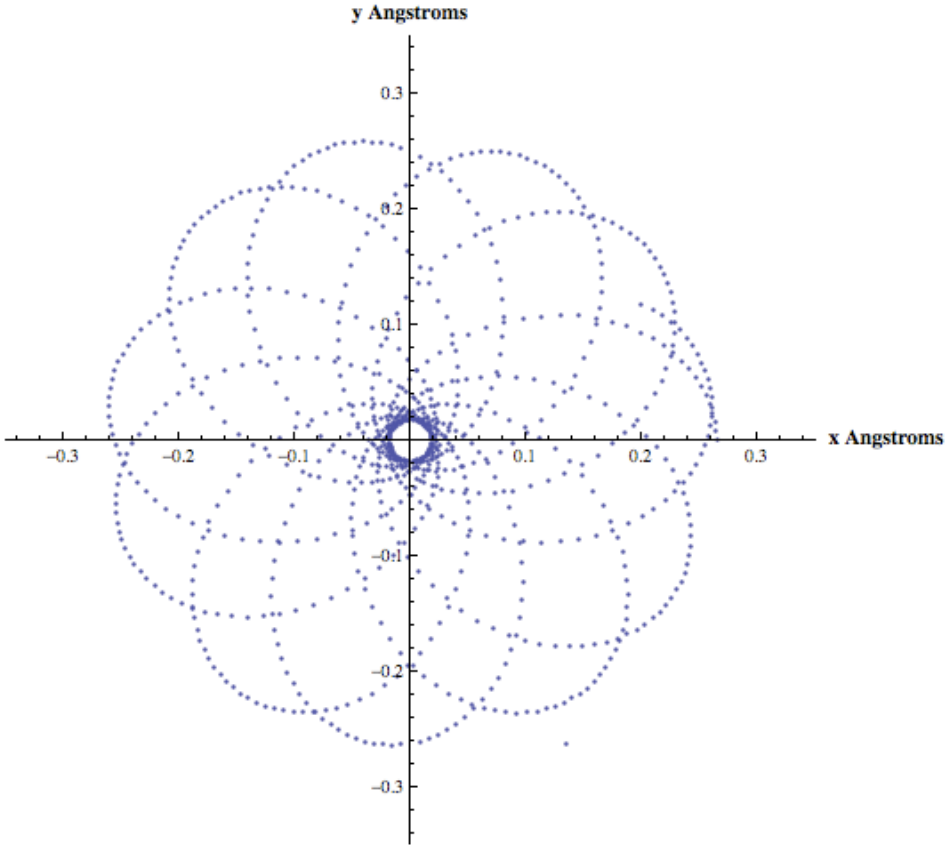

Figure F.4. The phase match minimum found near 38.5 eV corresponds to an orbit that is almost, but not exactly closed, in 11 trips. At 40 eV, there is a 6-orbit closed path, but it destructively interferes.

point in phase space, even if they're off by a few percent of the initial starting positions and launch angles. Path integral techniques would be a more favorable, though computationally intensive approach to this system. In this approach, we would split the ray into many rays, trace them forward, and split those rays into many rays, superimpose rays that end up at the same point in phase space, in a phase sensitive manner, and continue the process until an orbit is formed.

Another potentially useful technique for identifying when a ray returns to its

wavefront is to intentionally generate a caustic by launching rays at slightly different starting angles, as illustrated in figure F.5.. When the rays return to the same point in space, with the same phase, at the same time, presumably they have returned to the same wavefront. When we launch rays at near tangential, but not exactly tangential angles, we find that the rays form a caustic at the minimum turning radius, and at the maximum turning radius. That a caustic is at the maximum radius serves to strengthen the argument that it is valid to quantize rays that return to the same point in phase space after many orbits. The initial challenge of this problem is to determine when rays return to the same wavefront with the same phase. Here, we have shown that we can start rays on the same wavefront, and we find that they return to the same point in space at the same time, with the same relative angle, after each ray has taken a different trajectory towards the central potential and back.

Also, we did not include the $(Ze^2/r)^2$ relativistic corrections to the Coulomb potential that arise if we spatially vary both ϵ and μ according to the Coulomb potential. Most rays go close to the nucleus, and this term would affect both their travel time and bending angle. If an unambiguously good quantizing frequency is found, the next step would be to perturb the Bohr radius of the $R_{10}(r)$ orbitals, calculate a new refractive index perturbation potential, and find out whether the phase matching improves or degrades, while also re-checking adjacent frequencies to look for a better frequency quantization condition. If we begin adding $R_{2l}(r)$

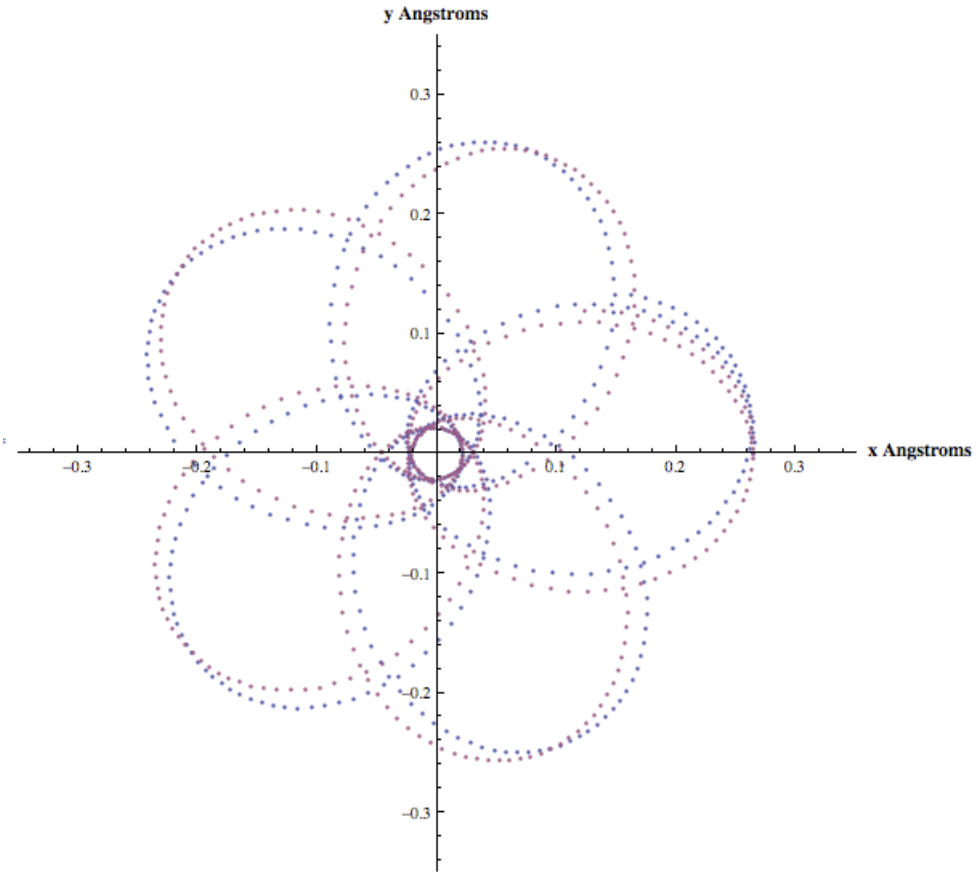

[b]

Figure F.5. One way to identify caustics is to form a caustic by starting rays at slightly different angles. Launching caustic on a quasi-periodic orbit indicates that they cross once at the minimum and again at the ray extreme turning point. This suggests that imposing quantization conditions on quasiperiodic rays that have traversed the cavity several times is valid. This may imply that we can also check for satisfaction of phase conditions from one maximum to the other, regardless of whether rays form quasiperiodic orbits in a reasonable amount of time.

perturbations to the shape of the refractive index, the search parameter space rapidly increases, which is an issue with most nonlinear problems.

Since charge density takes the form of energy density, we might try a fully semiclassical system in which an electron-like, massive vector field is coupled to Maxwell's equations, using energy density of $R_{nl}(r)$ solutions, in place of charge.

However, this approach runs into problems. A single mode would give itself a repulsive self-energy shift of $\frac{5}{4}\frac{Z}{a}$, and we would no longer be able to obtain hydrogen like solutions. Since Z/a is proportional to the radius of the wavefunction, we would need to couple a third semiclassical field to the system to cancel the repulsive self energy, and the field would need to fall off rapidly when outside the electron wavefunction. A Yukawa coupling to a massive, scalar field may accomplish this result. However, it is easier here to simply invoke quantum mechanical point particle arguments to avoid self-energy shifts.

Connection Between the Dirac and KG Equations

Here, we wish to show why solutions to the relativistic Dirac equation are also solutions to the KG equation, but not vice versa. To see the connection between the Dirac and KG wave equation, we will recall that the Dirac equation can be cast in the following form, where Ψ is a 4 spinor[38]:

$$\left(c\vec{\alpha}\cdot\mathbf{p}+\beta mc^2\right)\Psi = i\hbar\frac{\partial}{\partial t}\Psi \tag{F.3}$$

Solutions to the Dirac equation are also solutions to the KG equation, if we ignore complications with spin-orbit coupling. Not all solutions to the KG equation satisfy the Dirac equation, as not all solutions to a vector wave equation satisfy Maxwell's equations. We can find the KG equation from the Dirac equation with the following methodology. We first take the Dirac equation Hamiltonian operator,

and operate on the Dirac equation itself, squaring the left hand side of F.3, and introducing another energy operator on the right. The parameters α and β are 4 by 4 matrices. α is a vector of matrices with the Pauli sigma matrices in the off diagonal elements. β is composed of the identity matrices:

$$\alpha = \begin{pmatrix} 0 & -\vec{\sigma} \\ \vec{\sigma} & 0 \end{pmatrix} \tag{F.4}$$

$$\beta = \begin{pmatrix} I & 0 \\ 0 & -I \end{pmatrix} \tag{F.5}$$

The following permutations are now useful: $\alpha_i^2 = \beta_i^2 = 1$, and $\alpha_i, \alpha_j = \alpha_i, \beta = 0$. Applying these, we find:

$$\left(c\vec{\alpha} \cdot \mathbf{p} + \beta mc^2\right)^2 \Psi = \tag{F.6}$$

$$\left(c^2p^2 + m^2c^4\right) \Psi = -\hbar^2\partial_t^2\Psi \tag{F.7}$$

To add a potential to the diagonal elements of the Dirac equation in as in earlier chapters, we simply perform the following substitution: $-i\hbar\partial_t \rightarrow E - V$. Since the momentum operator acts on the potential, it isn't strictly valid to make this substitution after we have arrived at the KG equation. To account for spin-orbit and Darwin shifts, we must perform a spinor analog to the steps in chapter VI. However, we already know that the spin-orbit shifts will be small corrections to the Schrödinger energy, where $E_s = E - mc^2$. So we'll make that substitution here,

and arrive at a version of the KG equation that ignores spin, while also throwing out V^2 relativistic corrections discussed in chapters V and VI:

$$\left(c^2p^2 + m^2c^4\right) \cong (E - V)^2 \cong E^2 - 2EV \tag{F.8}$$

With little approximation, the following holds: $E = mc^2 >> V$. Now we arrive back at the KG equation.

$$\nabla^2\Psi - \frac{1}{c^2}{\partial_t}^2\Psi = \frac{{\omega_p}^2}{c^2}\Psi + \frac{2\omega_p}{\hbar c^2}V(r)\Psi \tag{F.9}$$

Conclusion

Quantizing a nonintegrable spherical cavity was initially undertaken on the hope that ray orbits would still be elliptical. Also it is interesting to test whether the success in quantizing hydrogenic refractive index potentials can be extended. When quantizing hydrogenic atoms, the phase matched extremely well, but not nearly as well in this system.

Using the Bogomolny transfer operator to quantize this cavity should give more concrete results. This will verify whether the attempts to quantize this cavity using quasiperiodic orbits is valid. We demonstrated in chapter IX that the Bogomolny operator works exceptionally well for quantizing nonintegrable scalar systems. In chapter IX, we deformed the shape from one integrable geometry, to another. One geometry was the half sphere and the other the half parabola. We crossed

all of the fundamental modes of this hybrid system through chaotic phase space without a problem. Work by D.A. Goodings leads the way for demonstrating the use of the Bogomolny operator to determine the energies of spherically symmetric potentials[70]. Goodings even quantized the hydrogen atom using Bogomolny's operator, and used it to near-exactly derive the modes of the hydrogen atom, complete with angular momentum dependence[71]. Goodings started from the Schrödinger Hamiltonian, but as we have demonstrated, we can readily traverse between Schrödinger, Klein Gordon, Dirac equation, and Maxwell's equations using the techniques described in this dissertation. Using the Bogomolny operator on this perturbative refractive index approximation to the ground state of helium will more readily give an unambiguous answer than the ray tracing methods that we have begun to explore. Transfer operator approaches related to Bogomolny's operator have been used to quantize multi-electron atoms, and a semiclassical version of the helium atom that accurately predicts energies using trace methods and point particle assumptions[72]. Alexandru Popa has used phase velocity arguments, and the Hamilton-Jacobi equation, to quantize states in helium, lithium, and beryllium to high accuracy[73]. Popa additionally assigned orbital magnetic moments, and screening coefficients to electrons in this system using quantum and classical arguments. We will continue to explore the ray methods that we have briefly described here. As mentioned before, ray methods have the potential to carry signals into and out of linear, and perhaps nonlinear ENZ microcavities.

Learning to manipulate signals and data in these systems is key towards finding new practical applications. For 1D problems, use of the Liouville NLS Hamiltonian is undoubtedly the best starting point for future work. Extending this formalism to 3D cavities would be a tremendous boon for solving nonlinear problems, and testing new ray methods.

APPENDIX G

DERIVING THE VECTOR INTERACTION HAMILTONIAN

The starting point for deriving the vector version of Pauli's spinor/electromagnetic interaction Hamiltonian is taken from chapter XIII:

$$\begin{aligned}\nabla\times\nabla\times\vec{\psi}-\frac{ie}{\hbar c}\Big(\nabla(\mathbf{A}\cdot\vec{\psi})-\mathbf{A}\times(\nabla\times\vec{\psi})-\vec{\psi}\times(\nabla\times\mathbf{A})\Big)\\ -\frac{ie}{\hbar c}\Big(-2(\mathbf{A}\cdot\nabla)\vec{\psi}+\mathbf{A}(\nabla\cdot\vec{\psi})-\vec{\psi}(\nabla\cdot\mathbf{A})\Big)\\ =\frac{i\omega}{c}\left(\mu_d(\nabla\times\vec{\chi})+\nabla\mu_d\times\vec{\chi}\right)\end{aligned} \tag{G.1}$$

From the $\mathbf{\Pi}\cdot\vec{\psi}=0$ condition, we know: $\mathbf{A}\cdot\vec{\psi}=\dfrac{-i\hbar c}{e}\nabla\cdot\vec{\psi}$, substituting, we find:

$$\begin{aligned}\nabla\times\nabla\times\vec{\psi}-\nabla(\nabla\cdot\vec{\psi})-\frac{ie}{\hbar c}\Big(-\mathbf{A}\times(\nabla\times\vec{\psi})-\vec{\psi}\times(\nabla\times\mathbf{A})\Big)\\ -\frac{ie}{\hbar c}\Big(-2(\mathbf{A}\cdot\nabla)\vec{\psi}+\mathbf{A}(\nabla\cdot\vec{\psi})-\vec{\psi}(\nabla\cdot\mathbf{A})\Big)\\ =\frac{i\omega}{c}\left(\mu_d(\nabla\times\vec{\chi})+\nabla\mu_d\times\vec{\chi}\right)\end{aligned} \tag{G.2}$$

This is fortuitous, because the vector Laplacian operating on radial functions multiplied by vector spherical harmonics gives us Schroedinger-like radial wave equation. Since $\vec{\psi}$ and $\vec{\chi}$ have nonzero divergence, the two $j!=l$ vector spherical harmonics are the TE-like and TM-like solutions to Schroedinger's equation if V

varies radially, and we assume that the electromagnetic vector potential is small compared to V. Finally, we'll get rid of $\vec{\chi}$ before we begin to simplify our wave equation.

$$\begin{aligned}\vec{\chi} &= \frac{-ic}{\omega\mu_d}\left(\nabla\times\vec{\psi} - \frac{ie}{\hbar c}\left(\mathbf{A}\times\vec{\psi}\right)\right)\\ \nabla\times\vec{\chi} &= \frac{ie}{\hbar c}\left(\mathbf{A}\times\vec{\chi}\right) - \frac{i\omega}{c}\epsilon_d\vec{\psi}\end{aligned} \tag{G.3}$$

$$\begin{aligned}-\nabla^2\vec{\psi} - \frac{ie}{\hbar c}\Big(-\mathbf{A}\times(\nabla\times\vec{\psi}) - \vec{\psi}\times(\nabla\times\mathbf{A}) - 2(\mathbf{A}\cdot\nabla)\vec{\psi} + \mathbf{A}(\nabla\cdot\vec{\psi}) - \vec{\psi}(\nabla\cdot\mathbf{A})\Big)&\\ = \frac{i\omega}{c}\left(\mu_d(\frac{ie}{\hbar c}\left(\mathbf{A}\times\vec{\chi}\right) - \frac{i\omega}{c}\epsilon_d\vec{\psi})\right)&\\ + \frac{i\omega}{c}\left(\nabla\mu_d\times\frac{-ic}{\omega\mu_d}\left(\nabla\times\vec{\psi} - \frac{ie}{\hbar c}\left(\mathbf{A}\times\vec{\psi}\right)\right)\right)&\end{aligned}$$

$$\begin{aligned}(-\nabla^2 - \frac{\omega^2}{c^2}\epsilon_d\mu_d)\vec{\psi} - \frac{iq}{\hbar c}\Big(-\mathbf{A}\times(\nabla\times\vec{\psi}) - \vec{\psi}\times(\nabla\times\mathbf{A}) - 2(\mathbf{A}\cdot\nabla)\vec{\psi} + \mathbf{A}(\nabla\cdot\vec{\psi}) - \vec{\psi}(\nabla\cdot\mathbf{A})\Big)&\\ = \frac{-\omega\mu_d q}{\hbar c^2}\left(\mathbf{A}\times\vec{\chi}\right) + \frac{\nabla\mu_d}{\mu_d}\times\left(\nabla\times\vec{\psi} - \frac{iq}{\hbar c}\left(\mathbf{A}\times\vec{\psi}\right)\right)&\end{aligned}$$

$$\begin{aligned}(-\nabla^2 - \frac{\omega^2}{c^2}\epsilon_d\mu_d)\vec{\psi} - \frac{ie}{\hbar c}\Big(-\mathbf{A}\times(\nabla\times\vec{\psi}) - \vec{\psi}\times(\nabla\times\mathbf{A}) - 2(\mathbf{A}\cdot\nabla)\vec{\psi} + \mathbf{A}(\nabla\cdot\vec{\psi}) - \vec{\psi}(\nabla\cdot\mathbf{A})\Big)&\\ = \frac{-\omega\mu_d e}{\hbar c^2}\left(\mathbf{A}\times\frac{-ic}{\omega\mu_d}\left(\nabla\times\vec{\psi} - \frac{ie}{\hbar c}\left(\mathbf{A}\times\vec{\psi}\right)\right)\right) + \frac{\nabla\mu_d}{\mu_d}\times\left(\nabla\times\vec{\psi} - \frac{ie}{\hbar c}\left(\mathbf{A}\times\vec{\psi}\right)\right)&\end{aligned}$$

Assuming the Coulomb gauge:

$$(-\nabla^2 - \frac{\omega^2}{c^2}\epsilon_d\mu_d)\vec{\psi} - \frac{ie}{\hbar c}\left(-\mathbf{A}\times(\nabla\times\vec{\psi}) - \vec{\psi}\times(\nabla\times\mathbf{A}) - 2(\mathbf{A}\cdot\nabla)\vec{\psi} + \mathbf{A}(\nabla\cdot\vec{\psi})\right)$$
$$= \frac{ie}{\hbar c}\left(\mathbf{A}\times\left(\nabla\times\vec{\psi} - \frac{ie}{\hbar c}\left(\mathbf{A}\times\vec{\psi}\right)\right)\right) + \frac{\nabla\mu_d}{\mu_d}\times\left(\nabla\times\vec{\psi} - \frac{ie}{\hbar c}\left(\mathbf{A}\times\vec{\psi}\right)\right)$$

$$(-\nabla^2 - \frac{\omega^2}{c^2}\epsilon_d\mu_d)\vec{\psi} - \frac{ie}{\hbar c}\left(-\vec{\psi}\times(\nabla\times\mathbf{A}) - 2(\mathbf{A}\cdot\nabla)\vec{\psi} + \mathbf{A}(\nabla\cdot\vec{\psi})\right)$$
$$= \frac{e^2}{\hbar^2c^2}\left(\mathbf{A}\times\left(\mathbf{A}\times\vec{\psi}\right)\right) + \frac{\nabla\mu_d}{\mu_d}\times\left(\nabla\times\vec{\psi} - \frac{ie}{\hbar c}\left(\mathbf{A}\times\vec{\psi}\right)\right)$$

$$(-\nabla^2 - \frac{\omega^2}{c^2}\epsilon_d\mu_d)\vec{\psi}$$
$$= \frac{\nabla\mu_d}{\mu_d}\times\left(\nabla\times\vec{\psi} - \frac{ie}{\hbar c}\left(\mathbf{A}\times\vec{\psi}\right)\right)$$
$$+\frac{ie}{\hbar c}\left((\nabla\times\mathbf{A})\times\vec{\psi} - 2(\mathbf{A}\cdot\nabla)\vec{\psi} + \mathbf{A}(\nabla\cdot\vec{\psi})\right) + \frac{e^2}{\hbar^2c^2}\left(\mathbf{A}\times\left(\mathbf{A}\times\vec{\psi}\right)\right) \quad \text{(G.4)}$$

Finally, we arrive at a vector analog of the interaction potential.

$$\frac{\hbar^2}{2m}(-\nabla^2 - \frac{\omega^2}{c^2}\epsilon_d\mu_d)\vec{\psi}$$
$$= \frac{\hbar^2}{2m}\frac{\nabla\mu_d}{\mu_d}\times\left(\nabla\times\vec{\psi} - \frac{ie}{\hbar c}\left(\mathbf{A}\times\vec{\psi}\right)\right)$$
$$+\frac{\hbar^2}{2m}\frac{ie}{\hbar c}\left((\nabla\times\mathbf{A})\times\vec{\psi}\right) - \frac{ie\hbar}{mc}(\mathbf{A}\cdot\nabla)\vec{\psi} - \frac{e^2A^2}{2mc^2}\vec{\psi} \quad \text{(G.5)}$$

Starting from the Dirac equation, we can obtain vector curl equations, and a scalar identity matrix that includes divergence conditions, by using Pauli sigma matrix identities used in chapter IV IV.9, and chapter XIII. If we insist that the

scalar diverence and dot product terms cancel each other out, we find that we can obtain a vector version of the Pauli interaction Hamiltonian. The above vector wave equation is different from the wave equation obtained from Maxwell's equations because it allows for solutions with non-zero divergence. In chapter 14 we propose how the above equation can be modified to construct a tensor refractive index metamaterial that acts like a magnetic field for light.

REFERENCES CITED

[1] D. H. Foster, A. K. Cook, and J. U. Nöckel, Physical Review A (Atomic, Molecular, and Optical Physics) **79**, 011803 (2009), URL http://link.aps.org/abstract/PRA/v79/e011803.

[2] E. Bogomolny, Nonlinearity **5**, 805 (1992).

[3] M. C. Gutzwiller, *Chaos in Classical and Quantum Mechanics* (Springer-Verlag, 1990).

[4] C.-H. Chang, Phys. Rev. E **67**, 046201 (2003), URL http://link.aps.org/doi/10.1103/PhysRevE.67.046201.

[5] R. Blümel, T. M. Antonsen, Jr., B. Georgeot, E. Ott, and R. E. Prange, Phys. Rev. Lett. **76**, 2476 (1996), URL http://link.aps.org/doi/10.1103/PhysRevLett.76.2476.

[6] D. H. Foster, A. K. Cook, and J. U. Nöckel, Opt. Lett. **32**, 1764 (2007), URL http://ol.osa.org/abstract.cfm?URI=ol-32-12-1764.

[7] V. G. Veselago, Soviet Physics Uspekhi **10**, 509 (1968).

[8] R. A. Shelby, D. R. Smith, and S. Schultz, Science **292**, 77 (2001).

[9] J. B. Pendry, D. Schurig, and D. R. Smith, Science **312**, 1780 (2006).

[10] F. Bilotti and L.Vegni, New Journal of Physics **10**, 115035 (2008).

[11] A. Alù and N. Engheta, Phys. Rev. B **78**, 045102 (2008).

[12] A. Alù, M. G. Silveirinha, A. Salandrino, and N. Engheta, Phys. Rev. B **75**, 155410 (2007).

[13] B. Wang and K. Huang, Progress in Electromagnetics Research **106**, 107 (2010), URL http://www.jpier.org/pier/pier.php?paper=10060103.

[14] J. Li and Z. Liu, Physics Letters A **332**, 461 (2004), URL http://dx.doi.org/10.1016/j.physleta.2004.10.003.

[15] V. Podolskiy and A. Zayats, Conference on Lasers and Electro-Optics/International Quantum Electronics Conference, OSA Technical Digest (CD) Optical Society of America (2009), URL http://www.opticsinfobase.org/abstract.cfm?URI=CLEO-2009-JWC3.

[16] R. Liu and D. Smith, Physical Review Letters **100**, 023903 (2008), URL http://prl.aps.org/abstract/PRL/v100/i2/e023903.

[17] B. Edwards and N. Engheta, Physical Review Letters **100**, 033903 (2008), URL http://prl.aps.org/pdf/PRL/v100/i3/e033903.

[18] N. Engheta, Science **317**, 1698 (2007).

[19] S. Savel'ev and F. Nori, Nature Physics **21**, 521 (2006), URL http://www.nature.com/nphys/journal/v2/n8/pdf/nphys358.pdf.

[20] S. Savel'ev and F. Nori, Phys. Rev. B **75**, 184503 (2007), URL http://prb.aps.org/abstract/PRB/v75/i18/e184503.

[21] S. Gleyzes and J. Raimond, **446**, 297 (2007).

[22] J. D. Jackson, *Classical Electrodynamics, 3rd edition* (Wiley, New York, 1999).

[23] C. W. Erickson, IEEE Trans. Microwave Theory Tech. **23**, 218 (1975).

[24] P. Yu and K. Luk, IEEE Trans. Microwave Theory Tech. **32**, 641 (1984).

[25] D. H. Foster, A. K. Cook, and J. U. Nöckel, Phys. Rev. A **79**, 011803 (2009), URL http://link.aps.org/doi/10.1103/PhysRevA.79.011803.

[26] M. Tabor, *Chaos and Integrability in Nonlinear Dynamics* (Wiley, 1989).

[27] N. A. Kobylinsky, S. S. Stepanov, and R. S. Tutik, Journal of Physics A: Mathematical and General **23**, L237 (1990), URL http://stacks.iop.org/0305-4470/23/i=6/a=001.

[28] M. A. Gatta, Annales de la Fondation Louis de Broglie **34** (2009).

[29] A. Popa, Journal of Chemical Physics **122**, 244701 (2005).

[30] F. Whooten, *Optical Properties of Solids* (Academic Press, 1972).

[31] F. Jensen, W. A. Kuperman, and M. B. Porter, *Computational Ocean Acoustics* (Springer, 1994).

[32] M. Brack and R. Baduri, *Semiclassical Physics* (Addison-Wesley, 2003).

[33] R. Pohl, A. Antognini, F. Nez, F. D. Amaro, F. Biraben, J. M. R. Cardoso, D. S. Covita, A. Dax, S. Dhawan, L. M. P. Fernandes, et al., Nature **466**, 213 (2010), URL http://dx.doi.org/10.1038/nature09250.

[34] I. Bialynicki-Birula, Acta Phys. Pol. A **86**, 97 (1994).

[35] J. Sipe, Phys Rev A. **52**, 1875 (1995).

[36] C. C. Leary, D. Reeb, and M. G. Raymer, New Journal of Physics **10**, 103022 (2008), URL http://stacks.iop.org/1367-2630/10/i=10/a=103022.

[37] C. C. Leary, M. G. Raymer, and S. J. van Enk, Phys. Rev. A **80**, 061804 (2009), URL http://link.aps.org/doi/10.1103/PhysRevA.80.061804.

[38] R. Shankar, *Principles of Quantum Mechanics* (Plenum Press, 1980).

[39] W. E. Baylis, *Clifford (geometric) algebras with applications to physics, mathematics, and engineering* (Boston:Birkhauser, 1996).

[40] Y. Kravtsov and Y. Orlov, *Geometrical Optics in Inhomogeneous Media, 312* (1990).

[41] V. S. Liberman and B. Y. Zel'dovich, Phys. Rev. A **46**, 5199 (1992).

[42] M. Zeppenfeld and P. W. H. Pinkse, Opt. Express **18**, 9580 (2010), URL http://www.opticsexpress.org/abstract.cfm?URI=oe-18-9-9580.

[43] Morse and Feshbach, *Methods of Theoretical Physics*, vol. 2 (Feshback Publisher LLC, 1953).

[44] Y.-S. Park, A. K. Cook, and H. Wang, Nano Letters **6**, 2075 (2006), http://pubs.acs.org/doi/pdf/10.1021/nl061342r, URL http://pubs.acs.org/doi/abs/10.1021/nl061342r.

[45] P. Yu and K. Luk, IEEE Trans. Microwave Theory **32**, 641 (1984).

[46] J. Jose and E. Saletan, *Classical Dynamics, a Contemporary Approach* (Cambridge University Press, 1998).

[47] A. Kohler and R. Blümel, Phys. Rev. E **59**, 7228 (1999), URL http://link.aps.org/doi/10.1103/PhysRevE.59.7228.

[48] S. Bauch, A. Błędowski, L. Sirko, P. M. Koch, and R. Blümel, Phys. Rev. E **57**, 304 (1998), URL http://link.aps.org/doi/10.1103/PhysRevE.57.304.

[49] M. Tachiki, Phys Rev. B **50**, 7965 (1990).

[50] L. N. Bulaevskii, M. Zamora, D. Baeriswyl, H. Beck, and J. R. Clem, Phys. Rev. B **50**, 12831 (1994), URL http://link.aps.org/doi/10.1103/PhysRevB.50.12831.

[51] S. Gasiorowicz, *Quantum Physics* (John Wiley and Sons, Inc., 1996).

[52] F. Nori, Nature Physics **2**, 521 (2006).

[53] H. A. Fertig and S. Das Sarma, Phys. Rev. B **44**, 4480 (1991), URL http://link.aps.org/doi/10.1103/PhysRevB.44.4480.

[54] S. R. Nagel and S. E. Schnatterly, Phys. Rev. B **9**, 1299 (1974), URL http://link.aps.org/doi/10.1103/PhysRevB.9.1299.

[55] P. Holden and R. Stewart, IEEE transactions on microwave theory and techniques **47**, 2075 (1999).

[56] A. Alu and N. Engheta, Opt. Express **14**, 1557 (2006).

[57] Argyropoulos, Christos, Chen, Pai-Yen, D'Aguanno, Giuseppe, N. Engheta, and A. Alù, Phys. Rev. B **85**, 045129 (2012), URL http://link.aps.org/doi/10.1103/PhysRevB.85.045129.

[58] E. D. Palik, *Hanbook of Optical Constants of Solids, Vol. 3* (Elsevier Science, 1997).

[59] Y. Liu and X. Zhang, Appl. Phys. A (2007).

[60] M. Desaix, D. Anderson, and M. Lisak, **40**, 2441 (1989).

[61] Y. Shen, *The Principles of Nonlinear Optics* (John Wiley and Sons, 1984).

[62] P. Palinginis, C. J. Chang-Hasnain, and H. Wang, Applied Physics Letters **87** (2005).

[63] P. Berczynski, Y. Kravsttov, and A. Sukhorukov, Physica D **239**, 241 (2010).

[64] R. Scharf and A. R. Bishop, Phys. Rev. E **47**, 1375 (1993), URL http://link.aps.org/doi/10.1103/PhysRevE.47.1375.

[65] V. E. Zakharov and S. V. Manakov, Theoretical and Mathematical Physics **19**, 551 (1974), ISSN 0040-5779, 10.1007/BF01035568.

[66] R. W. Boyd, *Nonlinear Optics, 2nd edition* (Academic Press, New York, 2003).

[67] M. S. Pindzola, D. C. Griffin, and C. Bottcher, Phys. Rev. Lett. **66**, 2305 (1991), URL http://link.aps.org/doi/10.1103/PhysRevLett.66.2305.

[68] K. C. Kulander, Phys. Rev. A **36**, 2726 (1987), URL http://link.aps.org/doi/10.1103/PhysRevA.36.2726.

[69] W. Kinney and A. Pierce, J. Acoust. Soc. Am. **67**, 1145 (1980).

[70] P. Tong and D. A. Goodings, Journal of Physics A: Mathematical and General **30**, 4065 (1997), URL http://stacks.iop.org/0305-4470/30/i=11/a=031.

[71] D. A. Goodings and N. D. Whelan, Journal of Physics A: Mathematical and General **31**, 7521 (1998), URL http://stacks.iop.org/0305-4470/31/i=37/a=012.

[72] G. Casati, B. Chirikov, and G. Tanner, *Quantum Chaos* (Cambridge University Press, Cambridge, 1995).

[73] A. Popa, The European Physical Journal D - Atomic, Molecular, Optical and Plasma Physics **49**, 279 (2008), ISSN 1434-6060, 10.1140/epjd/e2008-00176-1, URL http://dx.doi.org/10.1140/epjd/e2008-00176-1.